UNIVERSITY OF OKLAHOMA

GRADUATE COLLEGE

STUDIES OF THE USE OF THE [2.2]PARACYCLOPHANE MOIETY TO MEDIATE INTERACTION BETWEEN METAL CENTERS AND ELECTROPOLYMERIZATION OF 2,2'-BITHIOPHENE IN MICELLAR MEDIA

A DISSERTATION

SUBMITTED TO THE GRADUATE FACULTY

in partial fulfillment of the requirements for the

Degree of

DOCTOR OF PHILOSOPHY

By

SACHIN SHESHRAO CHAVHAN
Norman, Oklahoma
2013

STUDIES OF THE USE OF THE [2.2]PARACYCLOPHANE MOIETY TO MEDIATE INTERACTION BETWEEN METAL CENTERS
AND
ELECTROPOLYMERIZATION OF 2,2'-BITHIOPHENE IN MICELLAR MEDIA

A DISSERTATION APPROVED FOR THE
DEPARTMENT OF CHEMISTRY AND BIOCHEMISTRY

BY

_____
Dr. Daniel T. Glatzhofer, Chair

_____
Dr. Kenneth M. Nicholas

_____
Dr. Ronald L. Halterman

_____
Dr. Wai Tak Yip

_____
Dr. Lloyd A. Bumm

© Copyright by SACHIN SHESHRAO CHAVHAN 2013
All Rights Reserved.

Acknowledgements

. I would like to take this opportunity to acknowledge many individuals whom I am very thankful to complete this journey. First of all the most important person I am thankful to is my mentor Dr. Glatzhofer, for being the most amazing mentor ever. I really appreciate his patience and his commitment with me to achieve academic excellence and put me at ease to achieve my goals. Without his guidance and persistent help this dissertation would not have been possible.

I would also like to take this moment to thank my committee members, Dr. Nicholas, Dr. Halterman, Dr. Yip and Dr. Bumm, for their valuable inputs, suggestions and their commitment throughout my journey as a PhD student. I would also like to thank Dr. Morvant for giving me opportunity to excel in my teaching experience. I would also like to thank my present colleagues in the lab, Farid Ismail, Dan Bamper, Nick Godman, David Hickey, Abby Holmes and past members Dr. Rahul Kadam, Dr. Matt Meredith, Dr. Frank Yepez. Dr. Anna Jozwiuk. I would like to give special thanks to Dr. Anna for helping me in my project to accomplish this dissertation.

I would also like to thank all my friends at OU and in india for all their support and made my this journey enjoyable. Also I would like to acknowledge Department of Chemistry and Biochemistry at University of Oklahoma and all the staff members from the department.

Most important I would like to thank my family for all their support throughout my life and their sacrifice they made in their life and it is really unaccountable. Last and most importantly I would like to thank my wife Avanti for her motivation, her support to sail this journey successfully.

Table of Contents

Acknowledgements iv

Table of Contents v

List of Tables viii

List of Figures ix

List of Schemes xvi

Abbreviations xix

Abstract xxi

CHAPTER I **Introduction** 1

Background: 1

Structural Studies of [2.2]paracyclophane: 2

Transannular effects on reactivity: 5

Linear free energy relationship: 7

Reactivity of [2.2]paracyclophanes 9

Optoelectronic Properties: 15

Magnetic Interactions: 18

Electronic Delocalization in [2.2]paracyclophanes: 21

Project Goals: - 28

Target I 29

Target II 30

Approaches 30

Brief synopsis of this thesis: 34

References: 41

CHAPTER II **Electron Donating Ability of [2.2]Paracyclophane Towards the Redox Potential of Ferrocene** 47

Introduction 47

Results and Discussion 54

Conclusion 69

Experimental 70

References 83

Chapter III **Ferrocenyl Imine Schiff Bases Derived from Diamino-[2.2]Paracyclophane** 86

Introduction 86

Results and Discussion 95

Conclusion 119

Experimental Section 120

References 124

Chapter IV **[2.2]Paracyclophane-based Ligand Copper (II) Complexes: Synthesis and Investigation of Electronic Interactions** 128

Introduction 128

Results and Discussions 139

Conclusion: 174

Experimental 176

References 185

Chapter V **Electropolymerization of Bithiophene in Sodium Dodecylsulfate Micellar Media** 190

Introduction 190

Results and Discussion 206

Conclusion 222

Experimental 223

References 224

Appendix A 216

List of Tables

Table II.1 Various substituted aniline derivatives used to make ferrocenyl Schiff bases 56

Table II.2 Electrochemical data for various ferrocenyl imine Schiff-base derivatives compared against internal standard 1,1'-dimethylferrocene 59

Table II.3 Correlation of Kx and substituent constants (σ and σ^+) with potential difference 63

Table III.1 UV-vis spectra parameters of FcIAPC and ppFcIDAP 100

Table III.2 Electrochemical data of Bis(ferrocenylimino)[2.2]paracyclophane..... 106

Table III.3 Electrochemical data for oligo(pp-FcIDAP) 113

Table III.4 Electrochemical data of FcDCA, FcIAPC, pp-FcIDAP and poly(pp-FcIDAP) 116

Table IV.1 Visible spectral data of Schiff base ligands..... 147

Table IV.2 UV – vis spectral data of pp-DAPSA and pm-DAPSA 159

Table IV.3 Elemental analysis 171

Table V.1 Some known conducting polymers 192

Table V.2 Samples used for study 208

Table V.3 Oxidation potential and concentrations of SDS data..... 215

Table V.4 Micelle concentration data 219

List of Figures

Figure I.1 Structural parameters of [2.2]paracyclophane 3

Figure I.2 Iso-surface plot of the frontier orbitals of [2.2]paracyclophane 4

Figure I.3 Nomenclature parameters of [2.2]paracyclophane 5

Figure I.4 Transannular effect for complexation of [2.2]paracyclophane with $Cr(CO)_3$ 6

Figure I.5 Transannular charge transfer effect with respect to electron donating (EDG) and electron withdrawing (EWG) groups 7

Figure I.6 Planar and central chiral derivative 12

Figure I.7 Energy diagram for photolytic excitations in a organic molecule 15

Figure I.8 Electrooptical pathway for an excitation in conjugated molecule 16

Figure I.9 4-(4-dihexylaminostyryl)-16-(4-nitrostyryl)[2.2]paracyclophane 18

Figure I.10 Organic molecules containing radicals possessing magnetic properties 19

Figure I.11 Bis(phenylmethylenyl)[2.2]paracyclophane derivatives 19

Figure I.12 Spin distribution of diphenylcarbene in Bis(phenylmethylenyl)[2.2]paracyclophane derivatives 20

Figure I.13 Biverdazyl substituted pseudo ortho-, meta- and para, [2.2]paracyclophane derivative 21

Figure I.14 [3.2] and [2.2]Paracyclophane polymers 23

Figure I.15 Multilayered [2.2]paracyclophane 24

Figure I.16 Disubstituted [2.2]paracyclophane containing through-space conjugated polymers, pseudo-para (P1 and P2), Pseudo-ortho (P3 and P4) and pseudo-gem (P5) 25

Figure I.17 Transition metal (M) complexes at each face of [2.2]paracyclophane .. 26

Figure I.18 [2.2]paracyclophane layered polymer 27

Figure I.19 Project target polymers 29

Figure I.20 Ferrocenyl-4-imino[2.2]paracyclophane 32

Figure I.21 Pseudo-para-(bis-ferrocenyl)-4,12-imino[2.2]paracyclophane 32

Figure I.22 Poly(pseudo-para-(ferrocenyl)-4,12-imino[2.2]paracyclophane) 33

Figure I.23 N-Salicylidene-(4-imino[2.2]paracyclophane 33

Figure I.24 N,N-bis(salicyledene- 4-imino[2.2]paracyclophane) 33

Figure I.25 Pseudo-para-N,N'-bis(salicylidene)-4,12-imino[2.2]paracyclophane and its copper complex 34

Figure I.26 Pseudo-para-4,12-bis(salicylidinimine)[2.2]paracyclophane and Pseudo-meta-4,12-bis(salicylidinimine)[2.2]paracyclophane ligands 37

Figure I.27 *pseudo-ortho*-N,N'-bissalicylidene-4,12-diamino[2.2]paracyclophane copper (II) complex 38

Figure I.28 *pseudo-para*-N,N'-bissalicylidene-4,12-diamino[2.2]paracyclophane and *pseudo-meta*-N,N'-bissalicylidene-4,12-diamino[2.2]paracyclophane metal complexes 39

Figure I.29 Metallopolymers based on pseudo-para and pseudo-meta salicylidenimine[2.2]paracyclophane metal complexes 39

Figure II.1 Poly(vinyl ferrocene) 48

Figure II.2 Ferrocene containing polymers 49

Figure II.3 Aza-ferrocene polyme 53

Figure II.4 Target polymer 54

Figure II.5 Typical cyclic voltammograms (CV) for ferrocenyl imine Schiff base with internal standard as DMFc 57

Figure II.6 Hammett plot of Δ logKx vs σ for the redox potential of substituted ferrocenyl imine Schiff bases in AcCN. 65

Figure II.7 Hammett plot of Δ logKx vs σ^+ for the redox potential of substituted ferrocenyl imine Schiff bases in AcCN 66

Figure II.8 Typical cyclic voltammograms (CV) for N-(4-imino[2.2]paracyclophane) ferrocenyl Schiff base with internal standard as DMFc 68

Figure III.1 [2.2]paracyclophane dicarbene 88

Figure III.2 π-spin density distribution in dicarbene isomers 89

Figure III.3 Verdazyl substituted [2.2]paracyclophane 90

Figure III.4 4-(4-dihexylaminostyryl)-16-(4-nitrostyryl)[2.2]paracylophane 91

Figure III.5 π-Stacked [2.2]-paracyclophane and [3.3]paracyclophane 92

Figure III.6 Charge transfer interaction in bis(α-methyl bithiophene)[2.2]paracyclophane 93

Figure III.7 Rhenium (I) complex of [2.2]paracylophane-diimine 93

Figure III.8 UV-vis spectra of 4-ferrocenylimine[2.2]paracyclophane (FcIAPC) and pseudo-para-bis(ferrocenylimine)[2.2]paracyclophane (ppFcIDAP) taken in acetonitrile solvent 99

Figure III.9 Cyclic Voltammetry of pseudo-para-bis(ferrocenylimine)[2.2]paracyclophane (pp-FcIDAP) 101

Figure III.10 Cyclic voltammetry of Bis(ferrocenylimino)[2.2]paracyclophane in different solvent system, dichloromethane (blue), and THF (red) 105

Figure III.11 Cyclic voltammetry of Bis(ferrocenylimino)[2.2]paracyclophane in different solvent system, acetonitrile (blue), and propylene carbonate (PC) (red). 105

Figure III.12 ^{1}H NMR of an oligo(ferrocenylimine[2.2]paracyclophane) in deuterated acetonitrile 110

Figure III.13 Possible structures interpreted by ^{1}H NMR for an oligomer..... 111

Figure III.14 UV-vis spectrum of oligo(4,12-bis(ferrocenylimine)[2.2]paracyclophane) in dichloromethane 112

Figure III.15 Cyclic Voltammetry of oligo(4,12-bis(ferrocenylimine)[2.2]paracyclophane) 113

Figure III.16 Cyclic voltammetry of oligo(4,12-bis(ferrocenylimine)[2.2]paracyclophane at different scan rate..... 114

Figure III.17 Comparison of CVs for monoferrocenylimine, bis(ferrocenylimine) and oligomer..... 115

Figure III.18 Square root of scan rate vs current at first oxidation potential of FcIAPC 116

Figure III.19 Square root of scan rate vs current at first oxidation potential of pp-FcIDAP 117

Figure III.20 Plot of scan rate vs first oxidation peak current for oligo(4,12-bis(ferrocenylimine)[2.2]paracyclophane). 117

Figure III.21 UV – visible spectroscopy of Poly (pp-FcIDAP) in chloroform..... 120

Figure IV.1 Metal coordination polymer 131

Figure IV.2 Stereochemical notation of substituted [2.2]paracyclophane 132

Figure IV.3 Stereochemical description of [2.2]paracyclophane..... 133

Figure IV.4 Binuclear Rhenium(I) Complexes with Bridging [2.2]Paracyclophane−Diimine Ligands 138

Figure IV.5 Dimetal complexes of [2.2]paracyclophane 139

Figure IV.6 UV-visible spectrum of the APCSA in methylene chloride..... 141

Figure IV.7 N-(4-[2.2]paracyclophanyl)-2'-hydroxyacetophenone imine APCHAP 142

Figure IV.8 UV-vis spectra of DMASA (__), APCSA (---) and ANSA (…..)..... 145

Figure IV.9 UV-vis spectra of DMAHAP (__) APCHAP (----) and ANHAP (…). 146

Figure IV.10 Major steric effects in salen ligands 148

Figure IV.11 Conformation energy minima vs dihedral angle for (ANSA and ANHAP) 149

Figure IV.12 Conformation energy minima vs dihedral angle for (DMASA and DMAHAP) 150

Figure IV.13 Conformation energy minima vs dihedral angle for (APCSA and APCHAP) 150

Figure IV.14 Minimum energy conformation of ANSA 151

Figure IV.15 Minimum energy conformation of ANHAP..... 151

Figure IV.16 Minimum energy conformation of DMASA 151

Figure IV.17 Minimum energy conformation of DMAHAP 152

Figure IV.18 Minimum energy conformation of APCSA 152

Figure IV.19 Minimum energy conformation of APCHAP 153

Figure IV.20 UV- visible spectra of pp-DAPSA Schiff's base ligand in dichloromethane 159

Figure IV.21 UV- visible spectra of pm-DAPSA Schiff's base ligand in dichloromethane 159

Figure IV.22 UV-vis spectrum of $(APCSA)_2Cu$) 163

Figure IV.23 UV-vis spectrum of $(APCSA)_2Cu$ 163

Figure IV.24 d-d transition in $(DMASA)_2Cu$ 164

Figure IV.25 EPR spectrum of Cu(APCSA)2 in DMSO/toluene solvent mixture at 77K 165

Figure IV.26 EPR spectrum of $Cu(APCSA)_2$ in DMSO/toluene solvent mixture at room temperature 166

Figure IV.27 Coaxial NMR tube used in Evans method and Change in chemical shift in the ^1H NMR signal 167

Figure IV.28 Theoretical copper Schiff's base ligand complexes based on [2.2]paracyclophane. 170

Figure IV.29 UV – vis spectra of ligands and their copper complexes in toluene 172

Figure IV.30 EPR poly[(ppDAPSA)Cu] at room temperature (RT) and 77 K 173

Figure IV.31 EPR poly[(pmDAPSA)Cu] at room temperature (RT) and at 77K 173

Figure IV.32 IR spectrum of APCSA Ligand using KBr salt 181

Figure IV.33 IR spectrum of the $(APCSA)_2Cu$ 182

Figure V.1 Polyaniline conducting polymer 193

Figure V.2 Mechanism of polypyrrole formation 195

Figure V.3 Typical anions found in conducting polymers 198

Figure V.4 Micelle structure 199

Figure V.5 Micelle formation 199

Figure V.6 Polythiophene 200

Figure V.7 Polythiophene 204

Figure V.8 Cyclic voltammetry of SC118D 207

Figure V.9 Cyclic voltammetry of SC1211 208

Figure V.10 Cyclic voltammetry of SC1212 208

Figure V.11 Cyclic voltammetry of SC1213 209

Figure V.12 Cyclic voltammetry of SC1214 209

Figure V.13 Cyclic voltammetry of SC1215 210

Figure V.14 Cyclic voltammetry of SC1216 210

Figure V.15 Cyclic voltammetry of SC118D 212

Figure V.16 Plot of efficiency of polymer growth against # of scans 213

Figure V.17 Plot of oxidation potential against –log[SDS]. 214

Figure V.18 Micelles and bilayer formation 215

Figure V.19 Electropolymerization of BT in bilayer 216

Figure V.20 Polymer growth at different concentrations of SDS and constant BT . 219

Figure V.21 Polymer growth at different concentrations of BT and constant SDS . 220

Figure V.22 Polymer growth at different concentrations of BT and SDS 221

Figure V.23 Possible model for electropolymerization of BT 222

List of Schemes

Scheme I.1 Preparation of [2.2]Paracyclophane 1

Scheme I.2 Synthesis of [2.2]paracyclophane..... 1

Scheme I.3 Regioselective bromination of monoester [2.2]paracyclophane 10

Scheme I.4 Electrophilic substitution involving transannular proton shift 11

Scheme I.5 Stereoselective α-electrophilic functionalization of chiral amides based on [2.2]paracyclophane 12

Scheme I.6 Stereoselective allylation of [2.2]paracyclophane aldehydes and ketones 13

Scheme I.7 Hydrogenation of dehydroamino acids and esters..... 14

Scheme I.8 Cyclopropanation reaction stilbene using *pseudo-ortho*-N,N'-bisssalicylidene-4,12-diamino[2.2]paracyclophane 14

Scheme I.9 Condensation reactions ferrocenyl carboxaldehyde with aniline derivatives 35

Scheme I.10 Condensation reaction of 4,12-diamino[2.2]paracyclophane with ferrocenyl carboxaldehyde 36

Scheme I.11 Synthesis of 4-imino[2.2]paracyclophane salicylidine ligand..... 36

Scheme I.12 Enantioselective cyclopropanation of styrene using chiral catalyst copper II (bis(4-iminosalisalicylidine)[2.2]paracyclophane 38

Scheme I.13 Electrochemical polymerization of 2,2'-bithiophene in aqueous micellar medium 40

Scheme II.1 Schiff base formation 50

Scheme II.2 Substituted Ferrocenyl Schiff base formation 50

Scheme II.3 Synthesis of a bis(ferrocenyl) Schiff base 51

Scheme II.4 Synthetic routes to poly(ferrocenyl-Schiff's bases..... 52

Scheme II.5 Reactions of ferrocenylcarboxaldehyde with aniline derivatives..... 55

Scheme II.6 Synthesis of N-4-(ferrocenylimine)-[2.2]Paracyclophane 67

Scheme III.1 Synthesis of pseudo – para - bis(ferrocenylimine)[2.2]paracyclophane (pp-FcIDAP 98

Scheme III.2 Electrochemical reaction of bis(ferrocenylimino)[2.2]paracyclophane103

Scheme III.3 Synthesis of an oligo(ferrocenylimine[2.2]paracyclophane); (n=1) 109

Scheme III.4 Ferrocenylimine [2.2]paracyclophane polymer [poly(pp-FcIDAP)] ... 119

Scheme IV.1 Polymerization of a metal complex through functional groups 129

Scheme IV.2 Coordination of metal ions through polymer containing chelating groups 129

Scheme IV.3 Metal-donor coordination polymer..... 130

Scheme IV.4 Polyimines synthesis 130

Scheme IV.5 Enantioselective hydrogenation of dehydroamino acid methyl esters using [2.2]PHANEPHOS 134

Scheme IV.6 Asymmetric catalytic dialkylzinc addition to aldehyde using[2.2]paracyclophane based chiral salen ligand 134

Scheme IV.7 Palladium catalyzed allylic alkylation isomers of phosphinyl-oxazolinyl-[2.2]paracyclophanes chiral ligand..... 135

Scheme IV.8 Cyclopropanation of trans-4,4'-dimethyl stilbene pseudo-ortho-N,N'-bissalicylidene-4,12-diamino[2.2]paracyclophane copper (II) catalyst136

Scheme IV.9 Synthesis of N-4-salicylidine[2.2]paracyclophane ligand (APCSA) ... 140

Scheme IV.10 Synthesis of *pp*-DAPSA and *pm*-DAPSA 157

Scheme IV.11 Synthesis of $(DMASA)_2Cu$ and $(APCSA)_2Cu$ 161

Scheme IV.12 Synthesis of poly(Cu(ppDAPSA)) and poly(Cu(pmDAPSA)) 169

Scheme V.1 Synthesis of polythiophene 201

Scheme V.2 Synthesis of polythiophene 202

Scheme V.3 Synthesis of Polyalkylthiophene (PAT) 202

Scheme V.4 Synthesis of polybithiophene (PBT) 206

Scheme V.5 Oxidation of BT to form poly(2,2'-bithiophene) 215

Abbreviations

AcCN	Acetonitrile
AN	Aniline
ANSA	N-salicylidene aniline
ANHAP	N-(o-hydroxyacetophenoimine) aniline
APC	4-amino[2.2]paracyclophane
APCSA	N-4-salicylidene[2.2]paracyclophane
APCHAP	N-4-(o-hydroxyacetophenoimine)[2.2]paracyclophane
BT	2,2'-Bithiophene
CV	Cyclic voltammetry
DAP	4,12-Diamino[2.2]paracyclophane
DMSO	Dimethyl sulfoxide
DAPSA	N,N'-4,12-bis(salicylidene)[2.2]paracyclophane
DCM	Dichloromethane
DMA	2,5-Dimethylaniline
DMFc	1,1'-Dimethylferrocene
DMASA	N-salicylidene-2,5-dimethyleaniline
DMAHAP	N-(o-hydroxyacetophenoimine)-2,5-dimethylaniline
EPR	Electron paramagnetic resonance
EDG	Electron donating group
EDA	Ethyl diazoacetate
ee	Enantiomeric excess
EWG	Electron withdrawing group

Fc	Ferrocene
FcIAPC	4-ferrocenylimine[2.2]paracyclophane
FcIDAP	4,12-bis(ferrocenylimine)[2.2]paracyclophane
HAP	2-Hydroxyacetophenone
HOMO	Highest occupied molecular orbital
IR	Infrared
ISC	Intersystem crossing
Kc	Comproportionation constant
LUMO	Lowest unoccupied molecular orbital
M	Metal
MeOH	Methanol
MLCT	Metal –ligand charge transfer
NMR	Nuclear magnetic resonance
pg	Pseudo-gem
pm	Pseudo-meta
po	Pseudo-ortho
pp	Pseudo-para
PC	Propylene carbonate
SDS	Sodium dodecyl sulfate
UV-vis	Ultraviolet - visible
SCE	Saturated calomel electrode
$TBAPF_6$	Tetrabutylammonium hexafluorophosphate
THF	Tetrahedrofuran

Abstract

Organometallic polymers have been identified as a class of materials useful in various advanced applications due to their promising electrical, magnetic, optical and catalytic properties. Such properties depend on the orbital interactions between metal ions and ligands, which allow for a mechanism for electronic tuning of the metal environment and properties. [2.2]Paracyclophane has been extensively studied due its unusual structural and electronic properties that arise from the co-facial arrangement of two benzene rings bridged by ethano groups. In this work, ferrocenyl Schiff's bases derived from [2.2]paracyclophane were synthesized to study the electronic behavior of iron centers in ferrocene mediated through the [2.2]paracyclophane moiety. A Schiff's base ligand of 4-amino[2.2]paracyclophane has also been synthesized and studied with regards to its geometric constraints. Attempts were also made to synthesize polymeric copper Schiff's base complexes to study the electronic coupling of copper atoms mediated through [2.2]paracyclophane.

It has been well understood that the [2.2]paracyclophane moiety behaves as an electron donating group but how it behaves when attached to a redox center has not been explored or quantified. We report here the synthesis and electrochemical study of a series of ferrocenyl imine Schiff's bases, including the Schiff's base derived from 4-amino[2.2]paracyclophane. All these ferrocenyl Schiff's bases showed one-electron redox behavior in their cyclic voltammograms, and their redox potentials were found to correlate linearly with Hammett substituent constants (σ) and (σ^+), where the reaction constant (ρ) values were found to be ca. 0.95 and 0.8, respectively. A detailed

discussion of the interaction of the [2.2]paracyclophane moiety with the iron redox center will be presented.

Understanding the electronic ability of the [2.2]paracyclophane to modify the redox behavior of ferrocene, we report the synthesis and electronic interactions between the two iron centers in a bis(ferrocenyl Schiff's base) separated by [2.2]paracyclophane. This study was carried out using cyclic voltammetry, to monitor the electrochemical behavior. A mixed-valent state was observed in this system and the electronic effect of one iron center on the other iron center mediated through [2.2]paracyclophane was determined by calculating comproportionation constant (K_c), which is equal to 240. The result showed weak interactions between the two iron centers mediated through [2.2]paracyclophane moiety.

In another study, Schiff's base ligands of [2.2]paracyclophanes were synthesized by condensation reactions of amino[2.2]paracyclophanes with salicylaldehyde. Geometrical constraints were studied for the Schiff's base ligand derived from 4-amino-[2.2]paracyclophane using UV-visible spectroscopy and computational methods. The ligand geometry was found to be distorted from planarity with the [2.2]paracyclophane unit. Studies were carried out on the synthesis of copper complexes of Schiff's base ligands based on 4-amino[2.2]paracyclophane and pseudo-para-4,12-diamino[2.2]paracyclophane isomers.

Finally, the electrochemical growth of poly(2,2'-bithiophene) (PBT) from 2,2'-bithiophene in sodium dodecylsulfate (SDS) aqueous media was studied using cyclic voltammetry. Different concentrations of SDS and BT were used to optimize the polymer growth. The optimization of such growth depends on the number of BT

molecule per SDS micelles in aqueous media and the mechanism for film growth is discussed in detail.

CHAPTER I

INTRODUCTION

Background:

Cyclophanes are interesting molecules that have been extensively studied. In the preparation of poly(p-xylylene) from p-xylene, Brown and Farthing isolated [2.2]paracyclophane [1]. Gas phase pyrolysis of p-xylene at more than 550 °C produces [2.2]paracyclophane by formation of a diradicaloid, and then a quinodimethane as shown in Scheme I - 1 [2].

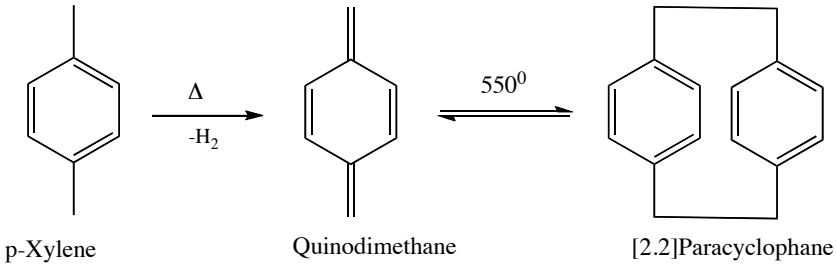

Scheme I - 1: Preparation of [2.2]Paracyclophane

Cram et. al. developed a synthesis of [2.2]paracylophane from p-methylbenzyltrimethylammonium hydroxide by quinodimethane formation as shown in Scheme I - 2.

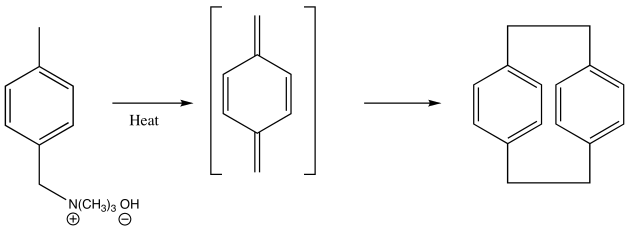

Scheme I - 2: Synthesis of [2.2]paracyclophane

[2.2]paracyclophane has attracted lot of attention due to its versatile use in many areas like stereoselective synthesis, where it can be used as the platform for chiral ligands, and in material sciences, particularly in polymer chemistry [3]. Various derivatives of [2.2]paracyclophane have been used in material science, such as in their polymerization to form poly-p-xylylenes[4] to be used in design of bioactive and biocompatible surfaces by coating them onto biomedical implants and microfluidic devices [5]. The use of paracyclophanes in material science has also been explored recently by incorporating the three dimensional extended π systems of mono-substituted paracyclophanes as an electro-active component in poly(3-butylthiophene), which showed a high photoelectric response [6]. Various conjugated polymer backbones containing paracyclophanes have attracted attention as next generation functional materials, such as poly(p-arylene)s and poly(p-arylenevinylene)s for applications as optoelectronic materials. These polymers contains disubstituted paracyclophane units in their backbones [7].

Structural Studies of [2.2]paracyclophane:

[2.2]Paracyclophane is an extensively studied compound because of its unusual structure. [2.2]paracyclophanes are very strained molecules with strain energies of ca. 31 Kcal mol^{-1} [8]. UV spectroscopy for [2.2]paracyclophane showed strong cofacial π-orbital overlap of its two benzene rings, and it's X-ray structure showed the benzyl-benzyl bonds are stretched with the bent and distorted benzene rings separated by a distance 2.78 of Å, as shown in Figure I -

1 [9]. The distance between non-bridged carbon atoms on both benzene rings is approximately 3.09 Å and the angle between the upper benzene planes and the ethyl bridging bonds is 12.6° [10, 11].

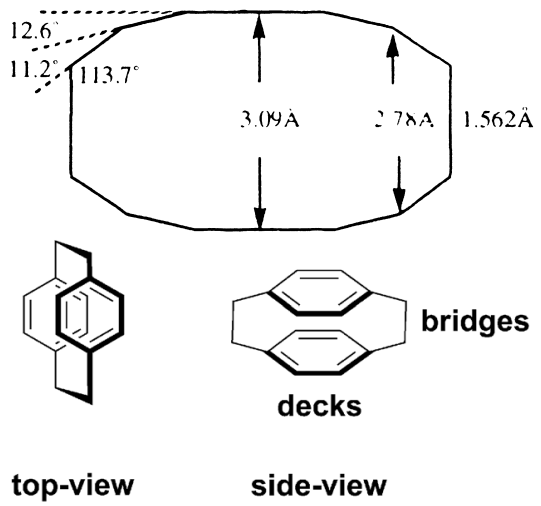

Figure I - 1: Structural parameters of [2.2]paracyclophane

[2.2]Paracyclophane is considered to have a conjugated π-system of two benzene rings even though there are non-conjugated ethyl bridges. Electron density distribution studies and potential energy density distribution studies showed that there is a repulsive interaction between the two rings through the ethylene bridges. It was also mentioned that transannular interaction is not optimal due to the ethylene bridges and distortions of the benzene ring into a boat conformation [12]. The orbital overlap of the two benzene rings in [2.2]paracyclophane shows strong interactions which can be analyzed [13].

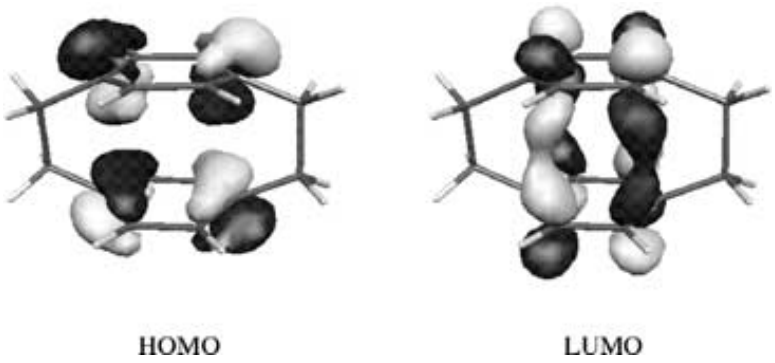

Figure I - 2: Iso-surface plot of the frontier orbitals of [2.2]paracyclophane

As shown in Figure I - 2, the HOMO shows the nodal surface between the two benzene rings, which shows antibonding characteristics, while the LUMO shows orbital overlap suggesting bonding character in the inter-ring region, and describes strong π – π electron correlations between the rings.

Cram introduced a systemic nomenclature of the cyclophanes. Cyclophanes are bridged between their benzene rings at the para-, meta-, or ortho- positions, hence their names denoted as para- or meta- or ortho-cyclophanes. The numbers in the brackets denotes the number of carbon atoms bridging the benzene rings. Hence [2.2]paracyclophane consists of two benzene rings bridged together at para position via two ethanyl groups. Cram and Steinberg suggested the name for this molecule as 'paracyclophane' as the two benzene rings are connected through the para positions on the benzene rings [14]. In the nomenclature of paracyclophanes, it is also important to designate the position of substituents on the benzene rings of paracyclophane. Figure I - 3 shows the established way of naming and numbering substituents in paracyclophanes. In a disubstituted [2.2]paracyclophane, when both substituents

are attached to different decks of [2.2]paracyclophane, *pseudo-* is used as prefix and is followed by, *ortho, para, meta* and *gem*, depending on where the other substituent is attached on the other deck. These four isomers, *pseudo-ortho*, *pseudo-para*, *pseudo-meta*, and *pseudo-gem* are shown in Figure I – 3.

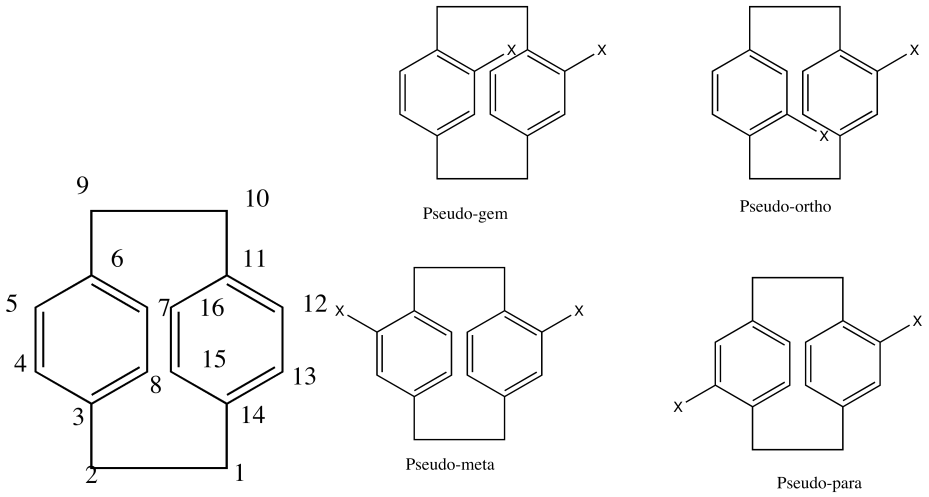

Figure I - 3: Nomenclature parameters of [2.2]paracyclophane

Transannular effects on reactivity:

[m.n]Paracyclophanes exhibit unique conformational and electronic properties based on the numbers of carbons, *m* and *n*, bridging the aromatic rings. Considerable differences in transannular electronic and steric effects have been shown by [m.n]paracyclophanes, where the $Cr(CO)_3$ moiety is complexed with the paracyclophane as seen in Figure I – 4 [15].

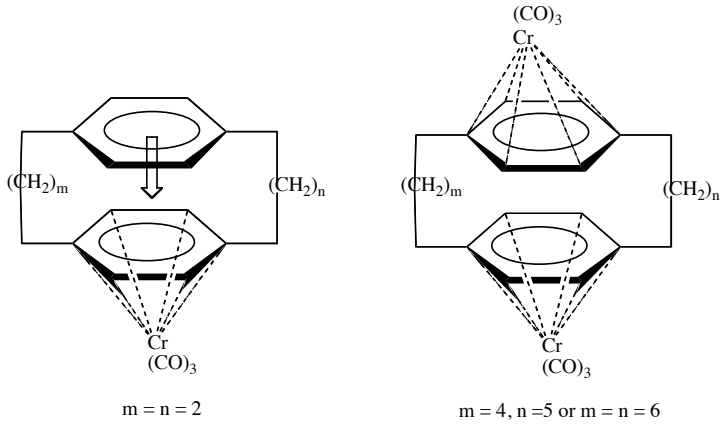

Figure I – 4: Transannular effect for complexation of [2.2]paracyclophane with $Cr(CO)_3$

When *m* and *n* ≤ 4, only mono-complexes formed (i.e. complexation with only one ring), while when *m* = 4, *n* = 5 and *m* = *n* = 6 reaction could be accomplished in the formation of bis-complexes (i.e. $Cr(CO)_3$ complexing with both rings). Using UV absorption spectroscopy, when *m* = *n* = 2, a greater bathochromic shift was observed on complexation than for the *m* = 4, *n* = 5 and *m* = *n* = 6 paracyclophane systems, which was attributed to transannular effects.

Cram and Singer studied transannular substituent effects in π-π complexes of [2.2]paracyclophanes by determining the equilibrium constant (K) for complexation with tetracyanoethylene (TCNE), as shown in Figure I – 5 [16]. The equilibrium constant value for complex formation of [2.2]paracyclophane with TCNE is found to be ca. 40, which is greater than that of p-xylene (K = 7.6), naphthalene (K = 12) and fluorene (K = 18), and pyrene (K = 30), indicating strong π-base strength and substituent effects. In case of ethyl as an electron donating group (EDG) (I) as in Figure I – 5, it increases

the base strength of the substituted ring in complexation to TCNE, while in case of substitution with acetyl and cyano groups as electron withdrawing groups (EWGs) (II), which deactivates the rings, showed the complexation of the unsubstituted ring with TCNE. In both the cases, EDG and EWG, the equilibrium constant values showed clear differences (for ethyl K = 52, acetyl K = 24.5, and cyano K = 8), which showed the effect on one benzene ring to another.

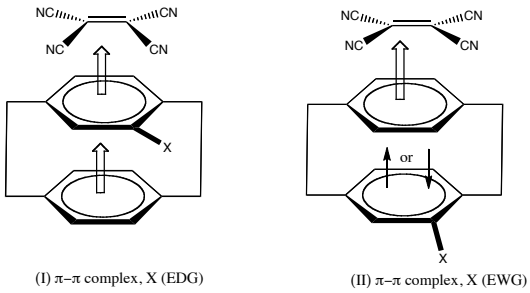

Figure I – 5: Transannular charge transfer effect with respect to electron donating (EDG) and electron withdrawing (EWG) groups

Linear free energy relationship:

Cram and Singer studied whether and how electronic effects of substituents in one ring are transferred to the second ring of the [2.2]paracyclophane [17]. For this study, two techniques were used: 1) complexation of tetracyanoethylene (TCNE) and monosubstituted [2.2]paracyclophanes, which was measured using electronic spectroscopy and 2) NMR studies to monitor chemical shifts of the aromatic hydrogens relative to monosubstituted [2.2]paracyclophane. By the first technique, a linear relationship was observed between the transition energies for the charge transfer

complexes and Hammett substituent constants (σ). Electron donating groups showed a stronger complexation with TCNE as shown in Figure I - 5. It is important to mention here that electron withdrawing groups showed transannular substituent effects but at the same time exhibited a homoannular substituent effect, as can be seen as in II, in Figure I – 5.

NMR can be used to study the transannular effect as well. In this case, the chemical shift of one of the aromatic protons adjacent to the substituent is sensitive to the nature of substituent, in which this proton is upfield with respect to other aromatic protons when the substituent is an EDG and dowfield when the substituent is an EWG. By both techniques, ring to ring electronic interactions in [2.2]paracyclophane were observed.

Cram and coworkers studied electronic effects transmitted between the two rings of [2.2]paracyclophane by measuring the acidity constants of substituted [2.2]paracyclophane carboxylic acids and amines [18]. The correlation between substituent and reaction center through the transannular transmission of electronic effects was determined by pKa values [19]. Acevedo and Bowden studied the transannular effect for pseudo-ortho substituted 4-carboxy[2.2]paracyclophanes using the electrostatic cavity model of Kirkwood and Westheimer [19]. Later, Cram and coworkers considered steric interactions between substituents and reaction centers for understanding the transannular effects between the two rings by measuring the acidity of pseudo-substituted 4-carboxy[2.2]paracyclophanes and 4-amino[2.2]paracyclophanes [20]. The correlation coefficient of the graph between the pKa values and substituent

constants for the electron withdrawing substituents in pseudo-para and pseudo-meta substituted 4-carboxy[2.2]paracyclophane and 4-amino[2.2]paracyclophane were calculated using the following equation 1, where K_x/K_o is the acidity constant ratio for substituted to parent 4-carboxy or 4-amino[2.2]paracyclophane, *m* is the slope of the correlation, and found to be 0.983 and 0.981 respectively.

$$\log (K_x/K_o)^{\Psi\text{-meta}} = m \log (K_x/K_o)^{\Psi\text{-para}} \qquad (1)$$

As both these correlation coefficients are similar in value, it is presumed that the effects on pKa values with different substituents are not particularly due to resonance effect as mentioned later concerning electrophilic substitution reactions on [2.2]paracyclophane [18, 21].

Reactivity of [2.2]paracyclophanes:

The reactivity of [2.2]paracyclophanes depends on the electrophiles reacting with them. Acylation, nitration and halogenation reactions are possible on the benzene rings of the paracyclophanes. Electron withdrawing groups on one ring deactivates both the rings toward electophilic attack. When subjected to electrophilic aromatic substitution reactions, a pseudo-gem effect was observed for the incoming electrophile [21]. The pseudo-gem effect was observed during bromination of a [2.2]paracyclophane monoester in excellent yield (82%). High regioselectivity results due to the formation of a σ-complex in which the

incoming bromine displaces the aromatic hydrogen atom directly opposite the most basic oxygen atom of the ester group as shown in Scheme I - 3.

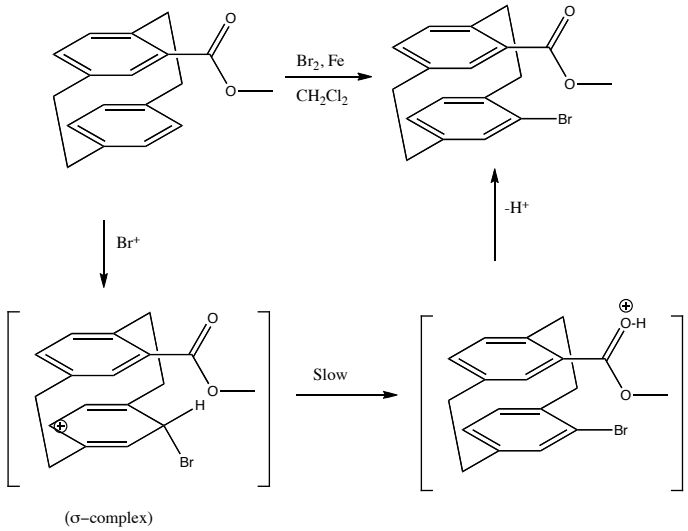

Scheme I – 3: Regioselective bromination of monoester [2.2]paracyclophane

The directing effect of 4-acetyl and 4-nitro substituents on one ring suggested that the bromination reactions predominantly favor pseudo-gem products [22]. This pseudo-gem direction is important as a significant intramolecular effect, which can be used in three ways for the modification of paracyclophanes in reactions such as: 1) to add additional bridges to the [2.2]paracyclophane nucleus, 2) stereocontrolled directed synthesis of pseudo-gem products, and 3) synthesis of multifunctionalized chiral [2.2]paracyclophane derivatives [23].

Transannular directive influences in mono-substituted [2.2]paracyclophanes were further studied in the formation of disubstituted paracyclophanes using electrophilic aromatic substitution reactions [21]. In the case of electrophilic substitution of substituted [2.2]paracyclophanes, attack by

electrophiles occurs on the unsubstituted ring opposite the most basic site in the substituted ring [24]. The reaction mechanism showed this attack is due to a transannualar proton shift as shown in the Scheme I - 4.

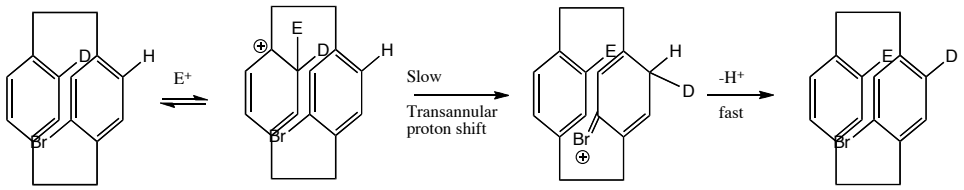

Scheme I – 4: Electrophilic substitution involving transannular proton shift

This transannular proton shift was studied by isotopic labeling as shown in the above scheme, and showed that the proton transfer is the rate-limiting step when one of the hydrogens is replaced with a deuterium. Bromination and acetylation reactions showed primary isotope effects for the transannular directive influence, but such a transannular directive influence was absent in electrophilic nitration [25]. These transannular effects are pronounced in the case of [2.2]paracyclophane, while [4.4]paracyclophane does not show such effects. [3.3]paracyclophane showed an intermediate level of effect.

Cram described the planar chirality of monosubstituted [2.2]paracyclophanes [20]. No stereoselective synthetic application was reported until the 1990s when it was realized that substituted [2.2]paracyclophanes are stable towards significantly high temperatures and towards acids and bases [23]. When a substituent is attached to the benzene ring, the derivative possesses planar chirality, and when the substituent is attached to one of the ethano

bridges, the derivative possesses central chirality. Increasing the number of substituents can generate different chiral derivatives of [2.2]paracylophane.

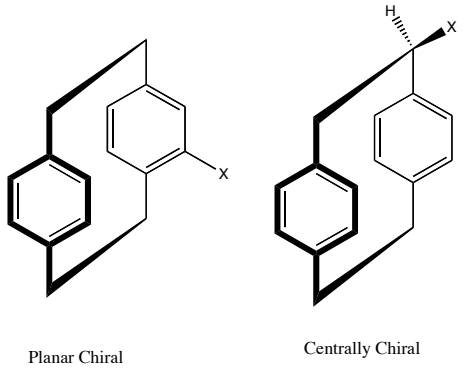

Figure I – 6: Planar and central chiral derivative

The Cahn-Ingold-Prelog system has been used for the description of the chiral [2.2]paracyclophane compounds [26]. The monosubstituted paracyclophanes as chiral auxiliaries has been used for stereoselective alkylations, halogenations, or phenylthiolations as shown in Scheme I - 5. In these reactions, racemic and homochiral N-substituted amines generated amides, which were used as model compounds for stereoselective enolization reactions to form substituted amides with an additional chiral center [27].

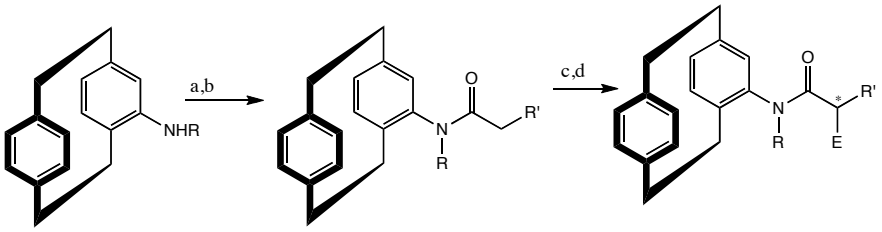

R = Me or Bn ; R' = Me, Bn, or Ph ; EX = MeI, BnBr, NCS, NBS, $PhSSO_2Ph$

a: MeMgBr; b: $R'CH_2COCl$; c:$LiN(SiMe_3)_2$, -78 ^0C, THF; d: EX, -78 to 22 ^0C

Scheme I – 5: Stereoselective α-electrophilic functionalization of chiral amides based on [2.2]paracyclophane

For these reactions, alkylation (82-92% ee) and phenylthiolation (72- 92 % ee) were more efficient than chlorination (58 – 98 % ee) and bromination (18 – 78 % ee). Use of optically active [2.2]paracyclophane derivatives has become important in stereoselective synthesis.

Enantiomers of mono-substituted [2.2]paracyclophane moieties bearing formyl, acetyl and hydroxyl functional groups, which were found to be chiral catalysts for asymmetric synthesis, were prepared by kinetic resolutions, and then chemically modified as required [28]. Carbonyl derivatives of [2.2]paracyclophane have been studied for asymmetric allylboration [29]. [2.2]Paracyclophane aldehydes and ketones possessing planar chirality will react to triallylboron to form boron esters, which form the corresponding homoallylic alcohols after alkaline hydrolysis as shown in Scheme I - 6.

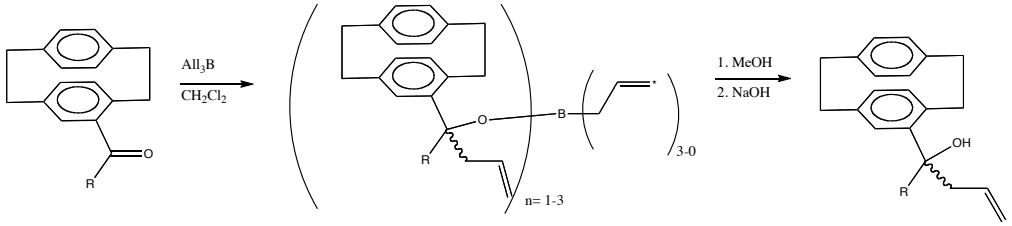

Scheme I – 6: Stereoselective allylation of [2.2]paracyclophane aldehydes and ketones.

Alcohols thus formed will have two elements of chirality, the planar chiral paracyclophanyl fragment and the newly formed asymmetric center.

Many chiral complexes of [2.2]paracyclophane have been used for asymmetric catalysis. As shown in Scheme I – 7, rhodium complexes derived from the phosphonites of chiral paracyclophanes were used to selectively hydrogenate dehydroamino acids and esters[30].

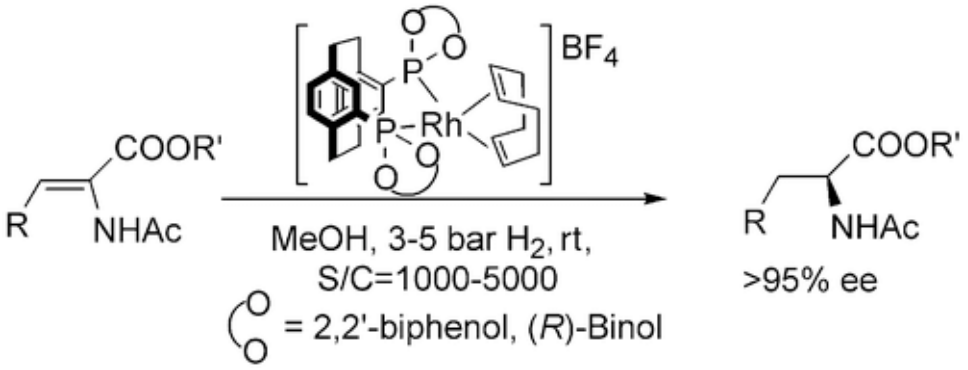

Scheme I – 7: Hydrogenation of dehydroamino acids and esters

Morvant showed the use of pseudo-ortho-4,12-diamino[2.2]paracyclophane as a precursor in the synthesis of a Schiff's base ligand with salicylaldehyde, which can be chelated with metal centers and used as a catalyst for cyclopropanation reactions [31].

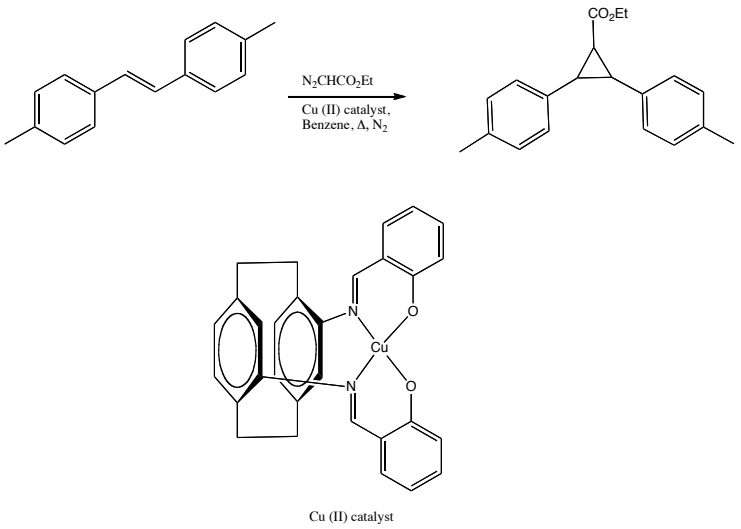

Scheme IV – 8: Cyclopropanation reaction of a stilbene using *pseudo-ortho*-N,N'-bis(ssalicylidene)-4,12-diamino[2.2]paracyclophane

The catalytic efficiency of the pseudo-ortho-N,N'-bis(salicylidene)-4,12-diamino[2.2]paracyclophane copper (II) catalyst was better than N,N'-bissalicylidene-1,2-diaminoethane copper (II) as a catalyst by ca. 45%.

Optoelectronic Properties:

In recent years, a great deal of interest has been focused on the optical properties of conjugated compounds. Organic optoelectronic devices are designed based on the synthesis of organic molecules with well-defined architectures. Optoelectronics is the study and application of electronic devices that source, detect, and control light. Organic molecules that act as electronic conductors are used in many optoelectronic devices, such as photovoltaic cells (PV) and organic light emitting diodes (OLED). Optoelectronic properties can be formulated based on the photonic or electronic excitations that evolve from the production of charge or release of photons.

Electrooptical properties depend on optical or electronic excitation, which in turn depends on the chemical structure of the material and its molecular organization. An energy diagram and electron-optical pathways for excitations in conjugated molecules is shown below in Figure I - 7 [32].

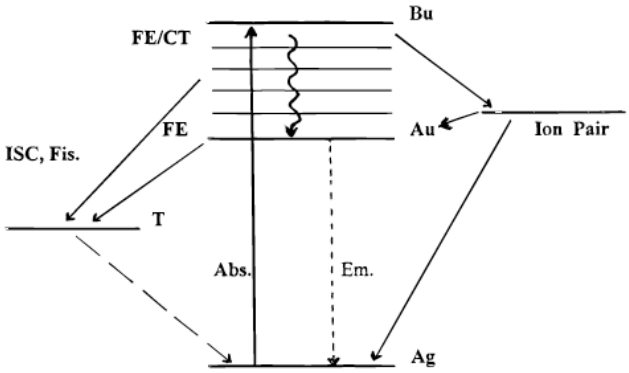

Figure I – 7: Energy diagram for photolytic excitations in a organic molecule

Excitations in conjugated molecules involve strong absorption from the ground singlet state to a higher singlet state, which releases Frenkel excitons and charge transfer excitons. Immediately after absorption, several processes can occur. Mostly the excited electron will go to a lower vibrational energy level in a process called 'internal conversion'. Various other pathways that are possible for this relaxation including intersystem crossing (ISC) to the lowest excited triplet state. Further relaxation from the triplet state may lead to the original ground state, resulting in phosphorescence, or transition back to the excited singlet state, resulting in delayed fluorescence.

The stepwise electro-optical pathway for an excitation in conjugated molecules is shown in Figure I - 8.

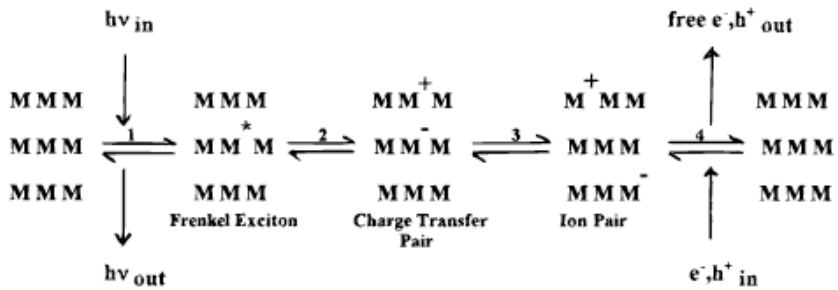

Figure I – 8: Electro-optical pathway for an excitation in conjugated molecule.

In the first reversible process, π – π* excitation leads to formation of Frenkel excitons, electron – hole pairs, which is followed by the dissociation of the electron hole pairs onto adjacent molecules leading to charge transfer pairs in the second process. The third process involves ion pair formation with adjacent molecules by electrostatic interactions, followed by ion pair relaxation.

The energy levels in processes 2 and 3 control the electrooptical properties of organic semiconductors.

The optoelectronic properties of [2.2]paracyclophanes make them potentially significant organic building blocks as applied in material science. Nonlinear optical applications are based on intramolecular charge transfer processes from a donor toward an acceptor moiety through a π-electron conjugated path such as in benzene, stilbene, polyene, thiophene derivatives, etc. Because [2.2]paracyclophane has a strained and π-stacked structure, its optical properties are important to study with modification by chromophore substitution and internal charge transfer between the two rings of the cyclophane core. The absorbance spectrum of [2.2]paracyclophane exhibits absorbance bands at 225 nm, 244 nm, 286 nm, and 302 nm. The spectroscopic properties are attributed to σ – π interactions and π – π through-space delocalization due to energy transfer throughout the cyclophane core. Intermolecular charge transfer (ICT) affects electronic communication in well defined paracyclophane based chromophores, which can result in absorbances and emissions near 500 nm and 600 nm, respectively [33]. Changes in the conjugation length and substitution patterns affects the emission, such as pseudo-para substitution leading to lower energy fluorescence than pseudo-ortho substitution, which may be because of increased electronic communication between the chromophores [34]. Through-space electronic interactions in [2.2]paracyclophanes have been considered to be an efficient pathway to nonlinear optical properties. A model dipolar compound, given in Figure I – 9, containing both donor and acceptor groups on a

paracyclophane, 4-(4-dihexylaminostyryl)-16-(4-nitrostyryl)[2.2]paracyclophane, was studied to elucidate the effects of inter-ring ICT between donor and acceptor [35].

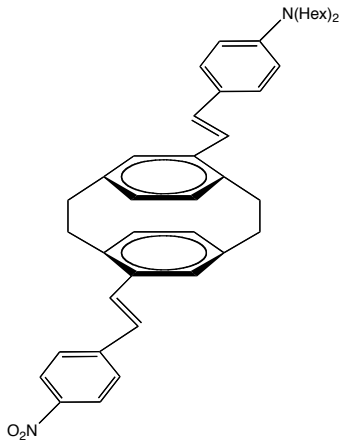

Figure I – 9: 4-(4-dihexylaminostyryl)-16-(4-nitrostyryl)[2.2]paracyclophane.

Magnetic Interactions:

Control of electron spin interaction through organic moieties such as conjugated π-systems is important to study the magnetic properties in organic molecules. While it is well known that iron and other metals possesses magnetic properties, it was not until the early 1980s that large efforts were made to synthesize stable, organic, high spin moieties [36]. Large numbers of organic molecules with radicals have been studied, a few listed below in Figure I - 10, for their magnetic properties [37, 38].

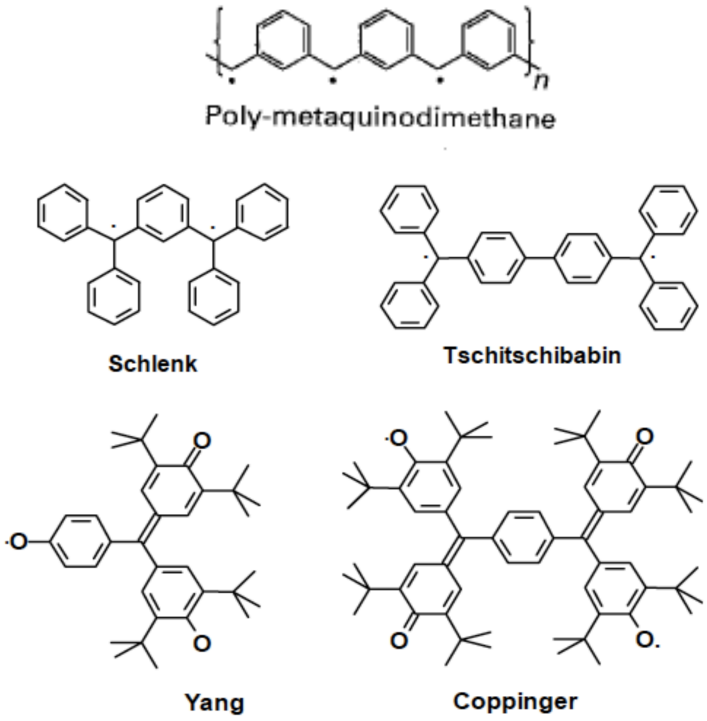

Figure I – 10: Organic molecules containing radicals possessing magnetic properties

Iwamura studied intermolecular magnetic interaction by controlling the spin multiplicity of substituted [2.2]paracyclophanes using bis(phenylmethylenyl diazo) groups and forming diphenyl carbene complexes as shown in Figure I - 11 [39].

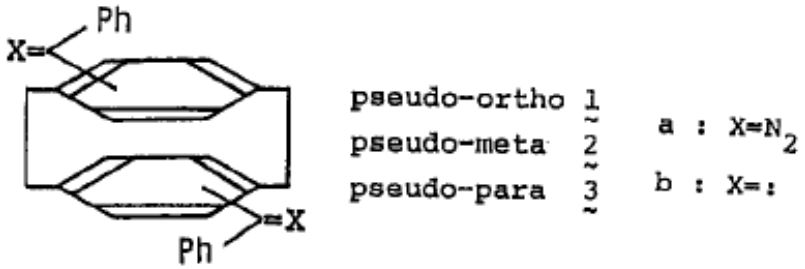

Figure I - 11: Bis(phenylmethylenyl)[2.2]paracyclophane derivatives

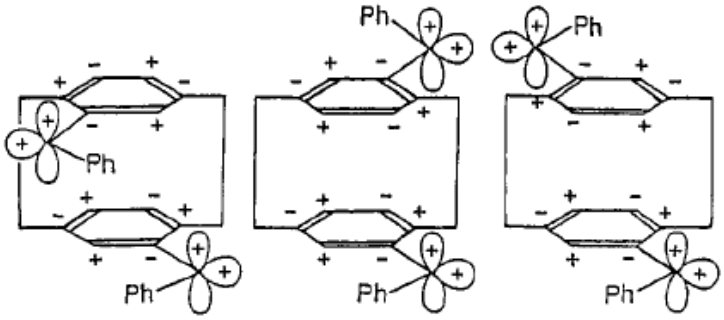

Figure I - 12: Spin distribution of diphenylcarbene in Bis(phenylmethylenyl)[2.2]paracyclophane derivatives

According to McConnell's condition, negative spin densities at two interacting sites on different molecules indicate intermolecular magnetic interaction for three isomers of these carbene complexes as shown in Figure I – 12. Negative signs of the spin density product occur for the pseudo-ortho and pseudo-para isomers and positive sign for the pseudo-meta isomer. According to this spin distribution, these carbene complexes showed different magnetic properties, in which the pseudo-ortho and pseudo-para isomers showed ferromagnetic behavior and the pseudo-meta isomer showed antiferromagnetic behavior.

Intermolecular magnetic interactions and interactions involving charge transfer were also studied for verdazyl derived [2.2]paracyclophanes [40]. Neugebauer's group studied the electronic coupling between two verdazyl radicals through the [2.2]paracyclophane moiety in the same fashion using NMR and ESR, and showed interactions were weak [41].

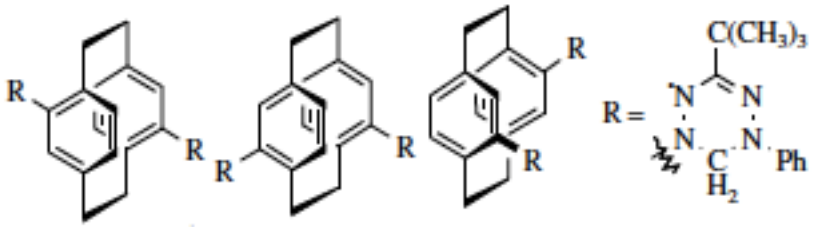

Figure I – 13: Biverdazyl substituted pseudo ortho-, meta- and para, [2.2]paracyclophane derivatives

As shown in Figure I – 13, three isomers of biverdazyl substituted [2.2]paracyclophane, pseudo-ortho, pseudo-para and pseudo-meta, were studied to explore trans-annular interactions between the two benzene rings. In case of pseudo-para- and pseudo-meta-biverdazyl isomers, only zero-field splitting parameters |D'| can be determined, which suggest the average distance between the two unpaired electrons in the verdazyls in the biverdazyl pseudo – ortho and the pseudo-meta-[2.2]paracyclophane compounds resulted from the midpoint of the verdazyl rings. While the distance between the two unpaired electrons in the pseudo-ortho moiety is shifted slightly beyond the verdazyl midpoints due to steric arrangements. Due to long distance between the verdazyl moieties, interactions between the two unpaired electrons in the verdazyl rings are weak.

Electronic Delocalization in [2.2]paracyclophanes:

Electron spin resonance (ESR) spectroscopy of the radical anions of [*n.n*]paracyclophanes were investigated and it was found that when *n* is more than three, the unpaired electron of the radical anion did not show any electron delocalization over both aromatic moieties [42]. The complexity of the ESR

spectrum of unpaired electrons in the [2.2]paracyclophane anions obtained in THF was explained based on the association of the radical anion and the gegenion. The radical anion of [2.2]paracyclophane was generated using potassium as a reducing agent in THF. Initial ESR studies with poorly resolved spectra indicated nine components and the coupling constant was not reported. Later, the ESR spectrum of the radical anion of [2.2]paracyclophane was analyzed to contain 41 components spaced by 0.63 G. The coupling constants were reported to be 2.52 and 0.63 G, corresponding to the methylene bridged protons and ring protons respectively [42].

ESR spectroscopy was found to be a useful method to determine the transannular effect in the case of radical anions on the [n.n]paracyclophanes [43]. When n = 2 or 3, both the benzene rings were involved in electron delocalization of the radical anions of [2.2] or [3.3] paracyclophanes. Both the radical anions showed hyperfine structure in ESR spectrum arising from transannular interactions. Later, Bramwell and Gendell carried out ESR experiments to show strong electron delocalization over both benzene rings [44].

So the question arises, whether such electronic and magnetic behavior can be observed in polymeric systems containing paracycophane moieties. For this purpose, paracyclophane could be either used in the backbone of a polymer or it could be used as a side chain of a polymer. The applications of transannular π-π interactions in the polymers containing cyclophane units as main chain or side chain units of the polymers have been reviewed extensively by Morisaki

and Chujo [45]. As discussed earlier, when two benzene rings are stacked in a paracyclophane system, transannular effects can be observed.

Research interest has been focused on examining such effects in polymer systems where aromatic rings are cofacially stacked [46]. Glatzhofer and Longone synthesized the structurally unique poly ((E,E)-[6.2]paracyclophane-1,5-diene) with the bridged aromatic rings pendant to the polymer backbone as seen in Figure I - 14 and studied the electronic effects in the polymer by fluorescence spectroscopy, ESR, and measuring conductivities after doping with iodine [47].

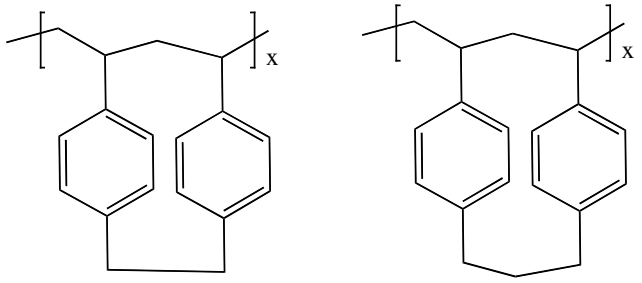

[3.2]paracyclophane containing polymer

[3.3]paracyclophane containing polymer

Figure I – 14: [3.2] and [2.2]Paracyclophane polymers

The polymerization of (E,E)-[6.2]paracyclophane-1,5-diene was carried out by cationic polymerization using $BF_3.Et_2O$ as an initiator [48]. The polymer containing [3.2]paracyclophane units, which has ring strain intermediate between [2.2] and [3.3]paracyclophane systems, showed a red shift in its emission maxima in fluorescence spectroscopy which is analogous to that seen in going from a double-layered [2.2]paracyclophane system (358 nm) to a

quadruple-layered [2.2]paracyclophane structure (395 nm) [49]. The multilayered [2.2]paracyclophanes are shown in Figure I – 15.

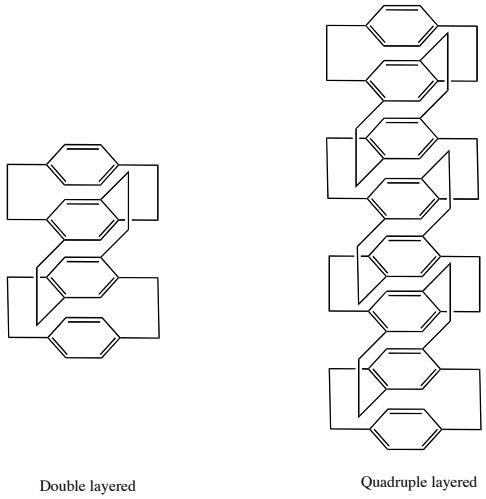

Figure I – 15: Multilayered [2.2]paracyclophane

Such shifts indicated the alignment and electronic interaction of multiple repeating units of aromatic rings. Conductivites and ESR studies of radical cations of the above mentioned polymers showed semiconducting behavior and electronic interactions in repeating units of the polymers. Later, substitution with electron donating groups on one of the benzene rings to stabilize the radical cations generated by doping with iodine showed very little effect in changing conductivities, and hence a direct comparison of the conductivity data could not be made [50].

Much attention has been focused on polymers containing cyclophane skeletons in which the π-stacked structure of the π-electron systems has been recognized as an important factor in the enhancement of the electronic properties in optoelectronic devices [51]. Various conjugated polymers such as

poly(p-arylene)s, poly(p-arylenevinylene)s and poly(p-arylene-ethynylene) have been used as charge transport materials due to their unique structural and electronic characteristics [52]. In the case of cyclophane-containing polymers, [2.2]paracyclophane is of particular interest due to the fact its benzene rings are fixed with ethylene bridges and π-stacking allows through-space interactions. Disubstituted [2.2]paracyclophane has several stereoisomers such as *ortho*-, *meta*-, *para*-, *pseudo-ortho*-, *pseudo-meta*-, *pseudo-para*-, and *pseudo-gem*-, which can result in different polymeric materials as can be seen in Figure I - 16.

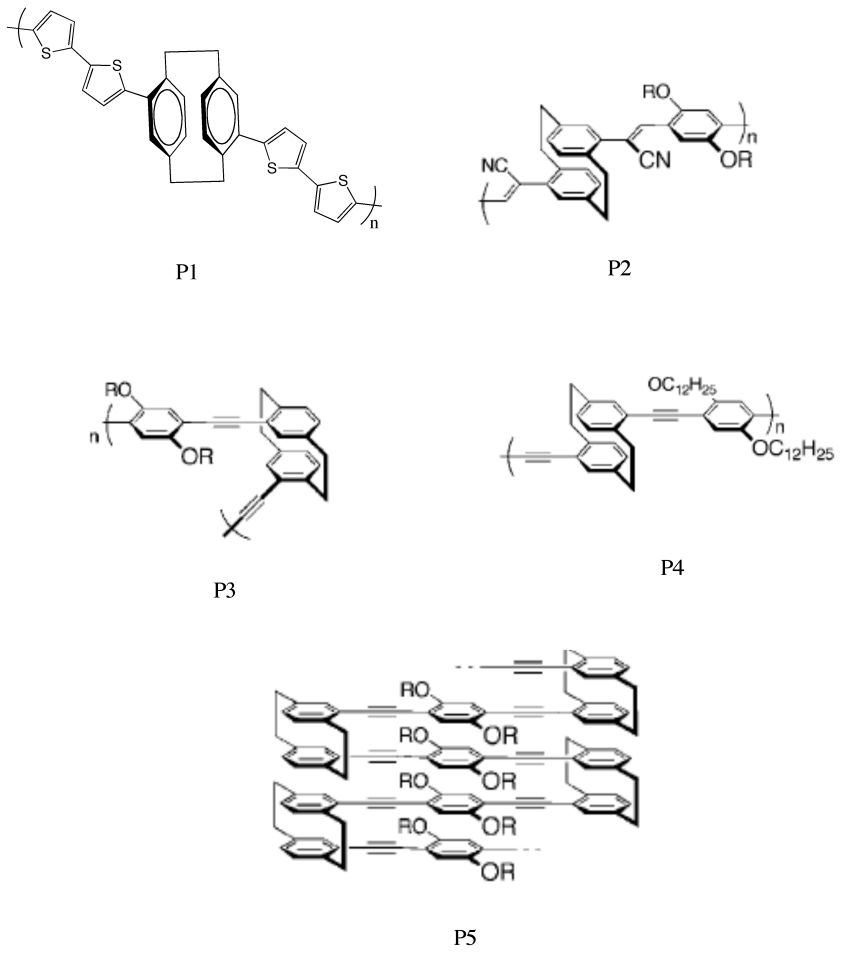

Figure I - 16: Disubstituted [2.2]paracyclophane containing through-space conjugated polymers, pseudo-para (P1, P2 and P4), Pseudo-ortho (P3) and pseudo-gem (P5). Figures adapted from reference [51].

These polymers showed energy and charge transfer properties stemming from π-stacking of the π-conjugated electronic systems.

Research interest in the area of organometallic polymers has evolved over the years due to orbital interactions between metals and the ligand which would allow a mechanism for charge transport [53]. Boekelheide and coworkers suggested the use of the [2.2]paracyclophane unit as a scaffold in complexing each benzene unit with the metal centers which would result in the formation of multilayered metal complexes of [2.2]paracyclophane as shown in Figure I -17 [54].

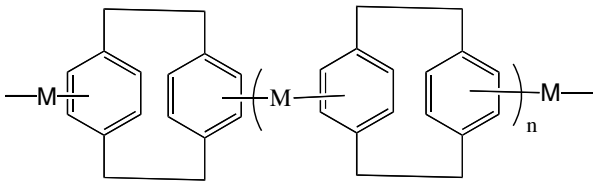

Figure I – 17: Transition metal (M) complexes at each face of [2.2]paracyclophane

The use of through-bond and through space interactions in a [2.2]paracyclophane polymeric system were exploited by synthesizing [2.2]paracyclophane layered polymers end-capped with ferrocene as shown in Figure I - 18 . A xanthane skeleton was used as the scaffold [55].

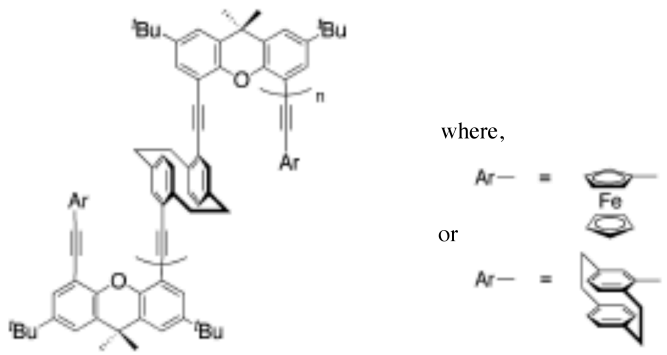

Figure I-18: [2.2]paracyclophane layered polymer. Figure is adapted from the reference [55].

It was concluded that there is enough space between the end capped ferrocene units and [2.2]paracyclophane to be aligned face to face but showed twisting, which lead to ineffective π-π stacking in the ground state with the result that the polymers did not show through-space interactions. Recently, Harvey and coworkers probed the electronic communications through [2.2]paracyclophane-containing conjugated organometallic polymers by studying triplet energy transfer using absorption, excitation, emission spectra [56].

So, considering the structural and transannular electronic properties of [2.2]paracyclophanes, it was of interest to attempt to exploit the electronic and magnetic properties of polymers containing the [2.2]paracyclophane moiety. In this project we planned to focus our attention on using [2.2]paracyclophanes as the aromatic units in conjugated, π-stacked polymers complexed with metals.

Considerations for the project:

1. As it was observed that the structural features of [2.2]paracyclophane play an important role in determining the electronic properties of polymers, it is necessary that the structure must allow direct interaction between the metal and [2.2]paracyclophane moieties.
2. In doing so, the metal centers should be easily redox accessible or have an unpaired spin, so that the interaction between metal centers through the [2.2]paracyclophane moiety can be studied.
3. It is also necessary that the metal centers should placed in such a way that the interactions between them can be directed through the [2.2]paracyclophane moiety.
4. Particularly, we planned to focus on pseudo-para moieties of [2.2]paracyclophane, as this isomer potentially allows for ferromagnetic interactions between spins.

Project Goals:

In order to fulfill these requirements, two systems were chosen as targets of this research project, as shown in Figure I -19:

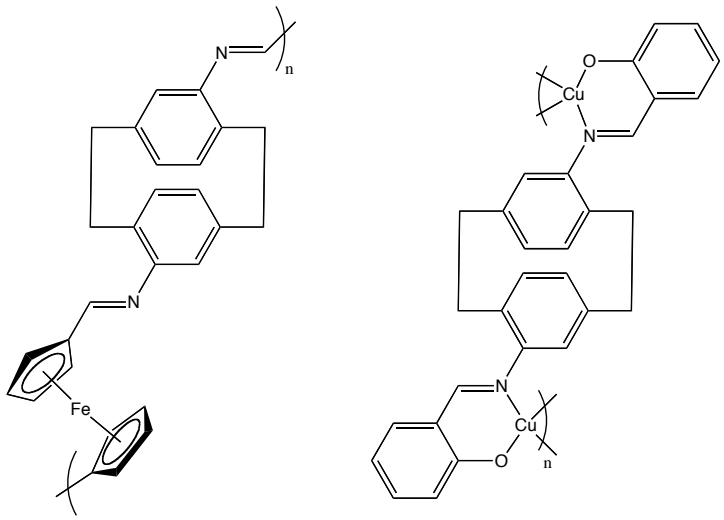

I II

Figure I – 19: Project target polymers

Target I:

The easily accessible redox properties of the ferrocene moiety would allow for:

A. Electrochemical probing of electronic interactions by studying the redox behavior of the ferrocene.

B. For the pseudo-para, bis-ferrocene moiety in [2.2]paracyclophane, a mixed valence system could be formed, resulting in tunable properties.

C. In doing so, a potential drawback could be anticipated that the spin may be highly localized on the ferrocenium ions (Fe (III)) upon electrochemical oxidation, and spatial and steric problem can be anticipated.

Target II:

Each Cu^{2+} ion has a d^9 electronic configuration and hence has one unpaired electron, which has spin state S of ½, and which would allow for,

A. Study of the unpaired electron interactions between the different copper metal centers using EPR
B. Study of spin exchange interactions, which would give rise to ferromagnetism, antiferromagnetism or ferrimagnetism, depending on the nature and relative orientations of the spins, which can be studied using magnetic susceptibility measurements.
C. In doing so, potential drawbacks could be anticipated that arise from the steric problems, which would twist the Schiff base moieties out of plane with the aromatic rings. This steric problem could potentially reduce orbital overlap and spin interactions.

Approaches:

Project Background:

The main goal of this thesis is to study the electronic behavior and stability of polymers of metal complexes of [2.2]paracyclophane derivatives and also the investigation of the possible applications of these derivatives. Paracyclophanes provide unique structural features, which include the strongly interacting π-moieties of the two benzene rings. Substituted paracyclophanes with donor/acceptor moieties offer the possibility of studying electronic effects leading to enhanced photophysical properties. Such unique properties have

motivated studies of the electronic effects of different paracyclophane derivatives. Aminoparacyclophane systems provide a useful platform for such studies. The ease of derivatizing amino paracyclophanes helps in studying electronic interactions with the cyclophane moiety. Condensation reactions of amino[2.2]paracyclophanes with aldehydes produces imine (Schiff's bases) with ease. Considering this, condensation of amino[2.2]paracyclophanes with ferrocene carboxaldehyde produces Schiff's bases. The purpose of using ferrocene is due to its electrochemical stability.

In this work, the first project goal is to explore synthesizing polymers containing ferrocenylimine moieties based on amino[2.2]paracyclophane. Secondly, derivatives of aminoparacyclophanes have been used as chiral ligands for the synthesis of copper complexes to use in catalysis reactions [57]. In this work, the synthesis of Schiff bases of amino[2.2]paracyclophane was made with salicylaldehyde, which were used as ligands to make copper (II) metal complexes. The synthesis of Schiff base metal complexes of diaminoparacyclophanes would allow for studies of electronic coupling between metal centers mediated by [2.2]paracyclophane.

Approach for target I:

1. Synthesize ferrocenyl aromatic imino-Schiff bases and determine the electron donating ability of the [2.2]paracyclophane moiety to study the

extent of interaction of ferrecene with [2.2]paracyclophane for the compound shown in Figure I - 20.

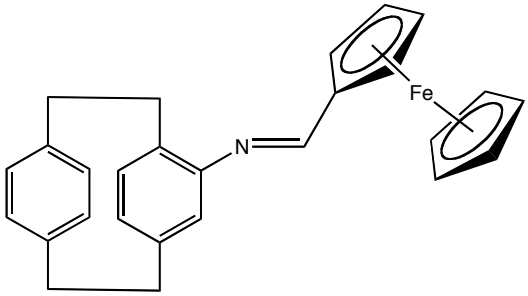

Figure I – 20: Ferrocenyl-4-imino[2.2]paracyclophane

2. Study the electronic communication between iron centers in ferrocenyl *pseudo-para*-diimino[2.2]paracyclophane Schiff bases and study the extent of ferrocene interaction through [2.2]paracyclophane moiety.

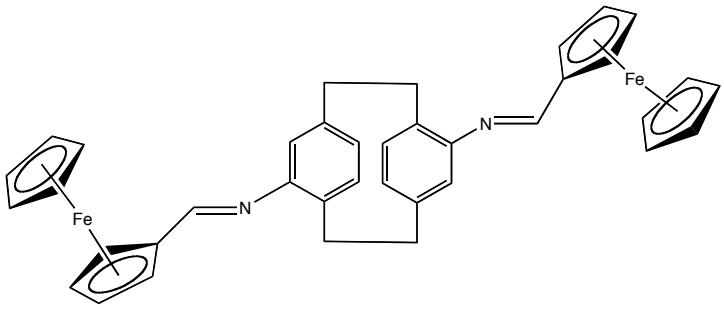

Figure I – 21: Pseudo-para-(bis-ferrocenyl)-4,12-imino[2.2]paracyclophane

3. If possible, synthesize and study the properties of poly(ferrocenyl imino[2.2]paracyclophane).

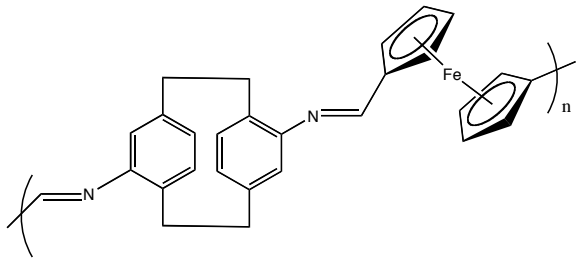

Figure I – 22: Poly(pseudo-para-(ferrocenyl)-4,12-imino[2.2]paracyclophane)

Approach for target II**:**

1. Synthesize and study the structural parameters of salicylidinimine ligands from amino[2.2]paracyclophane using UV-visible spectroscopy and computational studies.

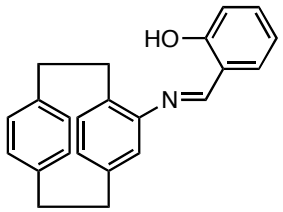

Figure I – 23: N- (4- Salicylidene [2.2]paracyclophane)

2. Synthesize and characterize copper complexes of salicylidinimine metal complexes based on 4-amino[2.2]paracyclophane.

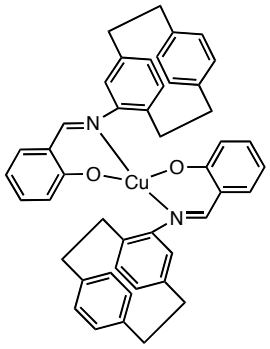

Figure I – 24: N,N-4-Bis(salicyledene)[2.2]paracyclophane)

3. If possible, synthesize and characterize polymers formed from *pseudo-para* and *pseudo-meta* DAP salen ligands and their metal complexes.

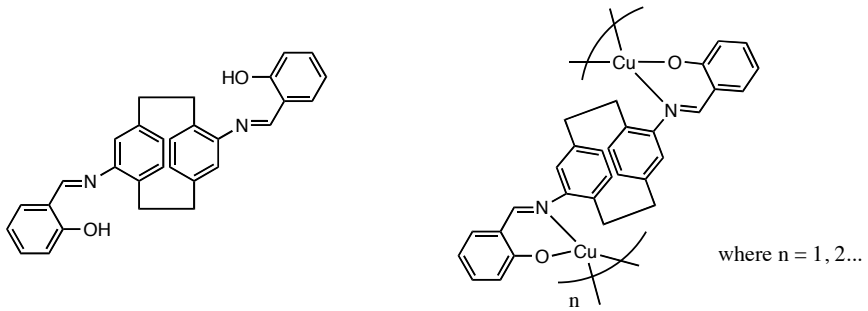

Figure I – 25: Pseudo-para-N,N'-4,12-bis(salicylidene)-[2.2]paracyclophane and its copper complex

Part C:

Studies of the electropolymerization of 2,2'-bithiophene in water using sodium dodecyl sulfate as a surfactant and electrolyte will be discussed.

Brief synopsis of this thesis:

Part A:

1) It has been well known that [2.2]paracyclophanes (PC) behave as electron donating groups but it has not been studied how [2.2]paracyclophane will behave electrochemically in the presence of a redox center attached to it. To study this electronic interaction electrochemically, a series of ferrocenyl imine Schiff bases has been synthesized by reactions of ferrocene carboxaldehyde and aniline derivatives to give analogues of amino[2.2]paracyclophane, as shown in Scheme I -9. Their redox behavior has been analyzed and compared with that of the ferrocenyl imine of *4-amino[2.2]paracylophane*.

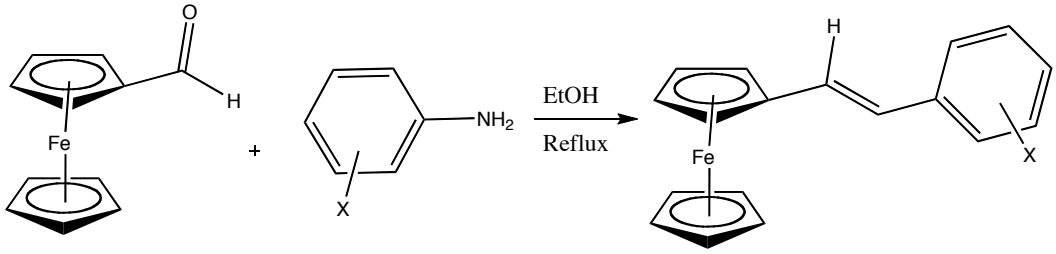

Scheme I – 9: Condensation reactions ferrocenyl carboxaldehyde with aniline derivatives

Ferrocene has been used widely in electrochemical processes because of its reversible redox behavior. It was thought to study the electrochemistry of substituted ferrocenyl Schiff base derivatives of aniline to investigate electrochemical behavior of 4-amino[2.2]paracyclophane (APC). The redox potentials of ferrocenyl imines of aniline derivatives were determined by cyclic voltammetry and correlated to σ values of the substituents on the aniline derivatives. This will allow the electron donating ability of [2.2]paracyclophane moiety to the redox center to be determined.

2) In this section we are interested in studying the electronic mediation effect of the [2.2]paracyclophane moieties when separating two redox centers through-space. The general synthetic route is shown below in Scheme I – 10.

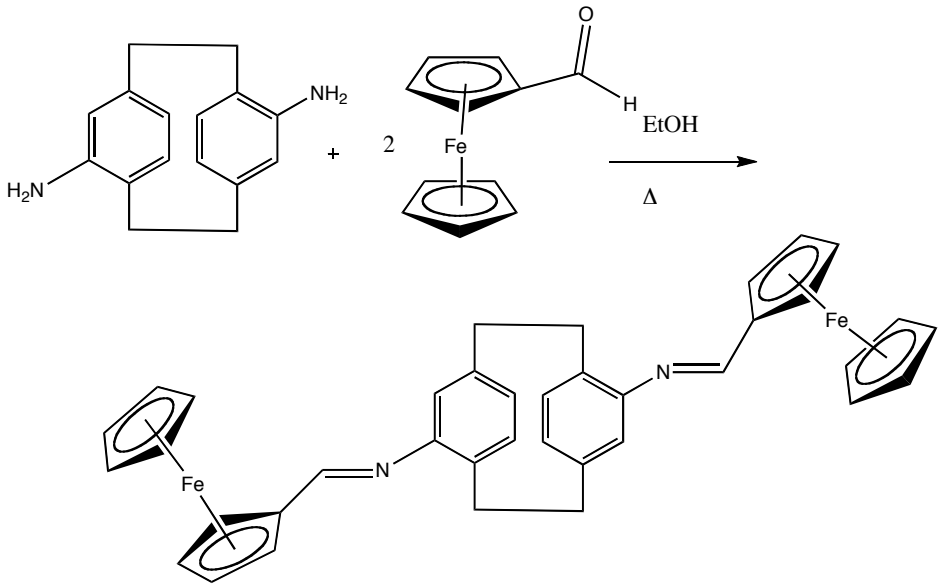

Scheme I – 10: Condensation reaction of 4,12-diamino[2.2]paracyclophane with ferrocenyl carboxaldehyde.

To assess the electronic interaction, a convenient means is to observe the redox potentials of two one electron redox-active centers, such as ferrocene, conjugated through formation of a Schiff base with [2.2]paracyclophane.

Part B:

1. Synthesis of 4-iminosalicylidine ligands of [2.2]paracyclophane:

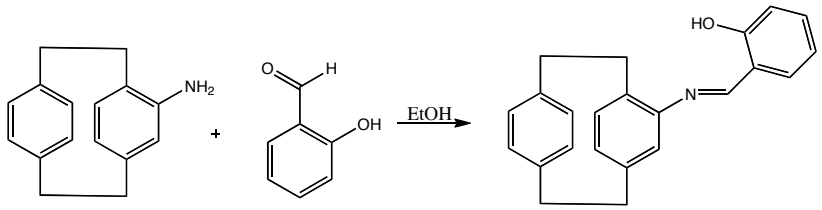

Scheme I – 11: Synthesis of N-4- salicylidine[2.2]paracyclophane ligand.

The synthesis of the salicylidinimine ligand by reaction between 4-amino[2.2]paracyclophane and salicylaldehyde was carried out in this section. The stability of the salicylidinimine ligand, its geometry, and its effect on the metal complexes of the Schiff's base ligands will be discussed. The synthesis of Schiff's base ligands from pseudo-para-diamino[2.2]paracyclophane and pseudo-meta-diamino[2.2]paracyclophane shown in Figure I – 26, was carried for further studies of metal complex formation.

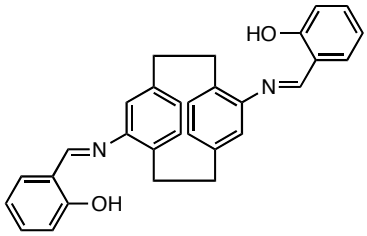

pp-DAPSA

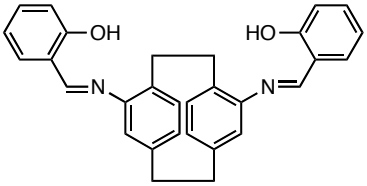

pm-DAPSA

Figure I – 26: Pseudo-para-4,12-bis(salicylidene)[2.2]paracyclophane and Pseudo-meta-4,12-bis(salicylidene)[2.2]paracyclophane ligands

2. Synthesis of metal complexes of salicylidinimine ligands:

Earlier our group has showed the promising catalytic enantioselective use of copper salicylidineimine complexes made from amino[2.2]paracyclophane in the catalytic conversion of aromatic olefins to form cyclopropanated products as shown in Scheme I -12 [58].

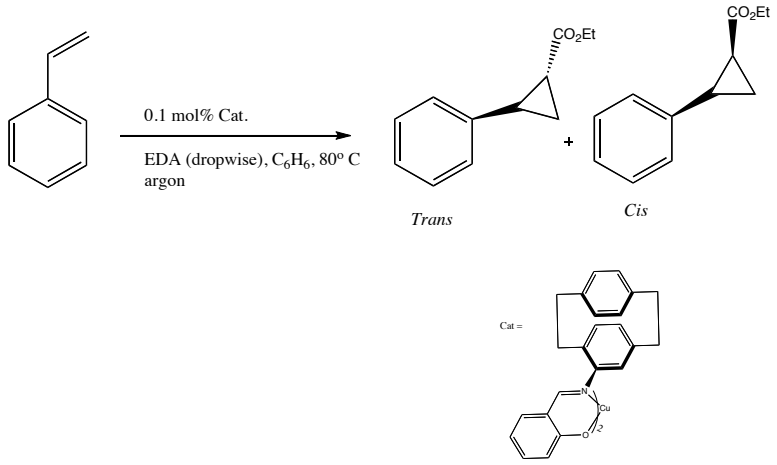

Scheme I – 12: Enantioselective cyclopropanation of styrene using chiral catalyst copper II (bis(4-iminosalisalicylidene)[2.2]paracyclophane)

The use of diamino[2.2]paracyclophane as a ligand by its conversion to a Schiff's base ligand, specifically *pseudo-ortho*-N,N'-bis(salicylidene)-4,12-diamino[2.2]paracyclophane, has also been shown to facilitate catalysis [31]. Morvant, investigated the cyclopropanation of trans-4,4'-dimethylstilbene with ethyl diazoacetate (EDA), using the copper complex of pseudo-ortho-N,N'-bis(salicylidene)-4,12-diamino[2.2]paracyclophane.

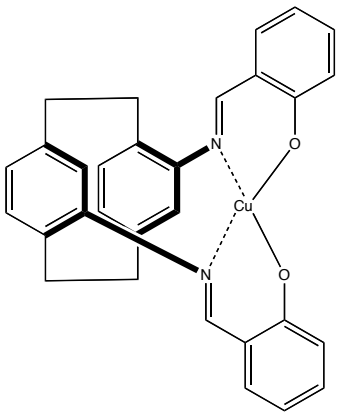

Figure I – 27: *pseudo-ortho*-N,N'-bis(salicylidene)-4,12-diamino[2.2]paracyclophane copper (II) complex

Although pseudo-ortho diamino[2.2]paracyclophane showed promising results for forming a ligand in previous studies, the other isomers of diamino[2.2]paracyclophane have not been explored. Here we report on attempts to synthesize and characterize bimetallic metal complexes of other isomers, such as pseudo-para and pseudo-meta diamino[2.2]paracyclophane as ligands.

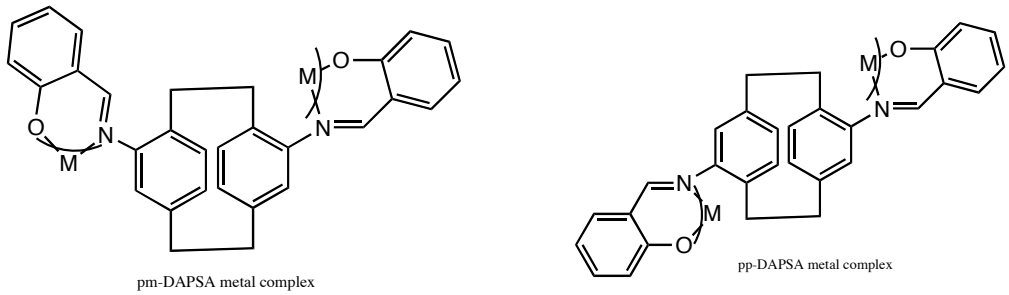

Figure I – 28: *pseudo-para*-N,N'-bis(salicylidene)-4,12-diamino[2.2]paracyclophane and *pseudo-meta*-N,N'-bis(salicylidene)-4,12-diamino[2.2]paracyclophane metal complexes

3. Synthesis of metallopolymers from pp-DAP and pm-DAP Schiff's base ligands:

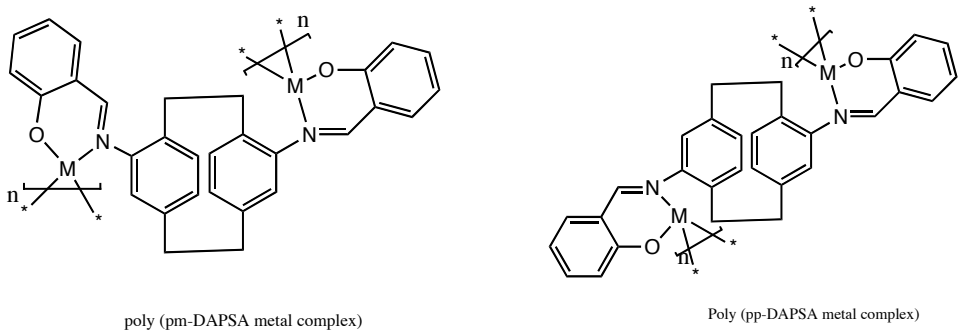

Figure I – 29: Metallopolymers based on pseudo-para and pseudo-meta bis(salicylidene)[2.2]paracyclophane metal complexes.

The fundamental focus of this project is to attempt to synthesize and characterize the electronic interaction between redox centers in the metallopolymers, poly((pp-DAPSA)metal complex) and poly(M(pm-DAPSA)metal complex), where redox active metal centers are separated by [2.2]paracyclophane moieties. Copper was used as the metal center for the synthesis of such metallopolymers. This research will include primary investigative studies using spectroscopic analytical methods and electrochemical studies.

Part C:

2,2'-Bithiophene (BT) is insoluble in water but it was shown that sodium dodecyl sulfate (SDS) increases the solubility of the bithiophene in water [59], allowing for polymerization.

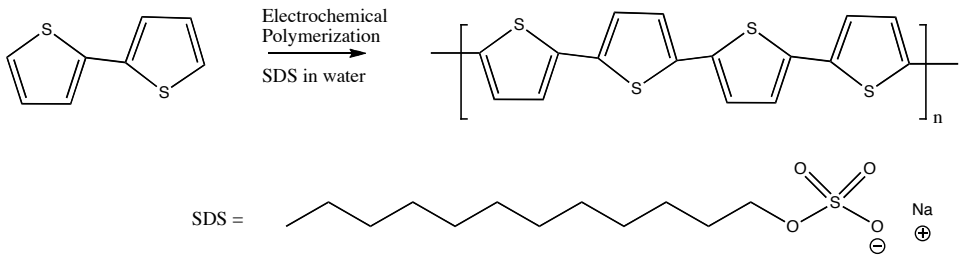

Scheme I – 13: Electrochemical polymerization of 2,2'-bithiophene in aqueous micellar medium.

In this part, electrochemical oxidation of 2,2'-bithiophene and its polymer growth at different monomer concentrations in an aqueous micellar medium (as shown in Scheme I- 13), will be discussed. These experiments were carried out in an effort to understand the mechanism by which the poly(2,2'-bithiophene) is formed.

References:

1. Brown, C.J. and A.C. Farthing, *Preparation and Structure of Di-p-Xylylene.* Nature, 1949. **164**(4178): p. 915.

2. Boekelheide, V., *[2n]Cyclophanes: Paracyclophane to Superphane.* Accounts of Chemical Research, 1980. **13**(3): p. 65 - 70.

3. Hopf, H., *[2.2]Paracyclophanes in Polymer Chemistry and Materials Science.* Angew. Chem. Int. Ed., 2008. **47**: p. 9808-9812.

4. Gorham, W.F., *A New, General Synthetic Method for the Preparation of Linear Poly-p-xylylenes.* J. Polym. Sci. Part A-1, 1966. **4**(12): p. 3027-3039.

5. Tan, C.P. and H.G. Craighead, *Surface Engineering and Patterning Using Parylene for Biological Applications.* Materials, 2010. **3**: p. 1803 - 1832.

6. Lucio Minuti, A.T., Assunta Marrocchi, Selvaggia Landi, Eszter Gacs-Baitz, *Synthesis and structure of [2.2]paracyclophanes incorporating alkyne units in the extended linear chain.* Tetrahedron Letters, 2005. **46**(34): p. 5735-5737.

7. Morisaki, Y. and Y. Chujo, *Through-space conjugated polymers consisting of [2.2]paracyclophane.* Polym. Chem., 2011. **2**: p. 1249-1257.

8. Shieh, C., D.C. McNally, and R.H. Boyd, *The heats of combustion and strain energies of some cyclophanes.* Tetrahedron, 1969. **25**: p. 3653.

9. Solladie-Cavallo, A. and M. Hibert, *1H and 13C NMR studies of two monosubstituted [2.2]paracyclophanes* Organic Magnetic Resonance, 1981. **16**(1): p. 44-46.

10. Marrocchi, A., I. Tomasi, and L. Vaccaro, *Organic Small Molecules for Photonics and Electronics from the [2.2]Paracyclophane Scaffold.* Israel Journal of Chemistry, 2012. **52**: p. 41 -52.

11. Dyson, P.J., B.F.G. Johnson, and C.M. Martin, *Ruthenium cluster - [2.2]paracyclophane complexes.* Coordination Chemistry Reviews, 1998. **175**: p. 59 - 89.

12. Lyssenko, K.A., M.Y. Antipin, and D.Y. Antonov, *The Transannular Interaction in [2.2]paracyclophane: Repulsive or Attractive ?* Chemphyschem, 2003. **4**: p. 817 - 823.

13. Grimme, S., *On the Importance of Electron Correlation Effects for the pi-pi Interactions in Cyclophanes.* Chem. Eur. J, 2004. **10**: p. 3423 - 3429.

14. Cram, D.J. and H. Steinberg, *Macro Rings. I. Preparation and Spectra of the Paracyclophanes.* J. Am. Chem. Soc., 1951. **73**(12): p. 5691-5704.

15. Cram, D.J. and D.I. Wilkinson, *Macro Rings. XXIII. Carbonylchromium Complexes of Paracyclophanes and Model Compounds1*. J. Am. Chem. Soc., 1960. **82**(21): p. 5721-5723.

16. Singer, L.A. and D.J. Cram, *Macro Rings. XXVII. Transannular Substituent Effects in π-π-Complexes of Paracyclophanes.* J. Am. Chem. Soc, 1963. **85**(8): p. 1080 - 1084.

17. Singer, L.A. and D.J. Cram, *Macro Rings. XXVII. Transannular Substituent Effects in π-π-Complexes of Paracyclophanes.* J. Am. Chem. Soc., 1963. **85**(8): p. 1080-1084.

18. Siegel, M.G., C.L. Liotta, and D.J. Cram, *Macro rings. 48. Transannular effects of acidity of heteroannularly disubstituted [2.2.] paracyclophane.* J. Am. Chem Soc., 1982. **104**(5): p. 1387-1391.

19. Acevedo, S. and K. Bowden, *Transmission of polar effects: prediction by the Kirkwood-Westheimer electrostatic field effect model.* Journal of the Chemical Society, Chemical Communications, 1977. **0**(17): p. 608-609.

20. Cram, D.J. and N.L. Allinger, *Macro Rings .12. Stereochemical Consequences of Steric Compression in the Smallest Paracyclophane.* J. Am. Chem. Soc., 1955. **77**(23): p. 6289-6294.

21. Reich, H.J. and D.J. Cram, *Macro rings. XXXV. Transannular directive influences in electrophilic substitution of monosubstituted[2.2]paracyclophanes.* J. Am. Chem. Soc, 1969. **91**(3): p. 3505 - 3516.

22. Cram, D.J. and J.M. Cram, *Cyclophane chemistry: bent and battered benzene rings.* Accounts of Chemical Research, 1971. **4**(6): p. 204 - 213.

23. Rolf Gleiter, H.H., *Modern Cyclophane Chemistry*, ed. W.-V.V.G. Co.2004, Germany: WILEY - VCH. 200 - 201.

24. Reich, H.J. and D.J. Cram, *Macro rings. XXXV. Transannular directive influences in electrophilic substitution of monosubstituted[2.2]paracyclophanes.* J. Am. Chem. Soc., 1969. **91**(13): p. 3505-3516.

25. Reich, H.J. and D.J. Cram, *Transannular directive influences in electrophilic substitution of 2.2-paracyclophane.* J. Am. Chem. Soc., 1968. **90**(5): p. 1365-1367.

26. Cahn, R.S., C.K. Ingold, and V. Prelog, *Specification of Molecular Chirality.* Angew. Chem. Int. Ed., 1966. **5**(4): p. 385 - 410.

27. Pelter, A., H. Kidwell, and R.A.N.C. Crump, *N-Methyl- and N-benzyl-4-amino[2.2]paracyclophanes as unique planar chiral auxiliaries* J. Chem. Soc., Perkin Trans. 1, 1997(21): p. 3137 - 3140.

28. Gibson, S.E. and J.D. Knight, *[2.2]Paracyclophane Derivatives in Asymmetric Catalysis.* Org. Biomol. Chem., 2003. **1**: p. 1256 - 1269.

29. N. V. Vorontsova, V.I.R., E. V. Vorontsov, O. L. Tok and Yu. N. Bubnov, *Stereoselective synthesis of homoallylic alcohols of the [2.2]paracyclophane series and their use a auxillaries in asymmetric allylboration of aldehydes.* Russian Chemical Bulletin, 2000. **49**(5): p. 912 - 919.

30. Zanotti-Gerosa, A., C. Malan, and D. Herzberg, *Phosphonites Based on the Paracyclophane Backbone: New Ligands for Highly Selective Rhodium-Catalyzed Asymmetric Hydrogenation.* Organic Letters, 2001. **3**(23): p. 3687 - 3690.

31. Morvant, M.C., *Synthesis, Properties and Applications of polynitro- and Polyamino[2.2]paracyclophanes*, in *Chemistry and Biochemistry*1996, University of Oklahoma: Norman.

32. Garnier, F., *Organic-Based Electronics a la Carte.* Accounts of Chemical Research, 1999. **32**: p. 209 - 215.

33. Bartholomew, G.P. and G.C. Bazan, *Bichromophoric Paracyclophanes: Models for Interchromophore Delocalization.* Accounts of Chemical Research, 2001. **34**(1): p. 30 - 39.

34. Elacqua, E. and L.R. MacGillivray, *From the Decks to the Bridges: Optoelectronics in [2.2]Paracyclophane Chemistry. Eur. J. Org. Chem.*, 2010: p. 6883 - 6894.

35. Joseph Zyss, I.L., Sergei Volkov, Vladimir Chernyak, Shaul Mukamel, Glenn P. Bartholomew and Guillermo C. Bazan *Through-Space Charge Transfer and Nonlinear Optical Properties of Substituted Paracyclophane. J. Am. Chem. Soc*, 2000. **122**: p. 11956 - 11962.

36. Masi, J.V., *Organic Magnetic Materials: An Overview.* Electrical Insulation Conference and Electrical Manufacturing & Coil Winding Conference, 1999. Proceedings, 1999: p. 117 - 120.

37. Allison, G., R.J. Bushby, and J.L. Paillaud, *Organic Molecular Magnets- The Search for Stable Building Blocks.* J. Mater. Sci. : Materials in Electronics, 1994. **5**: p. 67 - 74.

38. Baumgarten, M., *High Spin Molecules Directed towards Molecular Magnets*, in *In EPR of Free Radicals in Solids*, A.a.S. Lund, M., Editor 2003, Kluwer, Dordrecht. p. 491 - 528.

39. Akira Izuoka, S.M., Tadashi Sugawara, and Hiizu Iwamura, *Ferro- and Antiferromagnetic Interaction between Two Diphenylcarbene Units Incorporated in the [2.2]Paracyclophane Skeleton.* J. Am. Chem. SOc., 1985. **107**: p. 1786-1787.

40. Polumbrik, O.M., *Advances in the Chemistry of Verdazyl Radicals.* Russian Chemical Reviews, 1978. **47**(8): p. 1444 - 1478.

41. Neugebauer, F.A. and H. Fischer, *Verdazyls. Part 30.1 N-I ,N-I '-Linked Biverdazyls (Bis-I ,2,3,4-tetrahydro-s-tetrazin-I -yls) with a [2.2]Paracyclophanylene Bridge.* J. Chem. Soc., Perkin Trans. , 1981. **2**: p. 896 - 900.

42. Ishitani, A. and S. Nagakura, *Electronic absorption and E.S.R. spectra of the benzene and paracyclophane anions. Mol. Phys.*, 1967. **12**: p. 1 - 12.

43. Gerson, F. and W.B. Martin, *Electron spin resonance studies of the radical anions of [2.2]paracyclophane and related compounds.* J. Am. Chem. Soc., 1969. **91**(8): p. 1883-1891.

44. Bramwell, F.B. and J. Gendell, *ESR studies of the triplet state of [n.n] paracyclophanes.* The Journal of Chemical Physics, 1973. **58**(2): p. 420-427.

45. Morisaki, Y. and Y. Chujo, *Cyclophane-containing polymers.* Progress in Polymer Science, 2008. **33**(3): p. 346-364.

46. Diel, B.N., et al., *Cofacial assembly of metallomacrocycles as an approach to controlling lattice architecture in low-dimensional molecular solids. Chemical, structural, oxidation-state, transport, and optical properties of the iron coordination polymer [Fe(phthalocyaninato)(.mu.-pyrazine)]n and the consequences of halogen doping.* J. Am. Chem. Soc., 1984. **106**(11): p. 3207-3214.

47. Glatzhofer, D.T. and D.T. Longone, *Extended cooperative electronic effects in poly((E,E)-[6.2]paracyclophane-1,5-diene).* Journal of Polymer Science Part A: Polymer Chemistry, 1986. **24**(5): p. 947-954.

48. Longone, D.T. and D.T. Glatzhofer, *Cyclopolymerization of (E,E) -[6.2]paracyclophane-1,5-diene.* Journal of Polymer Science Part A: Polymer Chemistry, 1986. **24**(8): p. 1725-1733.

49. Boekelheide, V., *Syntheses and properties of the [2n]Cyclophanes*, in *Cyclophanes I*, F. Vögtle, Editor 1983, Springer Berlin Heidelberg. p. 87-143.

50. Longone, D.T. and J.H. Glans, *Synthesis and electrical properties of substituted paracyclophane polymers.* Journal of Polymer Science Part A: Polymer Chemistry, 1988. **26**(2): p. 405-417.

51. Morisaki, Y. and Y. Chujo, *Through-space conjugated polymers consisting of [2.2]paracyclophane.* Polymer Chemistry, 2011. **2**(6): p. 1249-1257.

52. Weder, C., *Synthesis, processing and properties of conjugated polymer networks.* Chemical Communications, 2005. **0**(43): p. 5378-5389.

53. Biswas, M. and A. Mukherjee, *Synthesis and evaluation of metal-containing polymers*, in *Photoconducting Polymers/Metal-Containing Polymers*1994, Springer Berlin Heidelberg. p. 89-123.

54. Laganis, E.D., R.G. Finke, and V. Boekelheide, *Multilayered iron complexes of [2.2]paracyclophane.* Proceedings of the National Academy of Sciences, 1981. **78**(5): p. 2657-2658.

55. Morisaki, Y., T. Murakami, and Y. Chujo, *Synthesis, Structure, and Properties of Aromatic Ring-Layered Polymers Containing Ferrocene as a Terminal Unit.* Journal of Inorganic and Organometallic Polymers and Materials, 2009. **19**(1): p. 104-112.

56. Clement, S., et al., *Probing excited state electronic communications across diethynyl-[2.2]paracyclophane-containing conjugated organometallic polymers.* Chemical Communications, 2012. **48**(69): p. 8640-8642.

57. Paradies, J., *[2.2]Paracyclophane Derivatives: Synthesis and Application in Catalysis.* Synthesis, 2011. **23**: p. 3749 - 3766.

58. Douglas S. Masterson, D.T.G., *Catalytic Enantioselective Cyclopropanation of Styrene Derivatives using N-(2',4'-di-tert-butyl) Salicylidene-4-amino[2.2]paracyclophane as an asymmetric ligand. J. Mol. Cat. A: Chemical*, 2000. **161**: p. 65 - 68.

59. Bazzaoui, E.A., S. Aeiyach, and P.C. Lacaze, *Electropolymerization of Bithiophene on Pt and Fe Electrodes in an Aqueous Sodium dodecylsulfate (SDS) Micellar Medium.* Synthetic Metals, 1996. **83**(2): p. 159 - 165.

CHAPTER II

Electron Donating Ability of [2.2]Paracyclophane Towards the Redox Potential of Ferrocene

Introduction:

A great deal of interest has been shown by material scientists and technologists in the synthesis of organometallic polymers as a result of properties needed for high technology materials, biomedical polymers and electrical inductors [1]. These inorganic based polymers are useful based on the following features [1, 2]:

- The number and variety of elements (over 40 elements) that can be used in such polymers
- High abundance of inorganic elements
- Possibility of attaching different side groups
- Stability at higher temperatures
- Many of the metals can be present in several oxidation states
- Useful properties such as conductivity, ferromagnetism, electroluminescence, and nonlinear optical properties

Due to these features, organometallic polymers, particularly ferrocene containing polymers, find application in semiconductor based devices, as nonlinear optical materials, magnetic materials, gas sensors, etc [3-6]. Ferrocene is an attractive molecule, containing an iron metal center sandwiched between two cyclopentadienyl rings, due to its unique electrochemical behavior and π-

conjugated system [7]. It shows one electron reversible redox behavior when electrochemically oxidized, in which ferrocene (Fe^{2+}) is oxidized to ferrocenium (Fe^{3+}) on a positive applied potential scan and vice versa on the reverse potential scan. Ferrocene is easy to prepare, cheap, commercially available, and air and thermally stable. Based on these considerations, ferrocene-based polymeric materials have been the focus of intense research [8]. Much of the interest was focused on the poly(vinylferrocene), (Figure II – 1), which was first synthesized soon after ferrocene was discovered, due to the presence of the redox active iron center.

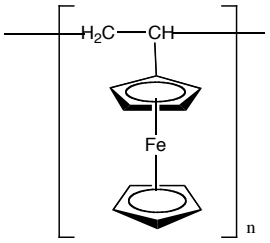

Figure II – 1: Poly(vinyl ferrocene)

In this polymer, the redox active centers are non-interacting and give a one reversible redox wave [9]. Further, various ferrocene-containing polymers (Figure II - 2) have been synthesized and studied such as poly(ferrocenylsilane), poly(ferrocenylthiophene), poly(ferrocenylalkene), poly(ferrocenylpyrrole), poly(ferrocenylaniline), etc [4].

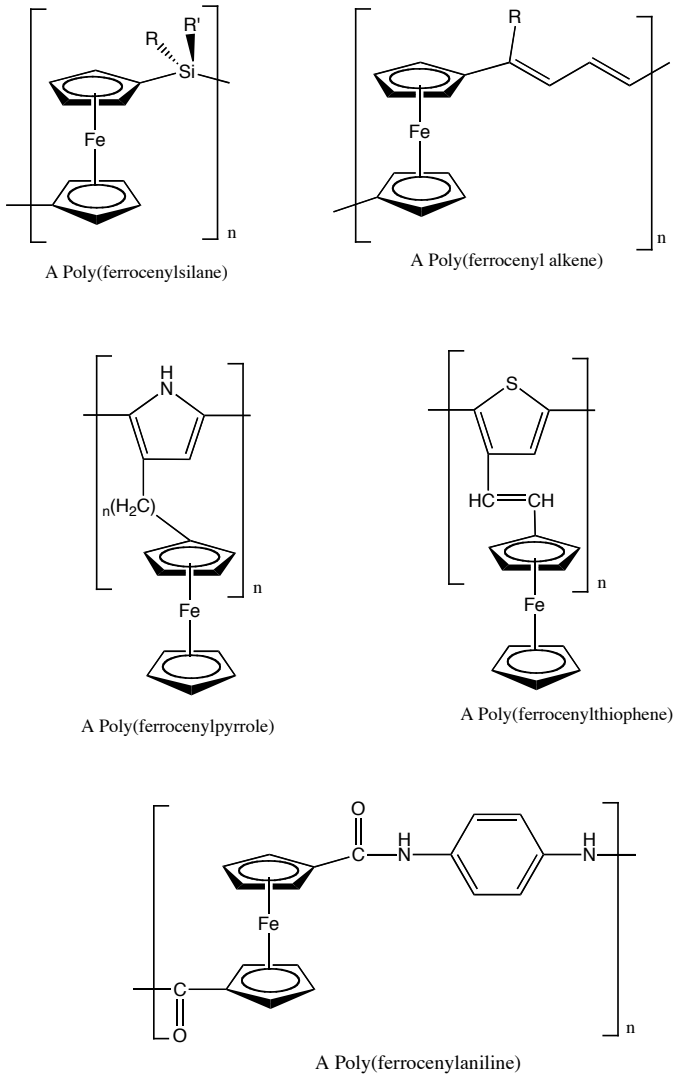

Figure II – 2: Ferrocene containing polymers

Schiff bases find potential applications in the areas of bioinorganic chemistry, catalysis and magnetochemistry. In particular, the contribution of Schiff's bases to the field of magnetochemistry has been focused on understanding the mechanism of exchange coupling between two metal centers through the Schiff's base moiety (C=N) [10]. The general procedure for the preparation of Schiff bases consists of condensation reactions of primary amines

with a carbonyl precursor as shown in Scheme II - 1. The final product contains an imine or azomethine group (C=N), which is referred to as a Schiff's base.

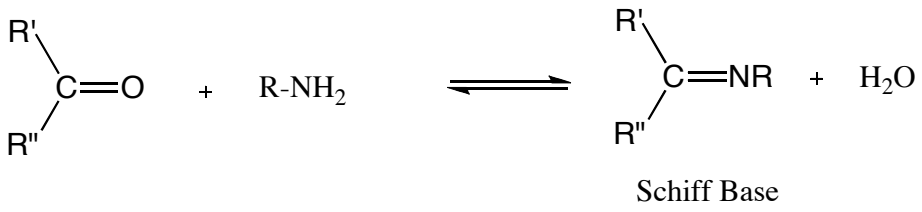

Scheme II -1: Schiff's base formation

A Schiff's base can coordinate with metal ions through its non-bonded lone pair of electrons on the nitrogen and also can transfer charges through the conjugated π-system.

The combination of the ferrocene moiety together with a Schiff base has been studied with regards to electrochemistry and further in the biological applications [11]. 4-Ferrocenyl aniline was treated with various substituted aromatic aldehydes to form the Schiff bases as shown in Scheme II - 2.

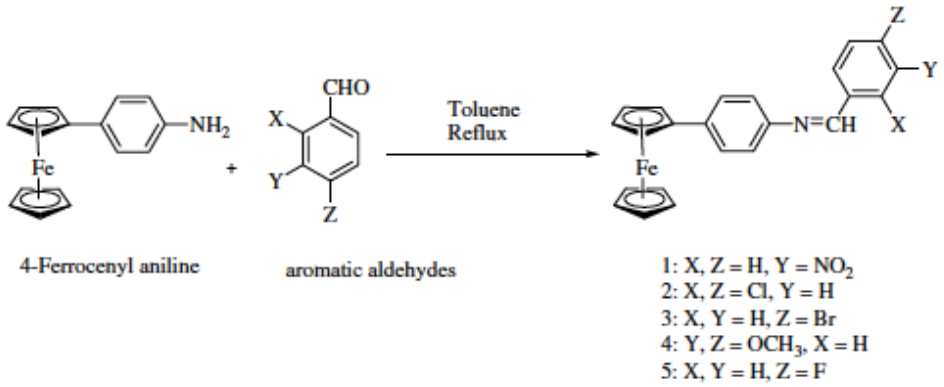

Scheme II – 2: Substituted Ferrocenyl Schiff base formation

It was observed that electron-withdrawing groups increase the oxidation potential of ferrocene towards positive potential while electron-donating groups reduce the oxidation towards negative potentials. Hence the effect of the electronic nature of substitutents can be used to modulate the oxidation potentials of ferrocene. In another case, a bis(ferrocenyl) Schiff-base has been synthesized by condensation between ferrocenecarboxaldehyde and p-phenylenediamine and it was doped with metal salts such as (Fe^{3+}, Al^{3+} and Ti^{3+}) for application as a semiconductor [12].

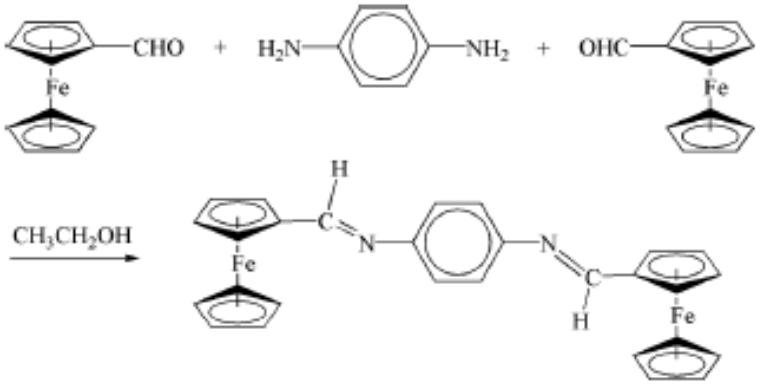

Scheme II – 3: Synthesis of a bis(ferrocenyl) Schiff base. Scheme adapted from the reference [12].

The results for this bis(ferrocenyl) Schiff base showed the formation of the charge transfer complexes with a 4-5-fold increase in conductivity values when doped with metal salts compared to monoferrocenyl Schiff's bases. This improved charge transfer complexation was further extended to three different polymers of poly(ferrocenyl-Schiff's bases), as shown in Scheme II – 4, and conductivity was measured by doping with iodine. A maximum conductivity at

room temperature of 3.17 x 10^{-4} S/cm was found for a poly-para-bis(ferrocenyl-Schiff's base)-I_2 complex [4]. Schiff's bases have also been of interest in organometallic research due to their stable coordination complexes with metal ions [13].

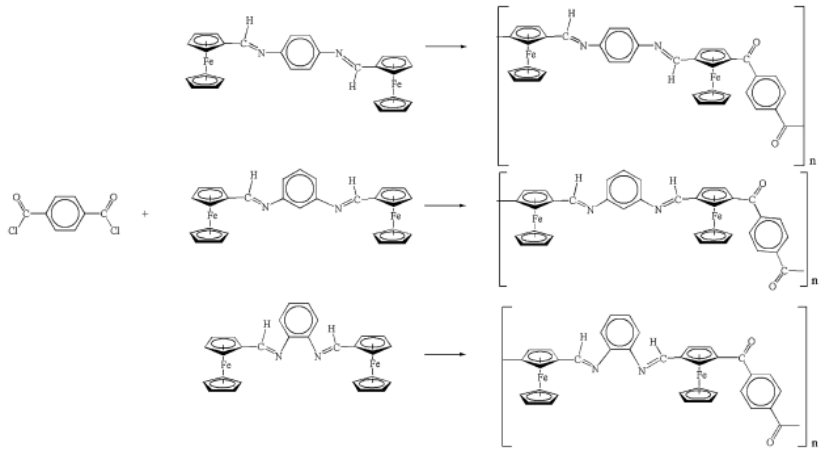

Scheme II – 4: Synthetic routes to poly(ferrocenyl-Schiff's bases). Figure adapted from Reference [4].

Various ferrocene-containing polymers have also shown a dependence of their redox and optical properties on neighboring-site interactions [14]. Nishihara and coworkers reported the redox and optical properties of aza-ferrocene oligomers and polymers as shown in Figure II - 3 [15].

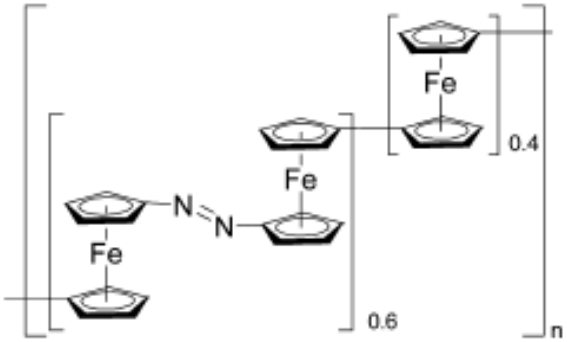

Figure II – 3: Aza-ferrocene polymer. Figure adapted from the reference [14].

Internuclear electronic interactions for the aza-ferrocene oligomer and polymers were monitored using electrochemistry and absorption spectroscopy, which showed the charge distribution among the ferrocene moieities.

[2.2]paracyclophane has been proven to be an excellent electron donating group for charge transfer complexation due to the presence of transannular electronic interactions between the two benzene rings in the cyclophane system [16-18]. As discussed in the introductory Chapter 1, polymers containing paracyclophane moieties in which the π-stacked structure of π-electron systems exists, show enhanced of electronic properties [19].

In summary, based on the electronic behavior of [2.2]paracyclophanes and Schiff's bases, and the redox behavior of ferrocene, we wanted to study the properties of the polymeric system proposed as shown in Figure II - 4.

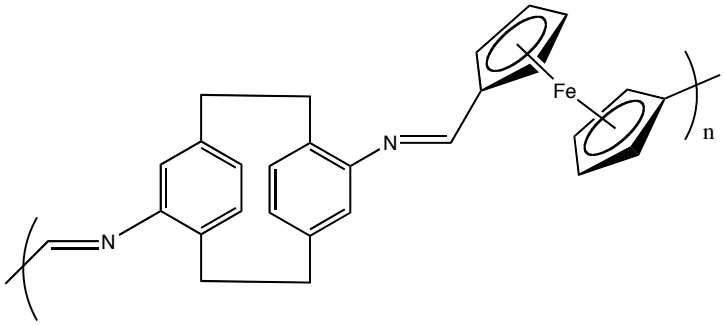

Figure II – 4: Target polymer.

In order to do so, it was desirable to study how the redox properties of ferrocene would change when attached to a [2.2]paracyclophane Schiff-base. As mentioned earlier, [2.2]paracyclophane is an excellent electron donating group, but its effect on redox properties has not been quantified electrochemically. To do so, we planned first to study the effect of substituents through the benzene rings of aniline on the oxidation potential of a ferrocene by forming appropriate ferrocenyl Schiff-bases. Linear free energy relationships can be used for this study to determine the substituents effect using electrochemistry [20]. Then, by using amino[2.2]paracyclophane to form the Schiff-base and determining its redox potential, the ability of the [2.2]paracyclophane moiety to donate electron density to the ferrocene can be quantified.

Results and Discussion:

In this study we investigated the electron donating ability of [2.2]paracyclophane by synthesizing the ferrocenyl Schiff's base from amino[2.2]paracyclophane and measuring its effectiveness in communicating electronically to the ferrocene redox center. The susceptibility of ferrocene

oxidation/reduction in ferrocenyl Schiff's bases was quantified electrochemically by synthesizing a series of redox active ferrocenyl imine Schiff's bases of ferrocenecarboxaldehyde and substituted anilines and measuring their redox potentials.

Synthesis of model compounds:

Cyclic voltammetry of ferrocene shows reversible, one electron oxidation at a low potential around 0.5 V vs saturated Calomel electrode (SCE) [21]. The ferrocenyl Schiff bases of aniline derivatives, which are analogues to amino[2.2]paracyclophane, were synthesized and characterized electrochemically. The synthesis of ferrocenyl imines from the reaction between ferrocene carboxaldehyde and aromatic amines has been reported previously [22]. The general reaction carried out is shown in Scheme II - 5.

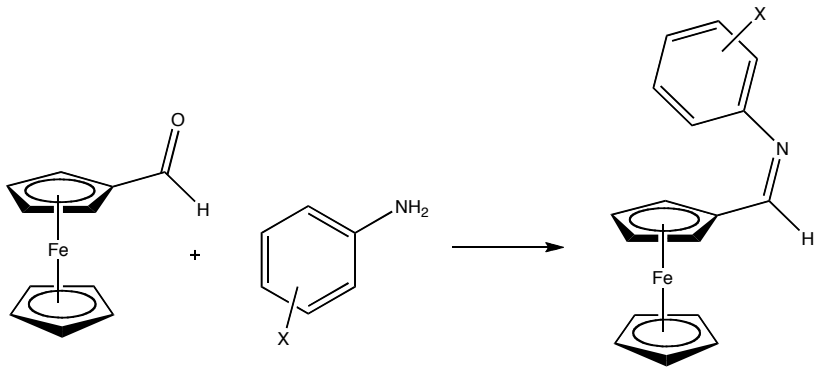

X = H, p-Me, o-Me, m-Me, p-OMe, p-NO_2, 2,5-$(Me)_2$, p-CN, p-Ph, 4-[2.2]paracyclophane.

Scheme II - 5: Reactions of ferrocenylcarboxaldehyde with aniline derivatives.

The ferrocene carboxaldehyde was heated with aromatic amines in presence of anhydrous ethanol to synthesize the imines. In a majority of the reactions, the product formed was purified by column chromatography or recrystallization. In most of the reactions, amines were used in slight excess to avoid any interference by traces of ferrocenecarboxaldehyde in the cyclic voltammetry. The products formed were analyzed by ^{1}H NMR in which the imine proton has a characteristic peak at approximately δ = 8.00 ppm. The following series of ferrocenyl imine Schiff base compounds was obtained.

Table II – 1: Various substituted aniline derivatives used to make ferrocenyl Schiff bases.

Ferrocenyl Imine Schiff bases	
Substituents (-X)	
-H	(FcCH=NPh)
-p-OMe	(FcCH=NC_6H_4-OMe-4)
-p-Me	(FcCH=NC_6H_4-Me-4)
-m-Me	(FcCH=NC_6H_4-Me-3)
-o-Me	(FcCH=NC_6H_4-Me-2)
-p-Ph	(FcCH=NC_6H_4-Ph-4)
-p-NO_2	(FcCH=NC_6H_4-NO_2-4)
-p-CN	(FcCH=NC_6H_4-CN-4)
-p-Cl	(FcCH=NC_6H_4-Cl-4)
2,5-Dimethylaniline	(FcCH=NC_6H_3-$(Me)_2$-2,5)
4-amino[2.2]paracyclophane	(FcIAPC)

Once the products were synthesized, the redox properties of these Schiff bases were characterized using cyclic voltammetry. Solutions (2 mM) of ferrocenyl imine Schiff base derivatives were prepared in acetonitrile using 0.1 M tetrabutyl ammonium hexafluorophosphate ($TBAPF_6$) as an electrolyte. A three-electrode cell was used with a Ag/AgCl reference electrode, a platinum wire as a counter electrode, and a platinum electrode as a working electrode.

1,1'-Dimethyl ferrocene (DMFc) was used as an internal standard. The use of DMFc as an internal standard was chosen due to its lower redox potential compared to the imine products. A representative cyclic voltammogram is shown in figure II - 5.

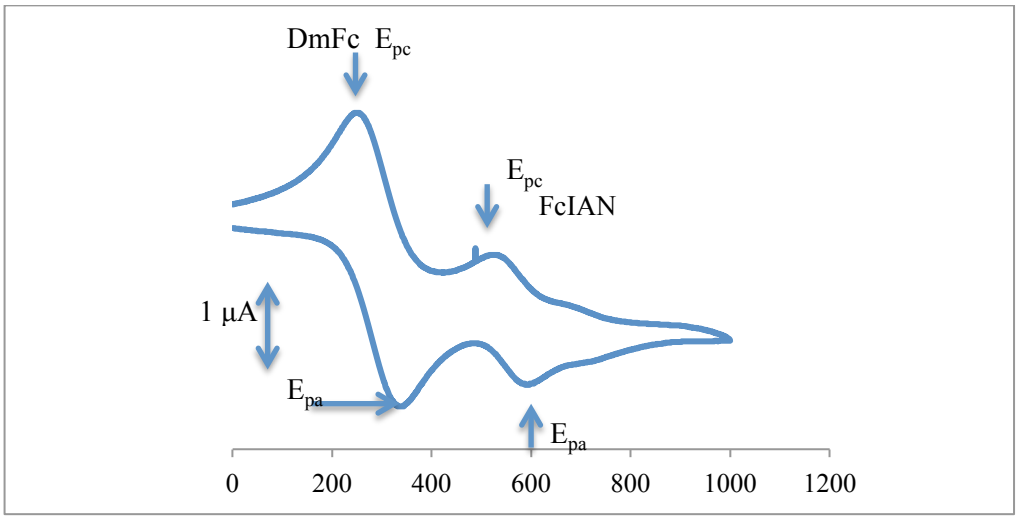

Figure II - 5: Typical cyclic voltammograms (CV) for ferrocenyl imine Schiff base with internal standard as DMFc. The example shown is for the 2 mM N-(ferrocenylmethylidene)aniline in AcCN solvent with 0.1M NBu_4PF_6 as an electrolyte; working electrode Pt; auxillary electrode Pt wire; reference electrode Ag/AgCl, initial coordinate 0 V; anodic limit 1.0 V; cathodic limit, 0 V. Scan rate 100 mV/sec; Y scale is at 5 µA.

The peaks at E_{pa} =335 mV and E_{pc} = 250 mV correspond to the internal standard DMFc, while for the ferrocenyl imine Schiff-base of aniline the redox wave is at E_{pa}= 595 mV and E_{pc} = 530 mV as shown in Figure II - 5. E_{pa} and E_{pc} are the anodic potentials and cathodic potentials of the redox wave, respectively. Redox potential data for the other ferrocenyl imine derivatives is summarized in Table II - 2.

Table II – 2: Electrochemical data for various ferrocenyl imine Schiff-base derivatives compared against an internal standard 1,1'-dimethylferrocene.

Schiff Base	1,1'-DMFc[a]		FcI Derivatives		ΔE_{pa}[b]	ΔE_{pc}[c]	$\Delta E^{d}_{1/2}$
	E_{pa} in V	E_{pc} in V	E_{pa} in V	E_{pc} in V	in V	in V	in V
Aniline	0.335	0.250	0.595	0.530	0.260	0.280	0.270
p-CN	0.344	0.267	0.643	0.581	0.299	0.314	0.307
p-OMe	0.472	0.394	0.708	0.644	0.236	0.250	0.243
p-Me	0.380	0.298	0.635	0.560	0.255	0.262	0.259
p-NO2	0.459	0.384	0.765	0.704	0.306	0.320	0.313
m-Me	0.430	0.347	0.692	0.613	0.262	0.266	0.264
DMA	0.447	0.358	0.700	0.623	0.253	0.265	0.259
o-Me	0.363	0.287	0.619	0.549	0.256	0.262	0.259
p-Cl	0.418	0.348	0.698	0.626	0.280	0.278	0.279
p-Ph	0.401	0.322	0.658	0.602	0.257	0.280	0.269
APC	0.448	0.358	0.676	0.624	0.228	0.266	0.247

Conditions: 2 mM compound, 0.1 M $TBAPF_6$, reference electrode Ag/Ag+, working electrode Pt, Scan rate 100 mV/sec.

[a] = Internal Standard

[b] = E_{pa} (FcI derivative) - E_{pa} (DMFc)

[c] = E_{pc} (FcI derivative) - E_{pc} (DMFc)

[d] = $(\Delta E_{pa} + \Delta E_{pc})/2$

The electrochemical behavior of the iron center, attached to the different aniline derivatives, showed one electron transfer behavior, where the redox peaks (E_{pa} and E_{pc}) are separated by *ca.* 60 mV/*n* and a ratio of anodic current to cathodic current (i_{pc}/i_{pa}) is approximately unity, where *n* is the number of electrons involved in electrochemical reaction, this suggests the reversibility of the electrochemical oxidation of the ferrocenes. The redox potentials for substituted ferrocenyl Schiff bases showed that the electron-donating groups lowered the oxidation potential of ferrocene, while electron withdrawing group showed higher oxidation potentials [23]. Ferrocene undergoes one electron reversible electrochemical oxidation to a π-ferricenium cation radical as shown in Equation (1).

$$\text{Fc(II)} \underset{+1e^-}{\overset{-1e^-}{\rightleftharpoons}} \text{Fc(III)}^{\oplus} \qquad (1)$$

For a reversible electrode process, the kinetics of this electron transfer are given by Equation (2),

$$\text{Ox} + e^- \underset{k_{ox}}{\overset{k_{red}}{\rightleftharpoons}} \text{Red} \qquad (2)$$

The kinetics of the above electron transfer process can be assumed to be first order, so that the rate of reduction of the ferrocenium cation depends on the rate constant and the concentration of ferrocenium cations at the site of electron transfers. For a reversible process in electrolytic cells, the kinetic expression of the electrochemical reaction is given by the Nernst Equation (3), which predicts the relationship between concentrations and the potential difference,

$$E = E^{o} - (2.303RT/nF)\ \mathrm{Log}\ (a_{red}/a_{ox}) \qquad (3)$$

where, E^{o} is standard electrode potential, E is the applied potential difference, R is the gas constant, F is the Faraday constant, T is the temperature in kelvins, and a is the chemical activity of the respective species respective to the concentrations of these species. In the correlation analysis used here for the reversible process, the half wave potential can be given by the Equation (4), which is similar to Nernst equation,

$$\Delta E_{1/2} = (2.303RT/nF)\ \Delta\mathrm{Log}\ (K_X) \qquad (4)$$

where, Kx is the equilibrium constant for the electrochemical reaction.

Under identical scan conditions and assuming equivalent transfer coefficients, differences in the magnitude of $E_{1/2}$ for differently substituted

compounds should reflect the free energy differences, which can be correlated using the Hammett linear free-enerrgy relationship given by Equation (5) [24],

$$\log K_{rel} = \rho\sigma \qquad (5)$$

In equation (5), σ is the substituent constant which is characteristic of the substituent, and ρ is the electrochemical reaction constant and is the measure of the sensitivity of the electrode reaction toward the substituents. If the E_{pa} is measured for each substituent by cyclic voltammetry using the same scan rate, working electrode, electrolyte concentration, and compound concentration, the difference in the oxidation potentials at 298 K can be written as:

$$\Delta\Delta E_x = (2.303RT/nF)\ \Delta Log\ (K_X) \qquad (7) \text{ and}$$

$$\Delta Log\ (K_X) = \rho\sigma \qquad (8)$$

where, $\Delta\Delta E_x = \Delta E_{1/2\ H} - \Delta E_{1/2\ X}$ in the Table II - 3

Table II – 3: Correlation of Kx and substituent constants (σ and σ^{+}) with potential difference

Entry	**Ferrocenyl Imine Schiff's bases**						
	Substituents (-X)	**$\Delta E_{1/2}$ in mV**	**$\Delta E_{1/2}$ in V**	**ΔΔEx**	**Δ logKx**	**$\sigma^{(a)}$**	**$\sigma^{+(a)}$**
1	-H	270	0.270	0	0	0	0
2	-p-Ome	243	0.243	-0.027	-0.459	-0.270	-0.780
3	p-Me	259	0.259	-0.011	-0.187	-0.170	-0.310
4	m-Me	264	0.264	-0.006	-0.102	-0.070	-0.070
5	o-Me	259	0.259	-0.011	-0.187	-0.170	-0.170
6	p-Ph	269	0.269	-0.001	-0.017	-0.050	-0.180
7	p-NO2	313	0.313	0.043	0.731	0.780	0.790
8	p-CN	307	0.307	0.037	0.629	0.660	0.660
9	p-Cl	279	0.279	0.090	0.150	0.380	-

[a] Values taken from Reference [25]

Values of $E_{1/2}$ for the particular compounds were calculated based on the difference between the redox potential of the ferrocenyl imine derivatives and the redox potential of the internal standard DMFc. Values of ΔLog (K_X) for the redox potentials of the substituted imine derivatives can be plotted against the substituent constants σ and σ^+ to study the linear free energy relationship. The values of σ and σ^+ were obtained from literature [25], where they indicate the characteristic properties of substituents and are important in studying the mechanism of the electrochemical reaction in ferrocenyl imine Schiff's bases.

A Hammett plot was drawn between Δlog K_x and simple substituent values (σ) is shown in Figure II - 6, and was found to obey the Hammett linear relationship. With respect to electron donating groups, the redox potential shifted towards negative potential, which confirms easier oxidation of the ferrocene moiety, while electron withdrawing groups shifted the oxidation potential towards positive potential, confirming more difficult oxidation of the ferrocene moiety. The positive ρ = -0.95 also indicates that electron donating groups favor the oxidation of ferrocene.

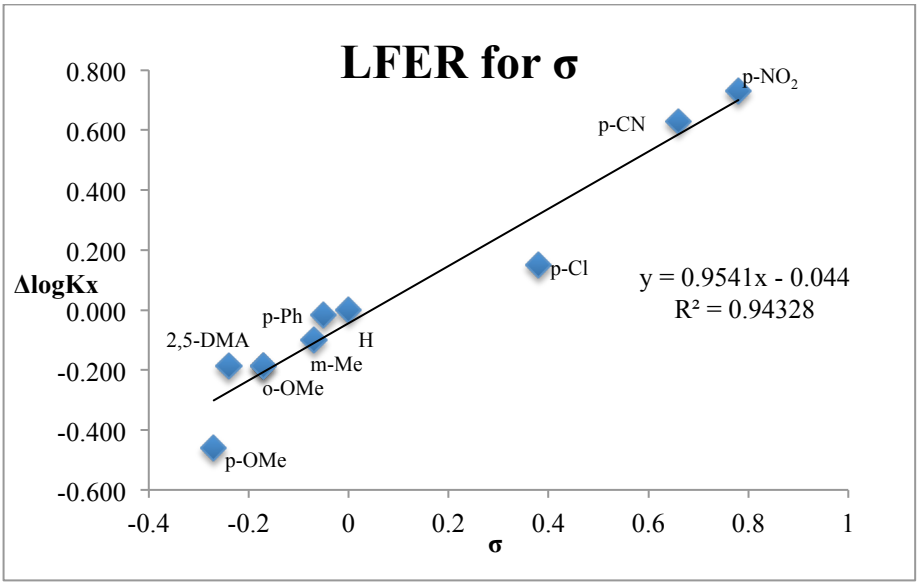

Figure II - 6: Hammett plot of Δ logKx vs σ for the redox potential of substituted ferrocenyl imine Schiff bases in AcCN.

As these ferrocenyl imine Schiff bases are conjugated in nature, the effect of resonance at the iron center was also studied by plotting Δlog K_x vs σ^+ as in Figure II - 7. There is less error in the Hammett relationship, which suggests that there is some resonance enhanced substituent effect involvement between the iron redox center and the substituent groups on the aniline derivatives e.g. p-OMe, p-NO_2. This resonance enhanced substituent effect gives the ρ^+ value as 0.8, which is somewhat lower than the simple resonance effect reaction constant ρ value, which nevertheless, showed the linear relationship clearly.

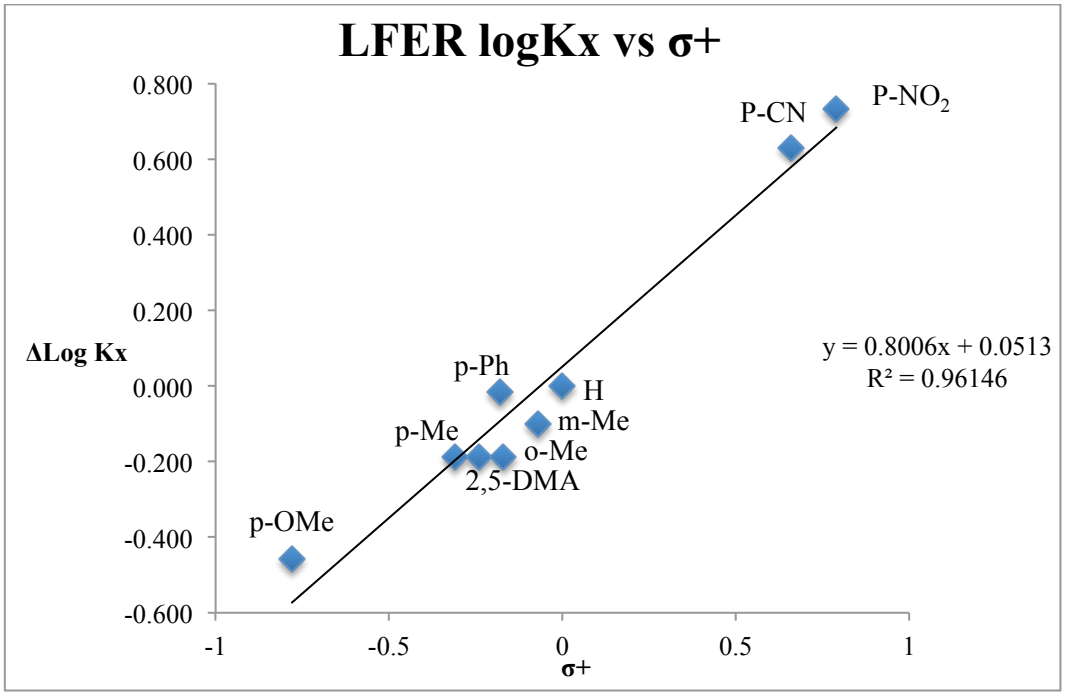

Figure II - 7: Hammett plot of Δ logKx vs σ^+ for the redox potential of substituted ferrocenyl imine Schiff bases in AcCN.

From the resonance substituent effect it can be inferred that the electron density from the electron-donating group can be delocalized to the redox center of the ferrocene on oxidation, which ultimately decreases the oxidation potentials. The stronger resonance effect of substituents on the oxidation potentials of the ferrocene redox center in such conjugated systems could be the result of the interaction of the p_z orbital of the sp^2 α – carbon atom with the ferrocenyl π system. The value ρ^+ indicates the sensitivity of the reaction mechanism to the character of the substituents. Here this value is positive and less than one, which indicates the substituent effect is small, with some resonance contribution.

Given the above results, we were interested in using the Hammet relationship to study the electronic effect of [2.2]paracyclophane as substituent

in the electrochemical oxidation of ferrocenyl imine Schiff's bases. Synthesis of N-4-(ferrocenylimine)-[2.2]Paracyclophane (FcIAPC) followed the same procedure as the other ferrocenyl imine derivatives, by condensation of 4-amino[2.2]paracyclophane with ferrocene carboxaldehyde in ethanol.

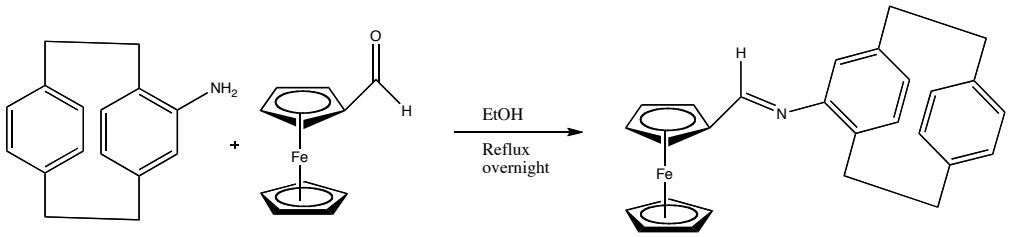

Scheme II – 6: Synthesis of N-4-(ferrocenylimine)-[2.2]Paracyclophane

It has been found that the electronic nature of [2.2]paracyclophane is electron releasing, but to the best of our knowledge it has not been established how it behaves with respect other substituents electrochemically. For this purpose we evaluated the electrochemical oxidation of the N-(4-imino[2.2]paracyclophane) ferrocenyl Schiff base (FcIAPC) using cyclic voltammetry.

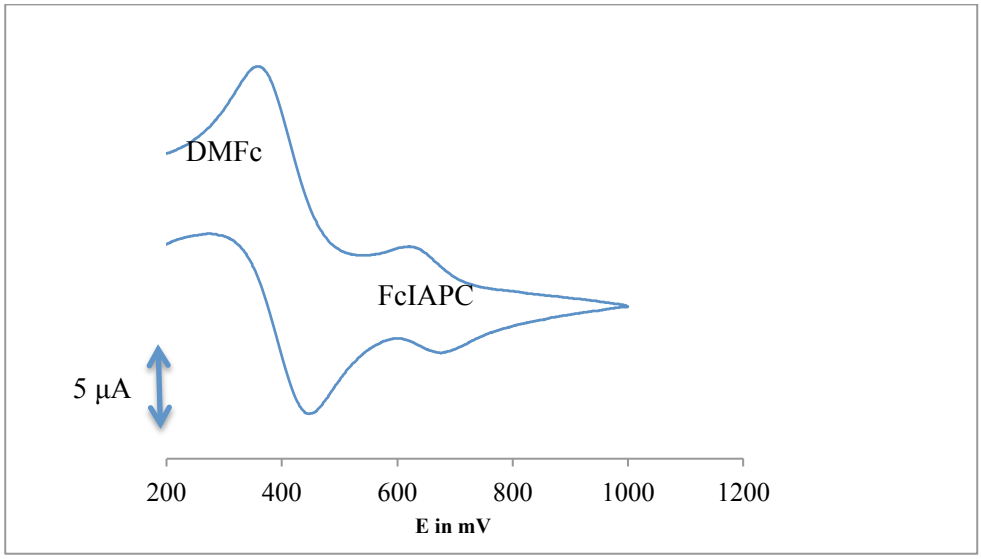

Figure II - 8: Typical cyclic voltammograms (CV) for N-(4-imino[2.2]paracyclophane) ferrocenyl Schiff base with internal standard as DMFc in AcCN solventwith 0.1M $TBAPF_6$ as an electrolyte; working electrode Pt; auxillary electrode Pt wire; reference electrode Ag/Ag+, initial coordinate 0 V; anodic limit 1.0 V; cathodic limit, 0 V. Scan rate 100 mV/sec; Y scale is at 5 µA.

The electrochemical redox behavior of FcIAPC showed properties similar to the other ferrocenyl imine derivatives. The half wave potential $E_{1/2}$ for FcIAPC is observed to be 0.247 V compared with DMFc at scan rate of 100 mV/sec and with Ag/AgCl as a reference electrode in presence of AcCN and 0.1 $TBAPF_6$ as an electrolyte.

The half wave redox potential obtained for FcIAPC from the cyclic voltammetry was used to calculate the total potential difference between the aniline substituted ferrocenyl imine base and 4-amino[2.2]paracyclophane based ferrocenyl imine using Equation (9):

$$\Delta\Delta E_x = \Delta E_{1/2\ H} - \Delta E_{1/2\ X} \qquad (9)$$

A $\Delta\Delta E_x$ value of -0.023 V was obtained, which was then used to calculate the equilibrium constant for this electrochemical reaction to obtain a σ^+ value of -0.39, which is closest to the value of aniline substituted with a para –OMe substituent. This value suggests the strong electron donating nature of the [2.2]paracyclophane which could be due to the through-space electronic effect of π – stacked aromatic benzene rings. Nonetheless, the low value of ρ^+ suggests that the spin interaction of the ferrocene on oxidation with the substituent is weak and mostly localized on the iron center.

Conclusion:

A linear free energy relationship for the substituted aniline derivatives of ferrocenyl imine Schiff bases was established by measuring their redox potentials and showing a linear correlation for the simple as well as resonance enhanced substituent effects. This linear correlation allowed us to determine the effect of [2.2]paracyclophane as a substituent on the redox potential of ferrocenyl imine Schiff bases. [2.2]Paracyclophane behaves much like a –OMe group as an electron donor, which will help us to interpret how it will behave in various applications, such as in electronic devices, molecular magnetic materials, etc.

Experimental:

Physical measurements:

1H NMR: ^{1}H NMR spectra were obtained using a Varian Mercury 300 spectrometer ($CDCl_3$ solvent). Cyclic voltammetry measurements were performed using a CV50W potentiostat electrochemical analyzer with Ag/AgCl reference electrode, a Pt working electrode and a Pt wire counter electrode, a scan rate of 100 mV/sec, with 2 mM ferrocenyl imine solutions in 0.1 M tetrabutylammonium hexafluorophosphate as electrolyte in AcCN at ≈ 20°C. 1,1'-dimethyl ferrocene was used as internal potential reference in the ferrocenyl imine solution.

Materials:

Ferrocenecarboxaldehyde, aniline, 2,5-dimethylaniline, p-anisidine, p-toluidine, m-toluidine, 4-aminobiphenyl, p-nitro aniline, 4-aminobenzonitrile were used as received from Sigma-Aldrich. o-Toluidine was prepared from o-nitrotoluene as per a literature procedure [26]. 4-Amino[2.2]paracyclophane was prepared from reduction of 4-nitro[2.2]paracyclophane [27]using a procedure as per the literature [26]. Ethanol, $CDCl_3$, hexanes, ether were all used as received. Activated neutral alumina, which was heated overnight at 60°C in an oven before being used, was used for column chromatography.

General procedure for synthesis of derivatives of ferrocenyl imine:

All the ferrocenylimine Schiff bases were prepared using the procedure as per the literature with little modification [28]. Ferrocene carboxaldehyde and aniline derivatives were dissolved in ethanol in 1:1.2 molar ratio. The mixture was heated to reflux solvent for 6 – 24 hours depending on the aniline derivative. The solutions were cooled down to room temperature and stirred for a day. The solvent was evaporated under reduced pressure and the product was purified by column chromatography using 50:50 hexane/ diethyl ether and neutral alumina.

1) FcCH=NPh:

Ferrocene caroxaldehyde (0.14 g, 0.65 mmol) and aniline (0.09 g, 1.00 mmol) was dissolved in 3 ml of ethanol. The reaction mixture was heated to reflux solvent overnight. The mixture was cooled to room temperature and solvent was evaporated under reduced pressure. The product (0.08 g, 45%) as red oil was isolated using column chromatography with neutral alumina using (50/50 v/v) hexane and diethyl ether as eluent. (R_f = 0.68). ^{1}H NMR (300 MHz, $CDCl_3$, 293K) δ 4.25 (s, 5H), 4.49 (s, 2H), 4.79 (s, 2H), 7.10-7.20 (m, 2H), 7.33 – 7.40 (m, 3H), 8.33 (s, 1H) [28].

2) $FcCH{=}NC_6H_4Me$-4

Following the general procedure, ferrocene carboxaldehyde (10.0 mg, 0.05 mmol) and p-toluidine (7.0 mg, 0.07 mmol) was used in 2 ml ethanol. The product was formed as a red solid (8.4 mg, 42.5 %). ^{1}H NMR (300 MHz, $CDCl_3$, 293K) δ 2.35 (s, 3H) 4.24 (s, 5H), 4.47 (s, 2H), 4.79 (s, 2H), 7.02-7.11 (m, 2H), 7.12 – 7.21 (dd, 2H), 8.32 (s, 1H) [29].

3) $FcCH{=}NC_6H_4Me$-2

Ferrocene carboxaldehyde (85.6 mg, 0.4 mmol) and o-toluidine (46.8 mg, 0.44 mmol) were dissolved in 2 ml ethanol and heated to reflux solvent overnight. The solution was cooled to room temperature and solvent was evaporated under reduced pressure. The solid was dissolved in methylene chloride and dried over sodium sulfate. The methylene chloride solution was filtered and dried under reduced pressure. Red crystals formed which were triturated with hexane to get the product (67 mg, 55%).

^{1}H NMR (300 MHz, $CDCl_3$, 293K) δ 3.83 (s, 3H), 4.24 (s, 5H), 4.47 (s, 2H), 4.79 (s, 2H), 6.88 -6.94 (d, 2H), 7.10 – 7.22 (d, 2H), 8.33 (s, 1H).

4) $FcCH{=}C_6H_4OMe$-4: Red solid (45 %)

^{1}H NMR (300 MHz, $CDCl_3$, 293K) δ 3.83 (s, 3H) 4.23 (s, 5H), 4.47 (s, 2H), 4.79 (s, 2H), 6.82-6.91 (m, 2H), 7.12 – 7.21 (dd, 2H), 8.37 (s, 1H) [29].

5) $FcCH{=}NC_6H_4CN$-4: Red solid (48 %)

^{1}H NMR (300 MHz, $CDCl_3$, 293K) δ 4.26 (s, 5H), 4.56 (s, 2H), 4.81 (s, 2H), 7.10 -7.20 (d, 2H), 7.60 – 7.70 (d, 2H), 8.32 (s, 1H).

6) $FcCH{=}NC_6H_4NO_2$-4: Red solid (44 %) [29]

^{1}H NMR (300 MHz, $CDCl_3$, 293K) δ 4.28 (s, 5H), 4.58 (s, 2H), 4.82 (s, 2H), 7.12 -7.20 (d, 2H), 8.20 – 8.26 (d, 2H), 8.35 (s, 1H) [29].

7) $FcCH{=}NC_6H_3$-$(Me)_2$-2,5: Red oil 42 % yield (87 mg, 0.27 mmol)

^{1}H NMR (300 MHz, $CDCl_3$, 293K) δ 2.27 (s, 3H), 2.36 (s, 3H), 4.23 (s, 5H), 4.47 (s, 2H), 4.80 (s, 2H), 6.65 (s, 1H), 6.82 -6.88 (d, 1H), 7.04 – 7.10 (d, 1H), 8.20 (s, 1H).

8) FcIAPC: Red solid 43 % yield (7.1 mg, 0.017 mmol)

^{1}H NMR (300 MHz, $CDCl_3$, 293K) δ 2.60 – 2.77 (m, 1H), 2.82 – 3.20 (m, 6H), 3.60 – 3.77 (s, 1H), 4.28 (s, 5H), 4.46 (s, 2H), 4.85 – 4.95 (dd, 2H), 5.80 (s, 1H), 6.34 – 6.42 (m, 1H), 6.44 – 6.62 (m, 4H), 6.90 – 6.98 (dd, 1H), 8.05 (s, 1H).

^{1}H NMR spectrum:

1) FcCH=NPh

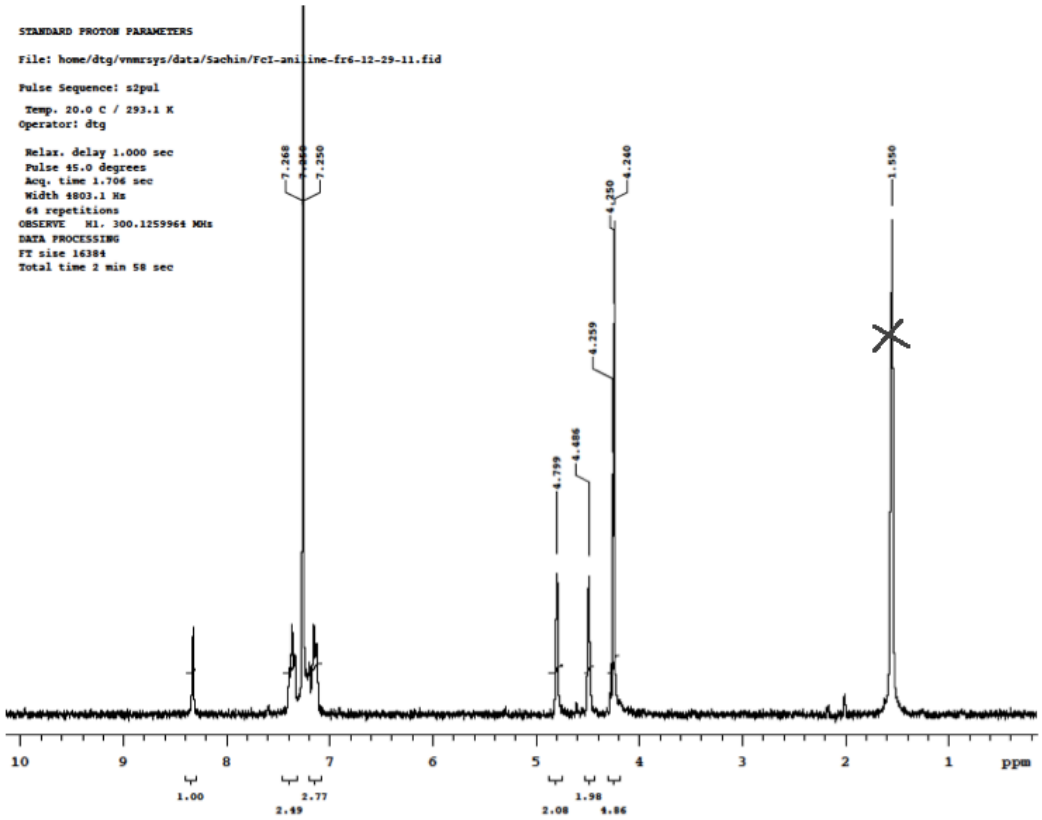

2) $FcCH{=}NC_6H_4Me\text{-}4$

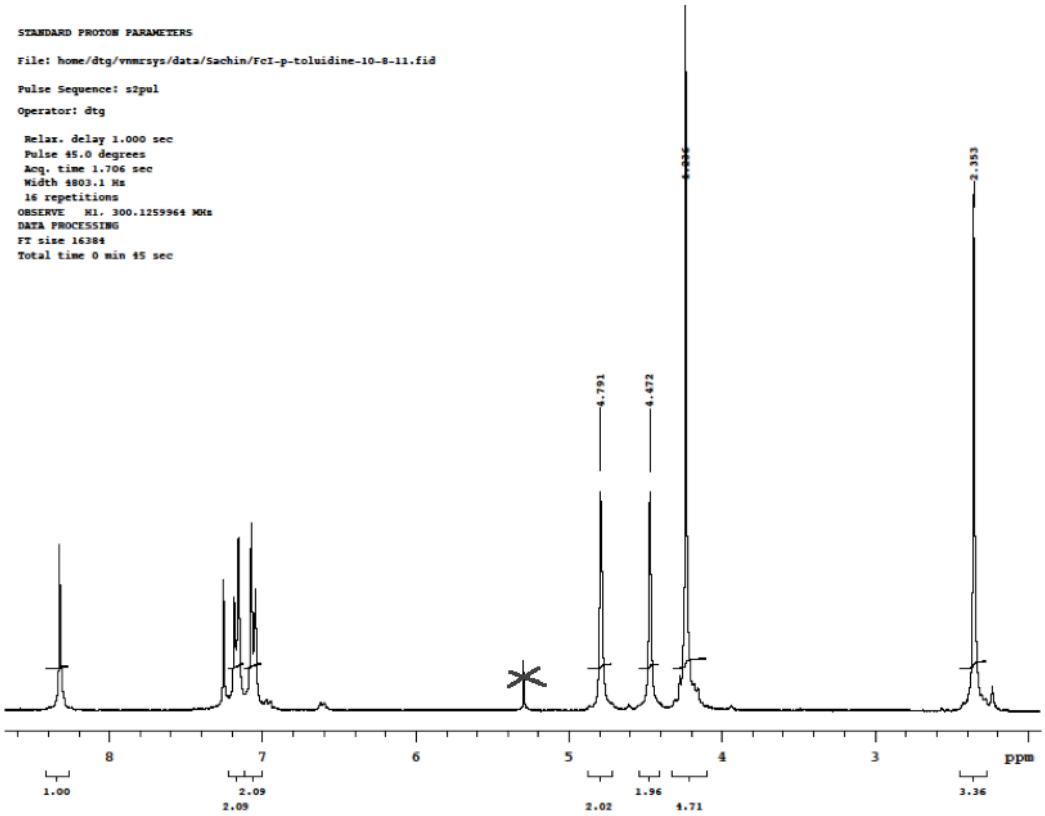

3) $FcCH{=}NC_6H_4Me$-2

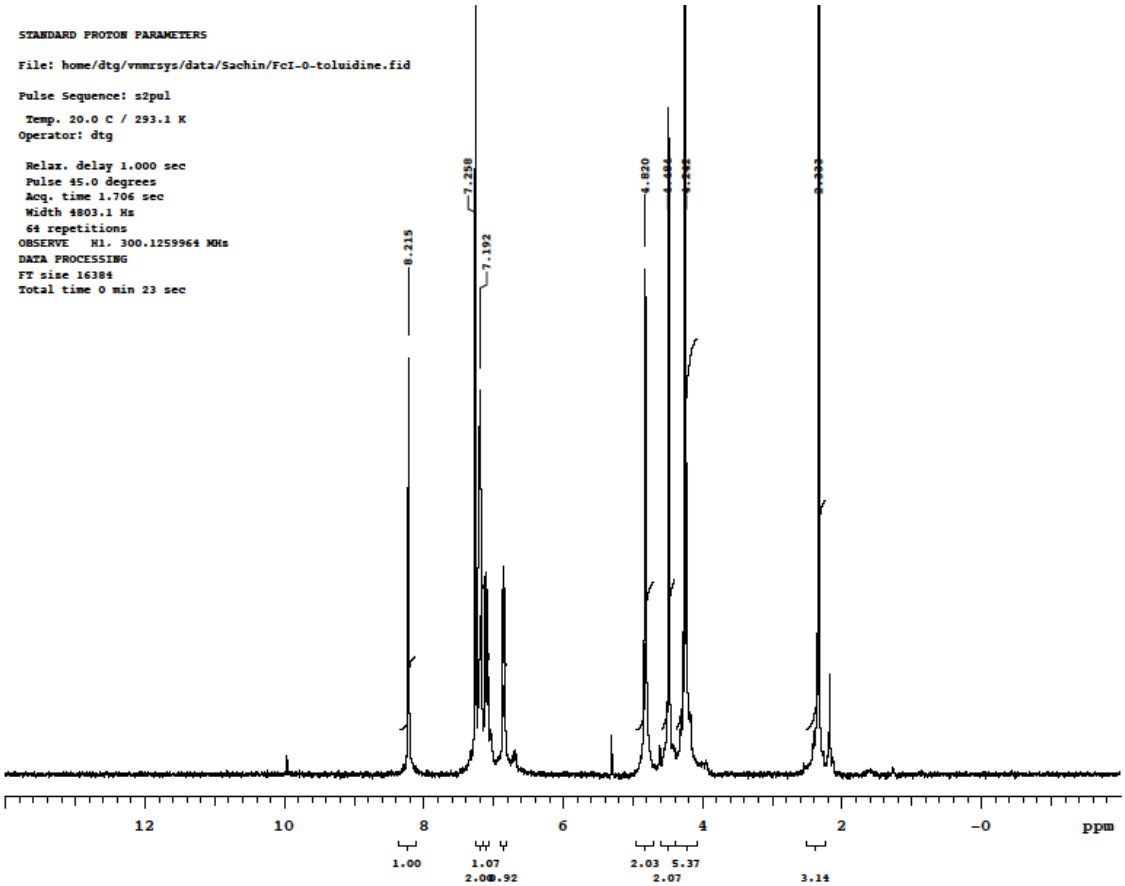

4) $FcCH{=}NC_6H_4OMe\text{-}4$

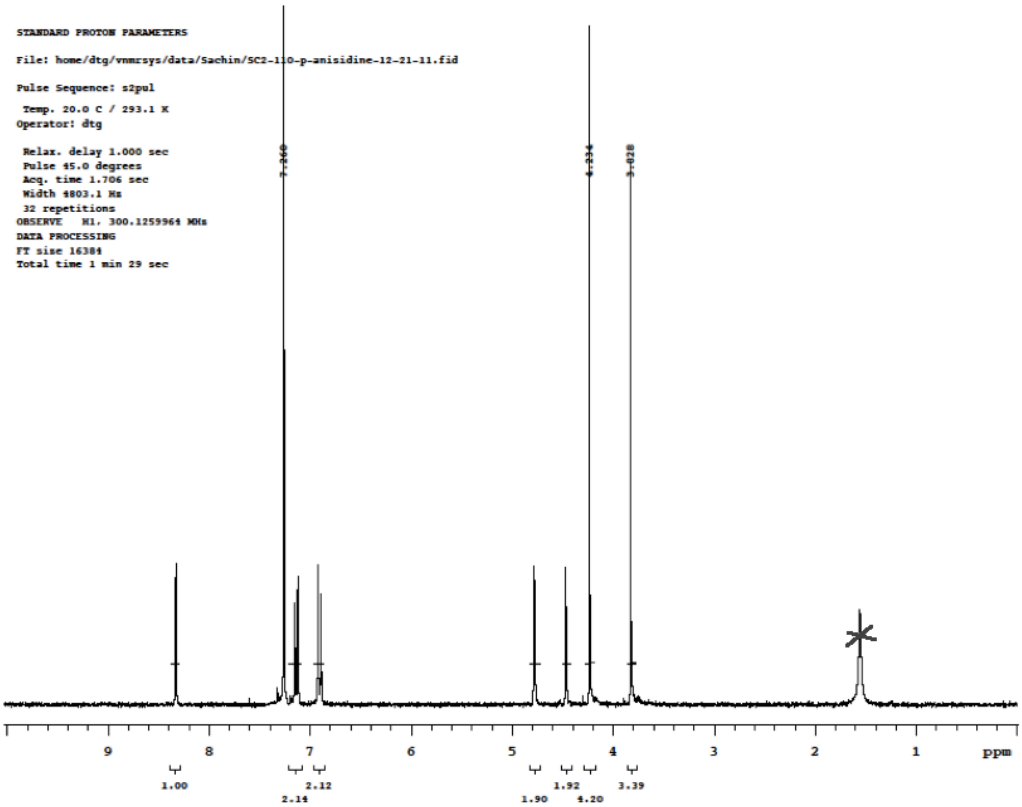

5) $FcCH{=}NC_6H_4Ph$-4

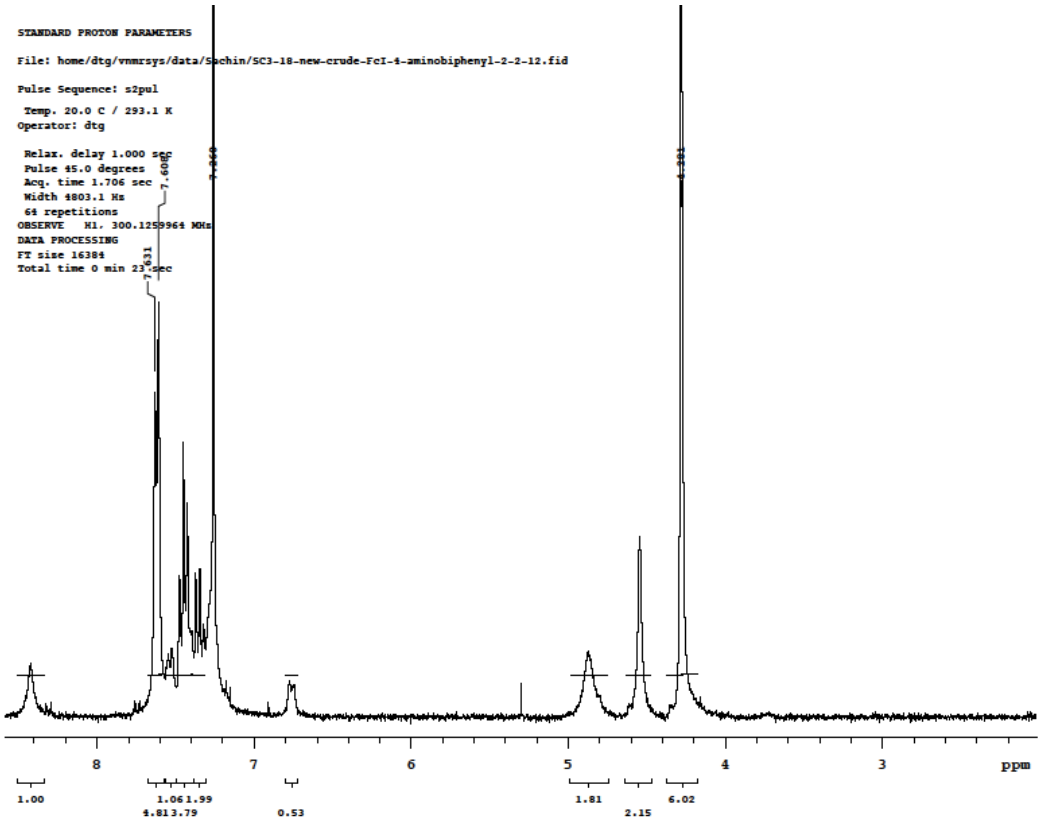

6) $FcCH{=}NC_6H_4NO_2$-4

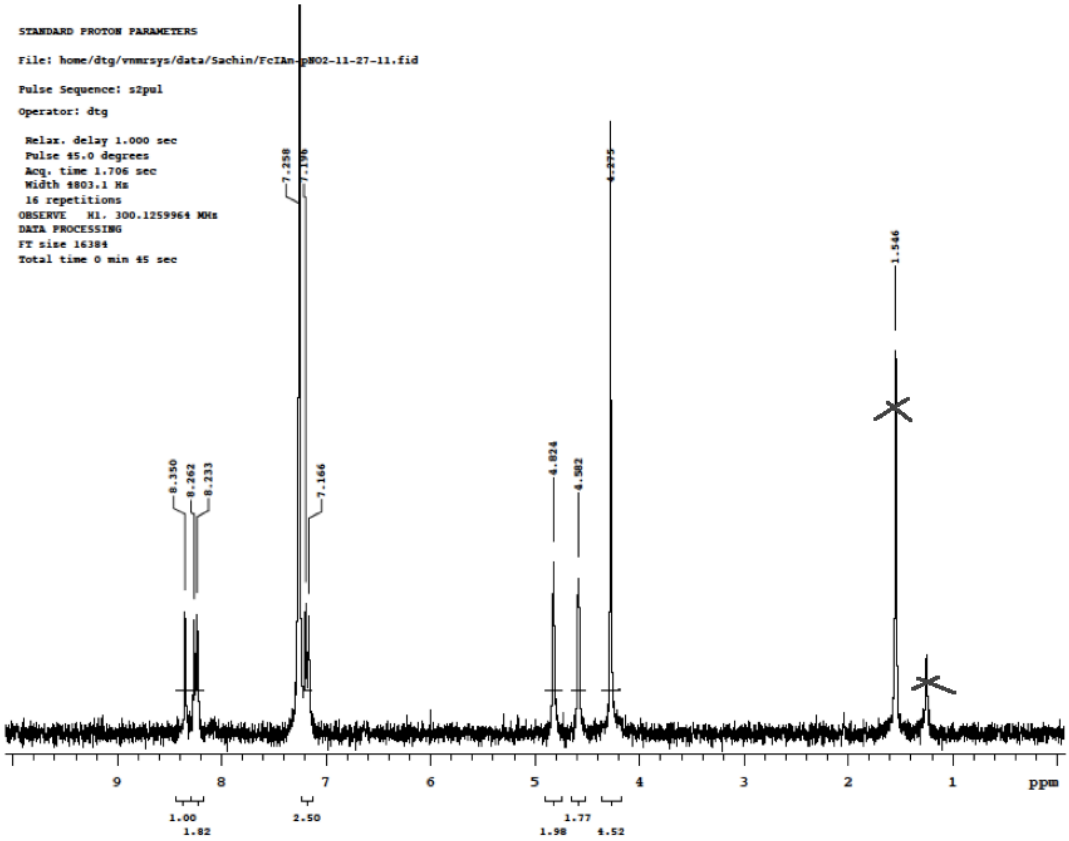

7) $FcCH{=}NC_6H_4CN$-4

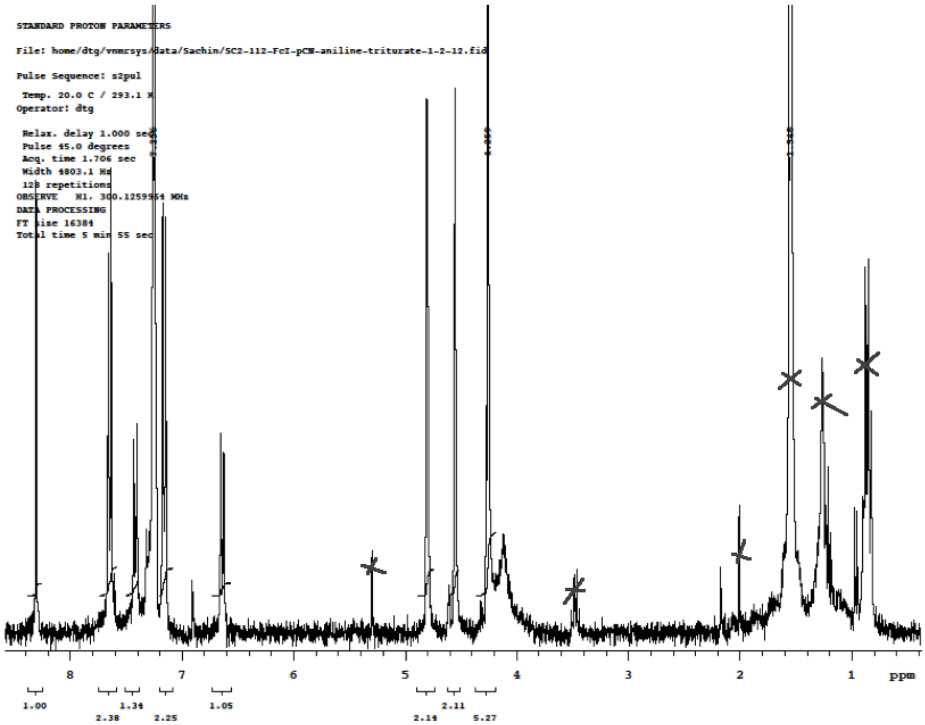

8)FcCH=$NC_6H_3(Me)_2$– 2,5

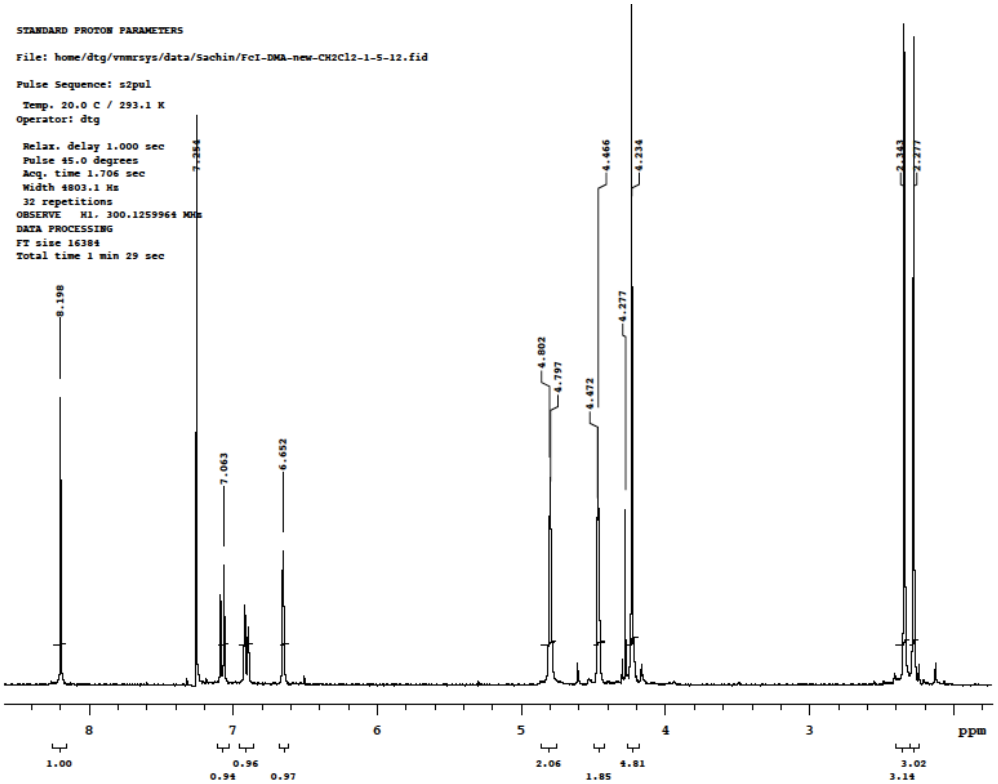

9) FcCH=N(amino[2.2]paracyclophane)-4

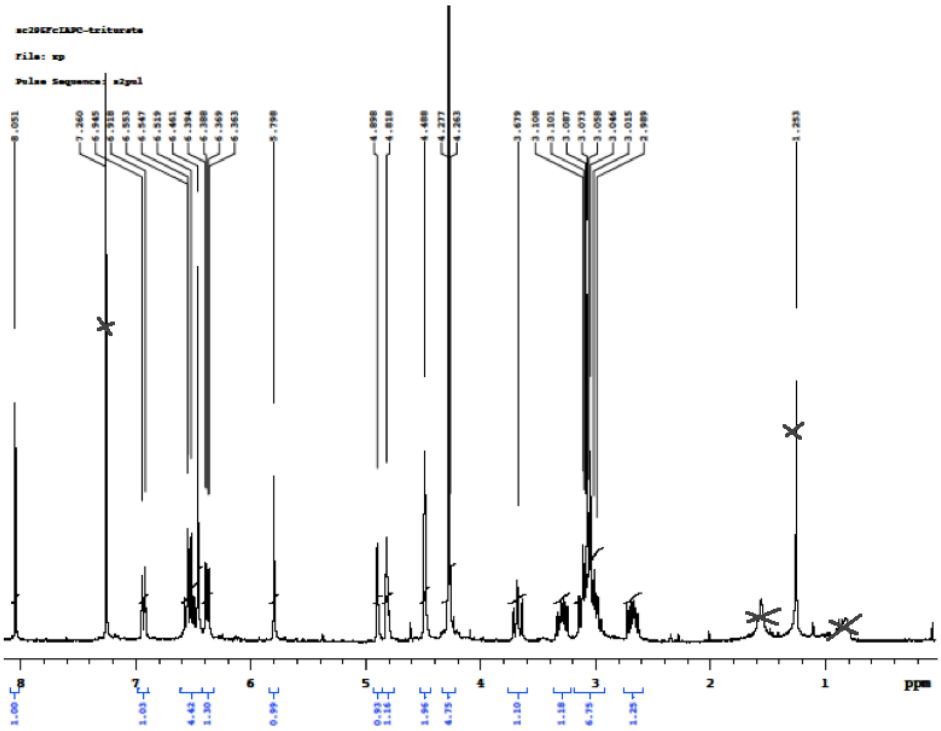

References:

1. Charles E. Carraher, J., *Organometallic Polymers. J. Chem. Edu*, 1981. **58**(11): p. 921 - 934.

2. Rahimi, A., *Inorganic and Organometallic Polymers: A Review.* Iranian Polymer Journal, 2004. **13**(2): p. 149 - 164.

3. Wright, M.E. and E.G. Toplikar, *New Ferrocene Complexes & Polymers for Nonlinear Optical Applicaitons.* Advances in New Materials, Contemporary Topics in Polymer Science, 1991. **7**: p. 000.

4. Liu, W.-J., G.-X. Xiong, and D.-H. Zeng, *Synthesis and Electrical Properties of Three Novel Poly(Ferrocenyl-Schiff Bases) and Their Charge Transfer Complexes with Iodine.* J. Inorg. Organomet. Polym., 2010. **20**: p. 97 - 103.

5. Refaei, M., L.I. Espada, and M. Shadaram, *Applications of Ferrocene-based Polymers in Optical Fiber Gas Sensing.* Chemical and Biological Sensing, 2000. **4036**: p. 123 - 130.

6. Huo, J., *Progress in Synthesis of Branched Ferrocene-based Polymers and Thier Applications in Supramolecular Recognition and as Precursors of Magnetic Materials.* Designed Monomers and Polymers, 2007. **10**(5): p. 389 - 404.

7. Herberhold, M., *Ferrocene Compounds Containing Heteroelements*, in *Ferrocenes*2007, Wiley-VCH Verlag GmbH. p. 219-278.

8. Togni, A. and R.L. Halterman, *Metallocenes: Synthesis, Reactivity, Applications*, ed. W.-V.V. GmbH. Vol. 2. 1998. 724.

9. Flanagan, J.B., et al., *Electron transfer to and from molecules containing multiple, noninteracting redox centers. Electrochemical oxidation of poly(vinylferrocene).* Journal of the american chemical society, 1978. **100**(13): p. 4248-4253.

10. Fenton, D.E. and P.A. Vigato, *Macrocyclic Schiff base complexes of lanthanides and actinides.* Chemical Society Reviews, 1988. **17**(0): p. 69-90.

11. Zaheer, M., et al., *Synthesis, characterization, electrochemistry and evaluation of biological activities of some ferrocenyl Schiff bases.* Applied Organometallic Chemistry, 2011. **25**(1): p. 61-69.

12. Liu, W.-J., G.-X. Xiong, and W.-P. Wang, *Research on synthesis and conductivity of ferrocenyl Schiff base and its salt.* Applied Organometallic Chemistry, 2007. **21**(2): p. 83-88.

13. Hernandez-Molina, R. and A. Mederos, *Acyclic and Macrocyclic Schiff Base Ligands.* ChemInform, 2004. **35**(48): p. no-no.

14. Nishihara, H. and M. Murata, *Electron Transfer in Ferrocene-containing π-conjugated Polymers.* Journal of Inorganic and Organometallic Polymers and Materials, 2005. **15**(1): p. 147-156.

15. Kurihara, M., *Synthesis and physical properties of azo-ferrocene oligomers and polymers.* Synthetic Metals, 1999. **102**(1–3): p. 1517-1518.

16. Singer, L.A. and D.J. Cram, *Macro Rings. XXVII. Transannular Substituent Effects in π-π-Complexes of Paracyclophanes.* J. Am. Chem. Soc, 1963. **85**(8): p. 1080 - 1084.

17. Sheehan, M. and D.J. Cram, *Macro Rings .40. Transannular Interactions in Tetracyanoethylene Complexes of [3.3]Paracyclophane and Derivatives.* J. Am. Chem. Soc., 1969. **91**(13): p. 3553-&.

18. Cram, D.J. and R.H. Bauer, *Macro Rings. XX. Transannular Effects in π-π-Complexes1.* J. Am. Chem. Soc., 1959. **81**(22): p. 5971-5977.

19. Morisaki, Y. and Y. Chujo, *Through-space conjugated polymers consisting of [2.2]paracyclophane.* Polymer Chemistry, 2011. **2**(6): p. 1249-1257.

20. Glatzhofer, D.T. and M.C. Morvant, *Substituent effects on the electrochemical oxidation ofN,N',N"-triphenyl-1,3,5-triaminobenzenes.* Journal of Physical Organic Chemistry, 1998. **11**: p. 731 - 736.

21. Tsierkezos, N., *Cyclic Voltammetric Studies of Ferrocene in Nonaqueous Solvents in the Temperature Range from 248.15 to 298.15 K.* Journal of Solution Chemistry, 2007. **36**(3): p. 289 - 302.

22. Imrie, C., V.O. Nyamori, and T.I.A. Gerber, *Solvent Free Synthesis of Ferrocenylimines.* Journal of Organometallic Chemistry, 2004. **689**: p. 1617 - 1622.

23. D'Silva, C., *Electrochemical characterisation of polyvinylferrocene polymers: substituent effects on the redox reaction. J. Mater. Chem.*, 1992. **2**(2): p. 225 - 230.

24. Glatzhofer, D.T. and M.C. Morvant, *Substituent Effects on the Electrochemical Oxidation of N,N',N"-triphenyl-1,3,5-triaminobenzenes.* Journal of Physical Organic Chemistry, 1998. **11**: p. 731 -736.

25. Isaacs, N.S., *Physical Organic Chemistry*. Longman Scientific and Technical, ed. L. Group1987, UK: Longman group and John Wiley & Sons.

26. Bellamy, F.D. and K. Ou, *Selective reduction of aromatic nitro compounds with stannous chloride in non acidic and non aqueous medium.* Tetrahedron Letters, 1984. **25**(8): p. 839-842.

27. Cram, D.J. and N.L. Allinger, *Macro Rings .12. Stereochemical Consequences of Steric Compression in the Smallest Paracyclophane.* Journal of the American Chemical Society, 1955. **77**(23): p. 6289-6294.

28. Meleshonkova, N.N., *Synthesis and redox properties of novel ferrocenes with redox active 2,6-di-tert-butylphenol fragments: The first example of 2,6-di-tert-butylphenoxyl radicals in ferrocene system. J. Organometallic Chemistry*, 2007. **692**: p. 5339 - 5344.

29. Wang, H.-X., *Ferrocenylamines 2. Reductive methylation of secondary ferrocenylamines and ferrocenylaldimines: Synthesis, characterization of [(N-methyl-N-aryl)amino]methylferrocenes,1-[(N-methyl-N-phenyl)amino]ethylferrocene and crystal structures of [(η5-C5H5)Fe(η5-$C_5H_4CH_2NHC_6H_4$-Cl-4)] and [(η5-C5H5)Fe(η5-C5H4CH2N(CH3)-C6H4-OCH3-4)].* Journal of Organometallic Chemistry, 2006. **691**(5): p. 987-993.

Chapter III:

Ferrocenyl Imine Schiff Bases Derived from Diamino-[2.2]Paracyclophane:

Introduction:

Electronic communication between two metal centers in intramolecular systems of inorganic or organic molecules has attracted lot interest in research due to its role in optoelectronic properties. Organic based semiconducting oligomers or polymers with conjugated systems have attracted even greater interest due to their applications in various electronic and optoelectronic applications. [2.2]paracyclophanes have shown interesting optical, electrical and topological properties due to their characteristic π – π interactions between the two co-facial arene systems [1]. [2.2]paracyclophanes have been studied extensively for their ability to delocalize charge carriers through π-stacks.

Iwamura has discussed transannular magnetic interaction in three isomers (*pp, pm, po*) of [2.2]paracyclophanedicarbenes using ESR, as shown in Figure III - 1 [2].

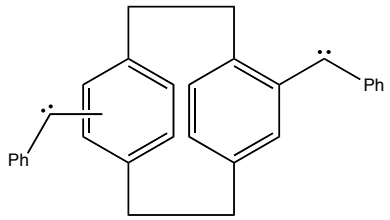

Figure III – 1: [2.2]paracyclophane dicarbene

The spin multiplicity of the dicarbenes was determined using ESR spectroscopy and their π-spin densities were determined considering the π-spin distribution

is an alternate diphenylcarbene system. According to McConnell's condition, the interaction between two aromatic radicals in [2.2]paracyclophanyl benzene rings is ferromagnetic when the product of π-spin density is negative at each most strongly interacting site between the two benzene rings, which can be observed from the Figure III - 2 [3, 4]. It was observed that such transannular interaction could be a through bond interaction via the ethano bridges or a through space interaction and only observed for pseudo-para and pseudo-ortho isomers. While in case of the pseudo-meta isomer, the product of π-spin density is positive at each interacting site between the two benzene rings and such interactions should be antiferromagnetic.

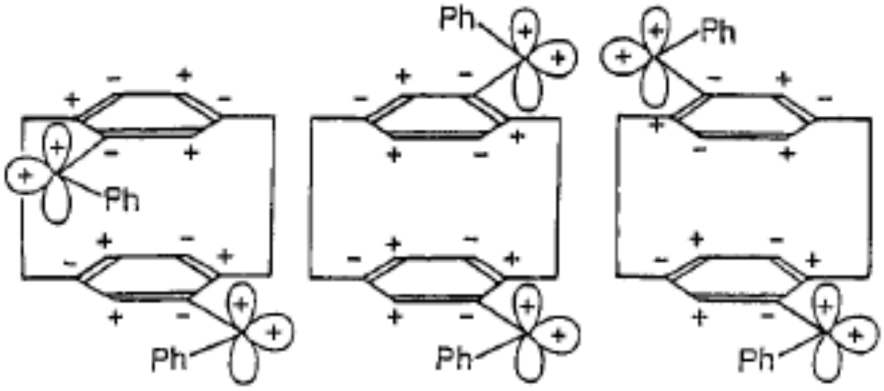

pseodo-ortho pseudo-meta pseudo-para

Figure III – 2: π-Spin density distribution in dicarbene isomers.

Figure adapted from reference [5].

Neugebauer and Fischer studied transannular interactions by attaching verdazyl radicals on to two arene decks of [2.2]paracyclophane, as shown in

Figure III - 3 [6]. The studies were carried out using ESR spectroscopy and NMR spectroscopy.

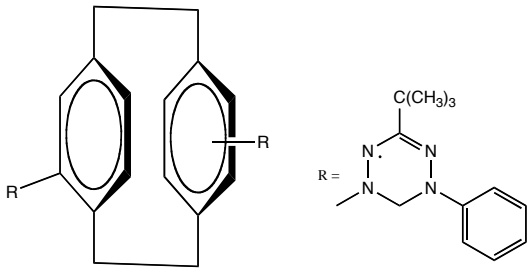

(verdazyl radical)

Figure III-3: Verdazyl substituted [2.2]paracyclophane

In this study, the authors synthesized three different isomers of bis(verdazyl)[2.2]paracyclophane viz. pseudo-para (*pp*), pseudo-meta (*pm*) and pseudo-ortho (*po*). The synthesis of pseudo-gem bis(verdazyl) isomer was not successful, which would have been good example to study for transannular interactions due to its fixed molecular structure. NMR studies indicated that there are no substantial transannular interactions within *pp, po*, and *pm* compounds. In case of the *pp* and *pm* isomers, the distance between the two unpaired electrons in the verdazyl substituents is located at the midpoints of the verdazyl rings and is significantly localized in the verdazyl ring, due to which no transannular interactions were observed between the biverdazyl moieties. In the case of the *po* isomer, the verdazyl rings are twisted out of conjugation from the paracyclophane decks which is due to steric requirements of the pseudo-ortho

substitution. This weakens or eliminates interactions with the [2.2]paracyclophane rings.

Bazan has reported donor – acceptor interactions through the π-π stacked arene system for dipolar 4-(4-dihexylaminostyryl)-16-(4-nitrostyryl)[2.2]paracylophane to use for non-linear optical applications as shown in Figure III - 4. They were able to show significant end to end charge transfer contributions through the [2.2]paracyclophane unit using quantum chemical calculations [7].

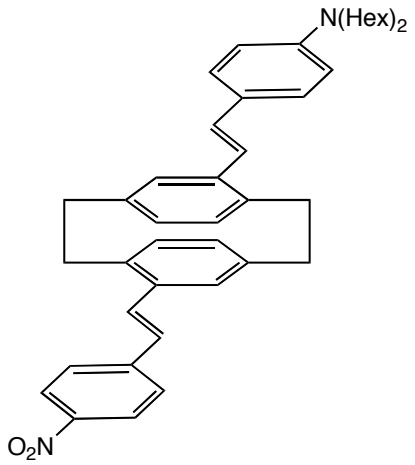

Figure III – 4: 4-(4-dihexylaminostyryl)-16-(4-nitrostyryl)[2.2]paracylophane

The influence of π – stacking in [2.2]paracyclophane and [3.3]paracyclophane, as shown in Figure III – 5, has been shown in radical cation delocalization of unpaired electrons resulting from strong intramolecular electronic interactions between two chromophores [8].

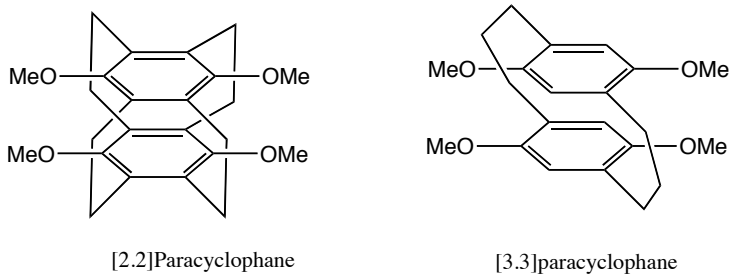

Figure III – 5: A π-stacked [2.2.2.2]-paracyclophane and a [3.3]paracyclophane.

Involvement of the conjugated π-stacked [2.2]paracyclophane system in a polymer backbone also showed promise in influencing the migration of electrons through conjugated conducting polymers. Collard et al. reported the effect of π-stacking in [2.2]paracyclophane and apparent electronic interaction using electrochemistry and fluorescence spectroscopy [9]. The bis(α-methyl bithiophene) para-substituted paracyclophanes, as seen in Figure III – 6, showed two separate, one electron oxidation peaks, which suggested the electronic influence of the π-stacked [2.2]paracyclophane. It was concluded that the influence of π-stacking on neutral and charged conjugated chains was observed in the electronic interactions between oligo-arenes.

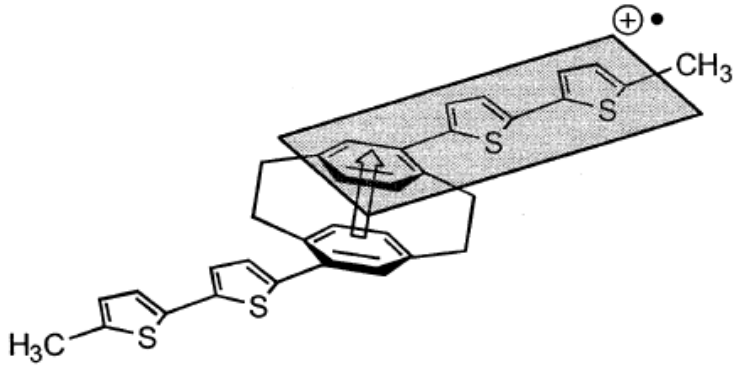

Figure III – 6: Charge transfer interaction in bis(α-methyl bithiophene)[2.2]paracyclophane

Electronic coupling in a mixed valence system based on the pseudo-para-dinitro[2.2]paracyclophane radical anion was investigated using Marcus-Hush theory, revealing that the electronic coupling in mixed valence pseudo-para-dinitro[2.2]paracyclophane radical anion system varies from a localized class-II to a delocalized class-III system by changing solvent polarity [10].

Connick et al. reported electronic coupling through π – π interactions in a binuclear rhenium (I) complex of [2.2]paracylophane-diimine, Figure III - 7 [11].

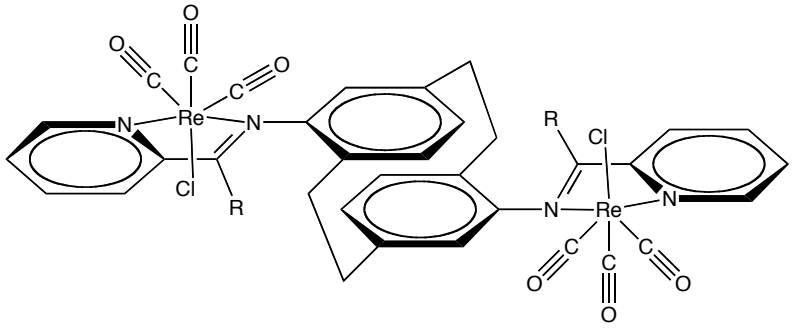

Figure III – 7: Rhenium (I) complex of [2.2]paracylophane-diimine

Two pseudo-para substituted bis-diimino[2.2]paracyclophane ligands were complexed with rhenium (I) tricarbonyl chloride, and the spectroscopic data and electrochemical data were determined. It was found that the comproportionation constants for these complexes, based on the diimine-centered electrochemical reduction process, suggested weak interactions between the diimine groups mediated by the paracyclophane bridging group. In this case, it was concluded that this weak interaction originated from steric

congestion caused by the carbonyl groups on the Re, which disfavors coplanarity of the diimine groups attached to [2.2]paracyclophane.

Richardson and Taube reported comproportionality based on binuclear complexes of ruthenium which undergo multiple step charge transfer processes [12]. For multistep charge transfer reactions of the type, in Equation (1),

$$A \xrightarrow{n_1 e^-,\ E_1^0} B \xrightarrow{n_2 e^-,\ E_2^0} C \qquad \text{Equation (1)}$$

The comproportionation constant (K_c) is a equilibrium constant related to the concentrations of A and C to B, by the given Equation (2),

$$Kc = \frac{[B]^{n1+n2}}{[C]^{n1}\,[A]^{n2}} = \exp\left[\frac{(E_1^0 - E_2^0)\, n_1 n_2 F}{RT}\right] \qquad \text{Equation (2)}$$

where n_1 and n_2 are the number of electrons participating in the reaction, E^0 is the standard potential for a particular step of the reaction, F is the Faraday constant, and R is gas constant at temperature T = 298 K. According to Sutton et al., if the values of K_c lies in the range of $4 < K_c < 200$, the obtainable standard potential range is 36 mV < ΔE° < 136 mV [13]. Also as K_c increases from 4, the peak – to – peak separation between the two-redox potentials increases, i.e. the two peaks in cyclic voltammetry for the two step charge transfer process become distinguishable. Hence when Kc is greater than 200, two redox stages for the

binuclear species can be clearly observed, which shows the interaction between two single step charge transfer systems [12, 13]. Multinuclear systems with several electroactive moieties have been of interest for their applications as magnetic materials, in electronic devices due to their electrical properties, and also for electrochemical recognition properties [14, 15].

Ferrocene has been studied for many years due to its well-characterized electrochemical properties. Many polymers containing ferrocenes have been studied as conductive polymers for their practical and fundamental applications. Ferrocene-modiefied polymers have various functions such as a photochemical quencher for triplet states in anthracene, a sensitizer in photochemical dimerization of isoprene, uses in absorption of UV and γ radiation, and polymers containing ferrocenium units are useful for special ionic adhesives [16].

Various polymers containing mixed valence ferrocene – ferrocenium moieties have been studied as semiconducting polymers, such as poly(vinylferrocene), ferrocene-o-anisaldehyde condensation polymers, and polyferrocenylene [17]. It was observed that upon oxidation of more than 70 % of the ferrocene units with DDQ, the polysalts with anions such as BF_4^- showed an increase in the conductivity. Electron transfer studies of poly(vinylferrocene) containing multiple redox centers suggested that all these redox centers are non-interacting but showed higher current density due to the high density of active redox centers [18]. Mixed valence compounds containing redox active sites held in close proximities, such as 1,1'-polyferrocene, where the oxidation of one

ferrocene has a distinctive effect on the oxidation potential of neighboring ferrocene moieties, showed intramolecular electronic interactions between different oxidation state sites [19].

Considering the factors involved in determining intramolecular electronic interactions between the electroactive sites (metals) discussed here, it is possible to consider interactions between redox active centers, specially the iron metal center in ferrocene, separated by a [2.2]paracyclophane moiety. In Chapter 2, we determined the electron donating ability of [2.2]paracyclophane, which influenced the oxidation of a ferrocene moiety. The diphenylcarbene [2.2]paracyclophane system showed electronic interactions between their spin densities, while for diverdazyl systems, it was shown that the interactions between pendant radicals depended in part on steric interaction of the verdazyl radicals, which showed no electronic interactions. But when the bis(rhenium) system with [2.2]paracyclophane was studied, weak interactions between the two Re redox centers are mediated by [2.2]paracyclophane, were observed. Hence it would be interesting to study a bis(ferrocenylimine) system and see how the spin interactions between the two ferrocene redox centers is mediated by the [2.2]paracyclophane. The use of ferrocenyl imine Schiff base of [2.2]paracyclophane is based on such factors as geometry, the redox properties of ferrocene, the electronic nature of [2.2]paracyclophane, and the conjugated system of the imine.

Results and Discussion:

Synthesis and characterization of pseudo-para-4,12-bis(ferrocenylimino)[2.2]paracyclophane (pp-FcIDAP):

[2.2]Paracyclophane has been used as mediator for electronic communication between two metal redox centers. This prompted us to investigate the effect of [2.2]paracyclophane on the electronic coupling between two ferrocene redox metal centers. From the linear free energy correlation studies in Chapter 2, it was established how [2.2]paracylophane interacts electronically with respect to the redox potential of the iron redox center of ferrocene. To continue the study of electronic mediation through the [2.2]paracyclophane moiety, we synthesized *pseudo-para*-4,12-bis(ferrocenylimino)[2.2]paracyclophane (ppFcIDAP).

In this synthesis two equivalents of ferrocene carboxaldehyde were reacted with *pseudo-para*-4,12-diamino[2.2]paracyclophanes (pp-DAP) by condensation in ethanol. A 10% excess of amino[2.2]paracyclophane was used to avoid any interaction of any ferrocenecarboxaldehyde impurities during cyclic voltammetry, as its redox potential is in the range of the imine products. The imine base was isolated as a red solid in 44% yield. The chemical reaction is shown in Scheme III - 1.

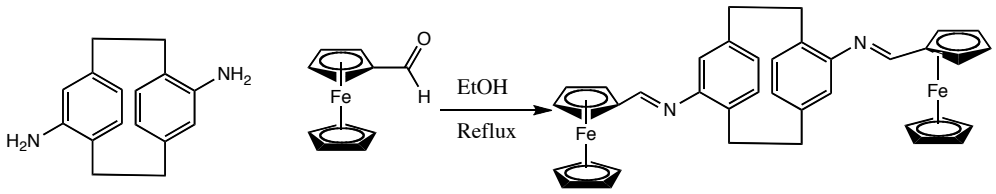

Scheme III - 1: Synthesis of pseudo – para - bis(ferrocenylimine)[2.2]paracyclophane (pp-FcIDAP)

The product was characterized using ^{1}H NMR, which showed a two proton singlet signal at δ ca. 8 ppm, typical for -CH=N imine proton. It can be observed that the peaks for the α-hydrogen atoms in the ferrocenyl moiety are singlets at 4.91 ppm and 4.83 ppm showing they are non-equivalent. In contrast N-4-ferrocenylimino[2.2]paracyclophane (FcIAPC) showed only a singlet at 4.92 ppm corresponding to equivalent α-hydrogen atoms in the ferrocenyl moiety. It is unclear what the source of this phenomenon is. It could be that the addition of the second ferrocenylimino moiety perturbs the electronic environment of the [2.2]paracyclophane enough to reveal the asymmetry of the ferrocenyl α-hydrogens. Because of their spatial distance apart, it is unlikely that the conformational constraints of the ferrocenyl imino groups, which could change the apparent electronic environment, are different for the two compounds. Peaks at 3.78 ppm, 3.30 ppm, 3.05 ppm, 2.72 ppm, correspond to hydrogens on the ethylene bridges of the [2.2]paracyclophane. IR-spectra were recorded using an Schimadzu IR spectrometer in the range of 400 – 4000 cm^{-1} at room temperature with the accumulation of 16 scans. The samples were made as KBr pellets. The IR spectrum for the imine Schiff base of pp-FcIDAP showed a characteristic C=N stretching band at around 1616 cm^{-1}. This band is 63 – 65

cm^{-1} wavenumbers lower that of the ferrocene carboxaldehyde carbonyl band, which was absent in the spectrum.

The model compound N-4-ferrocenylimino[2.2]paracyclophane was synthesized according to the procedure mentioned in Chapter 2.

UV/Vis spectroscopic measurements

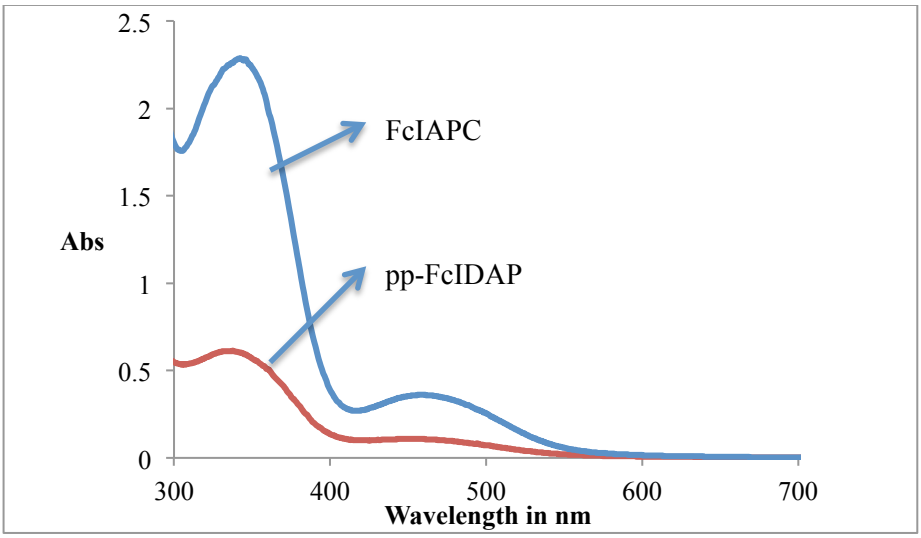

Figure III – 8: UV-vis spectra of 4-ferrocenylimine[2.2]paracyclophane (FcIAPC) and pseudo-para-bis(ferrocenylimine)[2.2]paracyclophane (ppFcIDAP) taken in acetonitrile solvent.

Table III – 1: UV-vis spectra parameters of FcIAPC and ppFcIDAP

	λmax (nm)	ε (mol^{-1} cm^{-1})	λmax (nm)	ε (mol^{-1} cm^{-1})
ppFcIDAP	480	2959	358	16353
FcIAPC	473	1639	353	10372

Electronic spectra for pp-FcIDAP and FcIAPC are shown above in Figure III - 8 and Table III – 1 in acetonitrile at room temperature. Both spectra are similar in their characteristics, in which both complexes exhibit characteristic absorption bands around 350 nm and 470 nm. But there is slight bathochromic shift observed in UV-visible spectrum for pp-FcIDAP, which is due to the electron donating nature of ferrocene. Also a difference in molar absorptivity values was observed. pp-FcIDAP showed increased molar absorptivity values compared to FcIAPC and corresponds to the attachment of the second ferrocenyl moiety to the other benzene ring of the [2.2]paracyclophane. These two absorption bands were assigned to the metal to ligand charge transfer (MLCT) band in which electron transfer occurs from the ferrocene *d* orbital transitions to the π* orbital of the azomethine group [20]. There is an absorption band at 290 for both the systems which corresponds to a π – π* transition for the [2.2]paracyclophane moiety. Attachment of the second ferrocenylimino group on the other deck of the [2.2]paracyclophane has only a small bathochromic effect on the absorption wavelength.

Electrochemistry:

The electrochemical properties of FcIAPC and pp-FcIDAP were invistigated using cyclic voltammetry in 0.1 M tetrabutyl ammonium hexafluorophosphate ($TBAPF_6$) at room temperature vs Ag/AgCl as reference electrode. The cyclic voltammagram for FcIAPC is shown in Chapter 2 Figure II - 8, showed typical one electron Fc/Fc^+ redox behavior.

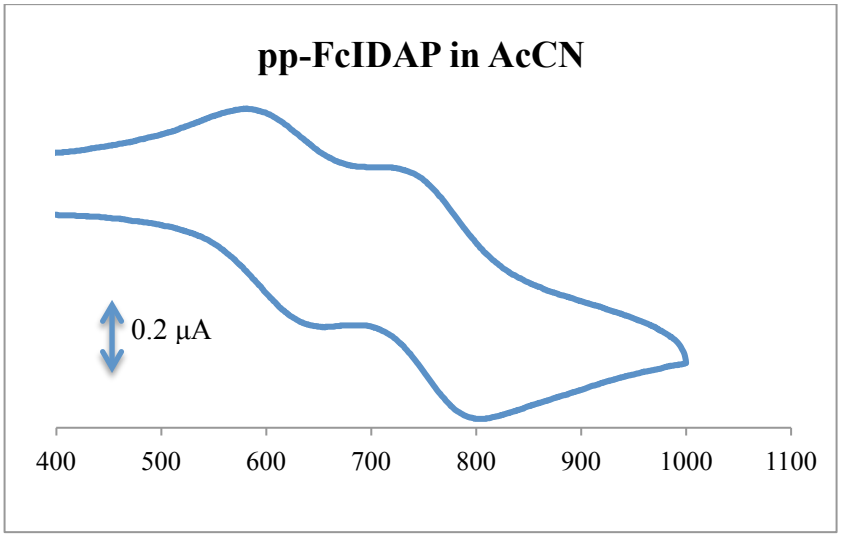

Figure III - 9: Cyclic Voltammetry of pseudo-para-bis(ferrocenylimine)[2.2]paracyclophane (pp-FcIDAP)
Conditions: 2 mM (pp-FcIDAP) in acetonitrile solvent with 0.1 M NBu_4PF_6 as an electrolyte; platinum as a working electrode, platinum wire as a counter electrode and Ag/AgCl as a reference electrode at 100 mV/S scan rate.

Cyclic voltammetry of the pp-FcIDAP in AcCN solvent showed two successive reversible redox couples at $E^1_{1/2}$ = 0.619 V and $E^2_{1/2}$ = 0.765 V, where the I_{pa} / I_{pc} ratio for both redox couples are about unity as shown in Figure III - 9. The potential differences between cathodic potentials and anodic

potentials for each of the redox potentials are 69 mV and 79 mV for the first and second redox peaks, respectively, which are consistent with one electron oxidation - reduction for each process. The first redox process at 0.619 V in the CV corresponds to the oxidation of ferrocene (Fc-PC-Fc) to a monoferrocenium moiety (Fc-PC-Fc^+) while the higher oxidation potential at 0.765 V corresponds to the oxidation of the monoferrocenium species (Fc-PC-Fc^+) to the bis(ferrocenium) species (Fc^+-PC-Fc^+). The representation of these electrochemical reactions is shown in Figure III – 10. The second oxidation potential shows that the two ferrocene moieties interact electronically, the first ferricinium acting as an electron withdrawing group toward the remaining ferrocene.

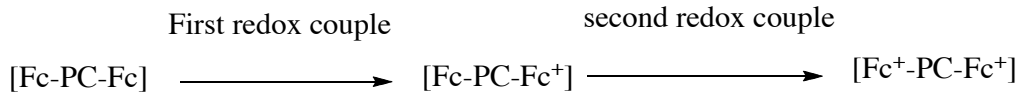

Figure III – 10: Redox moieties of Bis-(ferrocenylimino)[2.2]paracyclophane in cyclic voltammetry.

The differences between the redox potentials of the two sites was found to be $\Delta E_{1/2}$ = 139 mV larger than a previous literature value for (pseudo-*m*-[2.2]paracyclophane)[C≡C–FeCp*(dppe)]$_2$ (100 mV) [21]. The dynamic stability of these two mixed oxidation states with respect to disproportionation to produce fully oxidized and fully reduced species can be determined by calculating the comproportionation constant Kc. The electrochemical reaction for disproportionation of pp-FcIDAP can be written as shown in Scheme III - 2,

$$[Fc\text{-}PC\text{-}Fc] + [Fc^{+}\text{-}PC\text{-}Fc^{+}] \underset{}{\overset{K_c}{\rightleftharpoons}} 2[Fc\text{-}PC\text{-}Fc^{+}]$$

Scheme III – 2: Electrochemical reaction of bis(ferrocenylimino)[2.2]paracyclophane

The comproportionality constant for above reaction was calculated by using Equation (3) [22],

$$K_c = \exp\,[[(nF)/(RT)]\Delta E_{1/2}] \qquad \text{Equation (3)}$$

Where, n is number of electrons, F is faraday constant, R is the gas constant, T is temperature at 298 K and $\Delta E_{1/2}$ is the difference between the redox potential of two peaks in CV.

The magnitude of the Kc is diagnostic of the thermodynamic stability of the mixed valence system. The Kc value was found to be 224, which is greater than 4 (for the non interacting metal ions in a binuclear system [23]), and indicates that the two different redox species of ferrocene are interacting by delocalization of the unpaired electron, resulting in a fairly stable mixed-valent oxidation state (Fc-PC-Fc^{+}). This value of K_c suggests a relatively stable but weakly interacting mixed valence state, which would be categorized in between Class II – Class III according to the Robin – Day classification, where Kc ranges from 4 for weakly coupled Class II systems to Kc > 10^{13} in strongly coupled Class III systems [24]. As mentioned earlier, the value of K_c determines the stability of the [Fc-PC-Fc^{+}] state relative to [Fc-PC-Fc] + [Fc^{+}-PC-Fc^{+}]. There

are a number of factors which can influence the magnitude of K_c, such as through-space electronic interactions, solvation, entropy, steric interactions and any structural distortions upon oxidation [25].

Solvent effects:

The solvent plays an important role in the electrochemical kinetics of electrochemical reactions involving redox active compounds such that it influences the activation barrier of the reactions at the electrode surface and also solvent reorganization dynamics [26]. Here the effect of solvent properties such as dielectric constant was studied on the electrochemical behavior of the pp-FcIDAP. The solvents dichloromethane, tetrahydrofuran, acetonitrile, and propylene carbonate were chosen in this study based on their different dielectric constants. The electrochemical behavior of pp-FcIDAP in different solvents based on their dielectric constants was carried out using cyclic voltammetry as shown in Figure III – 10 and Figure III - 11. The concentration of the pp-FcIDAP was kept constant in all the solvent systems.

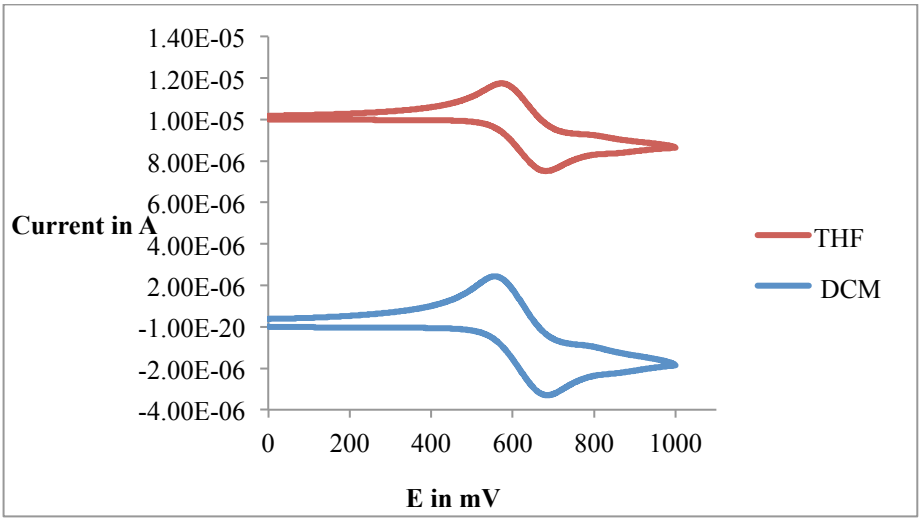

Figure III - 10: Cyclic voltammetry of bis(ferrocenylimino)[2.2]paracyclophane in different solvent systems, dichloromethane (blue), and THF (red). Conditions: 2 mM (pp-FcIDAP) in solvent with 0.1 M NBu_4PF_6 as an electrolyte; platinum as a working electrode, platinum wire as a counter electrode and Ag/AgCl as a reference electrode at 100 mV/S scan rate

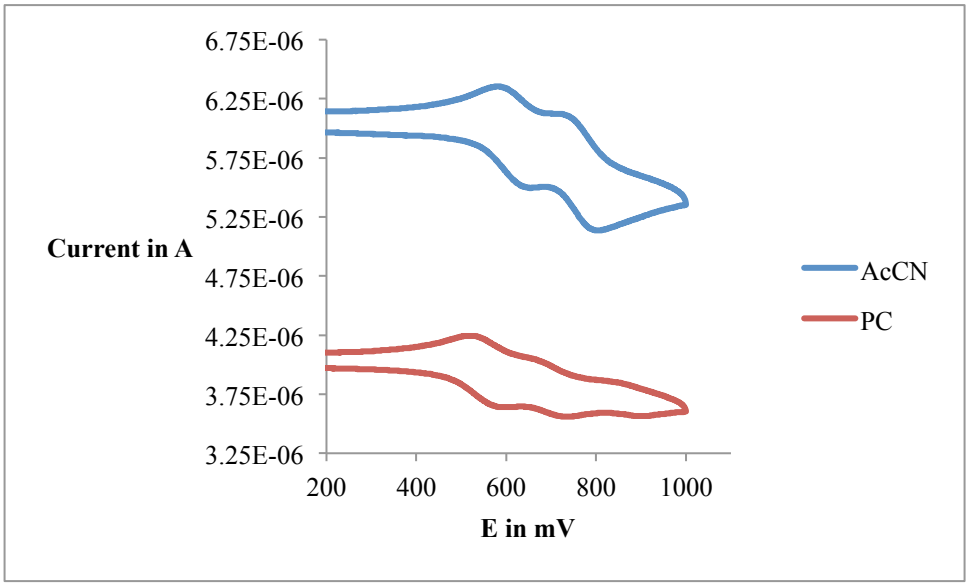

Figure III - 11: Cyclic voltammetry of bis(ferrocenylimino)[2.2]paracyclophane in different solvent systems, acetonitrile (blue), and propylene carbonate (PC) (red). Conditions: 2 mM (pp-FcIDAP) in solvent with 0.1 M NBu_4PF_6 as an electrolyte; platinum as a working electrode, platinum wire as a counter electrode and Ag/AgCl as a reference electrode at 100 mV/S scan rate

The oxidation - reduction potentials for the two separate redox waves for pp-FcIDAP appear to have I_{pa}/I_{pc} current ratios approximately of unity in acetonitrile (AcCN) and propylene carbonate (PC), and the areas under the redox peaks are equivalent. However, in dichloromethane (DCM) and tetrahydrofuran (THF), CV appears to show a single redox wave and I_{pa}/I_{pc} ratio approximately equal to unity. Such behavior could be arising from the low dielectric constants [27]. Solvent effects on internuclear interaction for azo-bridged ferrocene oligomers was studied and explained using the effect of solvents based on their solvent donor number (DN) or acceptor numbers (AN) by electrochemical and spectroscopic methods [28].

Table III – 2: Electrochemical data for bis(ferrocenylimino)[2.2]paracyclophane in acetonitrile (AcCN), dichloromethane (DCM), tetrahydrafuran (THF), and propylene carbonate (PC).

Entry	Solvents	E_{pa1} in mV	E_{pc1} in mV	ΔE^1 in mV	E_{pa2} in mV	E_{pc2} in mV	ΔE^2 in mV
1	AcCN	653	584	69	804	725	79
2	DCM	684	560	124			
3	THF	682	575	107			
5	PC	589	526	63	731	670	61

$\Delta E^1 = E_{pa1} - E_{pc1}$

$\Delta E^2 = E_{pa2} - E_{pc2}$

The electrochemical data is presented in the Table III - 2, which showed two redox waves for AcCN (with ΔE^1 = 69 mV and ΔE^2 = 79 mV) and PC (with ΔE^1 = 63 mV and ΔE^2 = 61 mV), each wave corresponds one electron electrochemical reaction. Such behavior indicates the stability of the [Fc-PC-Fc^+] intermediates in these solvents. While for DCM (with ΔE^1 = 124 mV) and THF (with ΔE^1 = 107 mV) only one redox wave was observed. This behavior could be due to fast disproportionation [Fc-PC-Fc and Fc^+-PC-Fc^+] of the mixed valent compound in these solvents. The higher currents for DCM and THF could be due to absorption onto the electrode surface creating locally high concentrations of electroactive species. This would also be consistent with the large I_{pa} - I_{pc} peak separations while I_{pa}/I_{pc} ratio is near 1.

Based on the above, it can be concluded that there are weak electronic interactions in the mixed valence iron center in ferrocene mediated through the [2.2]paracyclophane. It was therefore desirable to study an oligomeric system based on ferrocenylimino [2.2]paracyclophane before we make attempts to form polymers. As we observed a weak interactions in bis(ferrocenylimine)[2.2]paracyclophane, we would expecting the electronic interactions mediated through [2.2]paracyclophane in case of the polymer to be attenuated further due to geometry constraints and solvation effects .

Synthesis of an oligomer of pseudo-para (ferrocenylimine[2.2]paracyclophane) (pp-FcIDAP):

Synthesis and Characterizations:

The synthesis of an oligo(ferrocenylimine[2.2]paracyclophane) was attempted by condensation reaction of a 2:1 equivalent ratio of 1,1'-ferrocenyl dicarboxaldehyde and 4,12-diamino[2.2]paracyclophane at room temperature as shown in Scheme III - 3. The solution of 1,1'-ferrocenyl dicrboxaldehyde was prepared in MeOH and stirred until all the solid dissolved. A solution of 4,12-diamino[2.2]paracyclophane in MeOH / toluene (3:1 v/v) was added drop-wise over a period of 2-4 minutes. The MeOH/toluene mixture was used to make reaction mixture soluble, as pseudo-para-4,12-diamino[2.2]paracyclophane is soluble in toluene and not well soluble in MeOH. This reaction mixture was stirred for 3 hours at room temperature. During the first hour of the reaction the solution turned a greenish-brown color and was allowed to stir for another two hours for reaction completion. The solvent was evaporated and the brown product was collected.

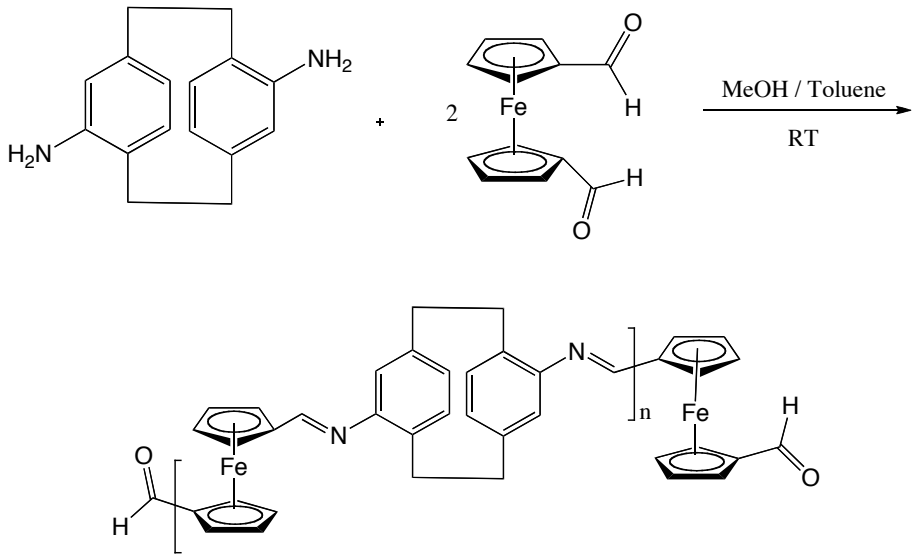

Scheme III - 3: Synthesis of an oligomer of pseudo-para-(ferrocenylimine[2.2]paracyclophane); (n=1)

^{1}H NMR and IR were used to characterize the final product. The FT-IR spectrum showed imine formation from the condensation reaction between 1,1'-ferrocene dicarboxaldehyde and pp-4,12-diamino[2.2]paracyclophane [29]. The characteristic peak for Schiff bases (C=N) stretching absorption appeared at 1622 cm^{-1}. Peaks at 2924 cm^{-1} are attributed to C-H stretching vibrations of the ethylene bridges and the peak at 1402 cm^{-1} can be assigned to C=C stretching vibrations of cyclopentadienyl groups. A peak at 1683 cm^{-1} corresponds to the C=O of the ferrocene carboxaldehyde.

The oligomer was characterized using ^{1}H NMR spectroscopy in deuterated acetonitrile, as deuterated chloroform showed only partial solubility for the oligomer, as shown in Figure III -12. The NMR spectra also confirmed the presence of ferrocene carboxaldehyde peaks at ca. 9.86 ppm

as well as imine peaks at 8.14 ppm which is consistent with ferrocenyl oligomer end capped with ferrocenyl carboxaldehyde [30]. However, the proton ratio for imine to aldehyde peaks (2 : 1) suggested a mixture of the possible structures shown in Figure III -13.

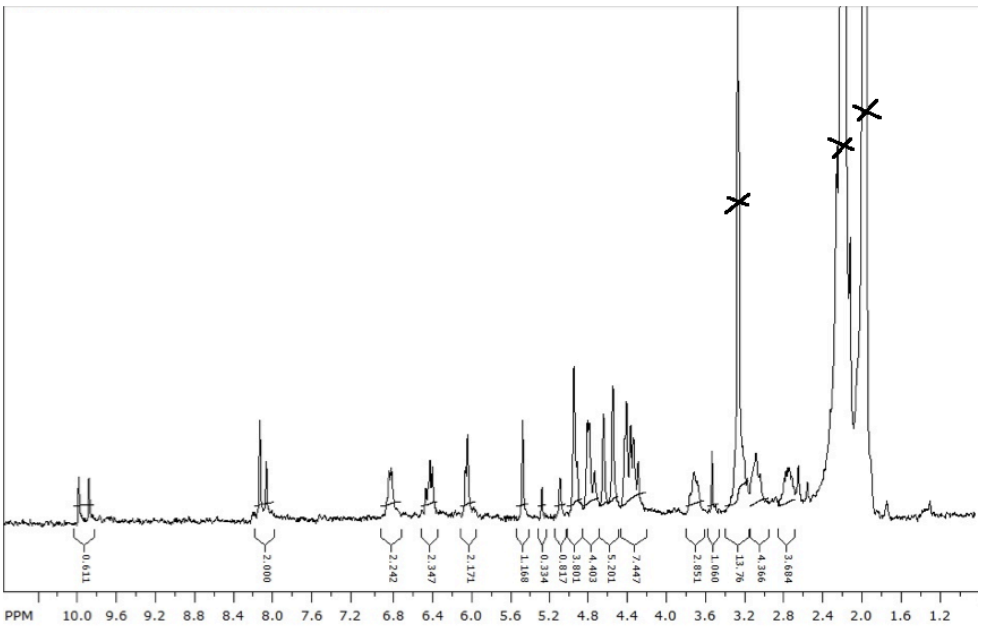

Figure III – 12: ^{1}H NMR of an oligo(ferrocenylimine[2.2]paracyclophane) in deuterated acetonitrile

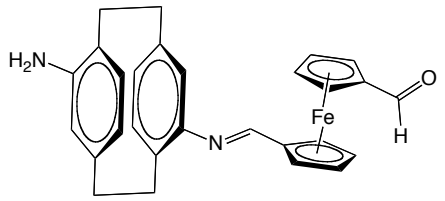

[APC-Fc-CHO]

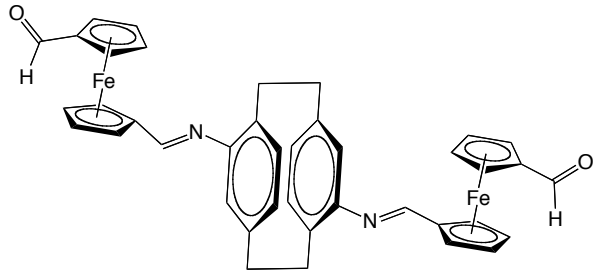

[CHO-Fc-DAP-Fc-CHO]

Figure III – 13: Possible structures for the oligomer of pseudo-para-(ferrocenylimine[2.2]paracyclophane) (pp-FcIDAP)

UV-vis:

The UV-vis spectrum for the oligomer, using dichloromethane as solvent is shown in Figure III -14. Poly(pp-FcIDAP) is dark brown in color, which showed characteristic bands at 235 nm , 360 nm, and 505 nm in the UV-vis spectrum. When compared with the ferrocene dimer of pp-4,12-diamino[2.2]paracyclohane the band at 450 is red shifted to 505 nm in case of the poly(pp-FcIDAP). This red shift could possibly due to the increased through space π-system interactions.

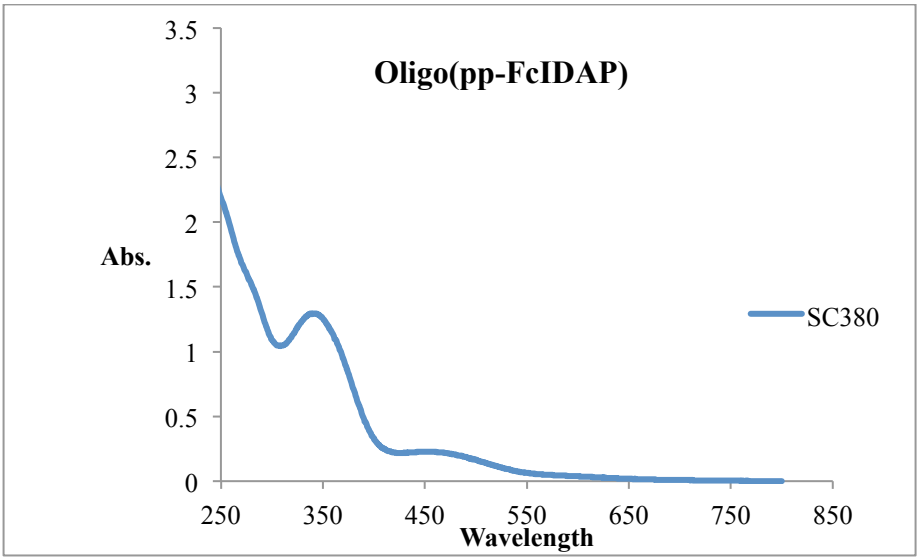

Figure III – 14: UV-vis spectrum of oligo(4,12-bis(ferrocenylimine)[2.2]paracyclophane) in dichloromethane

Electrochemical analysis:

Cyclic voltammetry for the oligo(4,12-bis(ferrocenylimine)[2.2]paracyclophane was carried out by dissolving it in AcCN/dichloromethane (1:1 v/v) with 0.1 M $N(Bu)_4PF_6$ as an electrolyte. The cyclic voltammagram shown in Figure III – 15, showed three quasi-reversible redox features for the oligomer. The electrochemical data for these peaks are given in the Table III – 3.

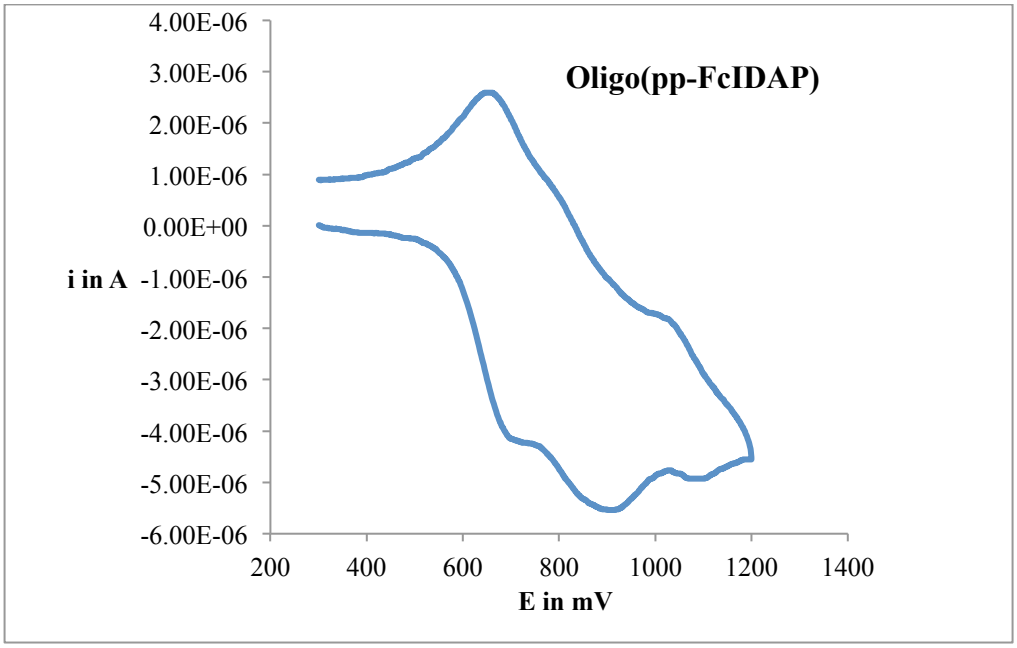

Figure III – 15: Cyclic Voltammetry of oligo(4,12-bis(ferrocenylimine)[2.2]paracyclophane) Conditions: 2 mM oligo(pp-FcIDAP) in acetonitrile solvent with 0.1 M NBu_4PF_6 as an electrolyte; platinum as a working electrode, platinum wire as a counter electrode and Ag/AgCl as a reference electrode at 100 mV/S scan rate

Table III – 3: Electrochemical data for oligo(pp-FcIDAP)

Oxidation Potential in mV		Reduction Potential in mV		$E_{1/2}$ in mV	ΔE_p in mV
E_{pa1}	710	E_{pc1}	655	683	55
E_{pa2}	890	E_{pc2}	790	840	100
E_{pa3}	1092	E_{pc3}	1022	1057	70

Cyclic voltammetry for oligo(pp-FcIDAP) was taken at different scan rate as shown in Figure III -16, and showed the similar features at all the different scan rates.

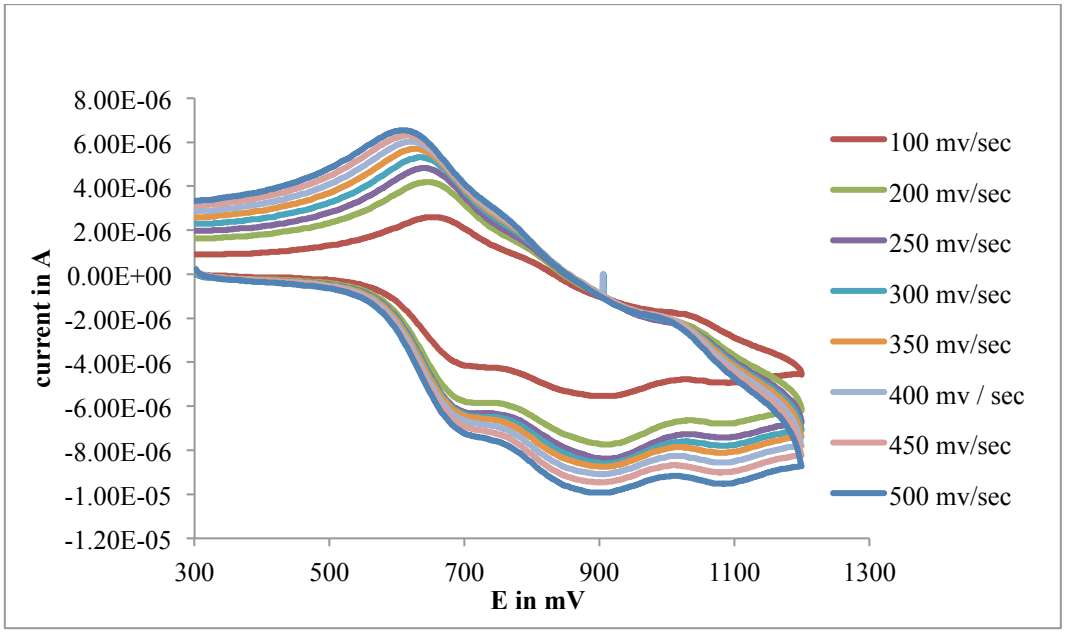

Figure III – 16: Cyclic voltammetry of oligo(4,12-bis(ferrocenylimine)[2.2]paracyclophane at different scan rate. Conditions: 2 mM oligo(pp-FcIDAP) in acetonitrile solvent with 0.1 M NBu_4PF_6 as an electrolyte; platinum as a working electrode, platinum wire as a counter electrode and Ag/AgCl as a reference electrode.

In general, in cyclic voltammetry for the reversible ferrocene – ferrocenium couple, the potential difference between the cathodic wave and the anodic wave ΔE_p is ca. 59 mV/ n, where n corresponding to the number of electrons involved in the electrochemical reaction. In Figure III – 21, three redox waves at $E_{1/2}$, 683 mV, 840 mV, and 1057 mV showed the potential differences ΔE_p of 55 mV, 100 mV, and 70 mV, respectively. To understand the electrochemical behavior of this oligomer, it is helpful to compare its behavior

with the electrochemical behavior of the monoferrocenyl imine and bis(ferrocenylimine) [2.2]paracyclophane compounds.

Comparison of 4-ferrocenylimine[2.2]paracyclophane (FcIAPC), pp-4,12-bis(ferrocenylimine)[2.2]paracyclophane (pp-FcIDAP), and 1,1'-ferrocene dicarboxaldehyde (FcDCA) was made with an oligo(4,12-bis(ferrocenylimine)[2.2]paracyclophane by using electrochemistry as shown in Figure III -17 and Table III – 4.

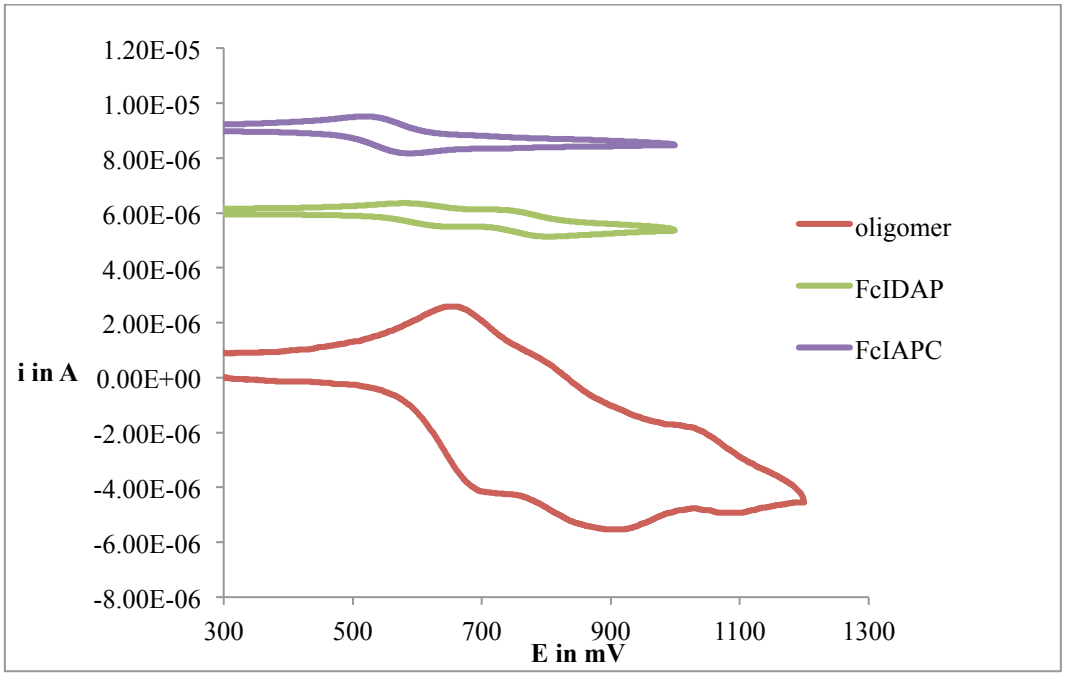

Figure III – 17: Comparison of CVs for monoferrocenylimine, bis(ferrocenylimine) and oligomer.

Table III – 4: Electrochemical data of FcDCA, FcIAPC, pp-FcIDAP and poly(pp-FcIDAP)

Compounds	$E_{1/2}(1)$ in mV	ΔE1 in mV	$E_{1/2}(2)$ in mV	ΔE2 in mV	$E_{1/2}(3)$ in mV	ΔE3 in mV
FcDCA	-	-	-	-	1010	90
FcIAPC	650	52	-	-	-	-
pp-FcIDAP	619	70	766	79	-	-
oligo(pp-FcIDAP)	683	55	840	100	1057	70

From the electrochemical data it can be seen that the first oxidation potential of pp-FcIDAP is lowered relative to that of the FcIAPC, which can be due to the additive electron donating nature of the [2.2]paracyclophane and other ferrocene moiety attached at pseudo-para position of the second ring of the [2.2]paracyclophane.

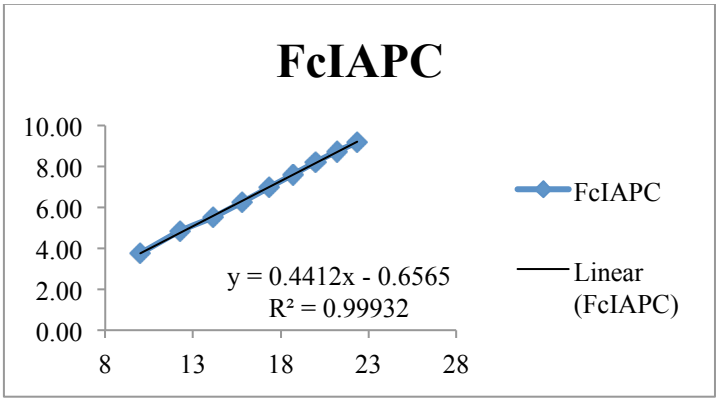

Figure III – 18: Square root of scan rate vs current at first oxidation potential of FcIAPC. Conditions: 2 mM FcIAPC in acetonitrile solvent with 0.1 M NBu_4PF_6 as an electrolyte; platinum as a working electrode, platinum wire as a counter electrode and Ag/AgCl as a reference electrode

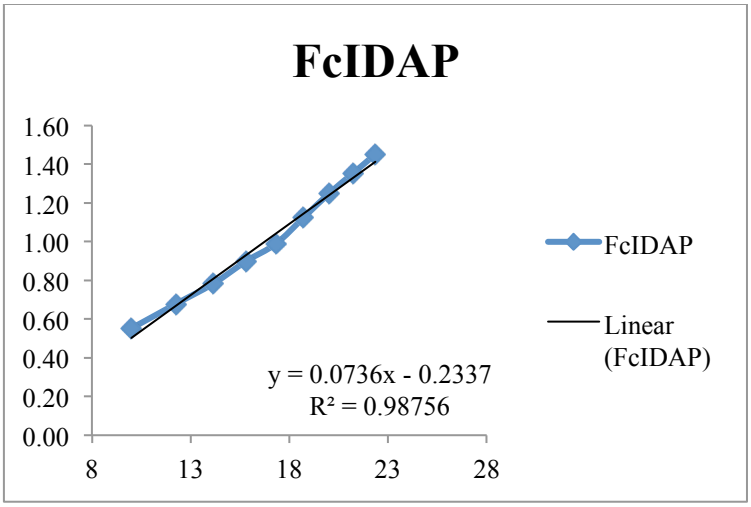

Figure III – 19: Square root of scan rate vs current at first oxidation potential of pp-FcIDAP. Conditions: 2 mM (pp-FcIDAP) in acetonitrile solvent with 0.1 M NBu_4PF_6 as an electrolyte; platinum as a working electrode, platinum wire as a counter electrode and Ag/AgCl as a reference electrode

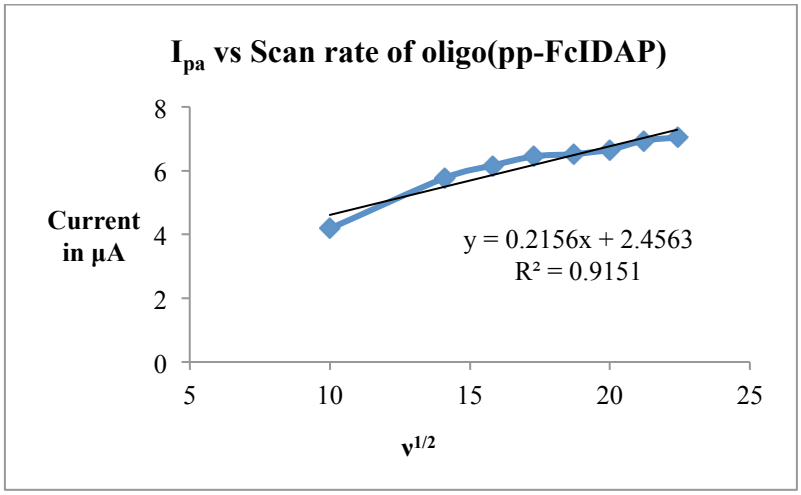

Figure III – 20: Plot of scan rate vs first oxidation peak current for oligo(4,12-bis(ferrocenylimine)[2.2]paracyclophane). Conditions: 2 mM oligo(pp-FcIDAP) in acetonitrile solvent with 0.1 M NBu_4PF_6 as an electrolyte; platinum as a working electrode, platinum wire as a counter electrode and Ag/AgCl as a reference electrode

When FcIAPC and pp-FcIDAP are compared for their electrochemical behavior with respect to scan rate, as seen in Figure III – 18 and Figure III – 19 respectively, the linearity of the relationship between the squre root of the scan rate ($\nu^{1/2}$) Vs. current for the pp-FcIDAP is lower. This could be possibly due to a diffusion-controlled process which is limited after reaching a 250 mV/S scan rate. Similar analysis of the first oxidation potential for the oligomer showed diffusion limitations after the 100 mV/S, as shown in Figure III - 20. This suggests there is an increasing tendency toward absorption onto the electrode surface as the molecules get larger and may reflect their increasing insolubility.

For the oligomer, the first oxidation potential ($E_{1/2}$ = 683 mV) of oligomer is higher than the pp-FcIDAP and FcIAPC, which could suggest the electron withdrawing group carbaldehyde endcapping the [APC-Fc-CHO]. But the redox potential of FcDCA (1010 mV) is much higher than the first redox potentials of the oligomer, which suggest the additive electronic contribution of ferrocenyl imine and endcapped carbaldehyde groups [31].

While the redox stability of the bisferrocenylimino compound (pp-FcIDAP) appeared to be promising, the interaction between the two ferrocene units was shown to be weaker. This is possibly due to localization of unpaired spin density on the iron atoms and may be further decrease by conformational twisting to lower interactions with the [2.2]paracyclophane core. Studies of an analogous oligomeric system were consistent with the data for the smaller molecule analogues but reactivity and solubility difficulties already manifested themselves. The above factors suggested that both the synthesis of the polymer

would be problematic and that the resulting polymer would not have the interesting properties that had been hoped for. Nonethless, several attempts to synthesize and characterize the polymer were made.

Polymer Synthesis:

The formation of a ferrocenylimino-[2.2]paracyclophane polymer [poly(pp-FcIDAP)] was attempted by a condensation polymerization process as shown in Scheme III – 4.

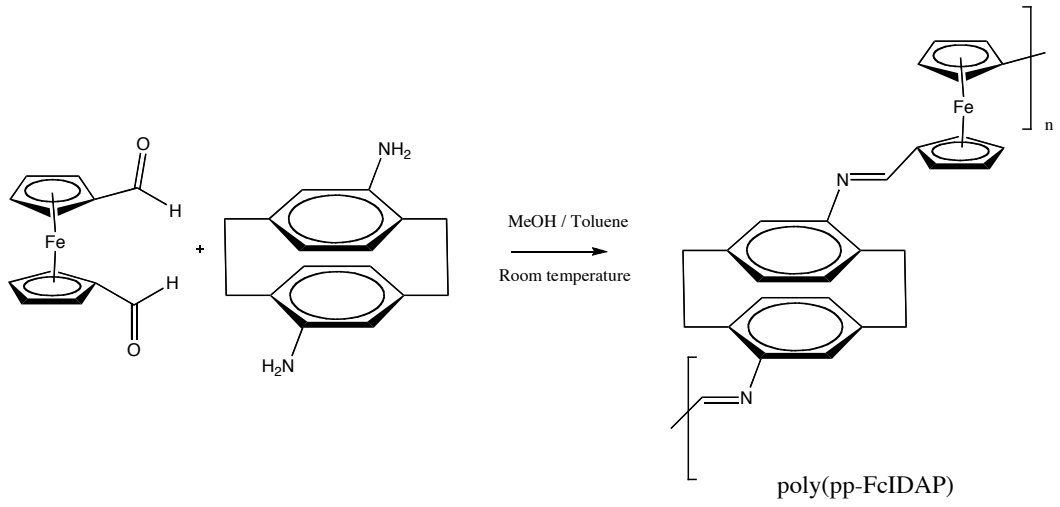

Scheme III – 4: Ferrocenylimine [2.2]paracyclophane polymer [poly(pp-FcIDAP)]

One equivalent of 1,1'-ferrocenyldicarboxaldehyde was dissolved in the methanol. One equivalent of pseudo-para-4,12-diamino[2.2]paracyclophane was dissolved separately in toluene / methanol mixture to solubilize it and added to the methanolic reaction mixture of 1,1'-ferrocenyldicarobxaldehyde. This reaction was stirred at room temperature, as ferrocene dicarboxaldehyde is very reactive towards pp-4,12-diamino[2.2]paracyclophane. The initial dark red

solution changes its color to dark brown solution. The precipitate that was formed after 3 hours was collected by filtration and rinsed with the methanol/toluene mixture. The melting point of the precipitate was observed to be more than 300° C. Further this solid product was characterized by ^{1}H NMR, IR and UV – visible spectroscopy. No peaks were observed in the ^{1}H NMR suggesting some oxidation to paramagnetic Fe^{3+} had already occured. IR spectroscopy showed the characteristic peak for azomethine (C=N) at 1620 cm-1 and the peak for the C=O (at 1685 cm-1) was not observed, suggesting the Schiff's base formation. The UV-visible spectroscopy of precipitate was taken in chloroform, as shown in Figure III - 21, which sowed partial solubility and showed the absorption at λmax 370 nm, which was assigned to ligand field d-d transition for the ferrocene.

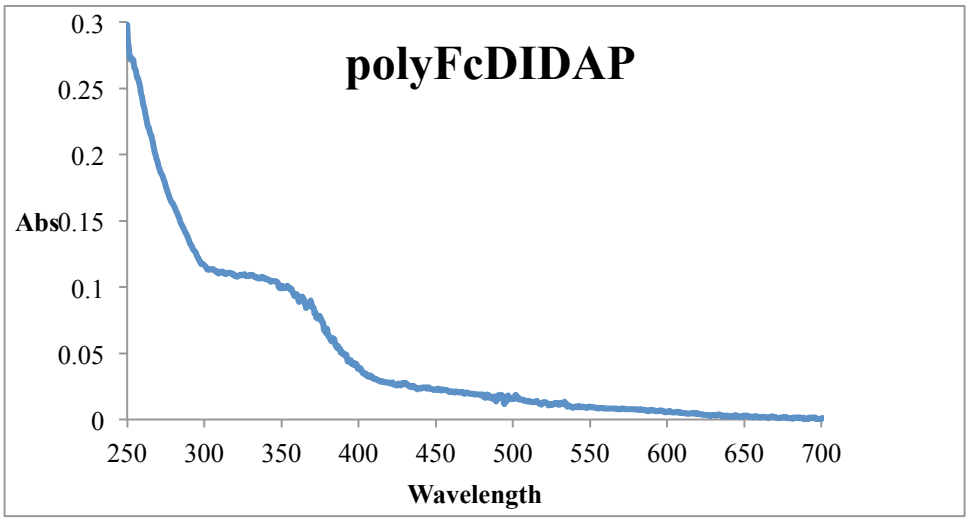

Figure III – 21: UV – visible spectroscopy of Poly (pp-FcIDAP) in chloroform

Attempts were made to study the electrochemistry of the poly(pp-FcIDAP) by dissolving in acetonitrile and 0.1 M NBu_4PF_6 electrolyte but significant redox behavior could not detected.

Conclusion:

We have prepared pp-4,12-bis(ferrocenylimino)[2.2]paracyclophane (pp-FcIDAP) and also attempted to synthesize its polymer analogue. We studied electronic interactions between the iron centers in ferrocene through the [2.2]paracyclophane using UV-vis spectroscopy and electrochemistry. From the UV-vis studies we observed that the absorption band near 400 – 500 nm is red shifted when monomeric ferrocene unit (FcIAPC) is changed to dimeric ferrocene unit (pp-FcIDAP). From the electrochemical data we could analyze the electronic interactions by determining the comproportionation constant, which showed weak interactions through the [2.2]paracyclophane moiety for pp-FcIDAP. Attempts to synthesize the polymeric analogue proved problematic and characterization of the resulting materials was not very fruitful.

Experimental Section:

Synthesis of 4,12-Bis(ferrocenylimine)[2.2]paracyclophane (pp-FcIDAP):

1-Ferrocenecarboxaldehyde (45 mg, 0.21 mmol) was dissolved with stirring in 3 ml of ethanol in a round bottom flask. 4,12-diamino[2.2]paracyclophane 25 mg (0.11 mmol) was introduced in this solution. A reflux condenser was attached to the flask and the reaction mixture was heated to reflux solvent for 18 hours. The reaction mixture was cooled to room temperature and dried under reduced pressure. The gooey product was mixed with chloroform and an uncharacterized precipitate was removed by filtration. The chloroform fraction was evaporated under reduced pressure to yield 28 mg of a red solid (percent yield 40% based on pp-4,12-diamino[2.2]paracyclophane) product (M. P. = more than 300° C).

^{1}H NMR data (300 MHz, $CDCl_3$): δ 8.09 (s, 2H), 6.84 (d, 2H), 6.35 (d, 2H), 5.87 (s, 2H), 4.91 (s, 2H), 4.83 (s, 2H), 4.49 (s, 4H), 4.29 (s, 9H), 3.78 (ddd, 2H), 3.30 (ddd, 2H), 3.05 (ddd, 2H), 2.72 (ddd, 2H).

FTIR (KBr pellet, cm^{-1}): 3400.5, 3117.9, 2925.6, 1653.0, 1617.8, 1401.8, 1103.8, 1021.3, 815.41, and 498.1.

Synthesis of oligo(4,12-bis(ferrocenylimine)[2.2]paracyclophane) (oligo(pp-FcIDAP):

In a 100 ml round bottom flask, 20 mg (0.0826 mmol) of 1,1-ferrocene dicarboxaldehyde and 2ml MeOH were introduced. The mixture was stirred to dissolve the solid. In a separate test tube 9.38 mg (0.0413 mmol) of 4,12-

diamino[2.2]paracyclophane was mixed with 1 ml of MeOH and 1 ml of toluene to dissolve it. This mixture was added drop-wise to the methanolic solution of 1,1'-ferrocenedicarboxaldehyde and stirred at room temperature. This reaction mixture was stirred for 3 hours. After an hour stirring the reaction mixture color changes to a dark brown solution. The reaction mixture was then dried under reduced pressure and the brown solid product (18 mg) was collected (M. P. = more than 300° C).

^{1}H NMR data (300 MHz, d-DMSO): 9.86, 8.14, 6.69, 6.37, 6.00, 4.90, 4.81, 4.37, 4.22, 4.15, 3.89, 2.72.

FTIR (KBr pellet, cm^{-1}): 3448, 3121, 2924, 1684, 1659, 1622, 1402, 1229, 1105, 1040, 968, 820, 739, and 664.

1H NMR of pp-FcIDAP

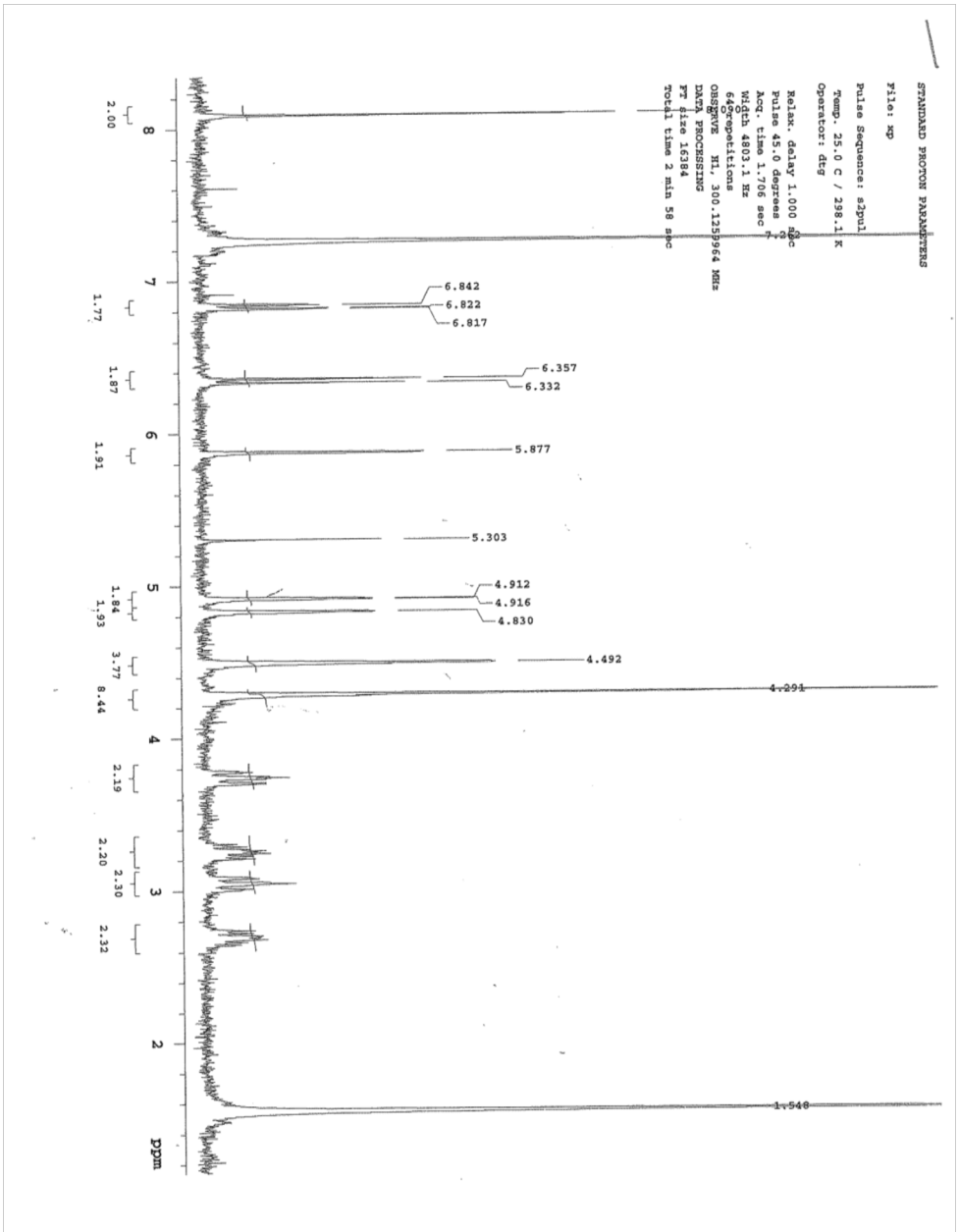

^{1}H NMR of oligo(pp-FcIDAP)

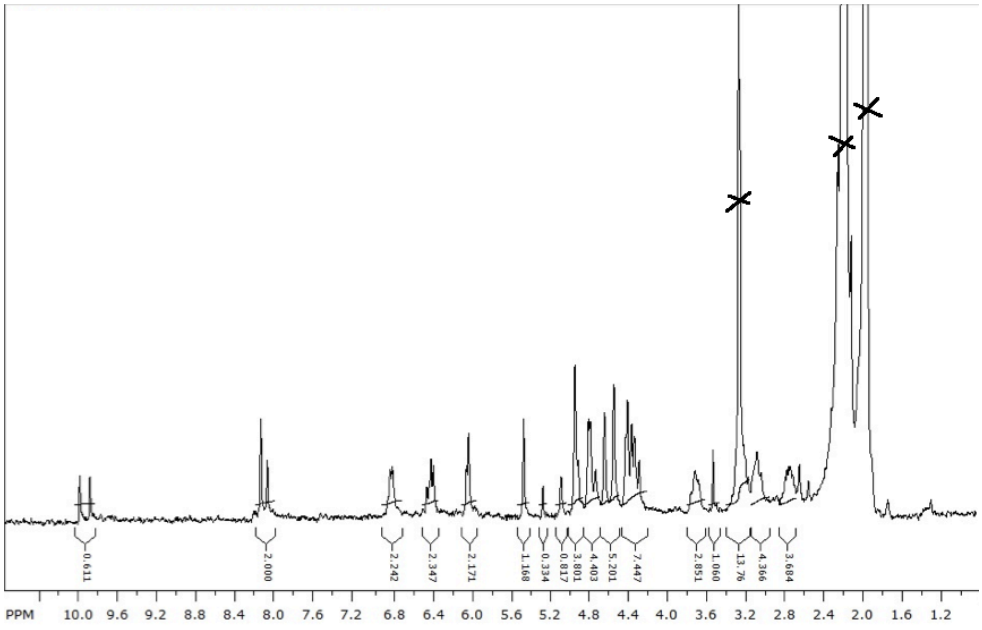

References:

1. Morisaki, Y. and Y. Chujo, *Cyclophane - Containing Polymers. Prog. Polym. Sci.*, 2008. **33**: p. 346 - 364.

2. Akira Izuoka, S.M., Tadashi Sugawara, and Hiizu Iwamura, *Molecular Design and Model Experiments of Ferromagnetic Intermolecular Interaction in the Assembly of High-Spin Organic Molecules. Generation and Characterization of the Spin states of Isomeric Bis(phenylmethylenyl)[2.2]paracyclophanes.* J. Am. Chem. Soc, 1987. **109**: p. 2631 - 2639.

3. McConnell, H.M., *Ferromagnetism in Solid Free Radicals.* The Journal of Chemical Physics, 1963. **39**(7): p. 1910-1910.

4. Izuoka, A., *Molecular design and model experiments of ferromagnetic intermolecular interaction in the assembly of high-spin organic molecules. Generation and characterization of the spin states of isomeric bis(phenylmethylenyl)[2.2]paracyclophanes.* Journal of the american chemical society, 1987. **109**(9): p. 2631-2639.

5. Akira Izuoka, S.M., Tadashi Sugawara, and Hiizu Iwamura, *Ferro- and Antiferromagnetic Interaction between Two Diphenylcarbene Units Incorporated in the [2.2]Paracyclophane Skeleton.* J. Am. Chem. SOc., 1985. **107**: p. 1786-1787.

6. Neugebauer, F.A. and H. Fischer, *Verdazyls. Part 30.1 N-I ,N-I '-Linked Biverdazyls (Bis-1,2,3,4-tetrahydro-s-tetrazin-1-yls) with a [2.2]Paracyclophanylene Bridge.* J. Chem. Soc., Perkin Trans. , 1981. **2**: p. 896 - 900.

7. Zyss, J., *Through-Space Charge Transfer and Nonlinear Optical Properties of Substituted Paracyclophane.* J. Am. Chem. Soc, 2000. **122**(48): p. 11956 - 11962.

8. Wartini, A.R., *Intramolecular Electron Transfer between 2,5-Dimethoxy-1,4-phenylene Units in [n.n]Paracyclophane Radical Cations.* Eur. J. Org. Chem., 1998: p. 139 - 148.

9. Salhi, F., *Influence of π-Stacking on the Redox Properties of Oligothiophenes: (α-Alkyloligo-thienyl)para[2.2]cyclophanes.* Organic Letters, 2002. **4**(19): p. 3195 - 3198.

10. Nelsen, S.F., A.E. Konradsson, and J.P. Telo, *Pseudo-para-dinitro[2.2]paracyclophane Radical Anion, a Mixed-Valence System Poised on the Class II/Class III Borderline.* J. Am. Chem. Soc, 2005. **127**(3): p. 920 - 925.

11. Ball, P., et al., *Binuclear Rhenium(I) Complexes with Bridging [2.2]Paracyclophane-Diimine Ligands: Probing Electronic Coupling through π-π Interactions.* Inorg. Chem., 2004. **43**: p. 622 - 632.

12. Richardson, D.E. and H. Taube, *Determination of E20-E10 in Multistep Charge Transfer by Stationary-Electrode Pulse and Cyclic Voltammetry: Application to Binuclear Ruthenium Ammines.* Inorg. Chem., 1981. **20**(4): p. 1278 - 1285.

13. Sutton, J.E., P.M. Sutton, and H. Taube, *Determination of the Comproportionation Constant for a Weakly Coupled Mixed-Valence System by Titration of the Intervalence Transfer Band: μ- (4,4'-Bipyridy1)-bis(pentaammineruthenium) (5+).* Inorg. Chem., 1979. **18**(4): p. 1017 - 1021.

14. Buda, M., *Electrosynthesis and coordination chemistry of poly(ferrocene–bipyridyl) films.* Journal of Electroanalytical Chemistry, 2000. **484**: p. 164 - 171.

15. Iwamura, H., *Organic - Synthetic and Supramolecular Approaches to Free Radical - Based Magnets. Proc. Japan Acad.*, 2005. **81** (Ser. B): p. 233 - 243.

16. Pittman Jr. C. U., *Polymerization of Ferrocenylmethyl Acrylate and Ferrocenylmethyl Methacrylate. Characterization of Their Polymers and Their Polymeric Ferricinium Salts. Extension to Poly(ferrocenylethylene).* Macromolecules, 1970. **3**(6): p. 746 - 754.

17. Cowan, D.O., *Organic solid state. VII. Semiconducting polymers. Mixed valence ferrocene-ferricenium polymers.* J. Am. Chem. Soc, 1972. **94**(14): p. 5110 - 5112.

18. Flanagan, J.B., *Electron transfer to and from molecules containing multiple, noninteracting redox centers. Electrochemical oxidation of poly(vinylferrocene).* J. Am. Chem. Soc, 1978. **100**(13): p. 4248 - 4253.

19. Brown, G.M., *Oxidation - State and Electron - Transfer Properties of Mixed - Valence 1,1' -Polyferrocene Ions.* Inorg. Chem., 1975. **14**(3): p. 506 - 511.

20. Gray, H.B., Y.S. Sohn, and N. Hendrickson, *Electronic Structure of Metallocenes.* J. Am. Chem. Soc, 1971. **93**(15): p. 3603 - 3612.

21. Tanaka Y., *Redox-active Polyiron Complexes with Tetra(ethynylphenyl)ethene and [2,2]Paracyclophane Spacers Containing Ethynylphenyl units: Extension to Higher Dimensional Molecular Wire. Dalton Trans.*, 2007. **0**: p. 928 - 933.

22. Creutz, C., *Mixed Valence Complexes of d5-d6 Metal Centers*, in *Progress in Inorganic Chemistry*2007, John Wiley & Sons, Inc. p. 1-73.

23. Kaim, W., A. Klein, and M. Glöckle, *Exploration of Mixed-Valence Chemistry: Inventing New Analogues of the Creutz-Taube Ion.* Accounts of Chemical Research, 2000. **33**(11): p. 755-763.

24. Robin, M.B. and P. Day, *Mixed Valence Chemistry-A Survey and Classification*, in *Advances in Inorganic Chemistry and Radiochemistry*, H.J. Emeléus and A.G. Sharpe, Editors. 1968, Academic Press. p. 247-422.

25. Roué, S., C. Lapinte, and T. Bataille, *Organometallic Mixed-Valence Systems. Electronic Coupling through an Alkyndiyl Bridge Incorporating Methylene Groups.* Organometallics, 2004. **23**(11): p. 2558-2567.

26. Gennett, T., D.F. Milner, and M.J. Weaver, *Role of Solvent Reorganization Dynamics in Electron Transfer Processes. Theory - Experiment Comparisons for Electrochemical and Homogeneous Electron Exchange Involving Metallocene Redox Couples.* J. Phys. Chem., 1985. **89**: p. 2787 - 2794.

27. Rieger, P.H., *Electrochemistry*1987: Prentice-Hall Inc.

28. Kurosawa, M., et al., *Synthesis of Azo-Bridged Ferrocene Oligomers and a Polymer and Electrochemical and Optical Analysis of Internuclear Electronic*

Interactions in Their Mixed-Valence States. Inorganic Chemistry, 1999. **38**(22): p. 5113-5123.

29. Abd-Elzaher, M.M., *Synthesis and Spectroscopic Characterization of Some Ferrocenyl Schiff Bases Containing Pyridine Moiety and Their Complexation with Cobalt, Nickel, Copper and Zinc.* Journal of the Chinese Chemical Society, 2004. **51**(3): p. 499 - 504.

30. Ossola, F., et al., *Synthesis, structure and properties of new ferrocene-containing compounds.* Inorganica Chimica Acta, 2003. **353**(0): p. 292-300.

31. Mahmoud, K. and H.-B. Kraatz, *Synthesis and Electrochemical Investigation of Oligomeric and Polymeric Ferrocenyl-Amides having Cyclohexyl, Phenylene, and Lysyl Spacers.* Journal of Inorganic and Organometallic Polymers and Materials, 2008. **18**(1): p. 69-80.

Chapter IV

[2.2]Paracyclophane-based Ligand Copper (II) Complexes: Synthesis and Investigation of Electronic Interactions

Introduction:

This chapter will include the preparation and characterization of electronic and steric interactions in [2.2]paracyclophane-based Schiff's base ligands, their copper complexes, and finally explore the possibility of synthesizing polymeric metal complexes. The majority of research in polymers has focused on purely organic polymers for variety of applications but interest in organometallic polymers continues to grow. Polysiloxanes started to be used commercially in the 1940s and contain an inorganic backbone (Si). Other polymers, which contain mixed inorganic-organic elements in the polymer backbones, include polyphosphazenes, polysilanes, organometallic polymers such as poly(vinylferrocene), and coordination polymers that have coordinate covalent bonds to metals in the polymer backbone [1].

Coordination polymers, a subset of organometallic polymers, can be formed either by coordination of metals with organic ligands to form a polymer, or by reaction of a coordination complex with an already formed polymer. Three common routes for the synthesis of coordination polymers are given below [2]:

- Polymerization of metal complexes through functional groups, where the actual polymer forming step involves condensation or addition reactions as shown in Scheme IV – 1.

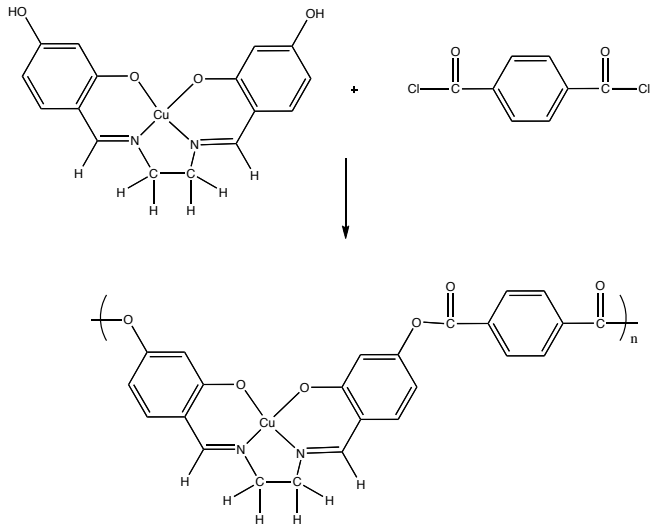

Scheme IV – 1: Polymerization of a metal complex through functional groups

- Coordination of a metal ion by a polymer containing chelating groups as shown in Scheme IV – 2

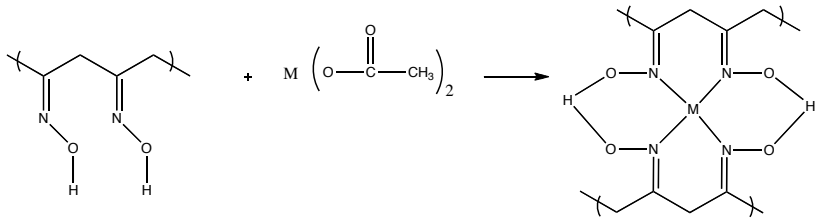

Scheme IV – 2: Coordination of metal ions through polymer containing chelating groups

- Polymerization through metal-donor atom coordination as shown in Scheme IV - 3.

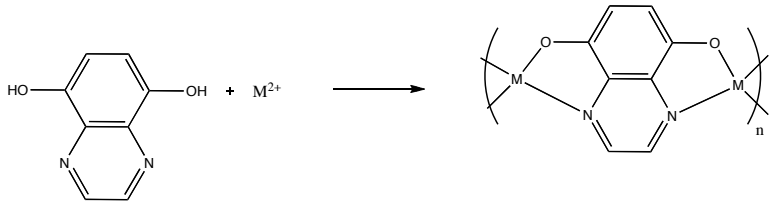

Scheme IV – 3: Metal-donor coordination polymer

There are number of condensation polymers that have been used commercially, such as polyimines, polyamides such as Nylon 66 and poly(p-phenyleneterephthalamide) (Kevlar), polyurethanes, etc. [1]. Polyimines are also called azomethine or Schiff's base polymers, which are prepared by condensation reaction of aldehydes with amines with the loss of water as shown in Scheme IV - 4.

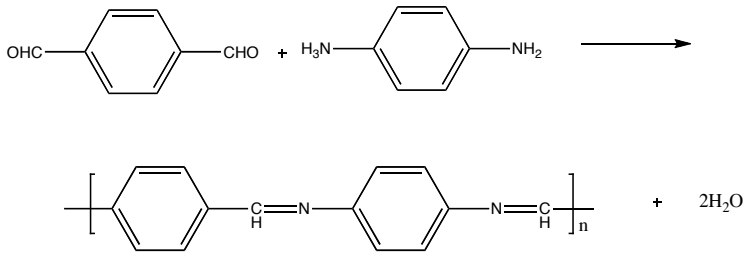

Scheme IV – 4: Polyimines synthesis

Polymers containing imine linkages are useful as chelating agents in preparing coordination polymers. An example of such a polymer is given in Figure IV – 1.

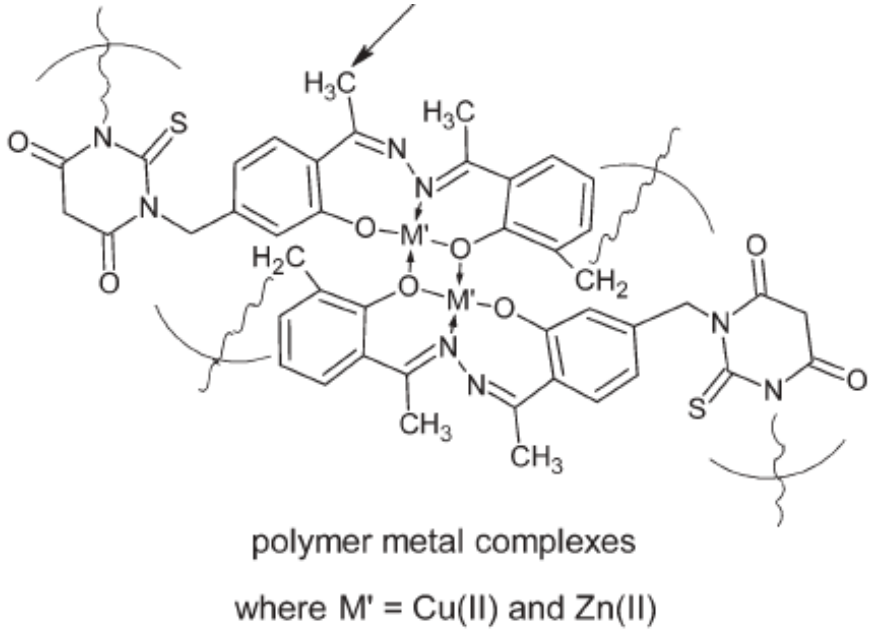

Figure IV – 1: Metal coordination polymer

The use of [2.2]paracyclophane as a scaffold for constructing chiral ligands has shown promising results in catalytic asymmetric syntheses [3]. Before going into the use of planar chirality of the [2.2]paracyclophane in asymmetric synthesis, it will useful to explain the stereochemical notation adopted for [2.2]paracyclophane [4]. As discussed earlier in the introduction chapter, when the substituent is attached to one of the ethano bridges, the derivative is called centrally chiral, while when the substituent is attached to one of the benzene rings then the derivative possesses planar chirality. In this chapter we will consider the planar chirality of [2.2]paracyclophane derivatives where substituents are attached to the benzene rings of the [2.2]paracyclophane. For example in Figure IV – 2 the stereochemical assignments are shown for a

carboxy mono-substituted [2.2]paracyclophane and a formyl and hydroxy disubstituted [2.2]paracyclophane.

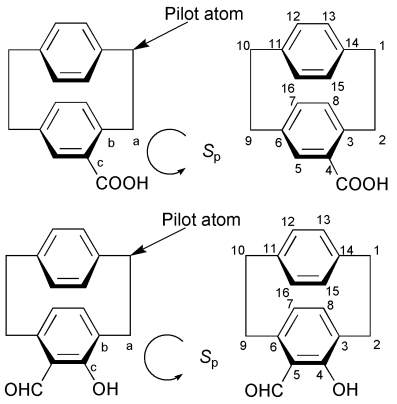

Figure IV – 2: Stereochemical notation of substituted [2.2]paracyclophane

According to Cahn-Ingold-Prelog (CIP) system a pilot atom, a point from which the chiral plane is viewed, as can be seen in Figure IV - 2, was selected for the molecules containing a plane of chirality. From the pilot atom, which is the out-of-plane atom closest to the chiral plane, the next three consecutive atoms were selected, labeled as *a*, *b* and *c* as shown in the Figure IV - 2, in the chirality plane, and the atom of the highest priority (CIP rule) is selected for the basis of counterclockwise or clockwise directions for the assignment of S_p or R_p configurations [5]. The subscripts *p* denotes the plane of chirality. For the di-substituted system with substituents on the same benzene ring of the [2.2]paracyclophane, numbering continues from the pilot atom towards the atom with higher priority atom and then around the paracyclophane unit, and it is identified as having either *Rp* or *Sp* chirality. The di-substituted example given in Figure IV -2 can be identified as (Sp)-5-formyl-4-hydroxy-

[2.2]paracyclophane. For substituents on both benzene rings, in case of di-substituted [2.2]paracyclophane, as shown in Figure IV - 3, either plane can be chosen to assign the stereo-chemical description [6].

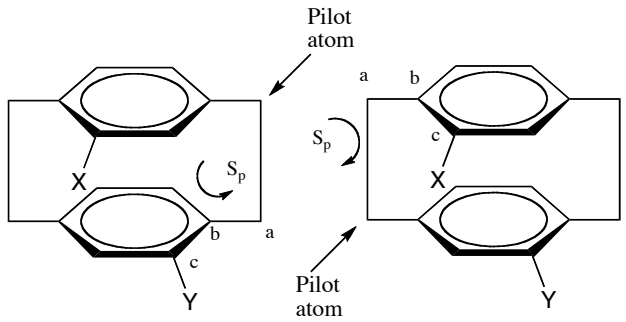

Figure IV – 3: Stereochemical description of [2.2]paracyclophane

A planar chiral [2.2]paracyclophane has been successfully used in rhodium catalyzed asymmetric hydrogenation reactions under mild conditions with high enantionselectivity [7]. In this case, [2.2]PHANEPHOS (4,12-bis(diphenylphosphino)[2.2]paracyclophane was used as a ligand to coordinate with rhodium, facilitating 1,4-reduction of dehydroamino acid methyl esters under mild conditions as shown in Scheme IV – 5, with high enantioselectivity (> 94 % ee).

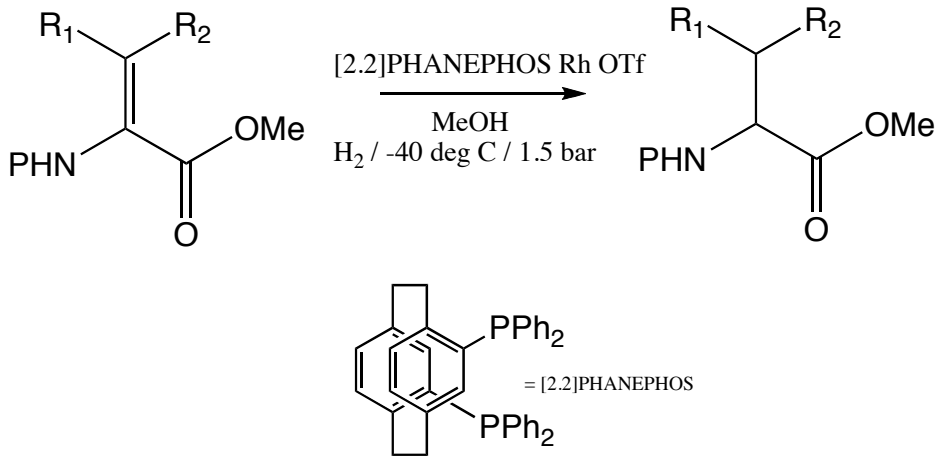

Scheme IV – 5: Enantioselective hydrogenation of dehydroamino acid methyl esters using [2.2]PHANEPHOS

Similar hydrogenation reactions were carried out using a ruthenium (II) catalyst system with [2.2]PHANEPHOS as a ligand for the asymmetric hydrogenation of β-keto esters [8].

Novel planar-chiral salen ligands based on the [2.2]paracyclophane analogue of salicylaldehyde (4-formyl-5-hydroxy[2.2]paracyclophane) and both achiral and chiral diamines have been synthesized and studied for their applications in asymmetric synthesis as shown in Scheme IV - 6 [9, 10].

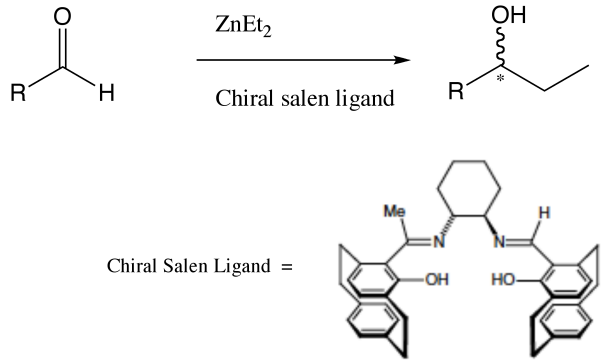

Scheme IV – 6: Dialkylzinc addition to aldehyde using[2.2]paracyclophane based chiral salen ligand.

[2.2]Paracyclophane based ketimine ligands have successfully been used in asymmetric catalytic dialkylzinc addition to imines to give high yield and high enantioselectivity[11, 12].

Bolm and Whelligan reported the synthesis of other examples of [2.2paracyclophanes used as planar chiral ligands for asymmetric catalysis, which include pseudo-geminal, pseudo-ortho and ortho phosphinyl-oxazolinyl-[2.2]paracyclophanes [13]. Pseudo-gem, pseudo-ortho and ortho are three geometrical isomers which can chelate with metals to achieve asymmetric catalysis. These phosphinyl-oxazolinyl-[2.2paracyclophane isomers has been used as ligands to carry out palladium catalyzed allylic alkylation as shown in the scheme IV - 7.

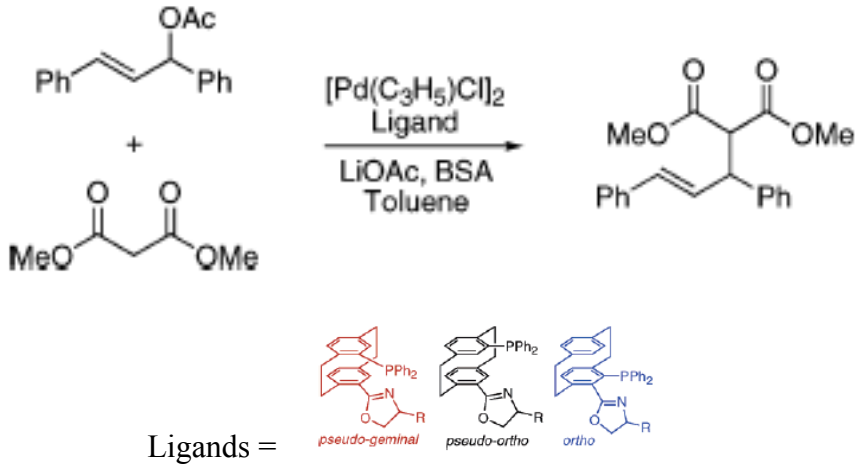

Scheme IV – 7: Palladium catalyzed allylic alkylation isomers of phosphinyl-oxazolinyl-[2.2]paracyclophanes chiral ligand.

It was suggested that of these isomers, the pseudo-ortho ligand is more effective to achieve high enantioselectivity (up to 89 % ee).

Morvant showed the use of pseudo-ortho-4,12-diamino[2.2]paracyclophane as a precursor in the synthesis of Schiff's base ligand with salicylaldehyde, which can be chelated with metal centers and used for asymmetric cyclopropanation reactions, as shown in Scheme IV - 8 [14].

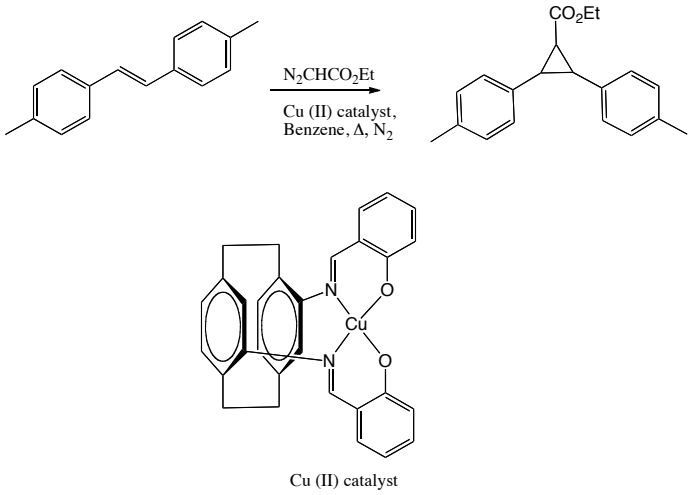

Scheme IV – 8: Cyclopropanation of trans-4,4'-dimethyl stilbene pseudo-ortho-N,N'-bissalicylidene-4,12-diamino[2.2]paracyclophane copper (II) catalyst

The catalytic efficiency of the pseudo-ortho-N,N'-bissalicylidene-4,12-diamino[2.2]paracyclophane copper (II) catalyst was better than N,N'-bissalicylidene-1,2-diaminoethane copper (II) as a catalyst by ca. 45%. Similar catalytic enantioselective cyclopropanation of olefins with diazoesters was reported to be carried out using N-salicylidine-4-amino[2.2]paracyclophane as an asymmetric ligand (Cu Catalyst A in Figure IV – 9) [15]. Later, when planar chiral N-(4-[2.2]paracyclophanyl)-2'-hydroxyacetophenone imine was used as a chiral ligand for the copper catalyzed cyclopropanation of styrene (Cu Catalyst

B in Figure IV – 9)and stilbene with diazoesters, an increase in the average enantioselectivity of ca. 60% for various substrates was observed [16].

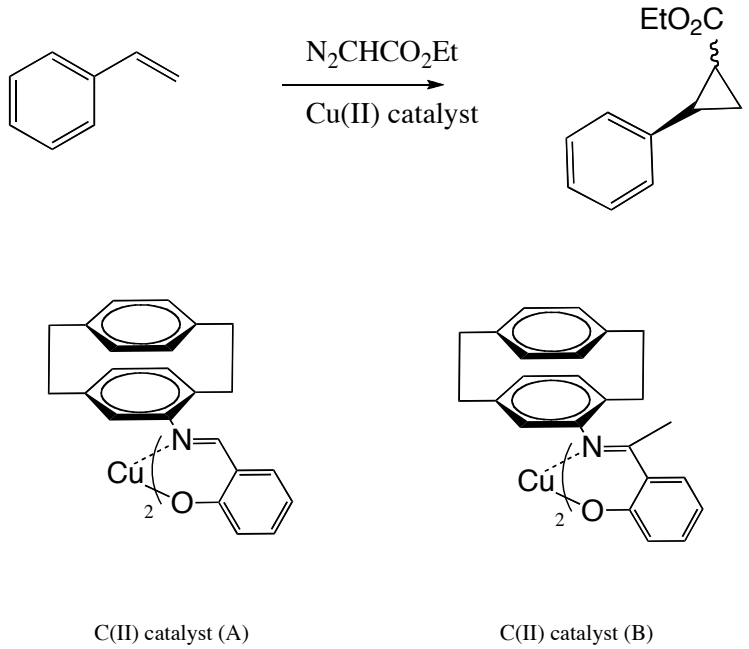

Scheme IV – 9: Cyclopropanation of Styrene

A conformational difference in the ligands when the imine hydrogen is substituted with a methyl group was necessary to achieve this dramatic change in enantioselectivity. To do so, computational studies, as well as spectroscopic studies and crystal structure analysis, will help to determine the effect of the methyl group to increase the enantioselectivity. At the same time, such conformational studies will also help in determining the metal complex geometry.

In the cases of pseudo-para and pseudo-meta [2.2]paracyclophane, formation of ligands and their metal complexes have potential for studying electronic coupling between the metal centers through the [2.2]paracyclophane

moiety. There is one example of a metal complex based on the pseudo-para [2.2]paracyclophane which was studied with regard to mediating electronic communication between the redox active Re metal centers, as shown in Figure IV - 4 [17].

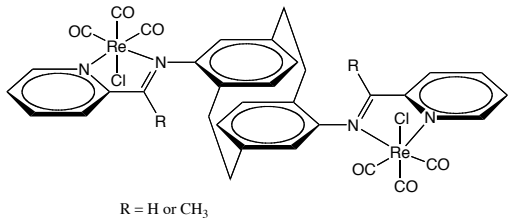

Figure IV – 4: Binuclear Rhenium(I) Complexes with Bridging [2.2]Paracyclophane−Diimine Ligands

In this example the role of the [2.2]paracyclophane bridge in electronic communication between metals was studied by using UV-visible spectroscopy, emission spectroscopy and cyclic voltammetry. There was not enough evidence of metal – metal interactionby UV-visible and emission spectroscopy to conclude if, or how, electronic coupling is mediated through the [2.2]paracyclophane. A better understanding was achieved using cyclic voltammetry, where two closely spaced, reversible, one electron reduction waves were observed for weakly interacting pyridine carboxaldimine groups. For such behavior, the comproportionation constant (K_c) for the mixed valence system was calculated to be 23 ± 9, which corresponds weak electronic interactions according to Robin and Day classification [18]. Strong electronic coupling have been observed, as in case of Figure IV - 5, where the redox centers are coupled with both decks of the [2.2]paracyclophane [19, 20].

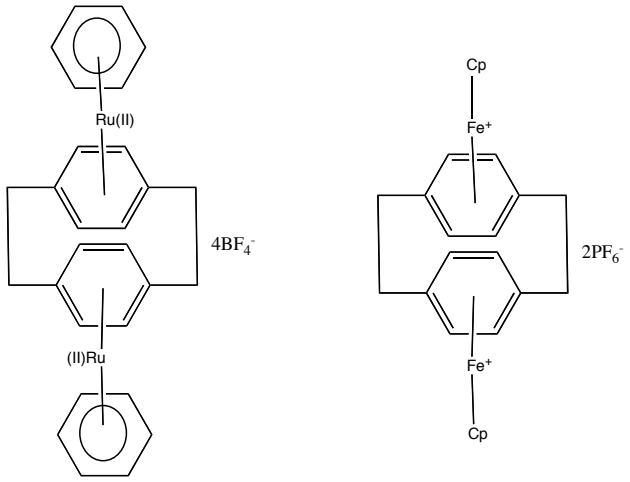

Figure IV – 5: Dimetal complexes of [2.2]paracyclophane

Hence, it was of interest to investigate such electronic interactions in copper complexes made from Schiff's base ligands of pseudo-para-4,12-diamino[2.2]paracyclophane as well as pseudo-meta-4,13-diamino[2.2]paracyclophane.

Results and Discussions:

Conformational studies of Schiff base ligands:

Synthesis of N-4-salicylidine[2.2]paracyclophane (APCSA) ligands:

The formation of salen-type ligands was carried out by a condensation reaction between 4-amino[2.2]paracyclophane and salicylaldehyde in a 1 : 1 ratio, as shown in Scheme IV - 9 [21]. The mixture was heated to reflux ethanol solvent and cooled to form a yellow crystalline precipitate. The product was dried under vacuum at room temperature.

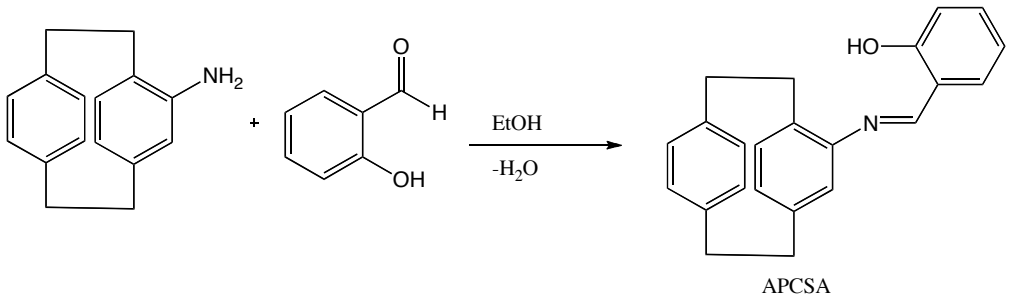

Scheme IV – 9: Synthesis of N-4-salicylidine[2.2]paracyclophane ligand (APCSA)

The salen-type ligand N-4-(salicylidene)[2.2]paracyclophane (APCSA) was characterized using IR, ^{1}H-NMR, UV-vis spectroscopy. The IR spectrum of the azomethine (C=N) showed an absorbance at 1614 cm^{-1} which was consistent with the stretching frequency of C=N bonds of the imine as shown in Figure IV – 32.

The ^{1}H-NMR was also consistent with the structural features of an imine and showed well-defined patterns for the protons at δ 3.5-3.8 ppm, 2.9 – 3.3 ppm, 2.8 ppm, which corresponds to the ethylene bridges of the paracyclophane, while protons on the aromatic rings of the [2.2]paracyclophane are appear at δ 6.01 ppm, 6.36 ppm, 6.83 ppm, 6.97 ppm, 7.10 ppm and 7.32 – 7.46 ppm. The chemical shift peak for protons on the benzene ring of the salicylaldehyde moiety occurs at δ 6.44 – 6.63 ppm. These assignments are consistent with the literature [21]. The UV-visible spectrum of the APCSA Schiff's base ligand is shown in Figure IV - 6.

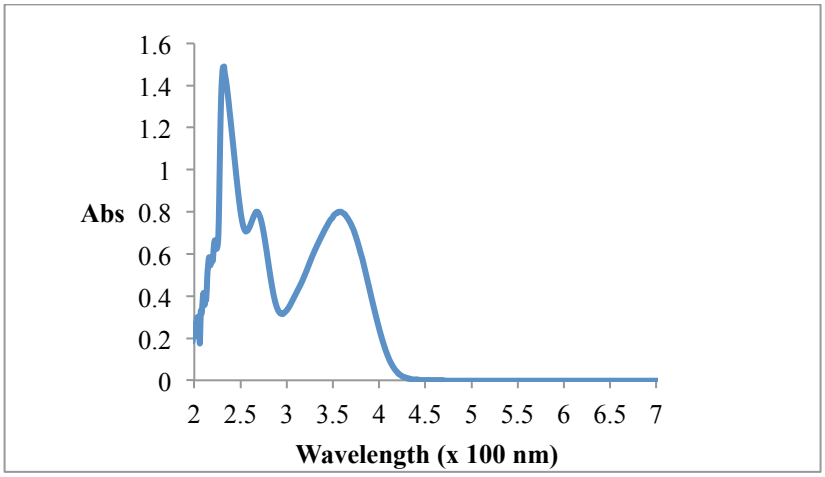

Figure IV - 6: UV-visible spectrum of the APCSA in methylene chloride.

The UV-Vis spectrum showed absorbance peaks at λ_{max} 360 nm and 280 nm and 240 nm. The peak at 360 nm corresponds to the π – π* transition involving the salen paracylophane moiety [22].

The geometry of APCSA is very important for metal complex formation and the orientation of Schiff's base ligands can determine the molecular properties of the resulting metal complexes. From molecular mechanics calculations, it was suggested that the easy rotation about the cyclophane – nitrogen bond give rise to number of conformations which ultimately decides the enantioselectivity in the cyclopropation of styrene using APCSA copper complexes. Glatzhofer and Masterson have shown the use of chiral Schiff's base ligands based on [2.2]paracyclophane for asymmetric cyclopropanation reactions of olefins by forming the copper (II) complex of APCSA but the complex was not characterized [21]. Further, the use of chiral complexes based on the N-(4-[2.2]paracyclophanyl)-2'-hydroxyacetophenone imine (APCHAP),

as shown in Figure IV – 7, showed an improved effect in the asymmetric cyclopropanation of styrene derivatives [23].

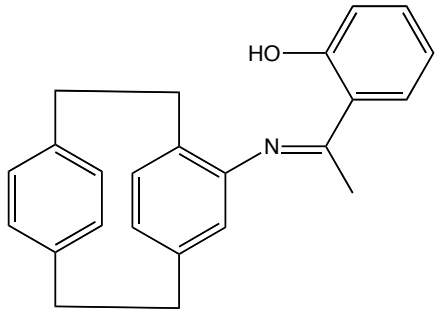

Figure IV – 7: N-(4-[2.2]paracyclophanyl)-2'-hydroxyacetophenone imine APCHAP

The differences in such reactivity and the nature of factors involved in such asymmetric induction are not well understood. To investigate this, and also to help understand electronic coupling between the metal and the [2.2]paracyclophane moiety in these complexes, it would be very important to study the geometry of the Schiff's base ligands. Computational and UV studies were used to investigate the conformations of such ligands. As model compounds, Schiff's base salen-type ligands based on aniline (ANSA), 2,5-dimethylaniline (DMASA) and 4-amino[2.2]paracyclophane (APCSA) as amines, and salicylaldehyde and 2-hydroxyacetophenone (abbreviation: ANHAP for aniline, DMAHAP for 2,5-dimethylaniline and APCHAP for [2.2]paracyclophane) were synthesized for these studies.

The molecular modeling that was done in this study was based on the following assumptions:

1. The co-planarity of the ANSA ligand, and

2. Strong hydrogen bonding between the hydroxyl group and nitrogen of C=N bond

The most important parameter in these molecular studies is the C=N dihedral angle which defines the overall conformation of the molecules. Braude and Sondheimer discussed the effects of steric congestion on the electronic spectra of conjugated systems [24]. Due to changes in the conformations, there are two spectral effects that can be observed:

1) Changes in absorption intensity alone, and
2) Wavelength displacements of the characteristic electronic bands as well as of changes in absorption intensity.

Effect type 1 usually showed up when there is weak steric inhibition of uni-planarity of conjugated systems, while effect type 2 occurs when the steric inhibition is strong. These effects can be used to study the conformations of the molecules based on the Equation 1:

$$\cos^2 \theta = \varepsilon / \varepsilon_0 \qquad \text{Equation (1).}$$

where, ε_0 is the absorption coefficient expected for the planar system ($\theta = 0°$) and ε is the absorption coefficient for the system being studied.

A steric effect of type 2 that showed no significant hypsochromic shift produced by substituents, such as alkyl groups, was first observed by Braude and coworker in connection with cyclohexene derivatives [25]. It was suggested that the steric interference would change the intensity of the peaks without any

changes in the displacements of the wavelengths, which in turn affects the co-planarity of the molecules. Studies of steric inhibition using UV absorption spectroscopy has been carried out by various groups in the 1950s [26, 27].

Hedden and Brown showed well-defined steric effects were observed in decreased intensity at the 240 nm maxima for ortho-alkyl substituted ketones related to acetophenones [27]. Braude suggested a more precise interpretation of the two types of steric effect inhibition in absorption spectroscopy, and indicated that a steric effect of type 1 in absorption spectroscopy is associated with the transitions between non-planar ground states and planar excited states. In the case of a steric effect of type 2, it is due to transitions between non-planar ground states and non-planar excited states [28]. Further Braude and Sondheimer explained the steric effect of type 1 by application of the Franck – Condon principle that the interplanar angle in the ground states can be deduced from the molar absorptivity values obtained from electronic absorption spectra [24, 29]. This investigation was carried out using ortho-alkyl substituted benzaldehydes, acetophenones and other related compounds.

Electronic absorption spectra of the model compounds for the [2.2]paracyclophane Schiff's base ligands were taken in dichloromethane solvent at known concentrations. All these compounds specifically exhibit intense bands near 265 nm and 340 nm which correspond to $\pi - \pi^*$ transitions. Superficially, absorption bands for all the Schiff's base ligands are similar. We were interested in the absorption band at 340 nm arising from the entire

conjugated π-system with the imine group held planar by hydrogen bonding with the hydroxyl group of the salicylidene benzene group. UV-vis spectra for all the compounds are shown below in Figure IV – 8 and Figure IV - 9. Molar absorptivities (ε) were calculated using Beer's law on data from carefully prepared solutions of the model compounds with known concentrations.

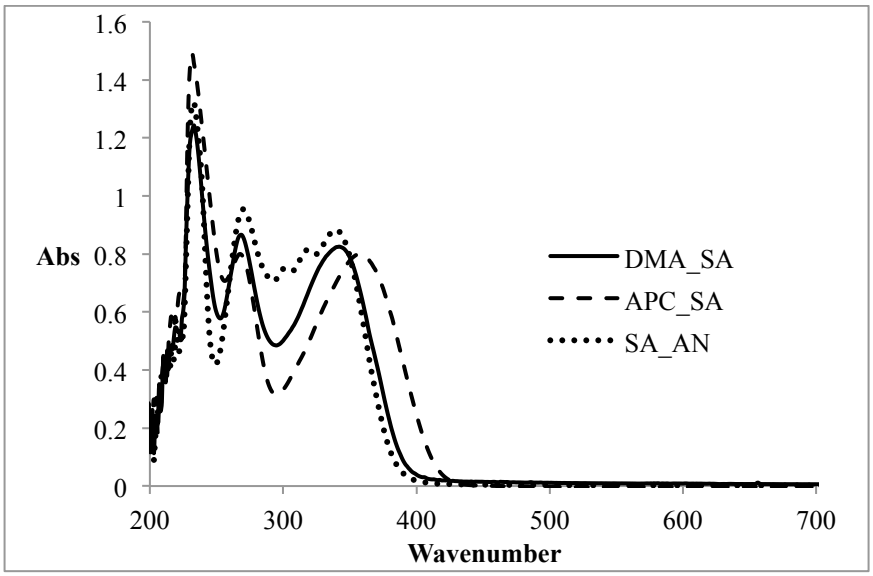

Figure IV – 8: UV-vis spectra of DMASA (__), APCSA (---) and ANSA (…..).

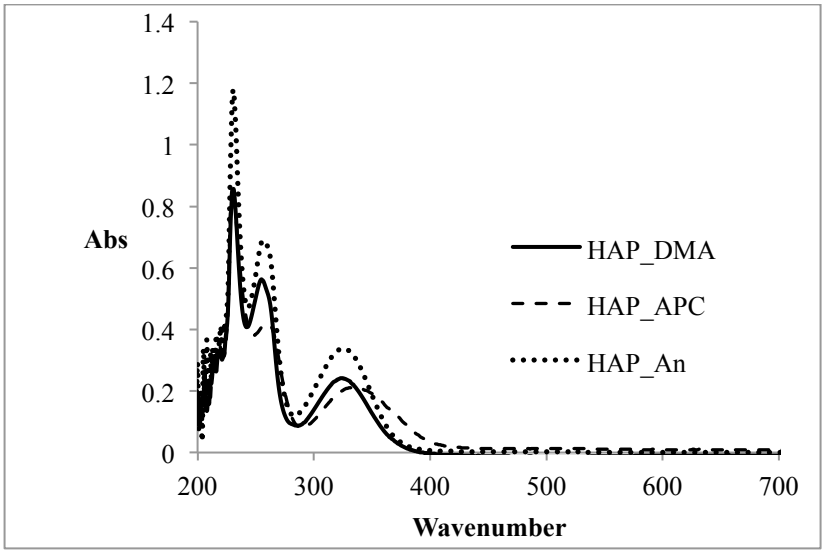

Figure IV - 9: -UV-vis spectra of DMAHAP (_____) APCHAP (----) and ANHAP (…)

The Braude equation (Equation 1) was used to calculate the dihedral angle for all the molecules to determine the molecular geometry. The values obtained using this equation are shown in Table IV - 1.

Table IV – 1: UV – Visible spectral data of Schiff base ligands

	ε in DCM ca.340 nm	Θ deg at 340 nm
ANSA	14029	0
DMASA	13437	12
APCSA	13216	14
ANHAP	8581	39
DMAHAP	7529	43
APCHAP	8011	41

In the treatment of the UV-visible data the value of the unhindered ANSA ligand is assumed to be 0°. For compounds DMASA and APCSA, the values for the dihedral angle calculated using Equation 1, were 12° and 14°, which are slightly twisted from the planar structures assumed for ANSA. This could be explained by the steric interactions between the iminium hydrogen and the methyl or methylene bridge group of 2,5-dimethylaniline [2.2]paracyclophane as shown in Figure IV - 10. When the iminium hydrogen is replaced with methyl group, the molecules should be twisted more from their planar counterpart ANSA. This is confirmed by the UV-visible data for ANHAP, DMAHAP and APCHAP. The dihedral angles for these compounds was calculated to be 39°, 43° and 41° for ANHAP, DMAHAP and APCHAP respectively.

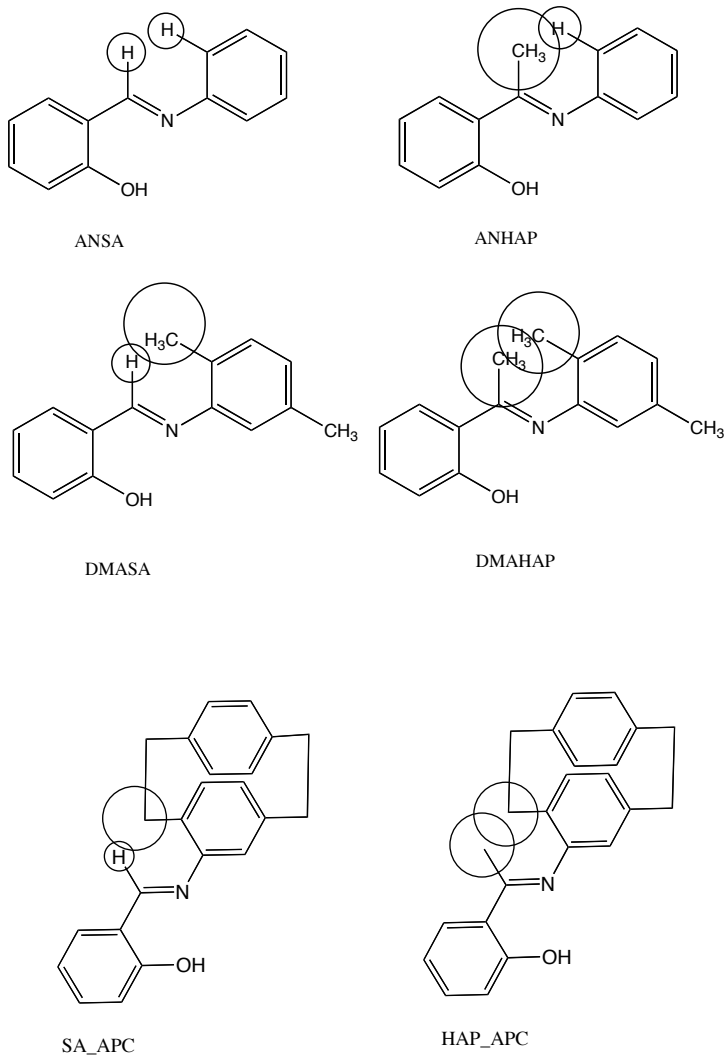

Figure IV - 10: Major steric effects in salen ligands

To try to understand the UV-visible measurements in more detail, a conformational study was performed for the geometry optimization using density functional theory (DFT) as implemented with Spartan® with the B3LYP function at the 6–31G** basis set level. To determine the conformational energy profiles, the optimized geometry was kept fixed and values of the total energy were calculated as a function of the dihedral angle θ (C1–C2–N1–C3) (atoms assigned in Figures IV-14 – IV-19) from 0 to 360°, varied every 10°. The

calculated lowest energy structures for the ANSA was for a dihedral angle (C1–C2–N1–C3) near 32°, although the minimum is shallow. As the iminium hydrogen is substituted with a methyl ($-CH_3$) group, the values in the dihedral angle changes due to steric inhibition, which ultimately twists the geometry of the molecule out of the plane. For all the Schiff base ligands, the energy minima were plotted against the dihedral angle for the atoms C1-C2-N1-C3, as shown in Figures IV-11, IV-12 and IV-13. From these energy plots, the predominant conformer will give the most stable conformation of the Schiff's base ligands as minima. The minimum energy conformations for all the six ligands are shown in Figures IV 14 – 19.

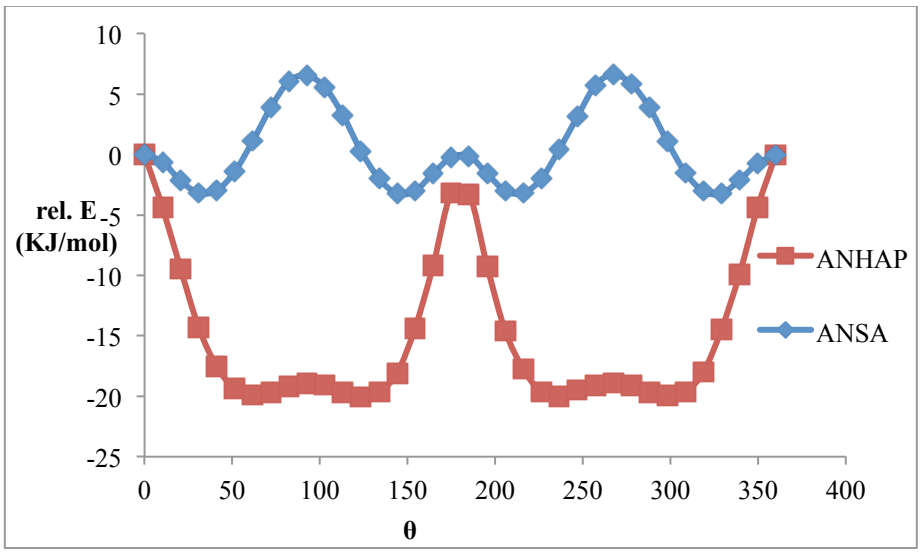

Figure IV – 11: Conformation energy minima vs dihedral angle for (ANSA and ANHAP)

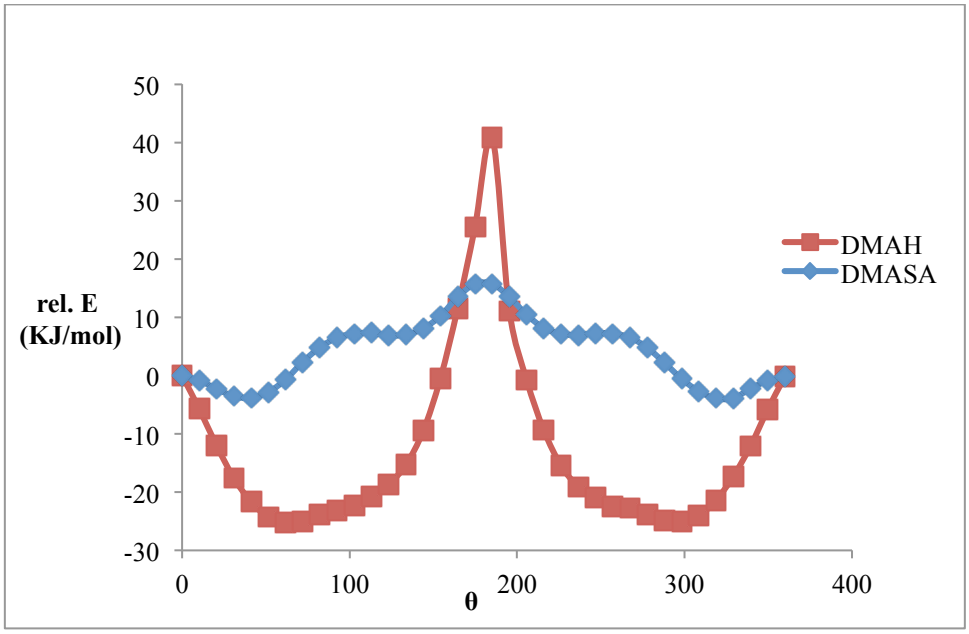

Figure IV -12: Conformation energy minima vs dihedral angle for (DMASA and DMAHAP)

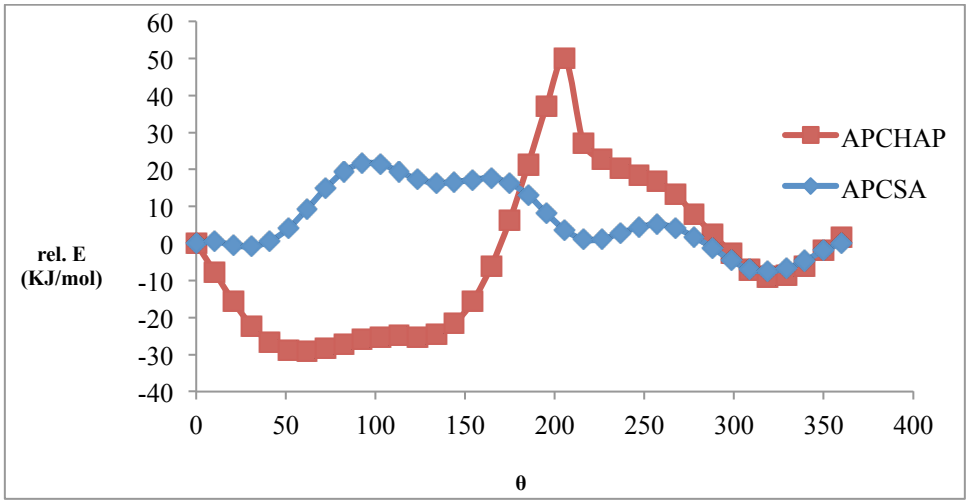

Figure IV - 13: Conformation energy minima vs dihedral angle for (APCSA and APCHAP)

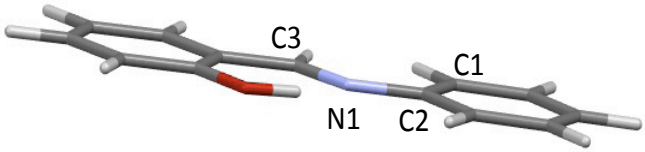

Figure IV - 14: Minimum energy conformation of ANSA

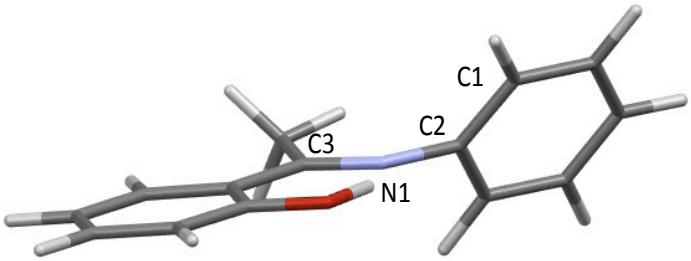

Figure IV - 15: Minimum energy conformation of ANHAP

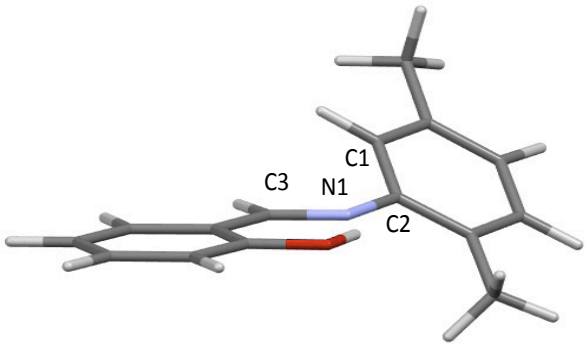

Figure IV - 16: Minimum energy conformation of DMASA

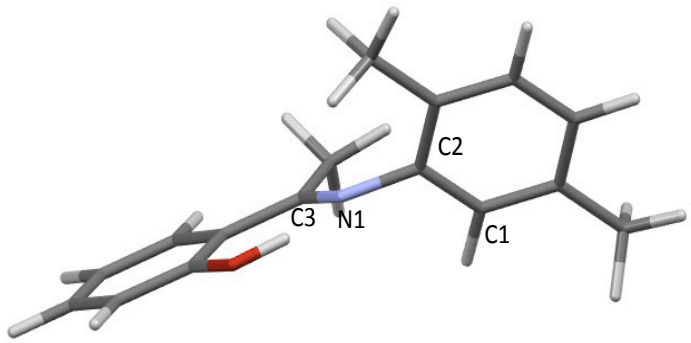

Figure IV - 17: Minimum energy conformation of DMAHAP

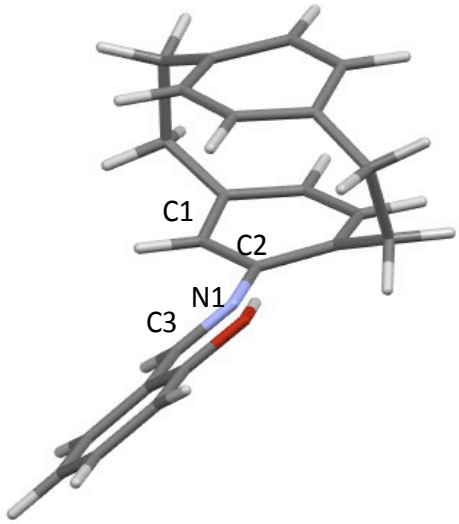

Figure IV - 18: Minimum energy conformation of APCSA

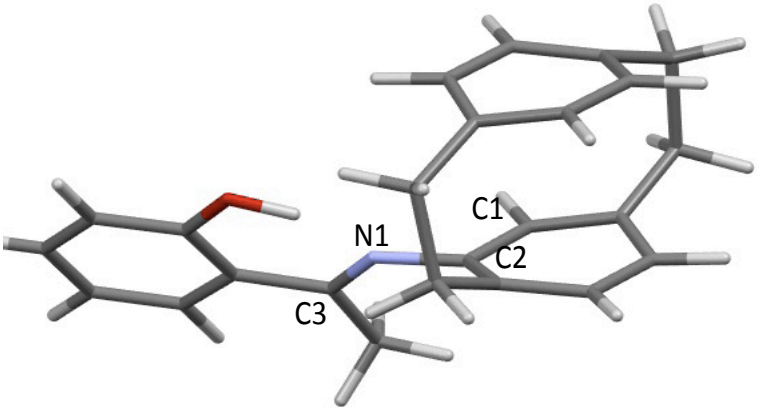

Figure IV - 19: Minimum energy conformation of APCHAP

The selected dihedral angles represented in Figures 15 – 20, showed a twist in the C1-C2-N1-C3 dihedral angles. The conformational studies show that the trends in dihedral twist angles calculated using the UV-visible spectra are generally correct. The methyl groups or [2.2]paracyclophane moiety in the 'aniline' portion of the molecule cause some twisting of the molecules. A methyl group placed on the imine carbon twists the molecules even more. However, the minima in the computational studies suggest that the Braude treatment underestimates the twist angles significantly. The calculations further suggest that the rotational barriers in the salicylaldehyde derivatives are relatively low and likely more easily overcome. The rotational barriers in the 2-hydroxyacetophenone derivatives are considerably steeper and likely "lock" the molecules in more twisted conformations. These contributions of conformations will need to be taken into account to form a more accurate picture of the

molecules and to explain the discrepancies between the calculations and the UV-visible data.

In summary, both the UV-visible data and the calculations show that all five ligands HAP_AN, DMASA, HAP_DMA, APCSA and HAP_APC have twisted geometries. In cases, where the imine hydrogen is substituted with the methyl group, the interference between methyl group and the ortho hydrogen of the aromatic ring and bridge of methylenes creates the steric hindrance. This steric hindrance does not allow the free rotation around the C1-C2-N1-C3 dihedral angle. Such steric interaction plays an important role in determining the geometries of the metal complexes formed from such ligands. In general neutral copper (II) complexes formed by chelation with Schiff's base ligands, prefer a planar coordination geometry [30]. But due to such steric interactions, when the metal complexes are formed, e.g. copper (II) complexes of some Schiff's base ligands will be distorted. If the UV-visible calculations are not correct, the distortion may be small and a coordinated metal center may interact strongly with the cyclophane system. If the calculations are correct, the conformations of the ligand may be much less favorable towards interaction of the metal with the cyclophane system.

Synthesis of copper metal complexes based on [2.2]paracyclophane Schiff base ligands:

Synthesis of Ligands:

To study the complex formation of N-salicylidene-4-amino[2.2]paracyclophane (APCSA) with the metal, it was thought to study complex formation of N-salicylidene-2,5-dimethylaniline (DMASA) with metal centers as it is the analog of the 4-amino[2.2]paracyclophane.

DMASA ligand:

The DMASA ligand was synthesized according to the procedure mentioned earlier in this chapter [31], by condensation of 2,5-dimethylaniline with salicylaldehyde (SA) in 1:1 ratio and isolated in high yields. DMA and SA was heated to reflux solvent (ethanols) overnight. The ethanol mixture was recrystallized to get pure yellow crystals, which were characterized by ^{1}H-NMR, IR and UV-vis spectroscopy.

Characterization of DMASA Ligand:

^{1}H-NMR shows characteristics signals for the iminic and phenolic protons at δ 8.2 and 13.2 respectively. IR spectroscopy of the free ligands shows a strong band in the spectrum of salen ligand around 1617 cm^{-1}, which corresponds to the typical C=N stretching mode, and about at 1276 cm^{-1} assigned to the C-O stretching mode. The structural characterization of DMASA was investigated by Elmali et al. to get a deeper insight into its structural

features, and its crystal structure suggested that the most stable conformation is a non-planar structure [31]. This was also confirmed by the Spartan conformational and UV-vis spectroscopic studies discussed earlier.

Further extending the synthesis of ligands to make metal complex macromolecules based on the *pseudo-para*-DAP, and *pseudo-meta*-DAP salen ligand systems, we prepared these complexes according to the procedure in the literature, and as shown in Scheme 10 [32]. The condensation of 4,12-*pp*-diamino[2.2]paracyclophane with 2 equivalents of salicylaldehyde gave the bis(Schiff's base) in high yield. An absolute ethanolic solution of these reagents was heated to reflux solvent for 2 hours and then cooled to form a yellow precipitate of the Schiff's base pp-DAPSA. This yellow precipitate is soluble in most organic solvents such as dichloromethane, chloroform, acetonitrile, toluene, etc. ^{1}H NMR, IR and UV-vis spectroscopy were used to characterize the ligand. The same procedure was followed for the synthesis of the Schiff's base ligand formation based on 4,13-*pm*-diamino[2.2]paracyclophane.

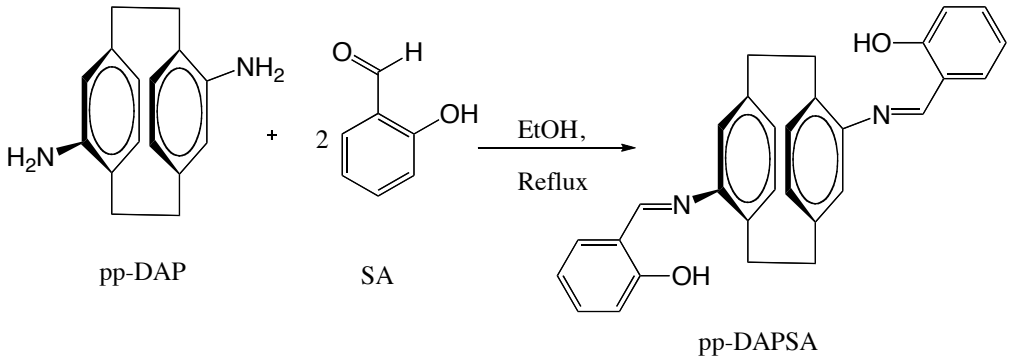

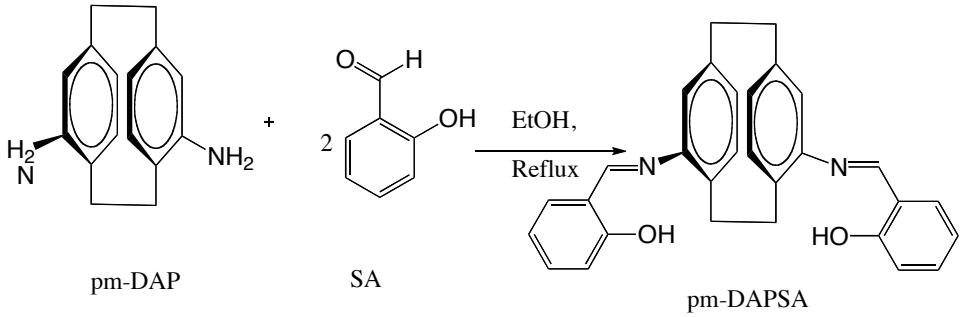

Scheme IV – 10: Synthesis of *pp*-DAPSA and *pm*-DAPSA

^{1}H NMR spectroscopy showed the typical iminic protons at δ 8.35 ppm for pp-DAPSA and δ 8.35 ppm for pm-DAPSA, phenolic proton at 13.82 ppm for pp-DAPSA and 13.79 ppm for pm-DAPSA. Protons of the aromatic rings of paracyclophane appeared at δ 6.1, 6.4, 6.8 and ethano bridge protons at δ 2.8, 3.2 and 3.7. The benzene ring protons from the salicylaldehyde showed peaks at δ 7.4, 7.0. The integration values gave the appropriate ratios for every proton, which confirms the formation of product. IR spectroscopy was used to further characterize the formation of the Schiff's bases. IR spectra for both pp-DAPSA and pm-DAPSA showed characteristic peaks for the C=N stretch at 1613 cm^{-1} and 1612 cm^{-1}. It also showed C-O stretching

at bands 1276 cm^{-1} and 1273 cm^{-1} for pp-DAPSA and pm-DAPSA respectively. The ring skeletal vibration C=C of both Schiff's base ligands appeared in the range of 1480 cm^{-1} – 1560 cm^{-1}. Both salen ligands based on the pp-DAP and pm-DAP are previously unknown.

UV-vis characterization of pp-DAPSA and pm-DAPSA ligands showed similar features in their spectra, Figures IV-20 and IV-21. These spectra were carried out using dichloromethane given in Table IV - 2. Both systems showed similar absorbances at λ_{max} 350 nm, 270 nm, and 230 nm [33].

Table IV – 2: UV – vis spectral data of pp-DAPSA and pm-DAPSA

Compounds	λ_{max} (nm)	ε (M^{-1} cm^{-1})	λ_{max} (nm)	ε (M^{-1} cm^{-1})	λ_{max} (nm)	ε (M^{-1} cm^{-1})
pp-DAPSA	230	37221	270	26087	350	29588
pm-DAPSA	230	44227	270	32832	350	30275

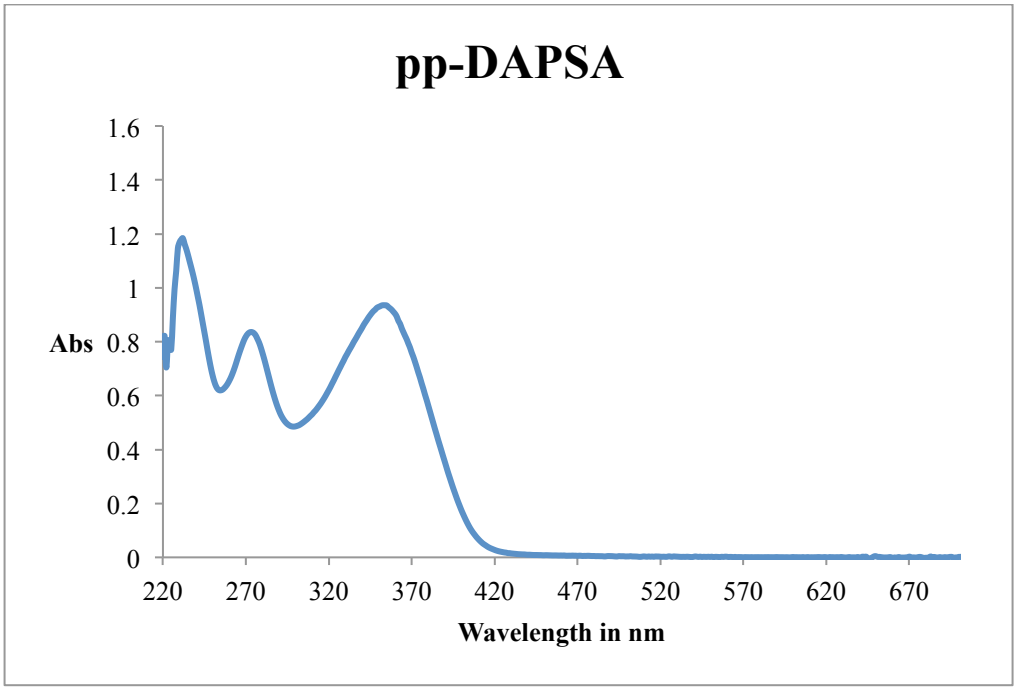

Figure IV – 20: UV- visible spectra of pp-DAPSA Schiff's base ligand in dichloromethane.

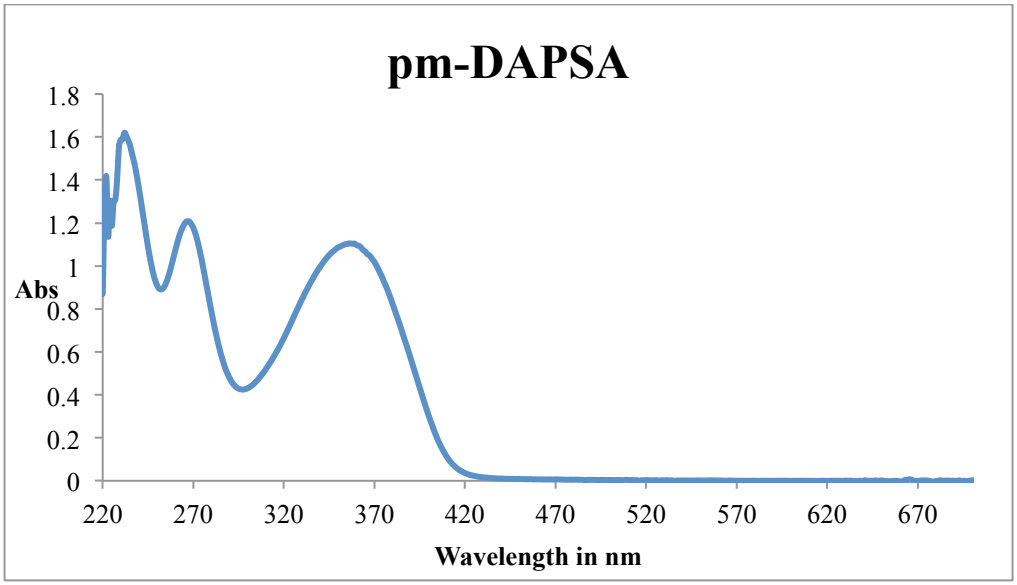

Figure IV – 21: UV- visible spectra of pm-DAPSA Schiff's base ligand in dichloromethane.

Synthesis of copper complexes:

The synthesis of copper complexes was investigated for the different ligands such as DMASA, which is a steric analogue of APCSA. Synthesis of copper complexes of salen ligands has already been studied [34]. For the purpose of understanding how the metal complex of APCSA ligand would behave, the copper complex of DMASA was studied.

Synthesis of $(APCSA)_2Cu$ and $(DMASA)_2Cu$ complexes:

The syntheses of copper complexes based on the APCSA and DMASA Schiff's base ligands were based on a procedure given in the literature [35]. The general scheme for the synthesis of the metal complexes is given in Scheme IV – 11. A solution of the Schiff's base ligand in methanol was prepared and stirred well. To this solution $Cu(CH_3COO)_2.H_2O$ was added slowly and stirred well for 1 hour at room temperature. After 1 hour, the solution turned brown and a greenish precipitate formed that was isolated by filtration. NMR signals were not observed for the precipitate and further characterized by IR and UV-visible spectroscopy.

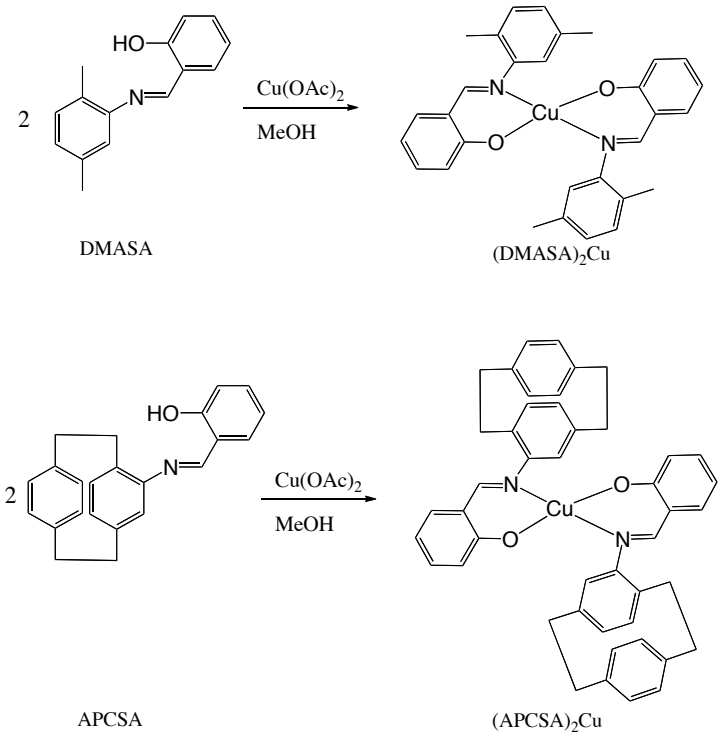

Scheme IV – 11: Synthesis of $(DMASA)_2Cu$ and $(APCSA)_2Cu$

Solubility test

Salen ligands based on DMASA and APCSA were shown to be soluble in most common organic solvents such as dichloromethane, chloroform, toluene, AcCN, etc., while the metal complexes of these salen ligands showed only partial solubility in toluene, dichloromethane, chloroform and AcCN but miscibility in DMSO and DMF solvents. This behavior can be explained based on the chelating effect of the salen ligands with metal complexes in which, due to metal ion chelation, a considerable delocalization of π electrons over the complete metal ligand complex changes the polarity of the complex and hence the solubility [32].

Infrared Spectroscopy:

The spectra provide valuable information regarding the nature of functional groups present in the ligand molecules and their metal complexes.

IR of $(DMASA)_2Cu$ and $Cu(APCSA)_2Cu$

As discussed earlier for the Schiff base ligand based on the 2,5-dimethylaniline (DMA), the IR spectra for the ligands showed strong absorption at 1617 cm^{-1} indicating the presence of C=N stretching band. This band shifted to lower frequency in the spectra of the $(DMASA)_2Cu$ complex, to 1606 cm-1. Also the IR spectrum of the ligand showed broad bands in the range of 3400 – 3500 cm^{-1}, which corresponds to intramolecular H-bonded –OH groups, which are absent in the metal complexes, indicating the oxygen of the –OH group is coordinated to the metal ion. In similar fashion, in the IR spectrum of the $(APCSA)_2Cu$ complex the absorption band for C=N in case of the metal complex showed at 1603 cm^{-1} vs 1614 cm^{-1} for the free ligand. This shift again shows the coordination of the C=N group to the copper [36]. The change in the C=N absorption band in the copper complex is due to C=N group coordinating to copper and reducing the electron density in the azomethine link [37].

UV of $(DMASA)_2Cu$ and $(APCSA)_2Cu$

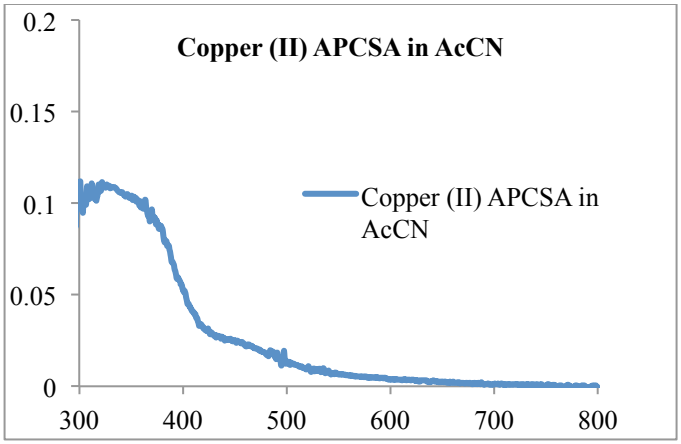

Figure IV – 22: UV-vis spectrum of $(APCSA)_2Cu$

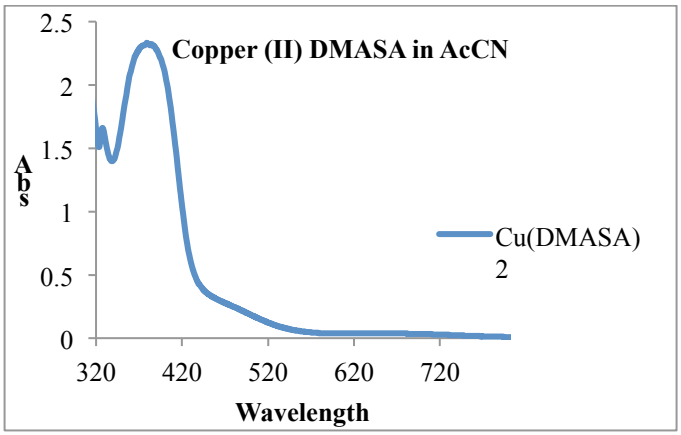

Figure IV – 23: UV-vis spectrum of $(APCSA)_2Cu$

The UV – vis spectra of $(APCSA)_2Cu$ and $(DMASA)_2Cu$ were taken in acetonitrile and shown in Figure IV – 22 and Figure IV – 23, respectively. Due to poor solubility, the region below 250 nm showed noise in the absorption spectrum for $(APCSA)_2Cu$. The absorption bands near the region 370 – 400 nm in case of both the copper complexes could be assigned to overlapped n → π* and ligand to metal charge transfer (LMCT) transitions [38]. The band observed

near the 670 nm in the visible spectrum for $(DMASA)_2Cu$ can be assigned to the copper d – d transitions in the square based pyramidal geometry as seen in Figure IV - 24 [39]. The absence of such peak in $(APCSA)_2$ Cu could be due to absence of square planar geometry in this complex. However, the concentration of the $(APCSA)_2Cu$ could be low but would otherwise show such d-d transitions as in case of $(DMASA)_2Cu$. Overall the spectral behavior of both the copper complexes are similar in nature.

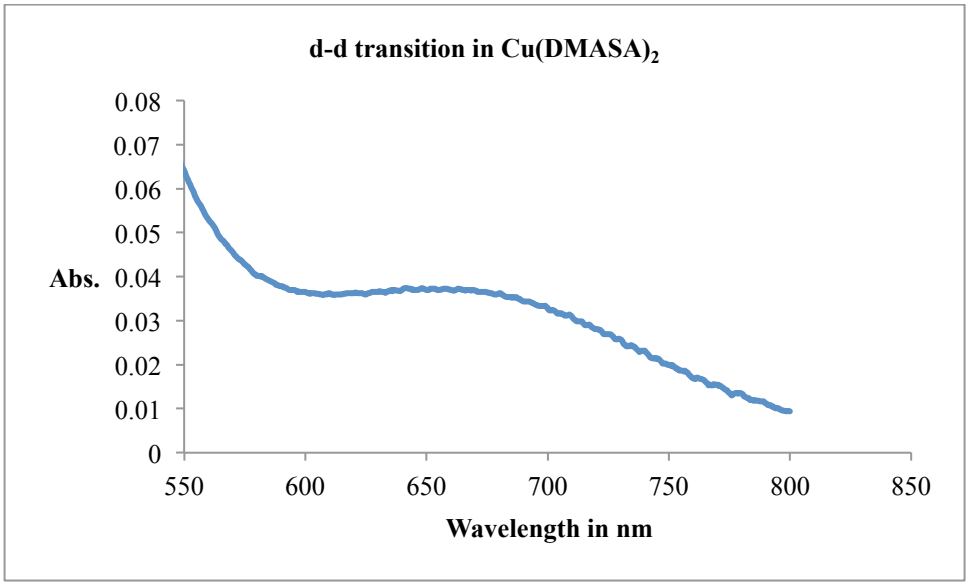

Figure IV – 24: d-d Transition in $(DMASA)_2Cu$

EPR:

The EPR spectrum of the $Cu(APCSA)_2$ complex was obtained at 77 K (liquid nitrogen) and room temperature in DMSO-toluene solution, because the metal complex tended to aggregate upon freezing. This complex exhibits axial spectra that are characteristic of Cu(II) complexes having $d_{x^2-y^2}$ ground state[40].

The four equally spaced EPR signals observed at low magnetic field are related to the hyperfine coupling of Cu(II) [41]. Three of the four features are well resolved while the fourth peak is partly overlapping with $\boldsymbol{g}_{\perp}$ as shown in Figure IV – 25, where the spectrum was taken at 77 K. The $\boldsymbol{A}_{\parallel}$ value was found to be 170 G and the $\boldsymbol{g}_{\parallel}$ value was found to be 2.24, while the $\boldsymbol{g}_{\perp}$ value was found to be 2.04.

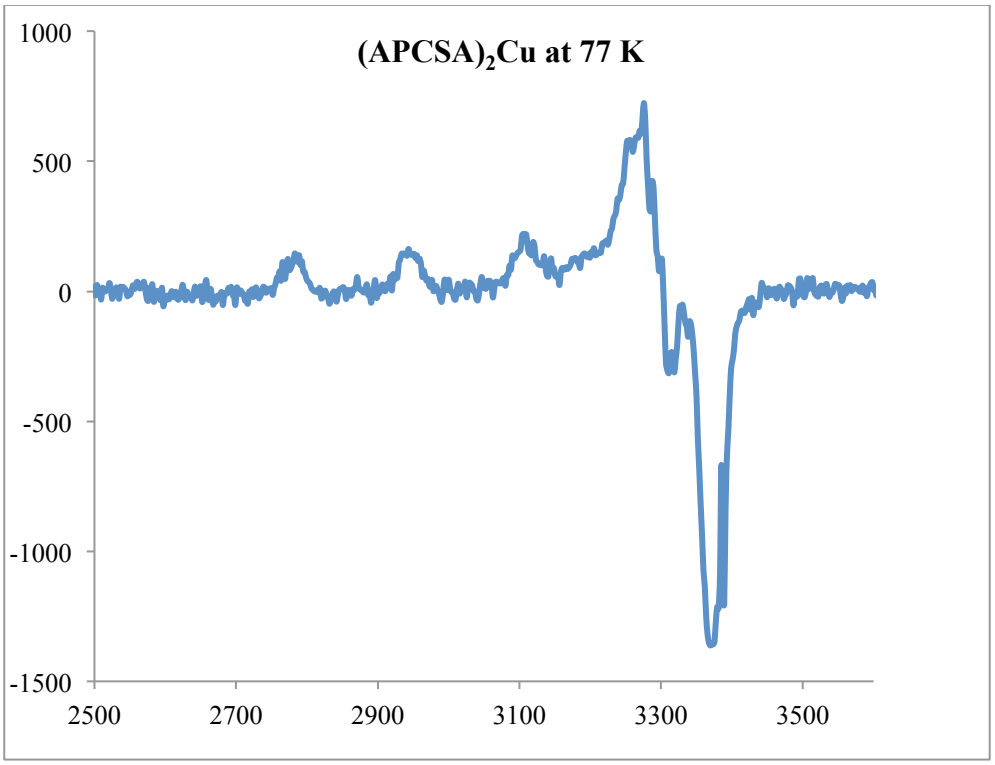

Figure IV – 25: EPR spectrum of Cu(APCSA)2 in DMSO/toluene solvent mixture at 77 K.

When the EPR spectrum of similar solution of $Cu(APCSA)_2$ complex in DMSO/toluene is taken at room temperature as shown in Figure IV - 26, the fourth peak of the parallel hyperfine component overlaps with the perpendicular

component [42]. As $g_{\parallel}$ (2.24) > $g_{\perp}$ (2.04), the unpaired electron is likely localized in the $d_{x^2-y^2}$ orbital of the copper ion [43].

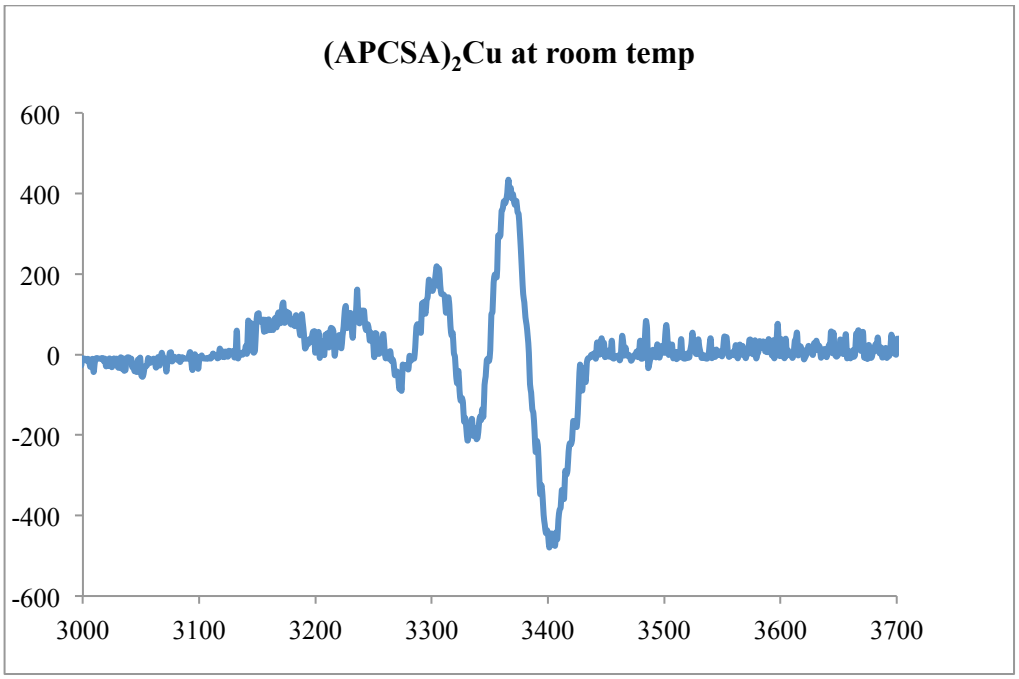

Figure IV – 26: EPR spectrum of $Cu(APCSA)_2$ in DMSO/toluene solvent mixture at room temperature.

Magnetic Susceptibility:

The paramagnetic behavior of copper (II) Schiff's base complexes has been well studied with regard to spin state. The lack of any NMR signals for the copper complex samples is problematic but results from the unpaired spin, which should impart paramagnetic properties to the system. The paramagnetic susceptibility of a substance in solution can be determined by using NMR spectroscopy [44]. Evans correlated the difference in the chemical shift of a signal from an inert reference material in the presence and absence of a

paramagnetic substance, which can be accomplished using coaxial NMR sample tube as shown in Figure IV – 27 [45].

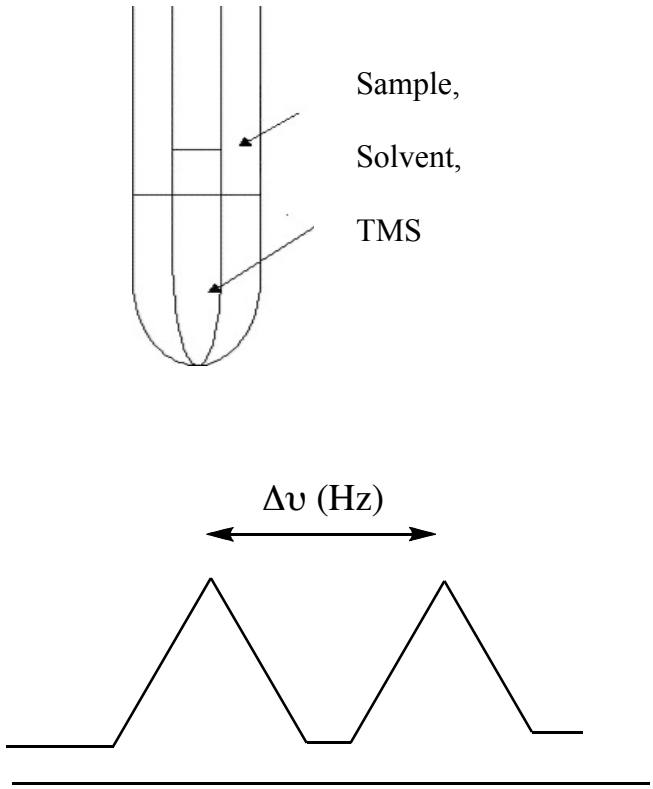

Figure IV - 27: Coaxial NMR tube used in Evans method and change in chemical shift in the ^{1}H NMR signal.

Hence considering the difference in the chemical shifts observed, the effective magnetic moment (μ_{eff}) and the spin state of the system could be calculated using the relationships given below,

$$\mu_{eff} = 3.57 \times 10^{-3} \left(\frac{T\,\delta\upsilon}{c} \right)^{1/2}$$

$$\mu_{eff} = 2(S(S+1))^{1/2}$$ Equation (2)

where μ_{eff} is the effective magnetic moment, T is the temperature at which this measurement taken (usually room temperature), $\delta\nu$ is the change in contact shift (in Hz), c is the concentration of the paramagnetic species, and S is the spin state of system in solution.

The effective magnetic moment calculated for the $Cu(DMASA)_2$ (II) system in $CDCl_3$, was found to be 2.01 μB, calculated from equation 2, in reasonable agreement with the copper (II)system spin only value of 1.73 μB corresponds to S = ½. Same method was used to calculate the effective magnetic moment for the $Cu(APCSA)_2$ complex, which was found to be 1.81 μB, in good agreement with the spin only value for Cu (II).

Metallopolymer Synthesis:

Synthesis of polymers based on copper complexes of the pp-DAP and pm-DAP Schiff's bases:

Insertion of copper into the Schiff base ligands is usually carried out by reaction with copper (II) salts. In our case the metal chelation was carried out using copper (II) chloride salt with a methanolic solution of pp-DAPSA and in another reaction, copper (II) chloride is reacted with methanolic solution of pm-DAPSA Schiff base ligands as shown in Scheme IV- 12.

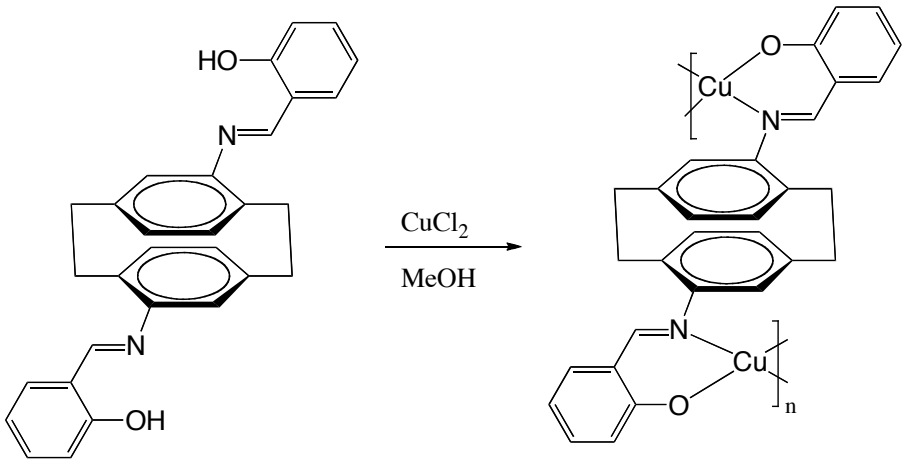

pp-DAPSA

Poly(Cu(pp-DAPSA))

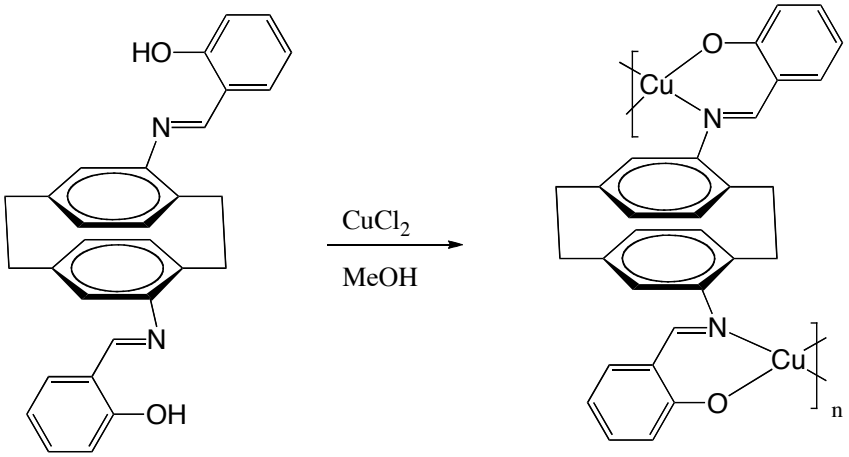

pm-DAPSA

Poly(Cu(pm-DAPSA))

Scheme IV – 12: Synthesis of poly(Cu(ppDAPSA)) and poly(Cu(pmDAPSA))

Both the reaction mixtures were stirred overnight and reaction was monitored by the color changes. Both reactions changed color to dark brown after 2-3 hours suggesting chelation of copper with the salen ligands. Both reactions gave a solid brown precipitate at the end of the reaction. The precipitates were washed with methanol and ether to clean the precipitates. Complexes thus formed showed poor solubility solvents such as CH_2Cl_2, $CHCl_3$,

moderate solubility in toluene and acetonitrile but satisfactory solubility in strong solvents such as DMF and DMSO. The precipitates were analyzed using elemental analysis, IR, UV and their electronic interactions were analyzed using EPR and Evan's method.

Table IV – 3: Elemental analysis

Element	$Cu(APCSA)_2$	Possible new structure ($(ppDAPSA)CuCl_2$)	Experimental Poly(ppDAPSA)Cu	Experimental Poly(pmDAPSA)Cu
	Theoretical	Theoretical	Found	Found
C	50.06	56.07	59.71	58.86
H	3.77	3.76	4.32	4.22
N	4.36	4.36	4.57	4.48

Elemental analysis of both putative polymers, poly(pp-DAPSA) and poly(pm-DAPSA), were carried out. For the comparison of the values, theoretical C, H, N values for $(APCSA)_2Cu$ and theoretical poly((pp-DAPSA)Cu) were calculated and found to be consistent with the structure shown in Figure IV - 28 and given with the data in Table IV – 3.

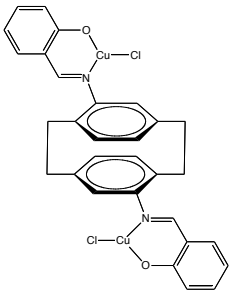

Figure IV – 28: Theoretical copper Schiff's base ligand complexes based on [2.2]paracyclophane.

It could be observed from the elemental analysis that the experimental values are in between theoretical values of monomer and polymeric structure. Further analysis, such as paramagnetic susceptibility and EPR spectroscopy, of the experimental polymers would give some insights into the number of copper centers involved in such copper Schiff's base complex formation based on [2.2]paracyclophane moiety.

IR and UV-vis Spectroscopy:

Infrared (IR) spectra of the samples including ligands (pp-DAPSA, pm-DAPSA) and copper metallated polymer complexes [poly(Cu(pp-DAPSA)) and poly(Cu(pm-DAPSA))] were recorded. The appearance of strong peaks for polymer copper complexes at 1607 cm^{-1} for poly (Cu (pp-DAPSA)) and 1608 cm^{-1} for poly (Cu (pm-DAPSA)) which are shifted to lower frequencies compared to their respective ligands, 1613 cm^{-1} for pp-DAPSA and 1612 cm^{-1} for pm-DAPSA, were observed. These bands shift to lower frequency suggesting the chelation of copper to the ligands. The UV-vis spectra of both the complexes with their respective ligands, as shown in Figure IV – 29, showed similar absorption at 360 nm (partially soluble in toluene), even though the colors of the complexes are brown. This band in case of brown copper complexes may be assigned to ligand to metal charge transfer transitions.

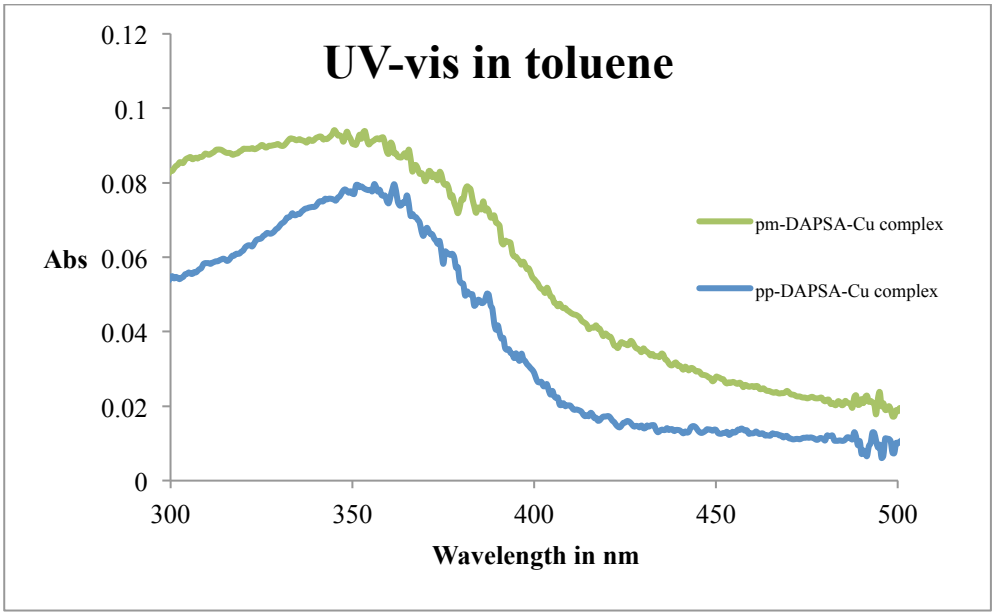

Figure IV – 29: UV – vis spectra of ligands and their copper complexes in toluene

EPR:

The coordination environment of the metal centers in the metal salen complexes can be determined using EPR spectroscopy, which is a very sensitive method to monitor the structural changes around the metal centers. The copper (II) EPR spectrum can give information for metal–metal short distance interaction, as well as the long distance dipole–dipole interaction [46]. The EPR spectra of the putative polymers of $(pp\text{-}DAPSA)_2Cu$ and $(pm\text{-}DAPSA)_2Cu$ were taken at room temperature and 77 K as shown in Figure IV – 30 and Figure IV – 31. The isotropic spectra observed at room temperature as well as 77 K for both samples suggested a distorted tetrahedral environment around the copper site [47]. This behavior could also be due to the increased metal content which corresponds to dipole – dipole interactions [46]. With no resolved hyperfine

structure in the spectrum, polymer-copper (II) complexes shows a single broad signal with Hamiltonian spin parameter values for poly (pp-DAPSA)Cu and poly (pm-DAPSA) of g = 2.08 and g = 2.09 respectively.

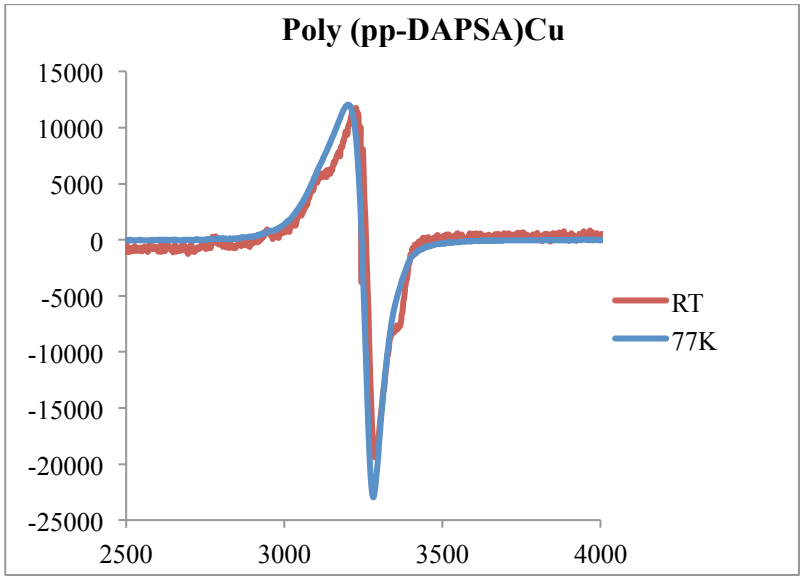

Figure IV - 30: EPR poly[(ppDAPSA)Cu] at room temperature (RT) and 77 K

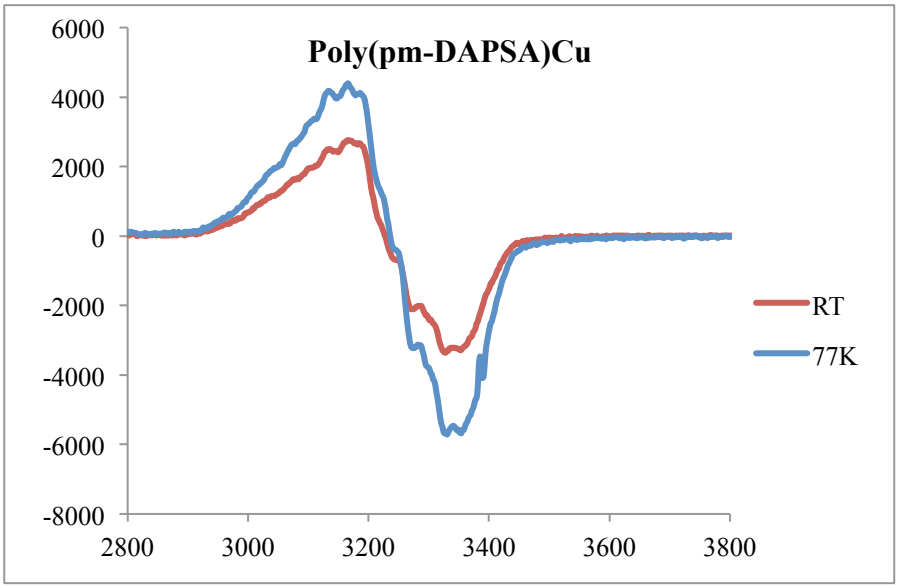

Figure IV - 31: EPR poly[(pmDAPSA)Cu] at room temperature (RT) and at 77K

According to literature for the metal containing polymers, specially for copper (II) containing salen complex polymers, the formation of divalent copper pairs is possible [48].

Evans method:

Magnetic moment measurements were carried out using Evan's method which showed the effective magnetic moment (μ_{eff}) values of 2.85 B. M. and 2.69 B. M. for poly ((pp-DAPSA)Cu) and poly ((pm-DAPSA)Cu), respectively, at room temperature.

Conclusion:

IR, UV-visible and ESR spectral data showed the reaction of pp-DAPSA and pm-DAPSA with copper (II) salts clearly produced some form of salen-Cu complexes. Elemental analysis for samples was clearly inconsistent with the putative polymeric structure. The effective magnetic moment measured for (pp-DAPSA)Cu, μ_{eff} = 2.85 B.M. was high for single S = ½ Cu(II) per molecule (μ_{eff} = 1.73 B.M). This could be evidence of ferromagnetic coupling between Cu(II) atoms but is more suggestive of a structure containing two largely independent S = ½ Cu(II) atoms per molecule (μ_{eff} = 2.45 B.M). If the molecular weight per repeat unit were higher, the observed μ_{eff} of ca. 2.85 B.M would be lowered and be closer to 2.45 B.M.. These observations suggest that the bis(salen) ligands are forming some type of bis(Cu(II)) complexes such as shown in Figure IV – 28.

Such a structure would have a theoretical elemental analysis of C = 56.07; H = 3.76; N = 4.36, in much better agreement with the experimental found values. Based on the molecular weight of the compound shown in Figure IV – 28, μ_{eff} would be measured as 2.69 B.M., significantly closer to 2.45 B.M. for non-interacting species.

The ESR data consistent with the tetrahedral coordination of the copper (II) atoms, suggesting that the structure may be "polymeric" through formation of Cu-Cl/Cl-Cu pairing interactions between molecules (or through some counterion other than Cl). Crystal structures would be needed to resolve this structure definitively but crystals have not been obtained.

These results suggest it may not be possible to form the desired coordination polymers. This may be due to collective steric congestion if the bis(salen)Cu coordination were to occur. The data further suggest that the interactions between Cu atoms are weak at best. The ligands have been shown to be twisted and coordination with the Cu and another ligand may increase the twist angle and decrease interaction with the [2.2]paracyclophane core. This would, in turn, decrease interaction between the metal centers.

Experimental:

All the chemicals were used as obtained from Aldrich. The Schiff's base ligands were prepared by the procedures as mentioned in the literature [49]. ANSA [50], ANHAP [51] and DMASA [52] were prepared according to literature procedures. ^{1}H NMR spectra were measured using a Varian 300 MHz instrument with solvent as an internal standard. UV-visible spectra were measured using a Hewlett Packard 8453 spectrophotometer in the range 200 to 1100 nm on solutions ranging in concentration from 1.0×10^{-4} M to 1.0×10^{-5} M. Conformational analyses were carried out using Spartan '08 for Windows molecular modeling software from Wavefunction Inc. Geometry optimization was performed using density functional theory (DFT) as implemented in Spartan using the B3LYP functional at the 6–31G** basis set level. To determine the conformational energy profiles, the optimized geometry was kept fixed and values of the total energy were calculated as a function of the dihedral angle θ (C–C–N–C) from 0 to 360°, varied every 10°.

Syntheses:

DMAHAP:

2,5-Dimethylaniline (DMA) (1.0 g, 8.3 mmol) and 2'-hydroxyacetophenone (HAP) (1.1 g, 8.3 mmol) were mixed in a flask equipped with a Hickman still. The reaction was heated for 1d at 120° C and water from the condensation collected in the still. The crude product was purified through column chromatography (silica gel, hexane). After removal of the solvent, pure

DMA_HAP was obtained as reddish oil in 3% yield (50 mg, 0.21 mmol). ^{1}H NMR (300 MHz, $CDCl_3$, 293K) δ 2.10 (s, 3H), 2.27 (s, 3H), 2.33 (s, 3H), 6.60 (s, 1H), 6.85–6.95 (m, 2H), 7.08 (dd, 2H, 7.4 Hz), 7.38 (t, 1H, 7.4 Hz), 7.63 (d, 1H, 7.8 Hz).

APCSA [21]:

4-Amino[2.2]paracyclophane (APC) (112 mg, 0.50 mmol) was dissolved in ethanol (2 ml) and stirred in a round bottom flask. To this solution ethanolic (2 ml) solution of salicylaldehyde (SA) (61.4 mg, 0.50 mmol) was added dropwise. The reaction mixture heated to reflux solvent for 2 h and then cooled to aid crystallization. After filtration APCSA was obtained as a yellow solid in 47% yield (76 mg, 0.23 mmol). ^{1}H NMR (300 MHz, $CDCl_3$, 293K) δ 2.74–2.88 (m, 1H), 2.96–3.27 (m, 6H), 3.56–3.69 (m, 1H), 6.01 (s, 1H), 6.36 (d, 1H, 8.1 Hz), 6.44–6.63 (m, 4H), 6.83 (d, 1H, 7.9 Hz), 6.97 (t, 1H, 7.5 Hz), 7.10 (d, 1H, 8.4 Hz) 7.32–7.46 (m, 2H), 8.32 (s, 1H), 13.83 (s, 1H).

APCHAP [23]:

4-Amino[2.2]paracyclophane (30 mg, 0.13 mmol), 2'-Hydroxyacetophenone (18 mg, 0.13 mmol) and p-toluene sulfonic acid (2.5 mg, 10 mol %) were dissolved in *n*-butanol (2 ml) and heated to reflux solvent for 24 h. The reaction mixture was cooled to room temperature and the solvent removed under reduced pressure. The crude residue was purified through column chromatography (silica

gel, hexane/ethyl acetate = 1:1) to give APC_HAP as a yellow solid in 48% yield (22 mg, 0.064 mmol). ^{1}H NMR (300 MHz, $CDCl_3$, 293K) δ 2.19, 2.26 (s, 3H), 2.61–2.81 (m, 1H), 2.87–3.33 (m, 7H), 5.77 (s, 1H), 6.35–6.58 (m, 4H), 6.62 (d, 1H, 8.2 Hz), 6.91 (t, 1H, 7.7 Hz), 7.10 (d, 2H, 8.2 Hz), 7.41 (t, 1H, 7.3 Hz) 7.61 (d, 1H, 7.7 Hz).

pp-DAPSA:

Pseudo-para-4,12-diamino[2.2]paracyclophane (60 mg, 0.25 mmol) and salicylaldehyde (62 mg, 0.50 mmol) were dissolved in 5 ml ethanol and heated to reflux solvent for 2 hour. After heating, the reaction mixture was stirred at room temperature for 1 hour. The precipitate that formed was collected by filtration and rinsed with absolute ethanol to get the final product as a yellow solid in 86 % yield (96 mg, 0.22 mmol). ^{1}H NMR (300 MHz, $CDCl_3$, 293K, given in Appendix:) δ 2.76 - 2.90 (m, 2H), 3.10 – 3.32 (m, 4H), 3.61 – 3.76 (m, 2H), 6.05 (d, 2H), 6.36–6.44 (dd, 2H), 6.84 -6.90 (dd, 2H), 6.94 – 7.02 (t, 2H), 7.08 – 7.14 (d, 2H), 7.38 – 7.48 (m, 4H), 8.35 (s, 2H), 13.82 (s, 1H (-OH)).

pm-DAPSA:

Pseudo-meta-4,13-diamino[2.2]paracyclophane (140 mg, 0.59 mmol) and salicylaldehyde (143 mg, 1.17 mmol) were dissolved in 10 ml ethanol and heated to reflux solvent for 2 hour. After heating, the reaction mixture was stirred at room temperature for 1 hour. The precipitate that formed was collected by filtration and rinsed with absolute ethanol to get the final product as a yellow

solid in 75 % yield (195 mg, 0.44 mmol). ^{1}H NMR (300 MHz, $CDCl_3$, 293K, given in Appendix:) δ 2.80 – 3.30 (m, 6H), 3.50 – 3.80 (m, 2H), 6.09 (d, 2H), 6.36–6.44 (dd, 2H), 6.84 -6.92 (dd, 2H), 6.94 – 7.02 (t, 2H), 7.06 – 7.14 (d, 2H), 7.36 – 7.46 (m, 4H), 8.35 (s, 2H), 13.79 (s, 1H (-OH)).

Synthesis of metal complexes:

Cu(DMASA)$_2$:

N-Salicylidene-2,5-dimethylaniline (230 mg, 1.02 mmol) was dissolved in 10 ml of methanol and stirred well. A copper acetate monohydrate (100 mg, 0.50 mmol) solution in 5 ml methanol was prepared and added slowly to the reaction mixture. The reaction mixture was stirred for 1 hour at room temperature. The resulting brown solution contained brown precipitate, which was isolated by filtration and rinsed with methanol and ether to get the final product as a brown solid in 45 % yield (140 mg, 0.22 mmol). IR (KBr pellets): (C=N stretch) 1606 cm^{-1}

Cu(APCSA)$_2$:

N-Salicylidene-4-amino[2.2]paracyclophane (29 mg, 0.09 mmol) was dissolved in 2 ml of acetonitrile and triethylamine (3-4 drops) was added dropwise. A copper perchlorate hexahydrate (16.5 mg, 0.045 mmol) solution in 2 ml of acetonitrile was prepared and added drop-wise to the reaction mixture. The

reaction mixture was stirred for 2 hours at room temperature. The resulting brown solution contained brown precipitate, which was isolated by filtration and rinsed with acetonitrile and ether to get the final product as a brown solid in 34 % yield (19 mg, 0.03 mmol). IR (KBr pellets):- (C=N stretch)1603 cm^{-1}

Poly(Cu(pp-DAPSA)) and poly(Cu(pm-DAPSA):

The general procedure for forming poly(Cu(pp-DAPSA)) and poly(Cu(pm-DAPSA) complexes is as follows: To a 3 ml methanolic solution of appropriate Schiff's base ligand [(pp-DAPSA) (30.0 mg, 0.070 mmol) and (pm-DAPSA) (50.0 mg, 0.11 mmol)], 3-4 drops of triethylamine was added and stirred. To this reaction mixture 2 ml of a methanolic solution of copper chloride [for pp-DAPSA (18.1 mg, 0.13 mmol) and for pm-DAPSA (30.1 mg, 0.22 mmol)] were added and the mixture stirred overnight at room temperature. The precipitate that formed was collected by filtration and rinsed first with methanol, and then with ether solvents.

Poly(Cu(pp-DAPSA): 33 mg brown solid product

Poly(Cu(pm-DAPSA): 66 mg brown solid product

Figure IV- 32: IR spectrum of APCSA Ligand using KBr salt.

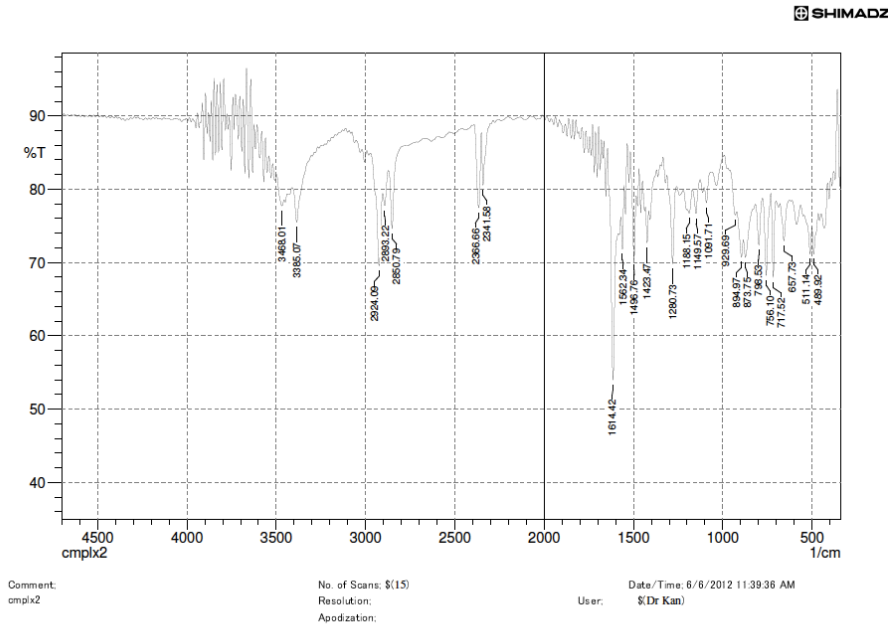

Figure IV – 33: IR spectrum of the $(APCSA)_2Cu$

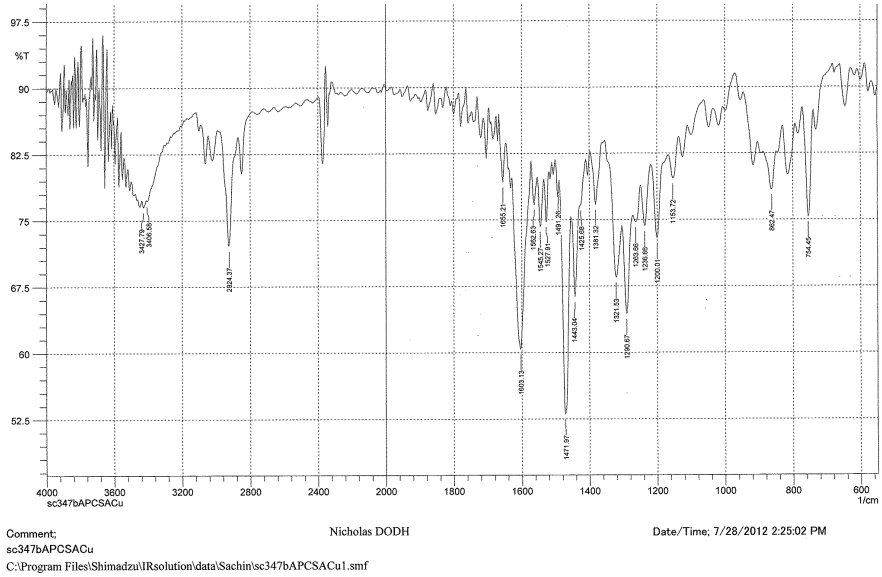

^{1}H NMR pp-DAPSA:

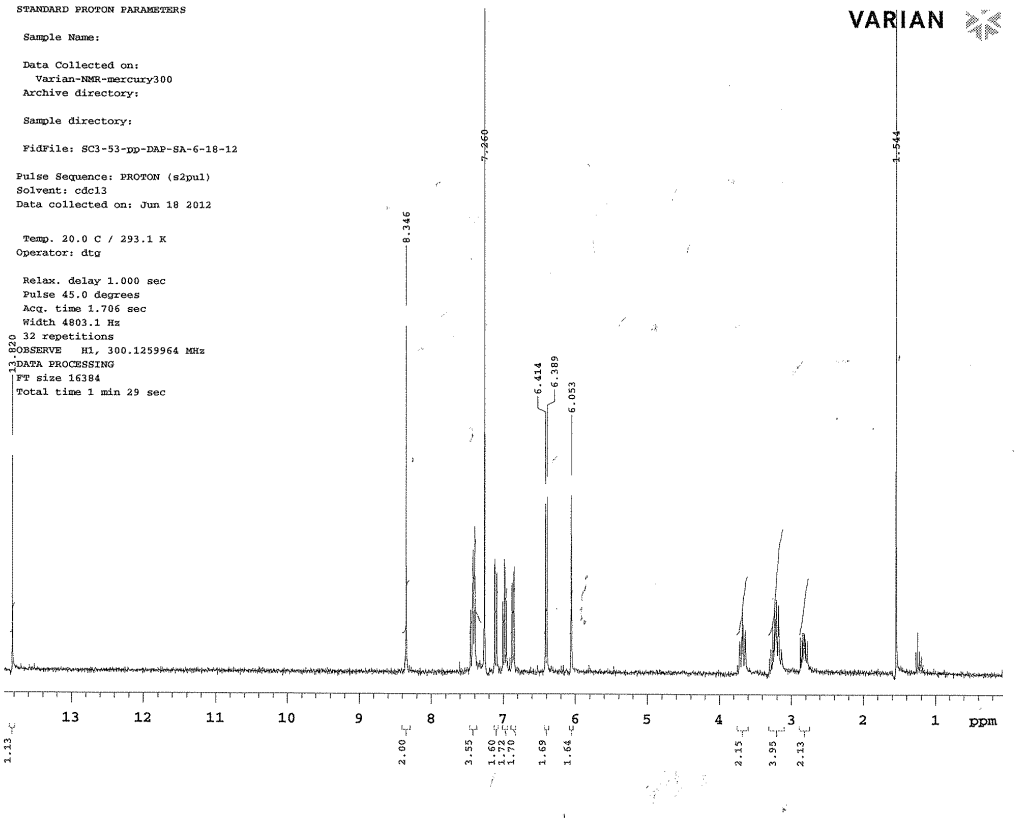

^{1}H NMR pm-DAPSA:

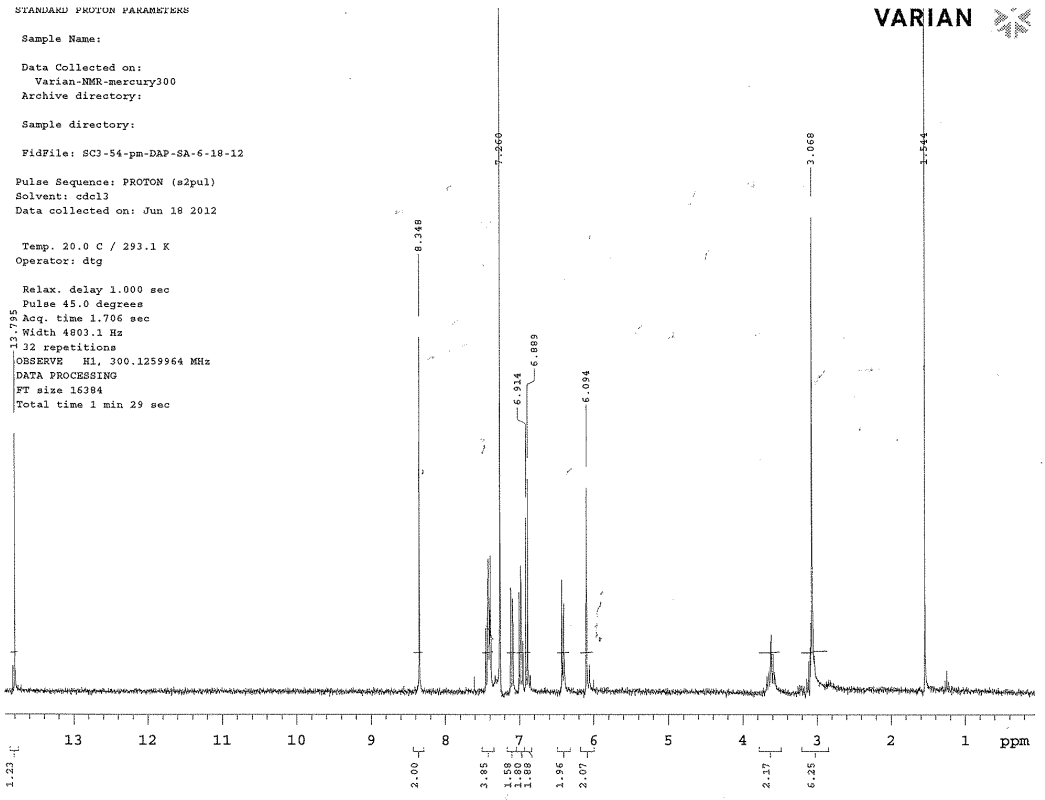

References:

1. Stevens, M.P., *Polymer Chemistry: An introduction*, ed. O.U. Press 1999, New York: Oxford University Press.

2. Charles E. Carraher, J., *Organometallic Polymers. J. Chem. Edu*, 1981. **58**: 921 - 934.

3. Gibson, S.E.; Knight, J.D., *[2.2]Paracyclophane derivatives in asymmetric catalysis.* Organic & Biomolecular Chemistry, 2003. **1**: 1256-1269.

4. Cahn, R.S.; Ingold, C.; Prelog, V., *Specification of Molecular Chirality.* Angewandte Chemie International Edition in English, 1966. **5**: 385-415.

5. Rolf Gleiter, H.H., *Modern Cyclophane Chemistry*, ed. W.-V.V.G. Co.2004, Germany: WILEY - VCH. 200 - 201.

6. Gibson, S.E.; Knight, J.D., *[2.2]Paracyclophane Derivatives in Asymmetric Catalysis.* Org. Biomol. Chem., 2003. **1**: 1256 - 1269.

7. Pye, P.J.; Rossen, K.; Reamer, R.A.; Tsou, N.N.; Volante, R.P.; Reider, P.J., *A New Planar Chiral Bisphosphine Ligand for Asymmetric Catalysis: Highly Enantioselective Hydrogenations under Mild Conditions.* Journal of the american chemical society, 1997. **119**: 6207-6208.

8. Pye, P.J.; Rossen, K.; Reamer, R.A.; Volante, R.P.; Reider, P.J., *[2.2]PHANEPHOS-Ruthenium(II) complexes: Highly active asymmetric catalysts for the hydrogenation of β-ketoesters.* Tetrahedron Letters, 1998. **39**: 4441-4444.

9. Danilova, T.y.I.; Rozenberg, V.I.; Vorontsov, E.V.; Starikova, Z.A.; Hopf, H., *A new family of planar-chiral symmetric and unsymmetric salens based on the [2.2]paracyclophane skeleton.* Tetrahedron: Asymmetry, 2003. **14**: 1375-1383.

10. Danilova, T.I.; Rozenberg, V.I.; Starikova, Z.A.; Bräse, S., *Planar-chiral salen and hemisalen [2.2]paracyclophane ligands for asymmetric diethylzinc addition to aldehydes.* Tetrahedron: Asymmetry, 2004. **15**: 223-229.

11. Dahmen, S.; Bräse, S., *Paracyclophanes in Action: Asymmetric Catalytic Dialkylzinc Addition to Imines Using [2.2]Paracyclophane-based N,O-Ligands as Catalysts.* Israel Journal of Chemistry, 2012. **52**: 139-142.

12. Antonov, D.Y.; Belokon, Y.N.; Ikonnikov, N.S.; Orlova, S.A.; Pisarevsky, A.P.; Raevski, N.I.; Rozenberg, V.I.; Sergeeva, E.V.; Struchkov, Y.T.; Tararov, V.I.; Vorontsov, E.V., *Synthesis, resolution and absolute configuration determination of (S)- and (R)-4-formyl-5-hydroxy [2.2]paracyclophane and its application in*

the asymmetric synthesis of [small alpha]-amino acids. Journal of the Chemical Society, Perkin Transactions 1, 1995. **0**: 1873-1879.

13. Whelligan, D.K.; Bolm, C., *Synthesis of Pseudo-geminal-, Pseudo-ortho-, and ortho-Phosphinyl-oxazolinyl-[2.2]paracyclophanes for Use as Ligands in Asymmetric Catalysis.* The Journal of Organic Chemistry, 2006. **71**: 4609-4618.

14. Morvant, M.C., *Synthesis, Properties and Applications of polynitro- and Polyamino[2.2]paracyclophanes*, in *Chemistry and Biochemistry*1996, University of Oklahoma: Norman.

15. Masterson, D.S.; Hobbs, T.L.; Glatzhofer, D.T., *Catalytic enantioselective cyclopropanation of olefins using N-salicylidene-4-amino[2.2]paracyclophane as an asymmetric ligand.* Journal of Molecular Catalysis A: Chemical, 1999. **145**: 75-81.

16. Masterson, D.S.; Shirley, C.; Glatzhofer, D.T., *N-(4-[2.2]paracyclophanyl)-2'-hydroxyacetophenone imine: An effective paracyclophane Schiff-base ligand for use in catalytic asymmetric cyclopropanation reactions.* Journal of Molecular Catalysis A: Chemical, 2012. **361–362**: 111-115.

17. Ball, P.J.; Shtoyko, T.R.; Krause Bauer, J.A.; Oldham, W.J.; Connick, W.B., *Binuclear Rhenium(I) Complexes with Bridging [2.2]Paracyclophane−Diimine Ligands: Probing Electronic Coupling through π−π Interactions.* Inorganic Chemistry, 2003. **43**: 622-632.

18. Robin, M.B.; Day, P., *Mixed Valence Chemistry-A Survey and Classification*, in *Advances in Inorganic Chemistry and Radiochemistry*, H.J. Emeléus and A.G. Sharpe, Editors. 1968, Academic Press. p. 247-422.

19. Plitzko, K.D.; Rapko, B.; Gollas, B.; Wehrle, G.; Weakley, T.; Pierce, D.T.; Geiger, W.E.; Haddon, R.C.; Boekelheide, V., *Bis(.eta.6-hexamethylbenzene)(.eta.6,.eta.6-[2n]cyclophane)diruthenium(II,II) complexes and their two-electron reduction to [2n]cyclophane derivatives having two cyclohexadienyl anion decks joined by an extremely long carbon-carbon bond.* Journal of the american chemical society, 1990. **112**: 6545-6556.

20. Bowyer, W.J.; Geiger, W.E.; Boekelheide, V., *An electrochemical study of the reduction of mono- and bis(iron) cyclophane complexes.* Organometallics, 1984. **3**: 1079-1086.

21. Masterson, D.S.; Hobbs, T.L.; Glatzhofer, D.T., *Catalytic Enantioselective Cyclopropanation of Olefins using N-salicylidene-4-amino[2.2]paracyclophane as an Asymmetric Ligand.* Journal of Molecular Catalysis A: Chemical, 1999. **145**: 75 - 81.

22. Cram, D.J.; Allinger, N.L.; Steinberg, H., *Macro Rings. VII. The Spectral Consequences of Bridging Two Benzene Rings Face to Face.* J. Am. Chem. Soc, 1954. **76**: 6132 - 6141.

23. Masterson, D.S.; Shirley, C.; Glatzhofer, D.T., *N-(4-[2.2]paracyclophanyl)-2'-hydroxyacetophenone imine: An Effective Paracyclophane Schiff-base Ligand for use in Catalytic Asymmetirc Cyclopropanation Reactions.* Journal of Molecular Catalysis A: Chemical, 2012. **361 - 362**: 111 - 115.

24. Braude, E.A.; Sondheimer, F., *Studies in light absorption. Part XI. Substituted benzaldehydes, acetophenones and related compounds. The effects of steric conformation on the electronic spectra of conjugated systems.* J. Chem. Soc., 1955. **0**: 3754 - 3766.

25. Braude, E.A.; Jones, E.R.H.; Koch, H.P.; Richardson, R.W.; Sondheimer, F.; Toogood, J.B., *Studies in Light Absorption. Part VI. Steric Inhibitionof Resonance in Natural and Synthetic derivatives of Cyclohexene.* J. Chem. Soc., 1949. **403**: 1890 - 1897.

26. Fehnel, E.A., *Steric Effects in the Ultraviolet Absorption Spectra of 2,4,6-Trimethylbenzoic Acid and Methyl Ester.* J. Am. Chem. Soc, 1950. **72**: 1404 - 1405.

27. Hedden, G.D.; Brown, W.G., *Ultraviolet Absorption Spectra of Hindered Ketones.* J. Am. Chem. Soc, 1953. **75**: 3744 - 3748.

28. Braude, E.A.; Sondheimer, F.; Forbes, W.F., *Steric Effects in the Electronic Spectra of Organic Compounds.* Nature, 1954. **173**: 117 - 119.

29. Braude, E.A.; Forbes, W.F., *Studies in Light Absorption. Part XIV. Steric Effects in ortho-Substituted Diphenyls.* J. Chem. Soc., 1955. **0**: 3776 - 3782.

30. Elias, H.; Hasserodt-Taliaferro, C.; Hellriegel, L.; Schoenherr, W.; Wannowius, K.J., *Effect of the coordination geometry and of substituent shielding on the kinetics of ligand substitution in copper(II) chelates.* Inorganic Chemistry, 1985. **24**: 3192-3198.

31. Elmali, A.; Elerman, Y.; Zeyrek, C.T., *Conformational Study and Structure of N-(2,5-methylphenyl)salicylaldimine.* Journal of Molecular Structure, 1998. **443**: 123 - 130.

32. Roy, G.B., *Synthesis and Study of Physico-Chemical Properties of a new Chiral Schiff base ligands and its Metal Complex.* Inorganica Chimica Acta, 2009. **362**: 1709 - 1714.

33. Bilge, S.; Kilic, Z.; Hayvali, Z.; Hokelek, T.; Safran, S., *Intramolecular Hydrogen Bonding and Tauterism in Schiff Bases: Part VI. Syntheses and Structural Investigation of Salicylaldimine and Naphthaldimine Derivatives.* J. Chem. Sci, 2009. **121**: 989 - 1001.

34. Baleizão, C.; Garcia, H., *Chiral Salen Complexes: An Overview to Recoverable and Reusable Homogeneous and Heterogeneous Catalysts.* Chemical Reviews, 2006. **106**: 3987-4043.

35. Vafazadeh, R.; Hayeri, V.; Willis, A.C., *Synthesis, crystal structure and electronic properties of bis(N-2-bromophenyl-salicydenaminato)copper(II) complex.* Polyhedron, 2010. **29**: 1810-1814.

36. Dudek, E.P.; Dudek, G., *Infrared spectra of 15N substituted copper complexes.* Inorganic and Nuclear Chemistry Letters, 1967. **3**: 241-244.

37. El-Tabl, A.S., *Synthesis and Characterization of Cobalt(II)/(III), Nickel(II) and Copper(II) Complexes of New 14, 15 and 16-Membered Macrocyclic Ligands.* Bulletin of the Korean Chemical Society, 2004. **25**: 1757 - 1763.

38. Kasumov, V.T.; Yerli, Y.; Kutluay, A.; Aslanoglu, M., *Synthesis, spectroscopy, magnetic and redox behaviors of copper(II) complexes with tert-butylated salen type ligands bearing bis(4-aminophenyl)ethane and bis(4-aminophenyl)amide backbones.* Spectrochimica Acta Part A: Molecular and Biomolecular Spectroscopy, 2013. **104**: 203-212.

39. Bosnich, B., *An interpretation of the circular dichroism and electronic spectra of salicylaldimine complexes of square-coplanar diamagnetic nickel(II).* Journal of the american chemical society, 1968. **90**: 627-632.

40. Knapp, S.; Keenan, T.P.; Zhang, X.; Fikar, R.; Potenza, J.A.; Schugar, H.J., *Preparation, structure, and properties of pseudotetrahedral, D2d complexes of copper(II), nickel(II), cobalt(II), copper(I), and zinc(II) with the geometrically constraining bidentate ligand 2,2'-bis(2-imidazolyl)biphenyl. Examination of electron self-exchange for the Cu(I)/Cu(II) pair.* Journal of the american chemical society, 1990. **112**: 3452-3464.

41. Klement, R.; Stock, F.; Elias, H.; Paulus, H.; Pelikan, P.; Valko, M.; Mazur, M., *Copper(II) complexes with derivatives of salen and tetrahydrosalen: a spectroscopic, electrochemical and structural study.* Polyhedron, 1999. **18**: 3617 - 3628.

42. Rieger, P.H., *Electron Spin Resonance*2007: The Royal Society of Chemitry.

43. Tharmaraj, P.; Kodimunthiri, D.; Sheela, C.D.; Priya, C.S.S., *Synthesis, Spectral Studies and Antibacterial Activity of Cu(II), Co(II) and Ni(II) complexes of 1-(2-*

hydroxyphenyl)-3-phenyl-2-propen-1-one, N,N-[(3,5-dimethyl-1H-pyrazol-1-yl)methyl]hydrazone. Journal of the Serbian Chemical Society, 2009. **74**: 927 - 938.

44. Evans, D.F., *The Determination of the Paramagnetic Susceptibility of the Substances in Solution by Nuclear Magnetic Resonance.* J. Chem. Soc., 1959: 2003 - 2005.

45. Schubert, E.M., *Utilizing the Evans method with a superconducting NMR spectrometer in the undergraduate laboratory.* J. Chem. Edu., 1992. **69**: 62.

46. Oriol, L.; Alonso, P.J.; Martinez, J.I.; Pinol, M.; Serrano, J.L., *Structural Studies of Copper(II)-Chelated Polymers Derived from Hydroxy-Functionalized Liquid Crystalline Homo- and Copolyazomethines.* Macromolecules, 1994. **27**: 1869-1874.

47. Coronado, E.; Gimenez-Marques, M.; Espallargas, G.M.; Brammer, L., *Tuning the Magneto-Structual Properties of Non-Porous Coordination Polymers by HCl Chemisorption.* Nature Communications, 2011. **3**: 828.

48. Marcos, M.; Oriol, L.; Serrano, J.L.; Alonso, P.J.; Puertolas, J.A., *Metal-containing homopolymers showing paramagnetic nematic mesophase.* Macromolecules, 1990. **23**: 5187-5191.

49. Abd-Elzaher, M.M., *Spectroscopic Characterization of Some Tetradentate Schiff Bases and Their Complexes with Nickel, Copper and Zinc. J. Chin. Chem. Soc.*, 2001. **48**: 153 - 158.

50. Misra, S.; Pandeya, K.; Tiwari, A.; Ali, A.; Saradamani, T.; Agawane, S.; Madhusudana, K., *Antihyperglycemic, α-glucosidase inhibitory and DPPH free radical scavenging activity of 5-bromosalicylaldehyde and schiff bases.* Medicinal Chemistry Research, 2011. **20**: 1431-1437.

51. Rai, M.; Singh, A., Ind. J. Chem. B, 1976. **14B**: 377.

52. Gündüz, T.; Kiliç, E.; Canel, E.; Köseo; gt; glu, F., *Protonation constants of some substituted salicylideneanilines in dioxan—water mixtures.* Analytica Chimica Acta, 1993. **282**: 489-495.

Chapter V

Electropolymerization of Bithiophene in Sodium Dodecylsulfate Micellar Media

Introduction:

Polymers have found various applications in everyday life. Conducting polymers have applications as optical and electronic materials for use in batteries, information storage, solar energy conversion, non-linear optics, sensor technology, etc. Conducting polymers can be further subdivide into three classes:

- Electron conducting polymers,
- Proton conducting polymers
- Ion conducting polymers.

Such polymers find many applications because of their ease of fabrication, flexibility of strength, lightness of weight, and chemical inertness. Because of these features research interest in conducting polymers continues to increase. In electronically conducting polymers, electronic conduction occurs by migration of electrons or positive holes along the polymer chain. This migration can occur due to the presence of conjugated, delocalized double bonds such as in polyacetylene. These conjugated polymers are studied for three main reasons. First, their high electronic conductivity in their doped form; second, in the case of undoped polymer forms, they behave as organic semiconductors which can be used in organic electronic devices such as solar cells, light emitting diodes, etc; and third, the ability of some to be processed electrochemically [1].

Interest in conducting polymers began to take off in the 1970's with the discovery of polyacetylene, prepared as a film by a modification of the Natta reaction [2]. Polymers such as polyethylene, polypropylene, poly(ethylene terephthalate), and polystyrene, obtained from their unsaturated monomers, are used as the insulators as they do not posses any mobile charges. Other polymers, such as polyacetylene, poly(p-phenylene), and polyheterocycles such as polypyrrole, polythiophene, polyfuran, polyindole, etc, given in Table 1, which possess extended conjugation, possess properties such as semiconductivity or conductivity, and strong interactions with light.

Table 1: Some known conducting polymers

Polymers	Structure	Polymer	Structure
Polypyrrole		Polyindole	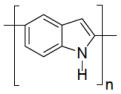
Polythiophene		Polyaniline	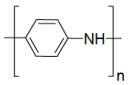
Polyfuran		Polyazulene	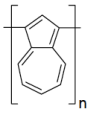
Polyselenophene		Poly *Para*-phenylene	

Poly(phenylene vinylene) showed electroluminescence properties when coated on the indium-tin oxide surface, which found application as an organic light emitting diode. This is possible because of the presence of π – electrons in the main chain of the polymer [3]. Other structural features these polymers

possess are planarity and large anisotropy ratios. Benzenoid and nonbenzenoid aromatic heterocycles have been used to generate the electrically conducting polymers. These polymers are formed from monomers such as pyrrole, thiophene, indole, furan, carbazole, and polycyclic aromatic hydrocarbons such as fluorine, azulene, pyrene, etc.

Electrically conducting polymers usually contain oppositely charged doping ions along the polymer chains (n and p doping). Doping of semiconducting/conducting polymers resulted in increased conductivity by introducing halogens. Due to this doping, charged species are able to move along the conjugated system of the polymer to form an electronically conductive polymer. Polyacetylene conductivity was increased seven orders when it was exposed to iodine vapor [2].

Conducting polymers can be synthesized chemically or electrochemically. Polyacetylene was first synthesized using an $Al(Et)_3/Ti(OPr)_4$ catalyst to get films up to 0.5 cm thick. Doping with halogens or AsF_5 was used to increase the conductivity of polyacetylene. Other chemicals such as ammonium persulfate, aluminum trichloride/copper chloride, $FeCl_3$, etc, have been used to synthesize conducting polymers [4, 5].

Polyaniline is often considered to be the most important conducting polymer, and has been made from anilines using oxidants such as $FeCl_3$ and MnO_2, $V_2O_5.nH_2O$ xerogels, and air oxidation using $Cu(NO_3)_2$ as a catalyst [6]. Polyaniline has been prepared chemically to study its conductivity properties and investigations to understand its mechanism are still continuing.

Electropolymerization of aniline is complicated in the sense that it typically forms as a powdery product but if a cycling voltage is kept between -0.2 and +0.8 V, it forms as a coherent film on the electrode surface. For polyaniline, various forms of the polymer were proposed depending on methods of preparation. Polyaniline bases may exist in a fully reduced form (leucoemeraldine, y = 1 on the scheme below), partially reduced form (emeraldine, y = 0.5 on the scheme below), and fully oxidized form (pernigraniline, y = 0 on the scheme below). Polyaniline bases may form polyaniline salts when treated with acids such as hydrochloric acid, or camphor sulfonic acids, as shown in Figure V - I.

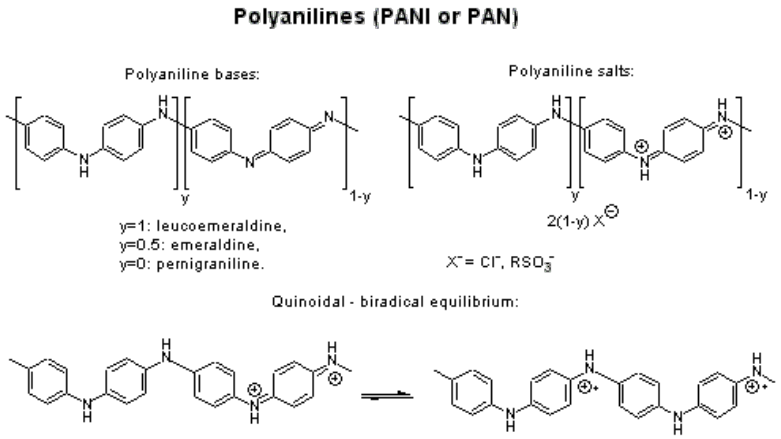

Figure V – I: Polyaniline conducting polymer

Conducting polymers synthesized electrochemically are generally formed by electrochemical oxidation of aromatic molecules. Electrodeposition of conducting polymers onto electrodes is of great interest due to the wide range of applications for such films. Formation of uniform films and simple processing

makes electropolymerization an especially attractive method to form conducting polymers. Various methods can be used to prepare films of electronically conducting polymers. Potentiostatic (constant-potential), galvanostatic (constant current) and potentiodynamic (potential scanning *i.e* cyclic voltammetry) methods can be used for such polymer preparation.

Polypyrrole is perhaps the most extensively studied of the various conducting polymers. The pyrrole monomer is easily oxidizable, water soluble, and commercially available and the polymer has certain advantages like environmental stability, good redox properties, and high electrical conductivity. Hence, polypyrrole finds applications in batteries, supercapacitors, electrochemical biosensors, conductive fabrics, mechanical actuators, anti-static coatings, and drug delivery systems etc [7]. Polypyrrole can be prepared by electrolytic oxidation of pyrrole. Different oxidizing methods, such as electrolytic and chemical, form polypyrrole films with different conductivity. Electrolysis of an acetonitrile solution of pyrrole with tetraethylammonium fluoroborate as an electrolyte gives highly conducting BF_4^- doped films of polypyrrole on the anode [8], while using a chemical oxidizing agent such as iron(III) chloride gives polypyrrole films with inferior conductivity [9].

The general mechanism for the polypyrrole formation is shown in Figure V – 2, which involves three steps, 1) formation of radical cations, 2) radical combination, and 3) deprotonation.

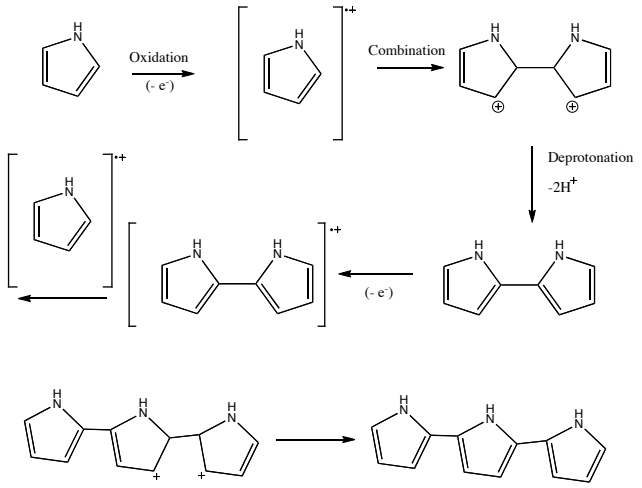

Figure V – 2: Mechanism of polypyrrole formation

The electrical conductivities of polypyrrole films depend on a number of factors such as the presence of counterions, temperature of the electrooxidation, and the potential applied during the polymerization process. Polypyrrole films are usually amorphous and homogenous with densitites around 1.5 g / cm^3. The polymer films usually contain one counterion for every three to four pyrrole units. To improve the stability and activity of films based on polypyrrole, numerous attempts have been made using different counterions such as BF_4^-, ClO_4^-, p-toluenesulfonate, tetrasulfonated metallophthalocyanins, etc [10, 11]. Yahovleva explained the links between the anion and the polymer matrix by studying the electrochemistry of polypyrrole films in aqueous solutions [11]. It was observed that the electrodeposition of polypyrrole on an electrode is limited to certain potentials as well as being dependent on pH, composition and hydrodynamic conditions. The nature of the anion showed an effect on polypyrrole synthesis such that the rate increases in the series ClO_4- > HSO_4^- >

Cl^-. The anion doped polypyrrole films electrodeposited from aqueous solution are black, compact, somewhat flexible in nature, insoluble in ordinary organic solvents, and degradatively soluble in hydrogen peroxide and hot chromic mixtures. In another study, reagents such as sulfuric, phosphoric, oxalic and acetic acid, were used in the polymerization of pyrrole to study electrical conductivity and temperature dependences [12]. Oxidative polymerization was carried using double distilled pyrrole and ammonium persulfate as an oxidant with different acids as dopant. It was noted that the electrical conductivity is dependent on the acidic strength, as more dissociated ions are present during polymerization. The acidic strength for the acids used is in the decreasing order H_2SO_4 > H_3PO_4 > $H_2C_2O_4$ > CH_3COOH. Although the acidic strength of phosphoric acid is less than sulfuric acid, the conductivity of polypyrrole in phosphoric acid is three fold higher. This is due to the triprotic nature of the phosphoric acid, which dissociates up to three times giving up H^+ each time and this can create more ionic species in the polymeric system to increase the conductivity. Temperature studies showed that higher electrical conductivity was observed at higher temperature, which may be due to an increase in lattice vibration resulting from chain stretching.

The choices of solvents and electrolytes are very important in determining the properties of the polypyrrole films. Water and organic solvents (such as acetonitrile, alcohols, tetrahydrofuran, etc) can be used for electropolymerization of polypyrrole. These solvents have to be inert under the operating conditions for electropolymerization (0.8 V to 1.0 V for oxidation of

pyrrole vs SCE) [13]. p-Toluene sulfonate or benzene sulfonate derivatives have been used as electrolytes for polypyrrole formation for which the mechanical strength was observed to be excellent. It was reported that such mechanical strength is due to strong interactions between the p-toluene sulfonate anions and the polypyrrole chains. The degree of insertion (x) of such anions is much higher (x = 0.69 in AcCN and x = 0.51 in aqueous solutions) than the small anions such as ClO_4^- and BF_4^- (x = 0.25) suggesting that there is higher charge per monomer in the polypyrrole system. It was also discussed that ordered polymer structures could be obtained with p-toluene sulfonate, while small anions will form random configurations of polymer. The flexibility of the polypyrrole films could be due to the p-toluene sulfonate anion being sandwiched between a spiral form of the PPy chains, with the sulfonate ion interacting with the chain while the phenyl groups interact in a hydrophobic fashion.

Polyanions such as sodium polyvinyl sulfonate, were used to study the changes in the growth rate and the structure of polymer films formed by electropolymerization [14]. The effect of the size of the anion plays important role in deciding the growth rate of polypyrrole films. Typical anions considered in polymerization are given in Figure V - 3 [15].

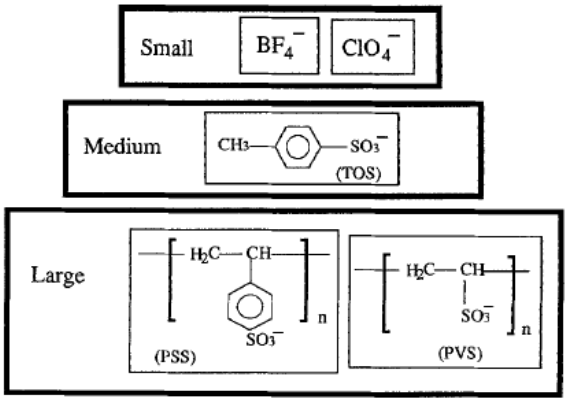

Figure V – 3: Typical anions found in conducting polymers

Polypyrrole films prepared with different anion sizes showed different rates of ion charge/discharge after the electropolymerization process. It was observed by using anode/electrolyte/polymer cathode cells, large anions as dopants gave higher energy density and only a small amount of electrolyte is needed to achieve this energy density. This effect may be due to the movement of anions near the pockets of pyrrole cation unit compensating the positive charge created by radical cations.

Sodium dodecylsulfate (SDS) and sodium dodecylbenzene sulfonate (SDBS) were used to study the electropolymerization of pyrrole, and the anion/cation exchange process in electropolymerized PPy films [15, 16]. Naoi et al. studied micellar effects of surfactants in the electropolymerization of pyrrole [17]. A micelle is an aggregate of surfactant molecules dispersed in liquid. The surfactant molecule typically has a strongly polar head and non-polar hydrocarbon tail. When the surfactant molecule is added to water, the non-polar hydrocarbon tail, hydrophobic in nature, clumps into the center of the ball-like

structure, while the strongly hydrophilic polar head interacts with the outside water. A typical micelle structure is shown in Figure V - 4,

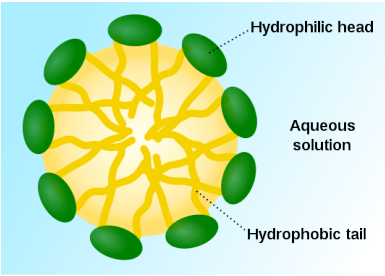

Figure V – 4: Micelle structure

Polypyrrole films grown in micellar solutions of anion surfactants showed perpendicularly oriented columnar structures. The growth rate in electropolymerization is dependent on the critical micelle concentration (CMC) of the surfactants.

The CMC is a characteristic of the surfactants, defined as the concentration above which any added surfactant molecule will form micellar aggregates [18]. So the typical behavior of surfactant molecules above CMC and below CMC is shown Figure V – 5.

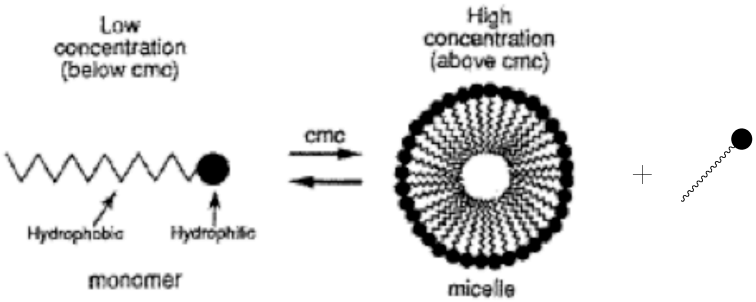

Figure V – 5: Micelle formation

Polythiophenes (PT) are one of the important classes of conjugated polymers that are used for various applications, such as electrical conductors, non-linear optical devices, polymer LEDs, antistatic coatings, solar cells, memory devices, nanoswitches, transistors, optical modulators and valves, etc [19]. The ability to modify polythiophenes made it one of the attractive conjugated polymers for the applications discussed above. Some of the features which polythiophenes provide based on different synthetic methods are π orbital overlap along the polymer backbone, interchain overlap, dimensionality, planarization of the polymer backbone, enhanced electrical conductivity, stability, etc. Polythiophene and its derivatives can be formed by coupling of monomeric units in the 2,5-positions, also called α,α'-positions. A typical polythiophene structure is shown in Figure V – 6. There is also possibilities of monomeric coupling at the 2,4-positions (α,β' positions) to synthesize polythiophenes [20].

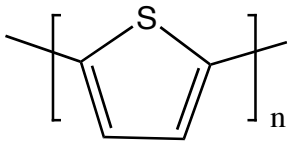

Figure V – 6: Polythiophene

One of the most useful methods for the synthesis of polythiophene is Ni-catalyzed polycondensation of dihalothiophenes. Yamamoto synthesized polythiophene using 2,5-dibromothiophene by reacting with Mg/THF in

presence of nickel (bipyridine) dichloride, which was similar to the system of Lin and Dudek, where the nickel catalyst was replaced by $M(acac)_n$ (where M = Pd, Ni, Co, Fe); both are shown in Scheme V - 1 [19].

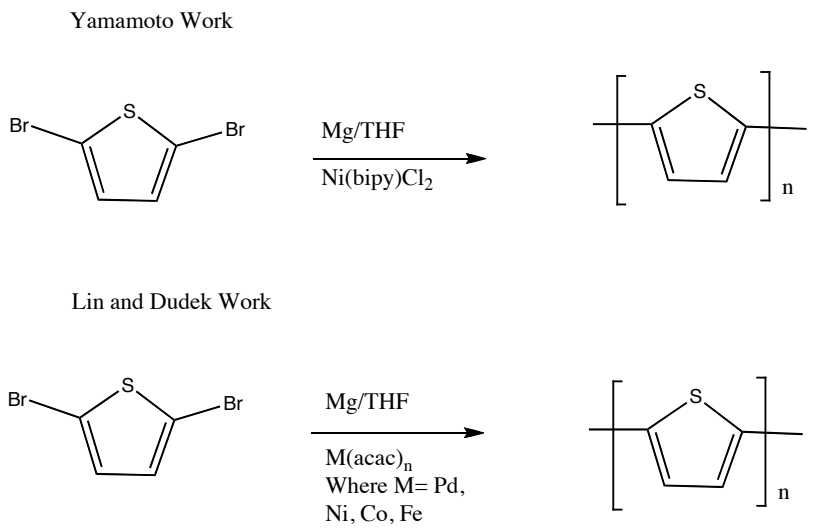

Scheme V – 1: Synthesis of polythiophene

Polythiophene can also be prepared, as shown in Scheme V – 2, by reacting thiophene with $FeCl_3$ [21] . When thiophene is reacted with butyllithium, it forms 2,5-dilithiothiophene which can be further polymerized with $CuCl_2$ to produce polythiophene [22].

Sugimoto Work

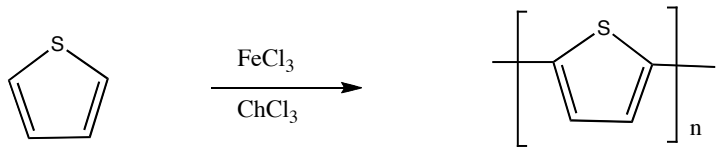

Sannicolo Work

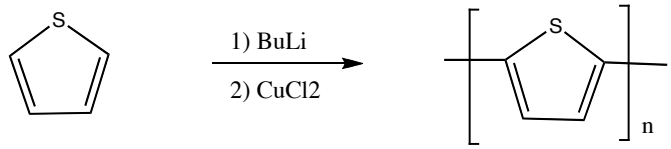

Scheme V – 2: Synthesis of polythiophene

The polythiophene synthesized this way showed little solubility and contains up to 3% of impurities. In the process of improving solubility and processability, alkylthiophenes were polymerized. The first chemically synthesized poly(3-alkylthiophenes) (PATs) showed improved stability and solubility properties as reported by Elsenbaumer et al. and as shown in Scheme V - 3 [23]. The polymers showed better melt moldability, better solubility, high conductivity, and formed environmentally stable complexes with electron acceptor dopants. However, these PATs showed poor thermal stability and have conductivity that may be due to dopant degradation.

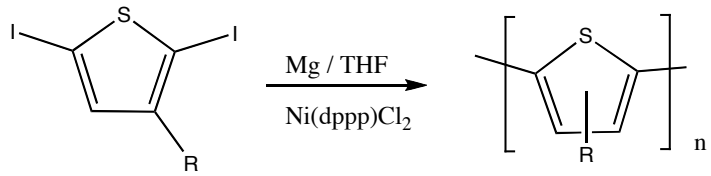

Scheme V – 3: Synthesis of Polyalkylthiophene (PAT)

Electrochemical polymerization of 3-alkylthiophenes has been carried out and the polymer showed higher conductivities than previous studies. The electropolymerization of 3-methylthiophene was carried out in a one compartment cell on an ITO electrode in the presence of propylene carbonate as solvent and tetraethylammonium hexafluorophosphate (Et_4NPF_6) as an electrolyte [24, 25]. Alkylthiophenes and alkoxythiophenes, being soluble in organic solvents, can be polymerized at lower oxidation potentials. Structurally, polymerization of 3-alkylthiophenes yields a mixture of randomly arranged, non-regular polymer chains, which is likely to influence the polymer properties. When symmetrically substituted 2,2'-bithiophene is polymerized, it yields only one polymer structure as shown in Figure V - 7 [26].

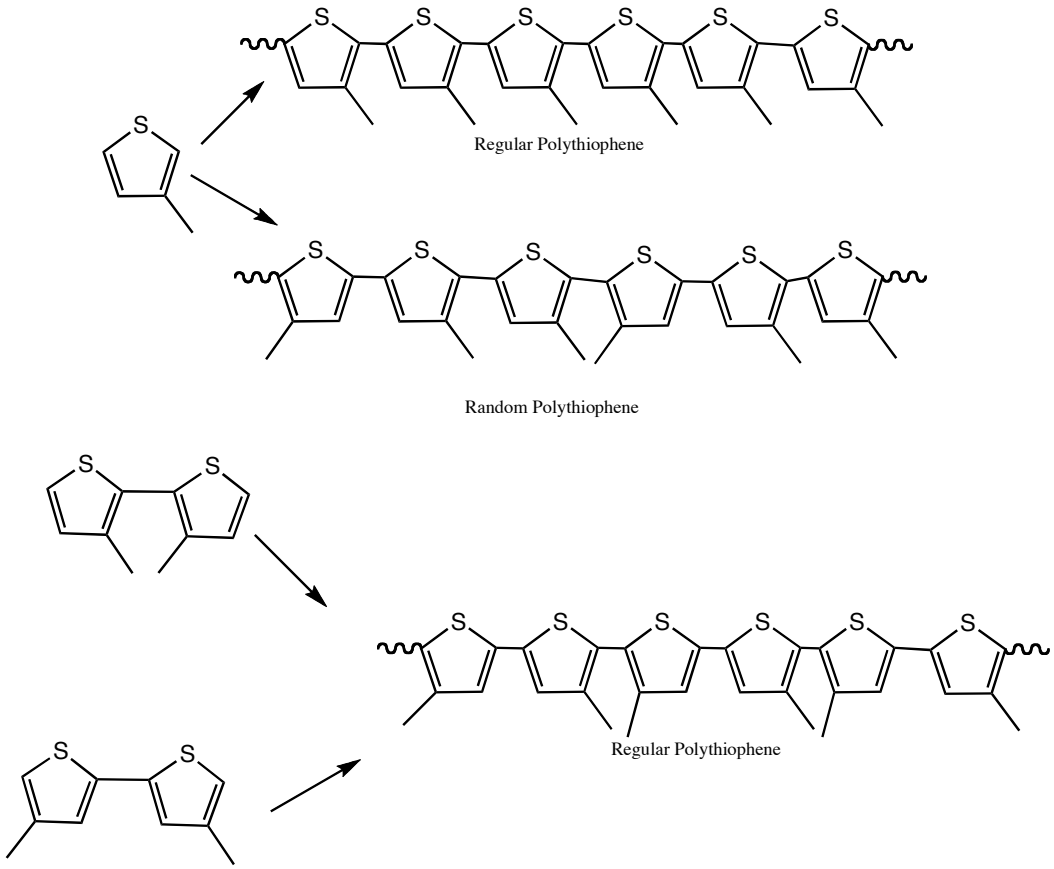

Figure V – 7: Polythiophene

The use of 2,2'-bithiophene as a starting monomer for the synthesis of polythiophene offers advantages over thiophenes, as reported by Krische et al. [26]. The properties reported for PBT are comparable to polythiophene except it has better solubility, a much shorter λ_{max}, CVs showed better resolved peaks, and Uv-vis spectra of polybithiophenes are temperature and solvent independent. The oxidative coupling mechanism for the BT is similar to pyrrole in polymer formation [27]. Electropolymerization studies so far have been carried out in organic solvents, mainly acetonitrile. Polymerization of thiophenes has not been investigated as much as aniline and pyrrole in aqueous

medium because its electropolymerization is difficult due to low solubility, higher oxidation potential, and high reactivity of its radical cation with a nucleophilic medium. Czerwinski and others reported the electrochemical polymerization to form poly(3-methyl-2,5-thienylene) films from aqueous emulsion media using a platinum electrode[28]. The polymer thus produced has different properties than that made in non-aqueous media with respect to its morphology and conductivity. Later, Dong and Zhang used 85% phosphoric acid to electropolymerize thiophene in water, but found that there are many carbonyl defects in the polymer [29]. Later, Lacaze et al. carried out electropolymerization of thiophene in perchloric acid on a platinum electrode. The resulting polythiophene showed better solubility and a lower oxidation potential, 0.9 V, as compared to 1.8 V from non-aqueous medium [30]. Later, for the first time, the same group used a micellar solution of SDS to electropolymerize BT in an aqueous medium on Pt and Fe electrodes [31]. The surfactant SDS improved the solubility of BT in water, lowering its oxidation potential, and improving the properties of the metal/solution interface by eliminating oxidation of the Fe electrode. Later, SDS was used to help synthesize polymers such as PEDOT (poly(3,4-ethylenedioxythiophene) and polybithiophene which showed better morphology and improved chain organization on the platinum electrode [32].

However, systematic studies of the electropolymerization of 2,2'-bithiophene (BT) in micellar media have not been done. Therefore, we wished to study growth and nucleation in the electropolymerization of 2,2'-bithiophene in

the presence of SDS. The optimization of concentration parameters for improved growth of the PBT in aqueous SDS will be discussed. The proposed synthesis of PBT is shown in Scheme V – 4.

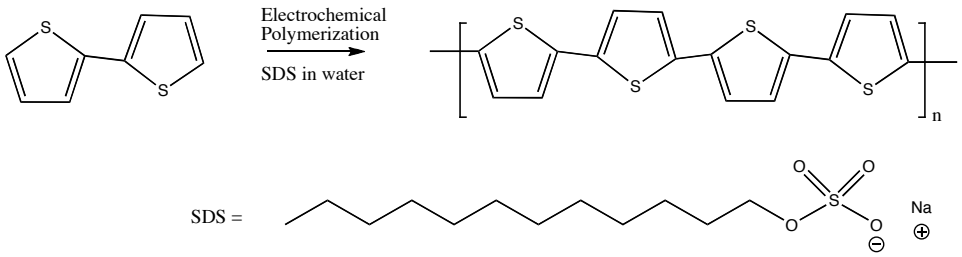

Scheme V – 4: Synthesis of polybithiophene (PBT)

Results and Discussion:

Electropolymerization of Bithiophene:

Synthesis of polythiophene from BT in aqueous SDS solutions was carried out. Different molar concentrations of BT:SDS were used in aqueous solution. Ultrasonic treatment was used to solubilize BT in SDS aqueous solution; the solutions formed were clear and transparent. The transparency is due to the microemulsion formation, which is thermodynamically stable and isotropic. Concentrations of BT and SDS were changed from 0.01 M to 0.04 for BT and 0.1 M to 0.4 M for SDS in water solution as shown in Table V - 2.

Table V -2: Samples used for study

Sample	SDS Concentration in M	BT concentration in M
SC118D	0.1	0.01
SC1211	0.2	0.01
SC1212	0.3	0.01
SC1213	0.4	0.01
SC1214	0.4	0.02
SC1215	0.4	0.03
SC1216	0.4	0.04

Successive cyclic voltammograms (CVs) on a platinum electrode at 100 mV/S were taken for up to 10 scans between -0.9 V to 1.5 V vs a SCE electrode for different concentrations of BT in aqueous solutions containing different concentration of SDS as shown in Figures V – 8 to Figures V - 14.

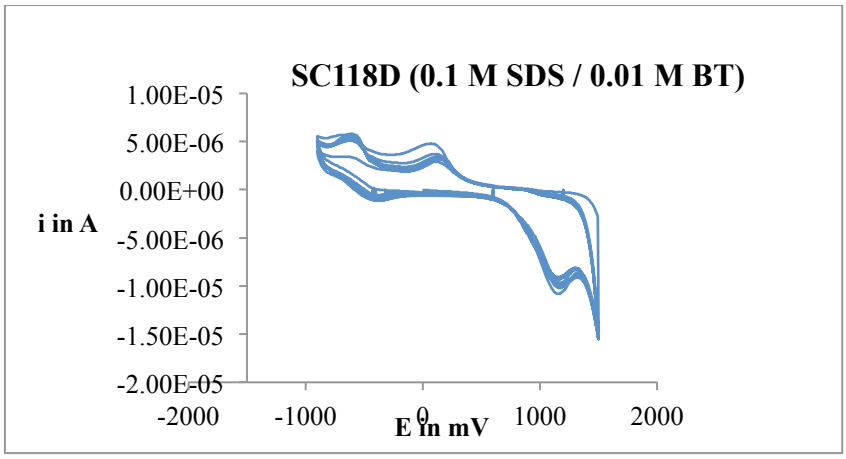

Figure V – 8: Cyclic voltammetry of SC118D. Conditions: 0.01 M BT in 0.1 M SDS aqueous solution; using platinum as a working electrode; platinum wire as auxillary electrode; saturated calomel electrode as reference electrode; at scan rate 100 mV/s.

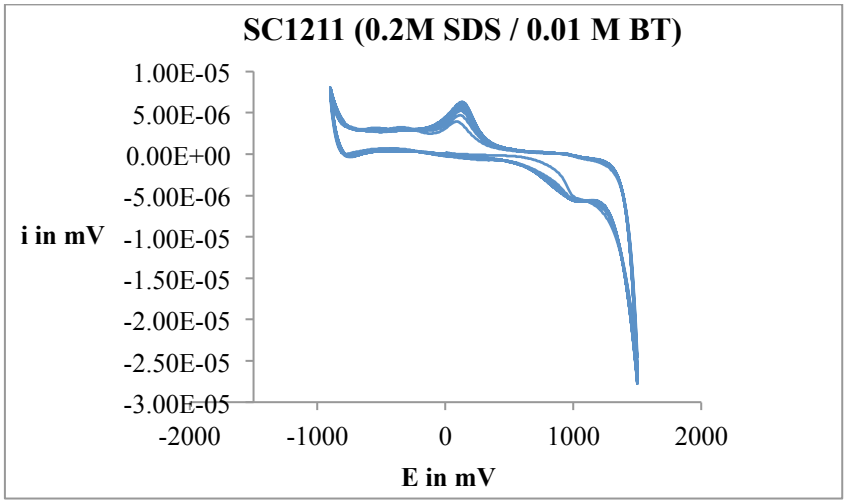

Figure V – 9: Cyclic voltammetry of SC1211 (0.2 M SDS / 0.01 M BT) Conditions: 0.01 M BT in 0.2 M SDS aqueous solution; using platinum as a working electrode; platinum wire as auxillary electrode; saturated calomel electrode as reference electrode; at scan rate 100 mV/s

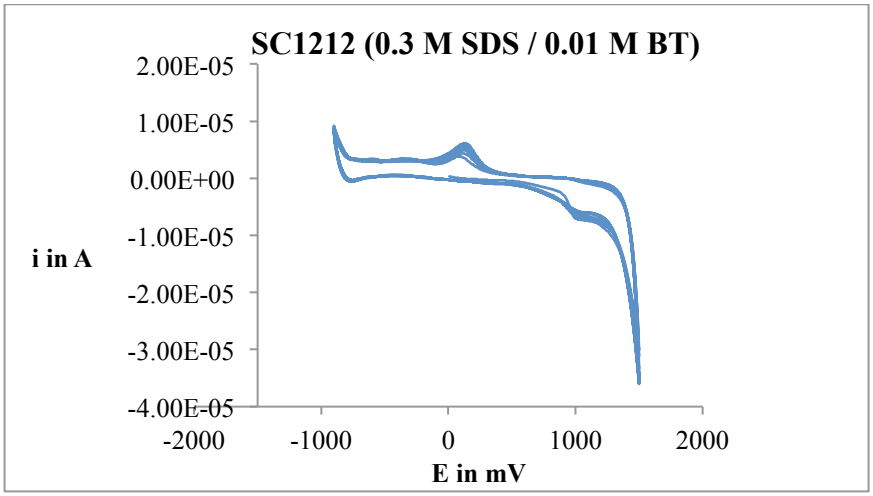

Figure V – 10: Cyclic voltammetry of SC1212 (0.3 M SDS / 0.01 M BT) Conditions: 0.01 M BT in 0.3 M SDS aqueous solution; using platinum as a working electrode; platinum wire as auxillary electrode; saturated calomel electrode as reference electrode; at scan rate 100 mV/s

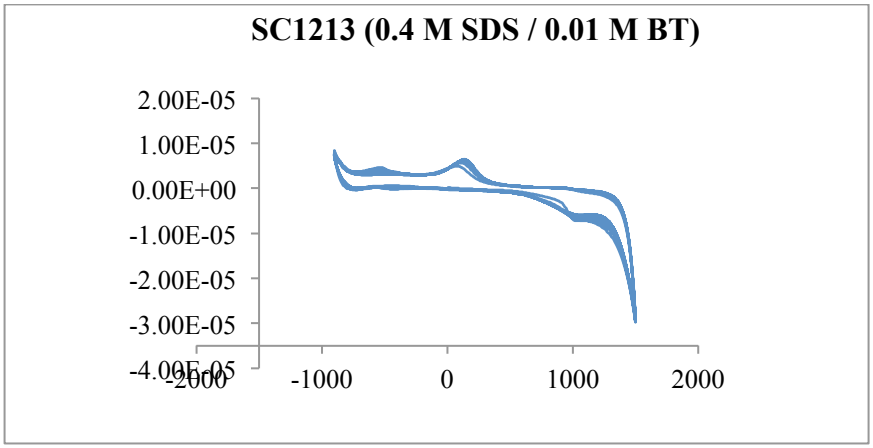

Figure V – 11: Cyclic voltammetry of SC1213 (0.4 M SDS / 0.01 M BT) Conditions: 0.01 M BT in 0.4 M SDS aqueous solution; using platinum as a working electrode; platinum wire as auxillary electrode; saturated calomel electrode as reference electrode; at scan rate 100 mV/s

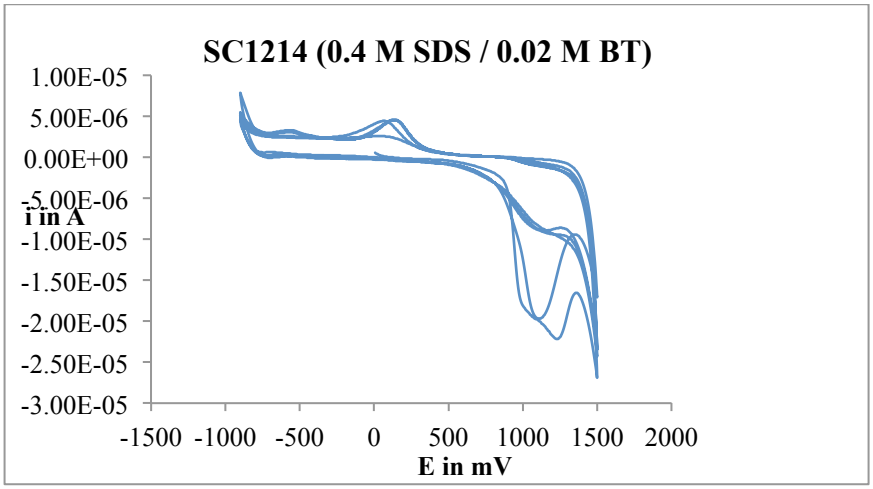

Figure V – 12: Cyclic voltammetry of SC1214 (0.4 M SDS / 0.02 M BT) Conditions: 0.02 M BT in 0.4 M SDS aqueous solution; using platinum as a working electrode; platinum wire as auxillary electrode; saturated calomel electrode as reference electrode; at scan rate 100 mV/s

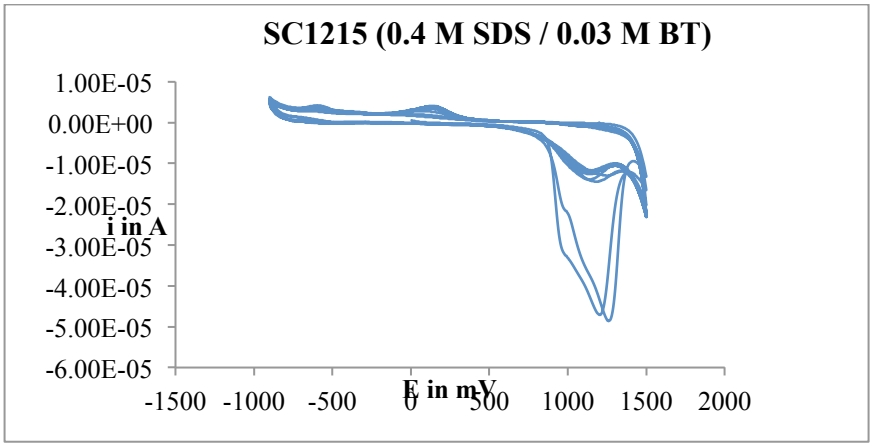

Figure V – 13: Cyclic voltammetry of SC1215 (0.4 M SDS / 0.03 M BT) Conditions: 0.03 M BT in 0.4 M SDS aqueous solution; using platinum as a working electrode; platinum wire as auxillary electrode; saturated calomel electrode as reference electrode; at scan rate 100 mV/s

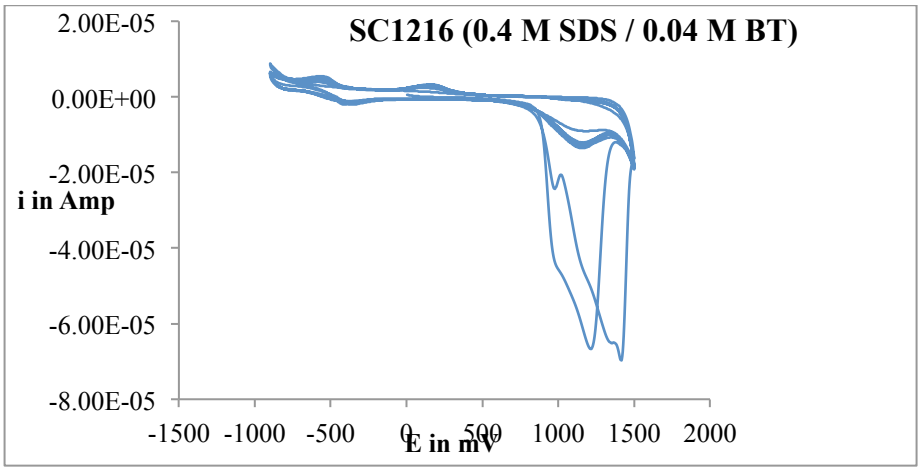

Figure V – 14: Cyclic voltammetry of SC1216 (0.4 M SDS / 0.04 M BT) Conditions: 0.04 M BT in 0.4 M SDS aqueous solution; using platinum as a working electrode; platinum wire as auxillary electrode; saturated calomel electrode as reference electrode; at scan rate 100 mV/s

All the CVs showed similar characteristic peaks for different concentrations of BT and SDS. The CVs displayed an oxidation potential at ca.

1.1 V in the first cycle of potential sweep, which corresponds to the anodic oxidation potential for the 2,2'-bithiophene monomer compared at 1.3 V to 2,2'-bithiophene in AcCN [27]. This decrease in the monomer oxidation potential has been attributed to a catalytic effect of the surfactants in the synthesis of conducting polymers [33]. This electrocatalytic effect of surfactant stems from the formation of micelles where hydrophobic and hydrophilic regions are formed at the metal/solution interface [34]. The oxidation reaction at this potential is irreversible and does not show a corresponding reduction peak in the reverse sweep. There was a reversible peak observed in the successive cycles at a cathodic potential of ca. -0.6 V and anodic potential of ca. -0.5 V vs SCE that is due to redox cycling of higher molecular weight oligomers/polymers. All the CVs showed the expected increase in the redox current with increasing numbers of cycles, which indicated electroactive polymer formation at the surface. To explain this polymer growth with respect to the number of cycles performed during the electrosynthesis, we designated the ratio of the growth of the polymer to the oxidation current of the monomer as *b/a*, which we call the efficiency (eff) of the polymerization, as Figure V – 15 shown here for reference.

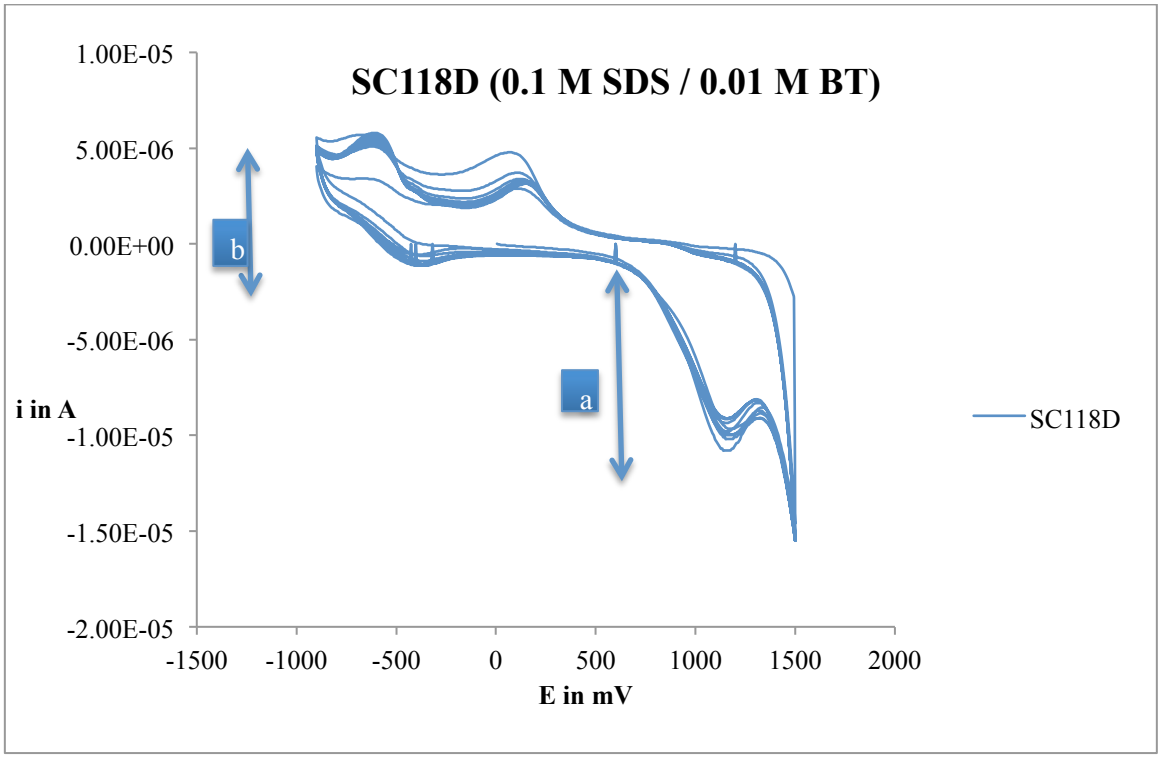

Figure V – 15: Cyclic voltammetry of SC118D. Conditions: 0.01 M BT in 0.1 M SDS aqueous solution; using platinum as a working electrode; platinum wire as auxillary electrode; saturated calomel electrode as reference electrode; at scan rate 100 mV/s.

Where *a* is assigned to the peak oxidative current of the monomer and *b* is assigned to sum of the peak redox currents for the polybithiophene.

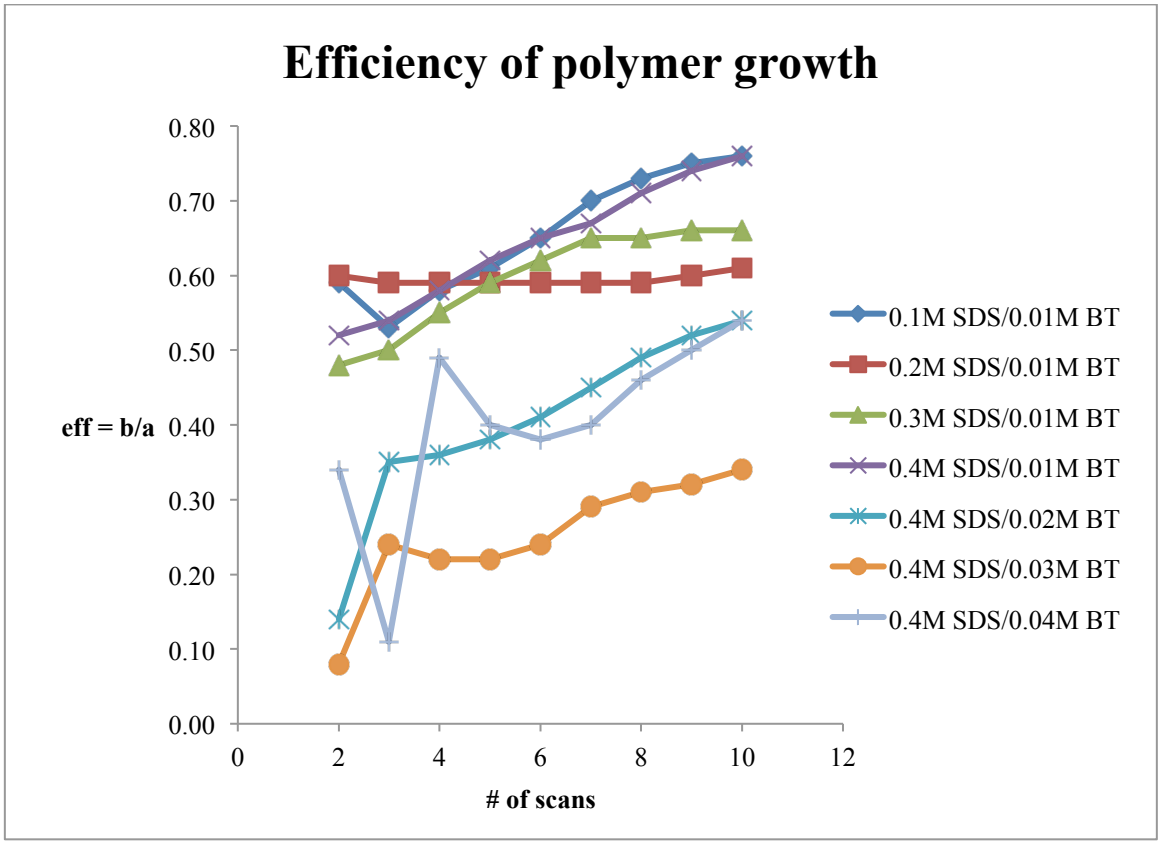

Figure V – 16: Plot of efficiency of polymer growth against # of scans

By plotting the efficiency vs the number of scans as shown in Figure V – 16, we could determine the optimal SDS and BT concentrations are 0.1 M SDS and 0.01 M BT for improved polymer growth. It was observed from the graphs that the different concentrations of SDS and BT showed different efficiencies, which could be due to the catalytic effect of the surfactant in adsolubilizing the BT in SDS aqueous solution. This catalytic effect of surfactants has been described as characteristic of the monomer oxidation potential [34]. Hence to study the catalytic effect of surfactants on the oxidation potentials of 2,2'-bithiophene monomer, the concentration of monomer BT was maintained at 0.01 M and SDS concentration was changed, as given in Table V - 3,

Table V – 3: Oxidation potential and concentrations of SDS data

	SDS conc M	log[SDS]	-log[SDS]	E_{pa} mV
SC118D	0.1	-1.00	1	1170
SC1211	0.2	-0.70	0.7	1050
SC1212	0.3	-0.52	0.52	1000
SC1213	0.4	-0.40	0.4	1010

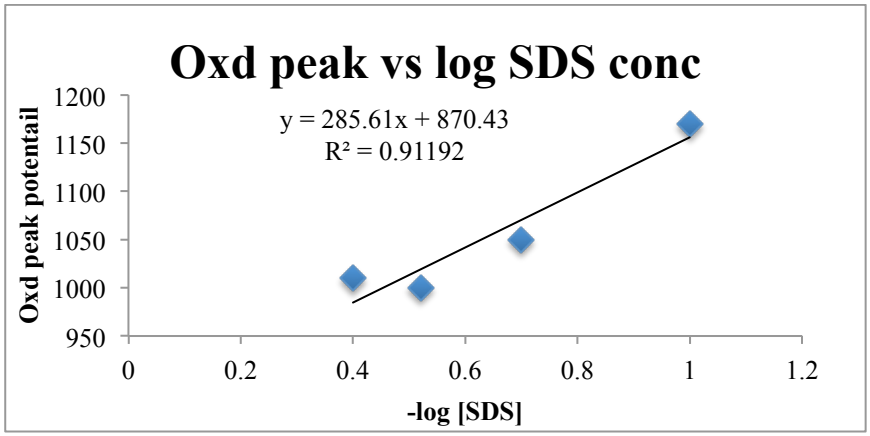

Figure V – 17: Plot of oxidation potential of monomer against –log[SDS]

From the Figure V – 17, it could be observed that there is significant effect of surfactant concentrations in lowering of the monomer oxidation potential. The oxidation potential decreases with an increase in the concentration of SDS. This behavior can be explained as characteristic of a nucleation process, stemming from the behavior of the SDS and the electropolymerization

mechanism of BT. The oxidation of BT to form polybithiophene can be found to be as given in scheme below,

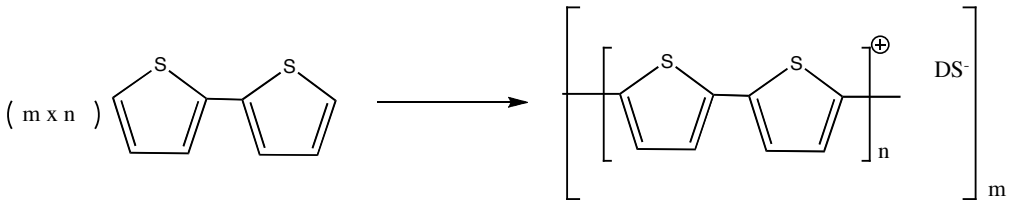

Scheme V – 5: Oxidation of BT to form poly(2,2'-bithiophene)
where *n* indicates degree of doping and *m* represents molecular weight.

Naoi et al. proposed a model for the catalytic activity of surfactants towards electropolymerizations and its behavior in the presence of a hydrophobic monomer [17]. The equilibrium process centers around micelle formation, in which the surfactant dopants in aqueous solution first appear as monomers that form micelles in solution and then bilayered micelles on the electrode surface at higher concentrations.

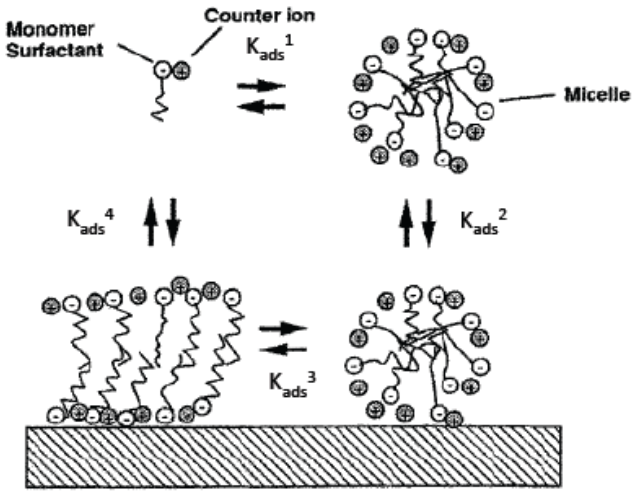

Figure V – 18: Micelles and bilayer formation

Harkins [35] explained the mechanism for the polymerization in presence of surfactants using a theory based on micelle formation. The

formation of polymer film in the presence of surfactants happens in three-step process. First, formation of micelles on the electrode surface, by proper control of surface charge and counterion concentration for ionic surfactants, results in a bilayered system being formed on the electrode surface. Second, hydrophobic polymerizable monomers insert into the hydrophobic part of micelles (called adsolubilization). Finally, oxidative polymerization of monomers takes place inside the admicelles on the electrode surface.

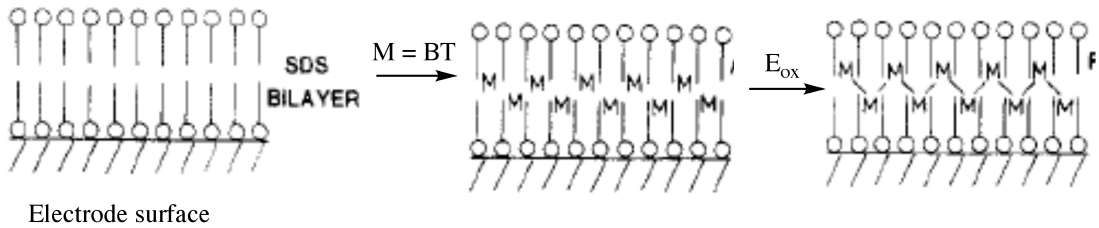

Figure V – 19: Electropolymerization of BT in bilayer

As the solubility of the BT in water is very poor (40.2 mg / Liter at 25° C), the use of surfactant enables higher solubility of BT in micelles or admicelles. To facilitate the admicellar assisted polymerization, it is necessary to understand the adsolubilization constant K_{ads}, where K_{ads} = (mole fraction of BT in the micelles/ the concentration of the free BT in the media) [36]. In order to quantify this solubilization of BT in micellar solution, and understand how the interaction between the monomer BT and the surfactant will affect the polymerization, it is useful to determine $K_{ads.}$ The adsolubilization constant, $K_{ads,}$ calculated by our group for the 0.1 M SDS at 25° C, was found to be 109 M^{-1} which basically suggests that more than 98 % of BT is incorporated in the

micelles [37]. The assumption can also be made that these BT molecules are present in both the micelles as well as in the bilayers.

The micelle concentration was determined based on the CMC values and aggregation number of surfactant SDS. The equation is given below,

$$\text{Micelle concentrations} = \frac{\text{Molar Concentrations} - \text{CMC}}{\text{Aggregation number}}$$

The CMC value was obtained to 0.01 M at pH 7 from the literature [38], and the aggregation number was found to be 62. The number of BT molecules per micelle was calculated based on the micelle concentration and the concentration of BT in the aqueous solution, as given in Table V - 4.

Table V – 4: Micelle concentration data

System	Sample Concentrations	Micelle Concentration	BT/Micelles	Slope (current in A (b/#of scans))
SC1211	0.2M SDS / 0.01M BT	0.003073	3.3	1.00E-08
SC1212	0.3M SDS / 0.01M BT	0.004685	2.1	6.00E-08
SC1213	0.4M SDS / 0.01M BT	0.006298	1.6	1.00E-07
SC1214	0.4M SDS / 0.02M BT	0.006298	3.2	2.00E-07
SC1215	0.4M SDS / 0.03M BT	0.006298	4.8	1.00E-07
SC1216	0.4M SDS / 0.04M BT	0.006298	6.4	2.00E-07
SC118D	0.1M SDS / 0.01M BT	0.001452	6.9	3.00E-07

The slope of the current was taken from plots of polymer formation current (b) vs number of scans as shown in Figure V - 20.

The trends in the CVs were different for different concentrations of SDS and BT. The polymer growth of BT was monitored by plotting the redox current of the polymer growth peaks (b) against the numbers of scans. From the graph, it was shown that at constant BT with different concentrations of SDS, the polymer growth was found to be better with an increasing number of scans when the concentration of SDS is 0.1 M. From Table V – 3 also it can be seen that when BT/micelle ratio was calculated, it was found to be higher in the case when 0.1 M SDS/0.01 M BT than any other combination of surfactants with BT.

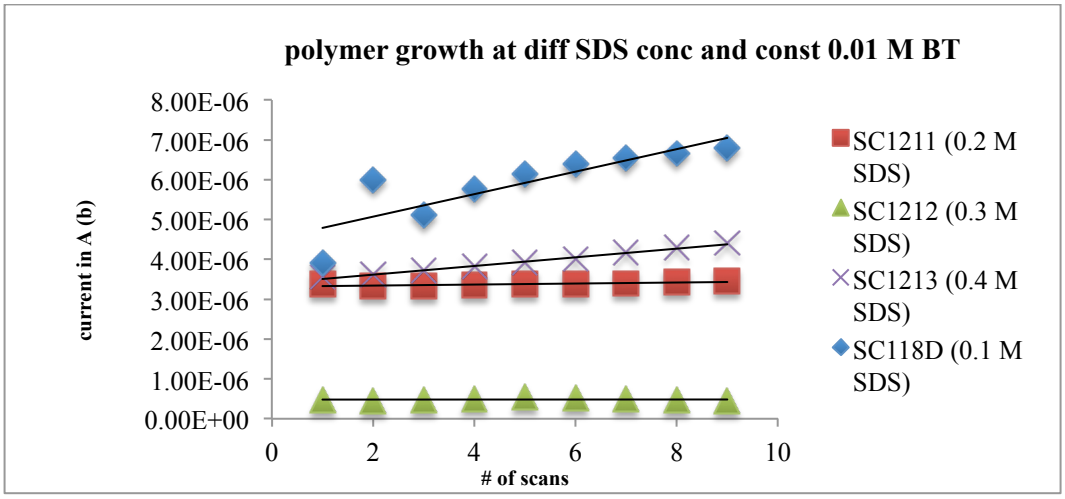

Figure V – 20: Polymer growth at different concentrations of SDS and constant BT

From Figure V – 20, it can also be observed that the polymerization rate was affected by increasing SDS concentration, but a clear trend can not be discerned. After 10 cycles the polymerization rates slow down which could signal that new polymer formation contributes less and less to the total redox current.

The effect of different concentrations of BT at constant SDS concentration (0.4 M) was also checked with regard to the polymerization growth rate.

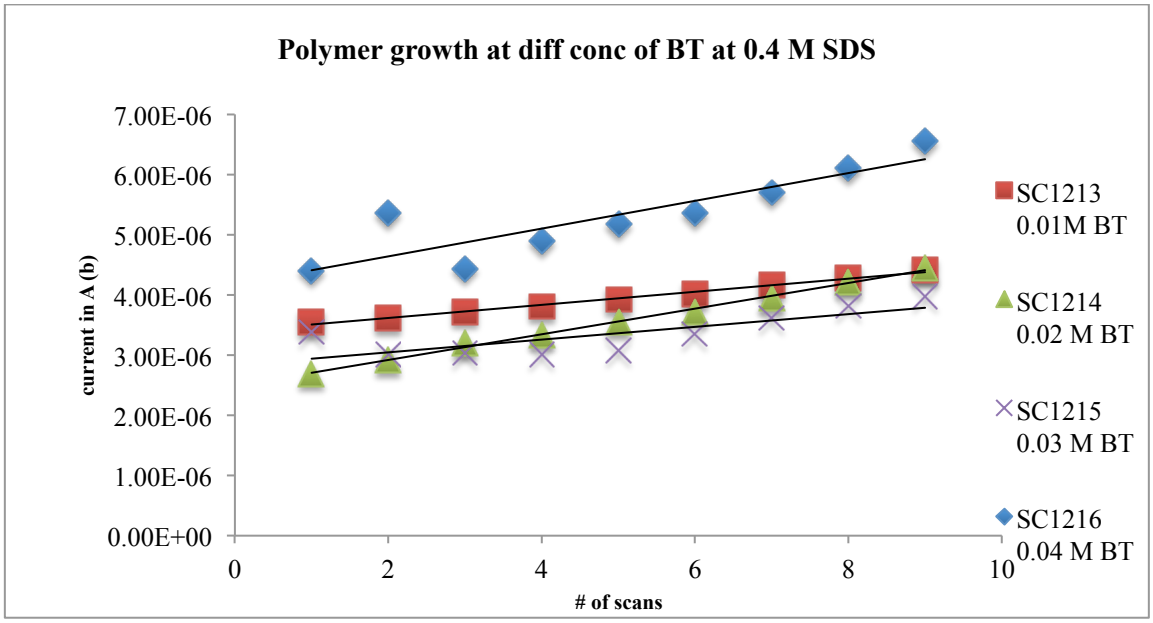

Figure V – 21: Polymer growth at different concentrations of BT and constant SDS

From the Figure V - 21 it can be observed that redox peak current increases with the increasing number of scans which shows the growth of the polymer film. But at high concentration of BT this polymer growth is prominent, which is clearly due to the increased concentration of electroactive BT moiety. As more BT molecules are available in the solution to adsolubilize in the micelles, the BT/micelle ratio increases.

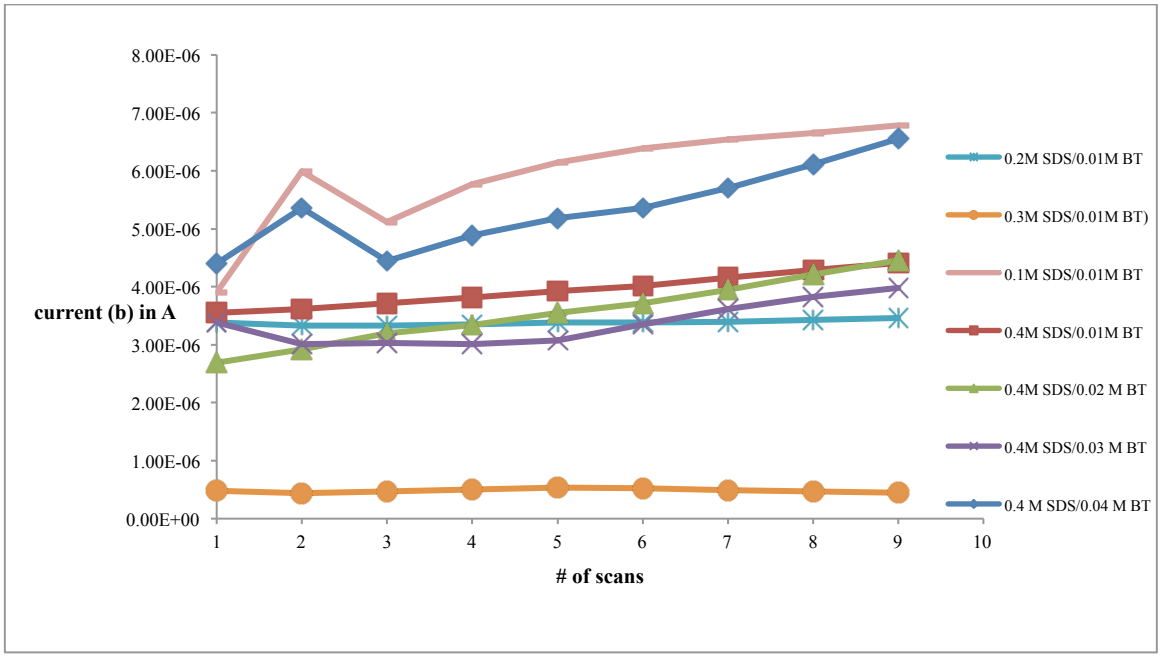

Figure V – 22: Polymer growth at different concentrations of BT and SDS

As the above plot, Figure V – 22, shows, the polymer growth is maximum when the concentration of SDS and BT is 0.1 M and 0.01 M or 0.4 M and 0.04 M, respectively. This could well be related to the number of BT molecules available in the micelles, which enhance the electropolymerization process. Such concentration dependencies can be as depicted in Figure V – 23, at low concentrations of SDS, adsolubilized BT molecules are present in the admicelles in a high enough concentration to facilitate polymerization. When the concentration of SDS is increased at constant BT concentration, more bilayers adsorbed onto the electrode surface form. However, at this point to keep K_{ads} constant some of the BT monomers move from the bilayer to the free micelles. This is consistent with the increase in oxidation potential and the lower efficiency of polymer growth. When the concentration of BT is increased, the

concentration of BT molecules adsorbed in the bilayer increases, lowering the oxidation potential and increasing the efficiency of polymer growth.

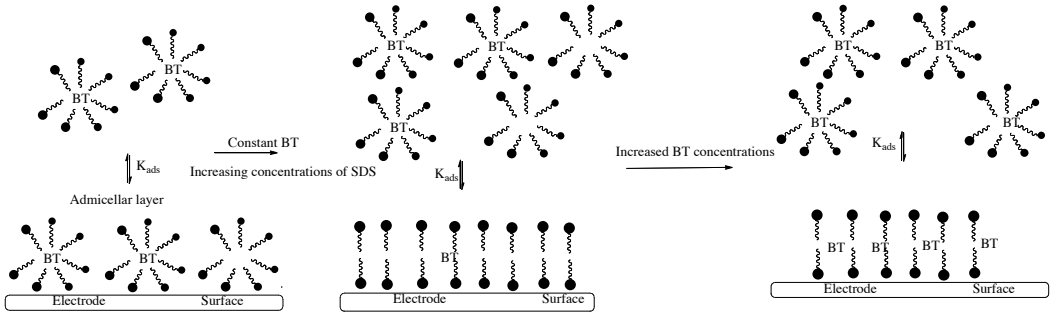

Figure V – 23: Possible model for electropolymerization of BT

Conclusion:

Stable polybithiophene films were prepared using SDS as an anionic surfactant electrolyte and as a solubilizing agent in the aqueous medium. The use of SDS has the advantage of solubilizing BT in aqueous solution and influences establishing the interface between the electroactive BT and the electrode surface. A Three-step process for the formation of polymer is discussed in which admicelle formation is followed by BT adsolubilization and finally polymerization in a surfactant bilayer on the electrode surface. It is quite interesting to notice that the effect of polymerization of BT in presence of SDS is not linear with the increasing concentration of SDS, while increasing the concentration of BT also has some effect on polymerization rate. However, polymerization clearly depends on how many molecules of BT can adsolubilize in the bilayer. It was observed that increased polymerizability of the BT depends on the BT/micelle ratio; if it stays sufficiently high, increased polymer growth can be observed.

Experimental:

Apparatus and Procedures:

Cyclic voltammetry data was obtained using a BAS CV 50W potentiostat. A three electrode one compartment cell was used at room temperature. For electrochemical studies, a 0.3 mm diameter platinum electrode used as the working electrode, a platinum wire used as the counter electrode and saturated calomel electrode (SCE) was used as the reference electrode.

Chemicals:

2,2'-Bithiophene (BT) (97%; Aldrich) and sodium dodecyl sulfate (SDS) (Aldrich) were obtained commercially and used without further purification. Deionized water was used as solvent.

Electrochemical procedures and measurements:

Electrochemical measurements and polymerization were performed in a one-compartment cell using potentiostat. BT 0.01 M was mixed with the 0.1 M SDS in DI water and was ultrasonicated to make sure all the BT molecules were dissolved in the SDS aqueous medium. Electrochemical measurements were performed as mentioned earlier in a one compartment cell with a platinum working electrode, a platinum wire counter electrode, and a SCE reference electrode. The working electrode was typically cycled between - 0.9 V to 1.5 V at a 100 mV/sec scan rate at room temperature. All the other concentration combinations of SDS and BT were prepared in a similar manner.

References:

1. Fisyuk, A.S., *Mixed Alkylthiophene-based Heterocyclic Polymers Containing Oxadiazole units via Electrochemical Polymerisation: Spectroscopic, Electrochemical and Spectroelectrochemical Properties. New J. Chem*, 2005. **29**: p. 707 -713.

2. Shirakawa, H., *Synthesis of Electrically Conducting Organic Polymers: Halogen Derivatives of Polyacetylene, (CH)x.* J. Chem. Soc., Chem Commun., 1977: p. 578 - 580.

3. Friend, R.H., *Conjugated polymers. New materials for optoelectronic devices. Pure Appl. Chem.*, 2001. **73**(3): p. 425 - 430.

4. Kovacic, P. and A. Kyriakis, *Polymerization of Benzene to p-Polyphenyl by Aluminum Chloride-Cupric Chloride.* J. Am. Chem. Soc, 1963. **85**(4): p. 454 - 458.

5. Wang, H.L., R.M. O'Malley, and J.E. Fernandez, *Electrochemical and Chemical Polymerization of Imidazole and Some of Its Derivatives. Macromolecules*, 1994. **27**(4): p. 893 - 901.

6. Bicak, N. and B. Karagoz, *Polymerization of aniline by copper-catalyzed air oxidation.* J. Polym. Sci. Part A, Polymer Chemistry, 2006. **44**: p. 6025 - 6031.

7. Sadki, S., *The mechanisms of pyrrole electropolymerization.* Chemical Society Reviews, 2000. **29**(5): p. 283-293.

8. Diaz, A.F., K.K. Kanazawa, and G.P. Gardini, *Electrochemical polymerization of pyrrole.* Journal of the Chemical Society, Chemical Communications, 1979(14): p. 635-636.

9. Toshima, N. and S. Hara, *Direct synthesis of conducting polymers from simple monomers.* Progress in Polymer Science, 1995. **20**(1): p. 155-183.

10. Saunders, B.R., K.S. Murray, and R.J. Fleming, *Physical Properties of Polypyrrole Films Containing Sulfonated Metallophthalocyanine Anions.* Synthetic Metals, 1992. **47**: p. 167 - 178.

11. Yakovleva, A.A., *Electrochemistry of Polypyrrole Films in Aqueous Solutions: The character of the Bond between the Anion and the Polymer Matrix.* Russian Journal of Electrochemistry., 2000. **36**(12): p. 1275 - 1282.

12. Shaktavat, V., K. Sharma, and N.S. Saxena, *Structural and Electrical Characterization of Protonic Acid Doped Polypyrrole.* Journal of Ovonic Research, 2010. **6**(6): p. 239 - 245.

13. Vork, F.T.A. and L.J.J. Janssen, *Structural Effects in Polypyrrole Synthesis. Electrochimica Acta*, 1988. **33**(11): p. 1513 - 1517.

14. Kuramoto, N., *Modification of Growth Rate and Structure of Electropolymerized Aniline by Sodium Polyvinyl Sulfonate. J. Chem. Soc., Chem Commun.*, 1990: p. 1478 - 1480.

15. Naoi, K., M. Lien, and W. Smyrl, *Quartz Crystal Microbalance Study: Ionic Motion Across Conducting Polymers. J. Electrochem. Soc*, 1991. **138**(2): p. 440 - 445.

16. Zhong, C. and K. Doblhofer, *Polypyrrole-based electrode coatings switchable electrochemically between the anion- and cation-exchanger states.* Electrochimica Acta, 1990. **35**(11 - 12): p. 1971 - 1976.

17. Naoi, K., *Electrochemistry of Surfactant - Doped Polypyrrole Film (I): Formation of COlumnar Structure by Electropolymerization.* J. Electrochem. Soc, 1995. **142**(2): p. 417 - 422.

18. Ruckenstein, E. and R. Nagarajan, *Critical Micelle Concentration. A Transition Point for Micellar Size Distribution.* J. Phys. Chem., 1975. **79**(24): p. 2622 - 2626.

19. McCullough, R.D., *The Chemistry of Conducting Polythiophenes.* Adv. Mater., 1998. **10**(2): p. 93 - 116.

20. Schopf, G. and G. Koßmehl, *Polythiophenes - Electrically Conductive Polymers. Adv. Polym. Sci.*, 1997. **129**: p. 1 - 166.

21. Yoshino, K., S. Hayashi, and R.-i. Sugimoto, *Preparation and Properties of Conducting Heterocyclic Polymer Films by Chemical Method.* Jpn. J. Appl. Phys., 1984. **23**: p. L899 - L900.

22. Berlin, A., G.A. Pagani, and F. Sannicolò, *New Synthetic Routes to Electroconductive Polymers Containing Thiophene Units.* J. Chem. Soc., Chem Commun., 1986(22): p. 1663.

23. Jen, K.-Y., G.G. Miller, and R.L. Elsenbaumer, *Highly conducting, soluble, and environmentally-stable poly(3-alkylthiophenes).* J. Chem. Soc., Chem Commun., 1986(17): p. 1346 -1347.

24. Sato, M.-a., S. Tanaka, and K. Kaeriyama, *Soluble Conducting Polythiophenes.* J. Chem. Soc., Chem Commun., 1986: p. 873 -874.

25. Sato, M.-a., S. Tanaka, and K. Kaeriyama, *Electrochemical Preparation of Highly Conducting Polythiophene Films.* J. Chem. Soc., Chem Commun., 1985: p. 713 - 714.

26. Krische, B., M. Zagorska, and J. Hellberg, *Bithiophenes as Starting Monomers for Polythiophene Synthese.* Synthetic Metals, 1993. **58**: p. 295 - 307.

27. Funt, B.L. and S.V. Lowen, *Mechanistic Studies of the Electropolymerization of 2,2′-bithiophene and of Pyrrole to Form Conducting Polymers.* Synthetic Metals, 1985. **11**(3): p. 129 - 137.

28. Czerwinski, A., et al., *The Electrochemical Deposition of Conducting Poly(3-Methyl-2,5-Thienylene) Films from Aqueous Media.* J. Electrochem. Soc, 1985. **132**(11): p. 2669 - 2672.

29. Dong, S. and W. Zhang, *Study on Conducting Polythiophene Electrochemically Polymerized in Phosphoric Acid Aqueous Solution.* Synthetic Metals, 1989. **30**(3): p. 359 - 368.

30. Bazzaoui, E.A., S. Aeiyach, and P.C. Lacaze, *Low Potential Electropolymerization of Thiophene in Aqueous Perchloric Acid.* j. Electroanal. Chem, 1994. **364**(1 - 2): p. 63 - 69.

31. Bazzaoui, E.A., S. Aeiyach, and P.C. Lacaze, *Electropolymerization of Bithiophene on Pt and Fe Electrodes in an Aqueous Sodium dodecylsulfate (SDS) Micellar Medium.* Synthetic Metals, 1996. **83**(2): p. 159 - 165.

32. Sakmeche, N., *Application of Sodium Dodecylsulfate (SDS) Micellar Solution as an Organized Medium for Electropolymerization of Thiophene Derivatives in Water.* Synthetic Metals, 1997. **84**(1 - 2): p. 191 -192.

33. Lima, A., *Electropolymerization of 3,4-Ethylenedioxythiophene and 3,4-Ethylenedioxythiophene Methanol in the Presence of Dodecylbenzenesulfonate.* Synthetic Metals, 1998. **93**(1): p. 33 - 41.

34. Sakmeche, N., *Anionic Micelles; A New Aqueous Medium for Electropolymerization of Poly(3,4-ethylenedioxythiophene) Films on Pt Electrodes. Chem. Comm.*, 1996: p. 2723 - 2724.

35. Harkins, W.D., *A General Theory of the Mechanism of Emulsion Polymerization. J. Am. Chem. Soc*, 1947. **69**(6): p. 1428 - 1444.

36. Funkhouser, G.P., *Solubilization and Adsolubilization of Pyrrole by Sodium Dodecyl Sulfate: Polypyrrole Formation on Alumina Surfaces. Langmuir*, 1995. **11**(5): p. 1443 - 1447.

37. Glatzhofer, D.T., O. Scherman, and G. Funkhouser, unpublished results.

38. Rahman, A. and C.W. Brown, *Effect of pH on the Critical Micelle Concentration of Sodium Dodecyl sulphate. J. Appl. Poly. Sci.*, 1983. **28**: p. 1331 - 1334.